Mechanical and Surface Properties of Polystyrene Fibers Reinforced with Cellulose Nanocrystals

by

Mahsa Kalantari

A thesis submitted in partial fulfillment of the requirements for the degree of

Doctor of Philosophy

in

Civil Engineering (Cross-Disciplinary)

Department of Civil and Environmental Engineering

University of Alberta

Abstract

Electrospinning of polystyrene (PS) as a ubiquitous polymer attracted tremendous attention. Though, different reinforcement techniques are commonly considered for the electrospun PS fibers because of their fragile structures. High mechanical properties of Cellulose nanocrystals (CNC) allow these nanoparticles to be used as effective reinforcing materials for a variety of nano-composite applications including electrospun fibers. However, hydrophilic characteristic of CNC makes it less favorable to disperse it uniformly in the hydrophobic polystyrene matrix. Therefore, to improve the interfacial interaction of CNC with polystyrene matrix, CNC nanoparticles were first modified by different functional chemical groups. In this work, three types of modified CNC were used. The modifications included replacement of hydroxyl groups through substitutive reactions with the para nitro benzene, three fluorocarbon benzene, and grafted polystyrenes. Firstly neat PS fibers were optimized by evaluation of the electrospinning solvents, and working parameters. The optimized electrospinning solutions were prepared using DMF as the solvent (20 wt. % of PS (Mn= 250000) was dissolved in DMF). Then, these modified CNCs were used to reinforce PS fibers. Five different loading levels of CNC (0, 0.5, 1, 1.5, 2 wt. % in solid fiber corresponding to 0, 0.01, 0.02, 0.03, 0.04 w/v % CNC dispersion in PS solution) were investigated. Electrospun samples were prepared in two forms of oriented and non-oriented structures. The effects of CNC modifications on the fiber morphologies were initially analyzed through SEM images. Subsequently, results obtained from SEM images were evaluated by turbidity, conductivity and viscosity of electrospinning solutions. The CNC modified with para nitro benzene and para three fluorocarbon benzene resulted in smoother fibers structure and an increase in fibers diameter. On the other hand, beaded fibers, with smaller diameters, were obtained by adding CNC grafted with PS. The effects of CNC inclusion and fiber alignments on the elastic modulus, strength and maximum strain of the fiber mats were investigated by conducting tensile tests. Using DMA results, storage moduli, loss moduli, and damping factors of the electrospun samples were measured and compared. The oriented PS mats with 0.5 wt. % CNC grafted with PS showed the best mechanical gain. The elastic modulus (E) and storage modulus (E') of this samples increased 910% and 250%, respectively. Finally, alignments of the electrospun fibers led to 450% improvement in stiffness, and 250% increment in storage modulus in avrage with inclusion of 2 wt. % various types of CNC. Finally, the surface properties and wettability of the electrospun samples were studied by means of contact angle and roughness measurements. Three different structures of the neat polystyrene including smooth electrospun fibers, beaded fiber, and electrosprayed spheres, were prepared by using different solvent collections. The beaded fiber structure resulted in the highest contact angle; however, there is a potential for electrosprayed samples to give a rise to superhydrophobic surface after longer times of electrospraying. Moreover, electrospun samples showed the rose petal effect which can be attributed to their hairiness and hierarchical surface structures. Addition of CNC could also change the surface properties due to the changes in roughness, and the surface energy based on the types of the CNC modification. Finally, alignment of the fibers caused a drop in the contact angle and roughness which can be explained by an increase in the structure order for the oriented CNC/PS samples.

Stop being drunk, all my life I will not

For I was not born when you entered my sight

Unlike the sun you do not come and go

Others come and go, you permanently glow

(Sa’di, Koliat, P. 606)

همه عمر برندارم سر از این خمار مستي   که هنوز من نبودم که تو در دلم نشستی

تو نه مثل آفتابي که حضور و غیبت افتد   دگران روند و آیند و تو همچنان که هستي

(سعدی، کلیات، صفحه ۶۰۶)

Acknowledgments

I would like to take this opportunity to thank all people who helped me directly or indirectly with the realization of this thesis work and throughout my study program. Firstly, I would like to express sincere gratitude and thanks to my supervisor, Dr. Yaman Boluk for his tireless patience, continues support, supervision, guidance, trusts on me and valuable suggestions on each step of my PhD research. I was really fortune to have him as my supervisors. Then, I would like to extend my sincere appreciation to my co supervisor, and Dr. Cagri Ayranci, for his valuable inputs, and his support during the course of this research.

I would also to extend my deep appreciation to my friends, and colleagues (Shahin Shadlou, Rongbing Du, Gregory Kaufman, Mounir El Bakkari, Hale Oguzlu, and Hafez Balavi) for their help, support and continues encouragement.

I am very thankful to the Agencies and Institutions that provided me financial support during my studies and thesis work; Alberta Innovative Technology Future (AITF) , Natural Sciences and Engineering Research Council of Canada (NSERC), Alberta Innovative Bio Solution, and Faculty of Graduate Studies and Research of the University of Alberta.

Finally I would express my endless gratefulness and love to my family members back in Iran. Thank you very much maman, baba, and Masih for your endless love, emotional and moral supports, and faith in me.

Contents

List of Tables

List of Figures

Nomenclature

A= Area

a_m & K_m = The Constant Values of Mark-Houwink equations

c= concentration

ΔG = Gibbs free energy

ΔH = Enthalpy

ΔS = Entropy

δ = Solubility parameter (or phase lag)

da= Areal density

D = Diameter

e = charge

ε = Strain

E= Modulus

F= Force

Fi= Attractive constant of chemical group

$F_{(d,h,p)}$= Fractionated solubility parameters

φ = Volume Fraction

G= compliance

χ = Polymer-solvent interaction parameters

$\chi *$= Wavenumber of perturbation

K= conductivity

γ = Surface tension

l= Filament length

λ = Wave length

ʎ= stress relaxation constant

M= Molecular weight

μ = Viscosity

η = Viscosity

ω = Frequency

ρ = Density

r = radius

R= Gas constant

r= radius

Ra= Interaction radius

τ = Shear strength

θ = Contact angle

T= Temperature

t= time

V= Volume

U= Velocity

W= Work

w= Weight

σ = Stress

Chapter 1

1. Introduction

Electrospinning is a convenient technique to produce polymeric nanofibrous webs where the fiber diameter can vary from several micrometers to tens of nanometers. This easily-tailorable technique can be used to produce fibers from various polymers and polymer blends. The simplicity of the particles incorporation or other functional material additions into the fibers are of the advantages of this technique (Ko and Wan 2014). In electrospinning, a polymer solution (Z. M. Huang et al. 2003; Rošic et al. 2012; Gupta et al. 2005) is subjected to a high electrical field to stretch and form continuous fibers and fiber mats. These nanofibrous structures have several outstanding functional characteristics, such as a large surface area to volume ratio, controllable pore size, and various remarkable morphological and mechanical properties (Ko and Wan 2014). Therefore, electrospun polymeric fibers are used in many areas such as composites (Rojas and Habibi 2009), biotechnology (tissue engineering, controlled/ sustained release systems) (Z. M. Huang et al. 2006; Zhang et al. 2005), membranes/filters (Zong et al. 2002; Cooper et al. 2013), and textiles (Deitzel et al. 2001).

Polystyrene (PS) is a commonly used amorphous polymer with high transparency, stiffness, high electrical resistance and low dielectric loss. PS is used in applications such as packaging, insulation, and filtration (Spychal, Lath, and Berek 1979). Numerous studies have reported the electrospinning of PS fibers (Roghani-Mamaqani, Najafi, and Salami-Kalajahi 2010; Jarusuwannapoom et al. 2005; Uyar and Besenbacher 2008; Rojas and Habibi 2009; Baker et al. 2006; Shin 2006; An, Shin, and Chase 2006; Jia et al. 2002; Aussawasathien, Sahasithiwat, and Menbangpung 2008; X. Lu, Wang, and Wei 2009; Sihn et al. 2008) for applications in tissue engineering (Baker et al. 2006), filtration (Shin 2006), ion exchanger (An, Shin, and Chase 2006), enzyme immobilization (Jia et al. 2002), sensors (Aussawasathien, Sahasithiwat, and Menbangpung 2008), catalysis immobilization (X. Lu, Wang, and Wei 2009) and composite materials (Sihn et al. 2008). However, brittleness and relatively low thermal and mechanical properties of PS limits its broader use. Consequently, incorporation of nano-sized fillers, such as gold nanoparticles (Huan, Liu, et al. 2015) and multiwalled carbon nanotubes (Worzakowska 2015), into the PS fibers attracted great interest. These composite fibers can be considered for high-performance applications that need high surface areas and other special material properties.

An alternative to the aforementioned particles is cellulose nanocrystals (CNC). CNCs are wood or plant-based novel nano-materials that offer an attractive combination of properties such as biocompatibility, and high mechanical stiffness and strength (Kargarzadeh et al. 2015), due to their orderly crystallized structure. These characteristics make them favorable in composites applications (Klemm et al. 2011) for improving mechanical properties of polymeric materials (Habibi, Lucia, and Rojas 2010).

CNCs can potentially improve the mechanical properties of PS electrospun fibers. However, the strong hydrophilicity of CNCs, due to the large amount of surface hydroxyl groups, is a disadvantage in terms of their reinforcement capacity in hydrophobic PS (i.e. the differences of polarity between PS and CNCs). Moreover, CNCs have a great tendency towards self-aggregation in continuous phase. This stems from their nanoscale dimensions and consequently large surface area (N. Lin and Dufresne 2014). This problem can lead to aggregation or nonhomogeneous dispersion of CNCs into nonpolar PS continuous matrix. To benefit from its nano-dimensional effect and other superior properties, a homogeneous dispersion of CNCs in the polymer matrix needs to be obtained (N. Lin and Dufresne 2013).

Adding amphipathic surfactant is an effective method to disperse CNCs homogeneously and to enhance their interfacial compatibility with nonpolar PS. PS and CNCs can be well mixed by adding a proper surfactant. However, the properties of PS/CNC nanocomposite materials may still deteriorate, due to the dynamic phase separation that can be induced by external stimuli during preparation (e.g. temperature and evaporation rate) (Rojas and Habibi 2009; Wanasekara et al. 2016). Surface modification or chemical functionalization of CNCs is the other possible route to improve their compatibility in nanocomposites, especially when used in combination with nonpolar or hydrophobic matrices. It helps to obtain better colloidal dispersion by tuning the surface characteristics of CNCs. Abundance of hydroxyl groups on the surface of cellulose makes it possible to do many different chemical modifications based on the type of polymeric matrix (Habibi, Lucia, and Rojas 2010). Considering the above-mentioned problems of surfactant application, modification of CNCs seems a more reasonable method to improve the interfacial interaction between CNC and polymeric matrix.

Both production and properties evaluation of the CNC reinforced polystyrene (PS) fibers mats were aimed in this PhD thesis. Based on these research goals, the objectives of this research are summarized as follows:

I. Analysis of the parameters affecting the electrospinning of polystyrene fibers

Finding a spinnable polystyrene solution is the first thing that should be taken into consideration. Therefore, first of all, our efforts were focused on finding a suitable solvent. Afterwards, we attempted to tailor fibers with desirable characteristics, by means of adjusting working parameters, including voltage and feeding rate.

II. Evaluation of the dispersion behaviour of modified CNCs in PS/DMF solution and their role in the electrospinning process

As described earlier, the dispersion behaviour of CNCs in PS matrix has significant influence on the final properties of nanofibrous web, and modification of CNC was considered to improve both dispersion of CNC in PS fibers, and interfacial interaction between them. Three modified CNCs, CNC-1, CNC-2, and CNC-g were considered for incorporation in PS fibers. The successful grafting of the modified CNC samples was verified by the FTIR spectroscopy. To determine the final dispersion of modified CNCs in PS matrix, their dispersion behaviour in DMF and PS/DMF solutions were studied.

III. Evaluation of the morphology and the structure of electrospun CNC/PS fibers

The diameter and morphology of fibers are important properties of electrospun fibers which influence directly the final function of nanofibrous mat. These properties can be tuned for diverse applications. In this part, how the presence of CNCs influences these specific properties of the fiber mat investigated and discussed.

IV. Mechanical properties of the CNC-reinforced fibers

In most of application for CNC-reinforced PS fibers, a developed mechanical properties of the final nanofibrous mat is an important requirement for a better functionality of the electrospun product. Therefore, evaluation of the mechanical improvement by CNC addition is an important objected in this thesis. Preparation of fibrous mats with aligned fibers was also took into consideration to further improve the mechanical properties. It is noteworthy that the evaluation of CNC effect is more reliable due to the more consistent structure of aligned fibrous web.

V. Surface properties of the CNC-reinforced fibers

Besides mechanical properties of the CNC/PS electrospun products, their surface characteristics should be taken into consideration for some specific applications. These applications include adhesive or superhydrophobic layers that can be manufactured by means of nanostrucutes, such as electrospun products. Therefore, a fundamental discussion of their surface properties is aimed in this thesis as well.

Chapter 2

2. Literature review

2.1. Electrospinning process and governing parameters

A simple electrospinning setup is composed of three parts: a high-voltage power supply, a syringe/syringe pump and a grounded collecting plate (collector). Figure 2.1 shows a schematic of a typical electrospinning system set-up with stationary surface. A high electric field is applied to the polymer solution pumped through a syringe. This electric field overcomes the surface tension of the solution, erupts from the tip of the needle, and forms a charged continuous jet of solution. The jet of solution accelerates towards the collector, whipping and bending rapidly. As the solution moves away from the needle and toward the collector, the jet quickly thins and dries as the solvent evaporates. On the surface of the grounded collector, a nonwoven mat of randomly oriented solid fibers is deposited (Seeram Ramakrishna, Kazutoshi Fujihara, Wee-Eong Teo, Teik-Cheng Lim 2005).

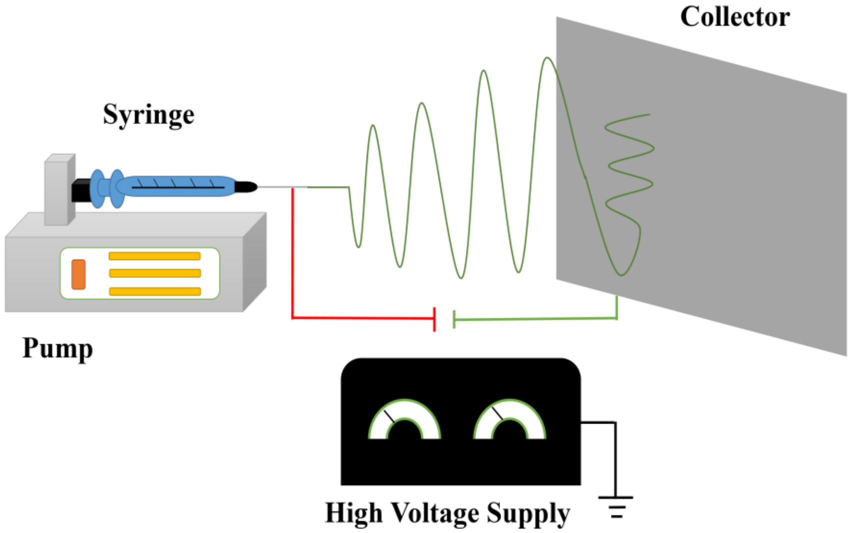

Figure 2. 1: Schematic representations of electrospinning set-up

2.2. Assemblies and alignments of electrospun fibers

One of the special advantages of electrospinning over the other fiber fabrication processes is the ability of this technique to produce fibrous structures with various assemblies. A particular assembly can improve the functionality of an electrospun product such as three dimensional arrangements of fibers for scaffold applications. Hence, it is necessary to devise new techniques that make the fabrication of the desired fibre assemblies, possible. Most popular fibre assemblies are nonwoven fibre mesh, aligned fibre mesh, patterned fibre mesh, random three-dimensional structures and sub-micron spring or convoluted fibres, respectively (Teo and Ramakrishna 2006; Baji, Mai, Wong, Abtahi, and Chen 2010). There are different application for these assemblies. For instance, nonwoven fibrous structure is more suitable for filtration application (Shin 2006); while, for uses such as nanowires, it is important to target exact locations of electrospun fiber deposition (Bashouti et al. 2006). Though, for most of the cases, assemblies can be an advantages. For example Xu and his colleagues found out that cells cultured on aligned fibers scaffolds were more proliferate in the direction of the fibre orientation (C. Y. Xu et al. 2004). However, assembly of the aligned fibers is mostly considered to improve the mechanical properties (Mathew et al. 2006; J. Lee and Deng 2012). Although rotating drum is the most convenient method to produce aligned electrospun fibers, there are other techniques where a list of the most popular system were presented in Table 2.1. This table is also presenting advantage and disadvantages of these systems.

Table 2. 1: Properties of different collector set-ups for various assemblies of electrospun products

(A more comprehensive list of the fiber collection systems is available on (Teo and Ramakrishna 2006))

System name	Schematic diagrams	Advantages	Disadvantages	References
Rotating drum	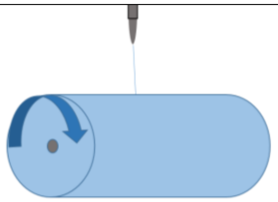	1) Straightforward system 2) Fabrication of aligned fibres with large area	1) Difficult fabrication of highly aligned fibrous assemblies 2) Fibre breakage at too high rotor speed	(Mathew et al. 2006) (Wannatong, Sirivat, and Supaphol 2004) (J. Lee and Deng 2012)
Parallel electrodes	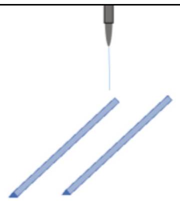	1) Straightforward system 2) Highly aligned fibres production 3) Easy separation of aligned fibres and transferring them to another substrate	1) Difficult fabrication of thicker layer of aligned fibres 2) limited length of the aligned fibres	(D. Li, Wang, and Xia 2003)
Rotating wire drum collector	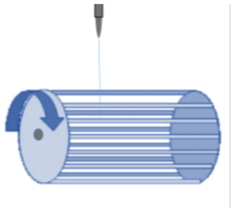	1) Straightforward system 2) Highly aligned fibres production	1) Difficult fabrication of thicker layer of aligned fibres 2) Imperfect fiber alignment on the whole assembly	(Katta et al. 2004)
Drum collector with wire wound on it	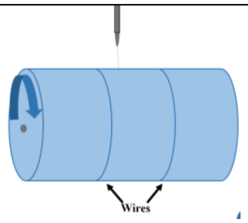	1) Straightforward system 2) Highly aligned fibres production 3) Adjustable area of aligned fibres by wire thickness variation	1) Concentration of aligned fibres on the wire rather than the whole drum	(Bhattarai et al. 2005)
Disc collector	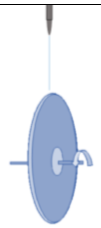	1) Straightforward system 2) Highly aligned fibres production	1) Difficult retention of high fibre alignment at the thicker layer of fibers 2) Small area of fibre alignment	(Theron, Zussman, and Yarin 2001) (C. Y. Xu et al. 2004)
Array of counter-electrodes	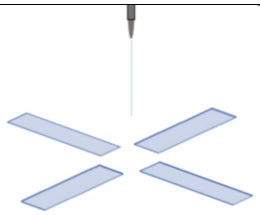	1) Straightforward system	1) Inconsistency of fibre pattern over the whole assembly 2) Limited area of the assembly 3) Difficult production of thicker fibrous samples	(D. Li and Xia 2004)

2.3. Influencing parameters on electrospinning

There are three groups of governing electrospinning parameters influencing the final characteristic of the fibers. These three groups include solution parameters, process parameters, and ambient parameters. Production of electrospun fibers with desired morphologies and diameters is possible by means of a proper control of these parameters (Seeram Ramakrishna, Kazutoshi Fujihara, Wee-Eong Teo, Teik-Cheng Lim 2005).

Solution parameter is the most significant influencing factor on electrospinning. It was proven that molecular weight, polymer concentration, solution viscosity (Casper and Stephens 2004; Shenoy et al. 2005a; C. Wang, Hsu, and Lin 2006) , solution conductivity (Fallahi et al. 2008; T. Lin et al. 2004) and the type of solvent (Wannatong, Sirivat, and Supaphol 2004; Eda and Shivkumar 2007; Jarusuwannapoom et al. 2005; Uyar and Besenbacher 2008) all are main solution characteristics which can significantly influence on the final morphology of the electrospun fibers.

Polymer concentration were found the first factor to control the transition of the bead-to-fiber structure (Gupta et al. 2005; McKee, Elkins, and Long 2004). As the concentration increases from very low to very high polymer contents, different polymeric structure can be obtained (Fong et al. 1999; Supaphol, Mit-Uppatham, and Nithitanakul 2005). As shown in Figure 2.2, polymeric micro (nano)-particles, a mixture of beads and fibers, smooth fibers and helix-shaped microribbons were observed by increase of the polymer concentration respectively (Yang et al. 2004). Two concentrations of the entanglement concentration (Ce) and the chain overlap concentration (C*) were introduced as critical hydrodynamic concentrations. The entanglement concentration (Ce) is usually several times of the overlap concentration, and the determining electrospinning concentration can vary based on the polymer type and its molecular weight. The higher the molecular weight, the lower of proportion of C* is needed to obtain a good electrospinning solution (Gupta et al. 2005).

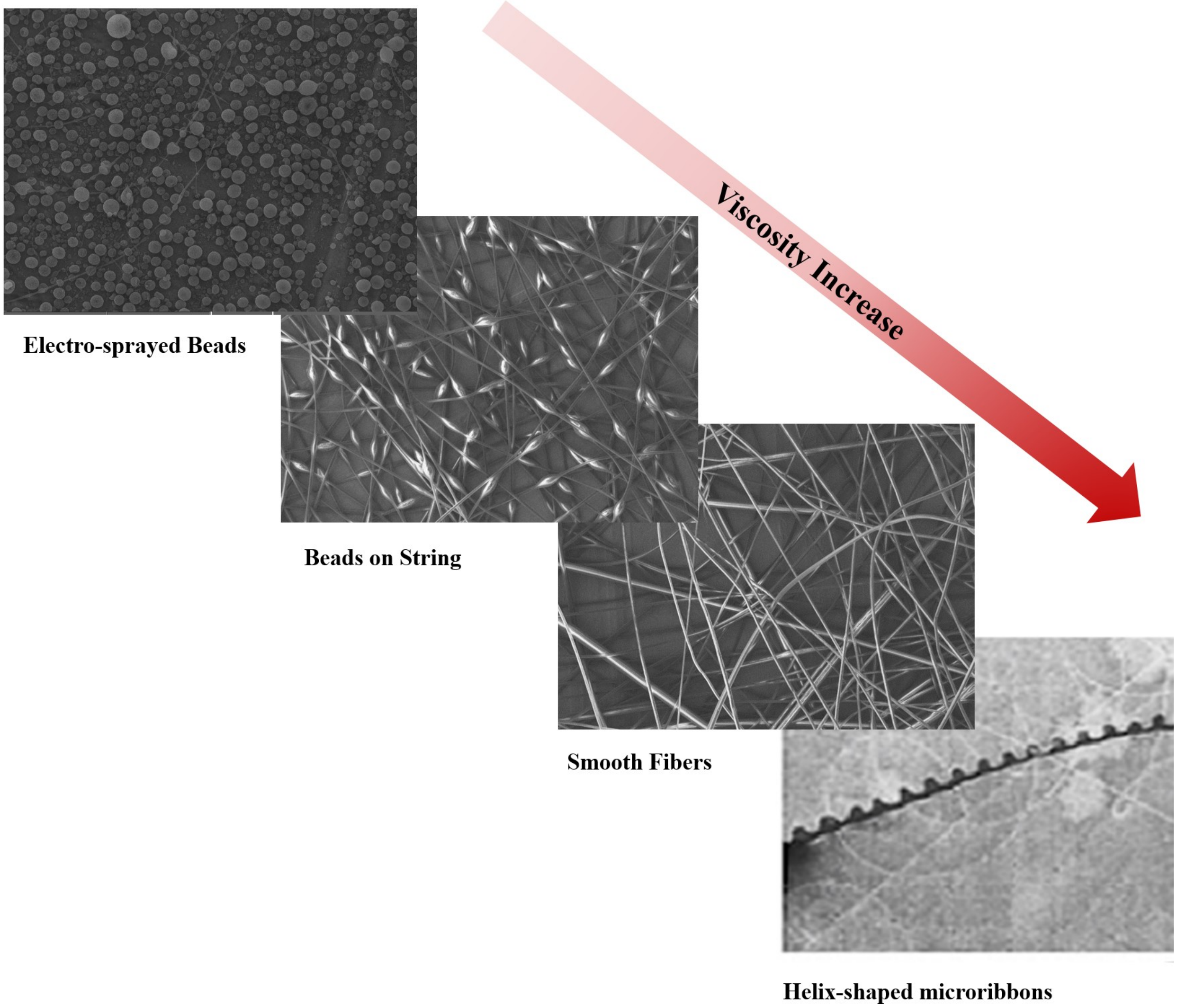

Electro-sprayed Beads

Beads on String

Smooth Fibers

Helix-shaped microribbons

Figure 2. 2: Different electrospun polymeric structure obtained from polymer solution with different concentration (Adopted by (Yang et al. 2004))

Viscosity can be adjusted by means of either the polymer concentration or polymer molecular weight. Viscosity, as a governing factor in electrospinning, should be adjusted over a suitable range to obtain smooth fibers; otherwise, electrospraying or hard ejection can happen at very low or very high viscosity respectively (Larrondo and Manley 1981; Sukigara et al. 2003). Moreover, in the case of a suitable range of polymer concentrations, a higher concentration of polymer solution can result in thicker fiber due to the higher solution viscosity of more concentrated solution.

Besides, the molecular weight of the polymer has an important effect on morphologies of electrospun fiber because it affects the entanglement of polymer chains in solutions, and consequently the solution viscosity. If the rest of the conditions are the same (e.g. solvent, solution surface tension, solution conductivity), the lower the molecular weight of the polymer, the higher the possibility to form beads rather than smooth fiber. However, increasing the molecular weight after a certain amount will result in micro-ribbon (Koski, Yim, and Shivkumar 2004).

The critical chain overlap concentration (C *) can be predicted by means of intrinsic viscosity [η], using the Equation 2.2 (Krause, Bellomo, and Colby 2001).

$$(C^{*} \sim 1/\,[\eta]) \qquad \text{Equation 2.1}$$

Mark-Howinks equation describes how the molecular weight and solubility in the selected solvent (polymer-solvent interaction) increase the intrinsic viscosity.

$$[\eta] = K_m M^{a_m} \qquad \text{Equation 2.2}$$

Where [η] and M are intrinsic viscosity and molecular weight (viscosity average) of polymer. The K_m and a_m are the constant values of the Mark–Houwink parameters. Constant a_m is a good representative factor of gyration radius of polymer chains. For solvents, a value of a=0.5 is an indicative of a theta solvent. A value of a=0.8 is typical for good solvents. For most flexible polymers, constant a_m between 0.5 and 0.8 distinguishes polymer solubility in solvent.

Hence, solvent as a carrier of a particular polymer in electrospinning has significant roles on the final properties of electrospun structures. The solvent type can also determine the minimum electrospinning concentration (Gupta et al. 2005). The degree of polymer-solvent interactions can estimate the amount of the viscous and elastic forces (viscoelasticity), and they can be evaluated by means of solubility parameters. The higher polymer-solvent interaction can lead to a lower entanglement concentration, and a higher elastic behaviour. Higher polymer/solvent interactions means a larger radius of gyration, or larger configurations of polymer chains in solvent. This can lead to the smaller entanglement concentration which is initiating elastic behaviour of the polymer solution, (Ferry 1948).

Surface tension is another important factor which is influenced by the compositions of the solution. Capillary action of high surface tension can cause Rayleigh instability resulting in the polymer solution jet breakage during electrospinning and finally the beaded structures. For fibers with uniform structure, the Rayleigh instability has to be suppressed by the viscoelastic forces during the elongational flow of electrospinning. Hence, a polymer solution with proper extensional viscosity and relaxation time can result into the smooth fiber (Yu, Fridrikh, and Rutledge 2006). Therefore besides viscoelastic forces, beaded fibers can be converted into smooth fibers by reducing the surface tension of the solution. This can be provided by means of different solvents combined with different surface tensions at the fixed concentration (Yang et al. 2004), or changing the mass ratio of solution components (Haghi and Akbari 2007; Pham, Sharma, and Mikos 2006; Zhang et al. 2005).

Solution conductivity is the other significant factor in electrospinning. It can be influenced by the solvent type, the addition of salt or surfactant, and the polymer type. Natural polymers are mostly polyelectrolytes, and their charge carrying ability increases by the ions resulting in thinner fibers with no beads. comparison with the synthetic equivalents (Zong et al. 2002). In the case of a neutral polymer solution, addition of the ionic salts such as KH2PO4 and NaCl can improve the electrical conductivity of the solution. Fibers with smaller diameters could be fabricated with the aid of ionic salts (Z. M. Huang et al. 2006). Based on the other project, application of organic acid as the solvent like formic acid was found helpful for nylon electrospinning due to the high solvent conductivity (Z. M. Huang et al. 2006).

Another main category of influential parameters is processing parameters. These parameters include applied voltage, flowrate, working distance, and collector type.

Applied voltage as a crucial factor can only result in the charged jets ejected from Taylor Cone when it is higher than the threshold voltage. However, there is no specific trend between the effect of the applied voltages and the diameter of electrospun fibers. For instance, researches (Fong et al. 1999) reported that there is no significant effect of voltage on the diameter of polyethylene oxide (PEO) fibers while some researchers found that higher voltages can result in the thinner fiber e.g., (Yuan et al. 2004). On the other hand, several groups proposed that the higher the voltages, the narrower the fiber can be due to the electrostatic repulsive force on the charged jet (Yuan et al. 2004). Additionally, the effect of higher voltage on the formation of beads was reported by several groups (Buchko et al. 1999; Demir et al. 2002). Consequently, voltage influences on fiber diameter can be more depended on the flowrate and on the distance between the tip and the collector (Yordem, Papila, and Menceloglu 2008).

Another effective process factor is the polymer solution flow rate from the syringe tip. For the polymer solution to have enough time for solidification, lower flow rate is more recommended because in case of high flow rate, formation of beaded fibers with thick diameter is more possible (Buchko et al. 1999). However, the amount of flow rate should be adjusted based on the polymer solution characteristic and applied electrical field.

Another processing factor is collector characteristics which was described in Section 2,2. Collector type not only determine the assembly of the electrospun product, but also influence on the fiber structures as well as the fiber collection form. Collectors are usually made of aluminum foil. However, transferring the collected fibers on foil to other substrates for various applications is not easy, so diverse collectors were devised such as wire mesh (X. Wang et al. 2005), pin (Sundaray et al. 2004), grids (D. Li et al. 2004), parallel or gridded bar (C. Xu et al. 2004), rotating rods or wheel (C. Xu et al. 2004), and liquid bath (Ki et al. 2005).

Working distance, the distance between the collector and the tip of the syringe is another subcategory of the processing parameters. It can also influence the morphologies of fiber (Ki et al. 2005). It is shown that the solvent cannot evaporate entirely if the distance is too short, and the fiber will not solidify before reaching the collector. On the other side of the spectrum, beaded fiber will be obtained if the distance is too long, so there is an optimum for working distance (Yuan et al. 2004).

However, sometimes preparation of fibers with desired characteristics cannot be achieved by adjusting these parameters, and it is needed to use some additives to polymer solution to improve the properties. For instance, salt is added to increase the conductivity of solution (Zong et al. 2002), or surfactant was suggested to decrease the surface tension (Zeng et al. 2003). Besides such additives, application of various nanoparticles in electrospinning attracted tremendous attention these days. These particles can bring about different improvement on final characteristics of electrospun fibers which will be discussed later.

2.4. Electrospinning of polymer solutions containing nanoparticles

Electrospinning of polymer solution that contains solid nano-particles is performed to embed fillers into fibers. In some cases, electrospinning is used to form fibrous structure of nanoparticles, and the concentration of nanoparticles are dominant. For instance, in order to electrospinning of lignin, which has a nano-spherical structure, high amount of lignin, around (95-99% w/w) and just tiny amount of polymer (1-5% w/w polyethylene oxide PEO) are added to the electrospinning solutions. In these cases, polymer is used as a processing aid to increase elongational viscoelasticity of the solution (Aslanzadeh et al. 2016). However, in most of the cases, just small amount of functional nanoparticles is considered in polymeric fibrous structure. These functional nanoparticles help to improve fibers, in terms of mechanical performance (J. Lee and Deng 2012) or thermal properties (Gao et al., n.d.), to develop sensor devices (Marega et al. 2015) and to incorporate medicine (Y. Wang et al. 2010) or nutrients (Sheikh et al. 2013). The high surface area to volume ratios of nanoparticles provide great interfacial interaction with the polymeric matrices. As a result, their effect on the properties of the final nanofibrous mat is more pronounced (Ko and Wan 2014). Incorporation of several different types of nanoparticles into the fibers was reported, and a list of the most typical functional nanoparticles and electrospun matrices is presented in Table 2.2.

Table 2. 2: Typical functional nanoparticles and matrix applied in electrospinning

Function	Nanoparticles	Polymer
Mechanical	CNT, Graphene	Poly acrylonitrile (PAN) (Kaur, Kumar, and Dhakate 2016), Polyvinylidene fluoride (PVDF) (Park et al. 2015)
Thermal	Clay	PAN (Esfandarani et al. 2011)
Electrical	CNT	Poly(styrene-butadiene-styrene) SBS (Costa et al. 2013)
Magnetic	Fe_3O_4	Poly acrylonitrile PAN (B. Wang, Sun, and Wang 2010)
Optical	CdS	Poly ethylene oxide (PEO) (Bashouti et al. 2006), Poly(methyl methacrylate) (PMMA)(Mthethwa et al. 2011)
Biological/antimicrobial	Ag	Poly vinyl alcohol (PVA)(Marega et al. 2015)

However, electrospinning of these nanocomposites as colloids of nanoparticles can be challenging. Colloidal particles in polymer solutions are usually complex fluids. Depending on the degree of adsorption or even non-adsorption of polymer chains onto particles (Feigin and Napper 1980), these nanoparticles can inevitably alter the overall rheological properties of the solutions (Nelson and Cosgrove 2004). This issue will effect on electrospun fiber structures. Drew et al. reported a significant beaded structures of poly (ethylene oxide) (PEO) fibers containing TiO_2 particles (Drew et al. 2003). They explained the bead formation by TiO_2 particle agglomeration in the polymer solution. However, they also attribute the uniform structure of fibers to the higher viscosity of the solution containing TiO2 particle. Moreover, Daga et al. claimed that laponite nanoclay addition into PEO solution resulted in strong viscoelasticity. They explained the high viscoelasticity by well dispersion of laponite particles and adsorption bridging of them by PEO macromolecules (Daga, Helgeson, and Wa 2006). In a different study, Sun et al. showed that addition of cellulose nanocrystals (CNC) can increase the sustainable viscosity of cellulose acetate solutions due to the formation of liquid crystals in suspensions (C. Sun, Boluk, and Ayranci 2015). They also reported that because of the higher viscosity and conductivity of CNC/Polymer solution, narrower fibers were obtained.

Additionally, the arrangement and distribution of these particles in the fibers has a tremendous effect on the overall properties and performance of the electrospun fibers. Some researchers claime electrospinning procedure will naturally maximize the uniform distribution of the nanoparticles in fibers (Huan, Bai, et al. 2015) while, some researchers reported the agglomeration of nanoparticles in electrospun fibers (H. Dong et al. 2012). In a few studies, it is reported that due to the electrostatic forces applied during electrospinning, nano-particles (especially in the case of cylindrical shapes) align parallel to the longitudinal fiber axis (D. Chen et al. 2009; Samir A, Alloin F 2005), and this maximizes their contribution to the improvement of the functional properties. Nevertheless, there are studies reporting the lack of alignment of nano cylindrical particles (Wanasekara et al. 2016). The other main factor that should be considered is the interfacial adhesion between nanoparticles and polymers because the lack of proper interfacial interaction can minimize the effect of nanoparticles on the final properties of electrospun mat (D. Chen et al. 2009).

2.5. Cellulose Nano Particles (CNC) as nanoparticles in electrospinning

Cellulose nanocrystal (CNC) is a novel nanofiller used in nano-composites. Their high modulus elasticity, low density renewability and biocompatibility make CNCs more favorable over other types of nanofillers (Samir A, Alloin F 2005; Eichhorn et al. 2010). CNC can be produced by means of acidic treatment and isolation of cellulose nano-whiskers from natural cellulose sources such as plants, algae, wood, and even a kind of sea animal called tunicates (Iwamoto et al. 2009). They have very desirable mechanical properties due to their high crystallinity. The elastic modulus of CNC is reported to be in the range of 120 - 180 GPa (Iwamoto et al. 2009), and their strength is reported as 10,000 MPa (Hubbe et al. 2008).

CNC is added to nanocomposites for different reasons. Biocompatibility and nontoxicity of CNC make it a good candidate for fibrous nanocomposites for biomedical applications, such as tissue engineering and wound healing (C. Zhou et al. 2013). Based on some studies (Liu, Yuan, and Bhattacharyya 2012; Zoppe et al. 2009), CNC was added to improve wettability of poly (lactic acid) (PLA) and poly (e-caprolactone) (PCL) fibers which improves the adhesion of living cell on the fiber scaffolds. However, CNC is mostly added to electrospun fibers because of its reinforcing ability (C. Sun, Boluk, and Ayranci 2015; Zhang et al. 2005; Zoppe et al. 2009).

Table 2.3 presents a list of studies considering the reinforcing effect of CNC on the fibers produced for different applications. CNC is originally hydrophilic with high compatibility for hydrophilic polymers. To reinforce nonpolar materials, either of surfactant application (Rojas and Habibi 2009; Wanasekara et al. 2016; Bercea and Navard 2000) or surface modifications of CNC (Iwamoto et al. 2009; Moon et al. 2011; Zoppe et al. 2009) were performed to improve the CNCs compatibility. However, surface modification of CNCs is preferred because the properties of surfactant stabilized PS/CNC nanocomposite materials may still deteriorate by external stimuli (e.g. temperature and evaporation rate) during preparation (Bercea and Navard 2000). As shown in Table 2.2, in case of electrospun fibers, except for a few cases, surface modification were not considered (Zoppe et al. 2009).

Table 2. 3: Reinforced fibers with cellulose nanocrystals (H. Dong 2015)

Polymer	**Source of CNCs**	**CNC content wt. %**	**Solvent**	**Surface Modification**	**Mechanical test**	**Reference**
Poly(vinyl alchohol)	Ramie fibers	0, 5, 10, 15	Water	None	Storage modulus É (DMA)	(M. Peresin et al. 2010; M. S. Peresin et al. 2014)
Lignin-Poly (vinyl alchohol)	Cotton	0, 5, 10, 15	Water	None	None	(Ago et al. 2012)
Polyethylene oxide	Microcrystalline Cellulose	0, 5, 10, 20	Water	None	Tensile Properties	(C. Zhou et al. 2011)
Cross-linked Polyethylene oxide	Cotton	0, 5, 10, 20	Water	Cross-linking of PEO	Tensile Properties	(C. Zhou, Wang, and Wu 2012)
EVOH (ethylene vinyl alchohol)	Bacterial Cellulose	0, 1, 5, 8	2-propanol-water	BCNW Bacterial Cellulose Nanowhiskers	None	(X. Wu, Moon, and Martini 2013)
Cellulose Acetate	Microcrystalline Cellulose	0-5	Acetic acid-Aceton	None	Storage modulus É (DMA)	(Herrera et al. 2011)
Poly(acrylic acid)	Cotton	0, 5, 10, 15, 20	Ethanol	None	Tensile Properties	(P. Lu and Hsieh 2009)
Poly caprolactone	Ramie fiber	0, 2.5, 5, 7.5	DMF-dichloromethane	Grafting of PCL	Storage modulus É (DMA)	(Zoppe et al. 2009)
Poly(lactic acid)	Microcrystalline Cellulose	0, 1, 10	DMF	None	Tensile Properties	(Liu, Yuan, and Bhattacharyya 2012)
Polystyrene	Cellulose filter paper	6, 9	THF	None	Storage modulus É (DMA)	(Rojas and Habibi 2009; Wanasekara et al. 2016; Huan, Bai, et al. 2015)
Poly(methyl methacrylate)	Soft wood pulp	0-41	DMF	None	Storage modulus É (nanoindentation)	(H. Dong et al. 2012)
Cellulose Acetate	Cotton	0-3	DMAC/Acetone	None	Storage modulus É (nanoindentation)	(C. Sun, Boluk, and Ayranci 2015)
Silk fibroin	Mulberry branch bark	0, 1, 2, 3, 4, 5	Formic Acid	None	Tensile Properties	(J. Huang, Liu, and Yao 2011)

2.6. Mechanical properties of nanofibrous mats containing CNC

Generally, adding CNCs to polymer fibers brings about both higher Young’s modulus and tensile strength, while CNC causes lower elongation at break and ultimate tensile elongation. For instance, Zhou et al. (C. Zhou et al. 2011) studied the tensile properties of polyethylene oxide (PEO)/CNC fibers electrospun from 7 wt. % PEO in H_2O with CNC content in the range of 0 to 20 wt%. They reported an increasing trend for the maximum tensile stress and Young's modulus, while the elongation at break had a decreasing trend (see Table 2.4). Huang and his colleagues reported that incorporation of only 2 wt. % of CNCs could enhance the tensile strength and Young's modulus of silk fibroin nanofiber mat to about twice as much as those of unreinforced nanofiber. Similar to the other project, the strain at break dropped gradually with the increase of CNC (J. Huang, Liu, and Yao 2011).

Table 2. 4: Tensile properties of electrospun PEO and PEO/CNC nanofibrous mats containing 10 and 20 wt. % CNC (Adopted by (C. Zhou and Wu 2012)).

Tensile Parameters	PEO + 0% CNC	PEO + 10% CNC	PEO + 20% CNC
Young's modulus (MPa)	~20	~40	~120
Strength (MPa)	~3.2	~6	~8
Strain (%)	~160	~125	~120

The effect of alignment of fibers on tensile properties of poly vinyl alcohol (PVA)/CNC fiber mats was examined in the mechanical study of the aligned and isotropic PVA/CNC nanofiber webs (J. Lee and Deng 2012). Oriented electrospun mats presented 30–45 % higher tensile strength and modulus than isotropic electrospun mats, unrelated to the CNC contents. Moreover, CNCs had a higher strengthening effect on the aligned PVA/CNC webs, compared with the isotropic PVA/CNC webs (J. Lee and Deng 2012).

The storage modulus of the fiber mats after incorporation of CNCs is generally investigated by means of dynamic mechanical analysis (DMA) in the tensile mode. It was shown that adding

CNC has a reinforcing effect on the storage modulus at either above or below T_g for several nanocomposite fibers. For instance, in the case of PCL fiber, the storage modulus was increased by several loadings of CNCs, and the reinforcement effect was observed to depend upon both the fiber diameter and the CNC content (Zoppe et al. 2009). In a similar study, uniaxially oriented arrays of PEO/CNC fibers with similar diameter in the range of 400-500 nm were prepared with CNC fillings of 5 wt. %, 10 wt. %, and 15 wt. % (Changsarn et al. 2011). The storage moduli of the PEO/CNC nanofiber arrays along the fiber axis were 1.5–2 times greater than neat PEO fiber array. Similar results were reported for PS nanofibrous oriented web containing cellulose nanowhiskers (CNW). The storage moduli of 20, 63, and 126 MPa were measured for samples containing 0, 6, and 9 wt. % CNW, respectively (Rojas and Habibi 2009).

Because of the small size and difficulty in handling single nanofibers, the fiber mats consisted of web of nanofibers are usually considered to be the best choice for the assessment of the mechanical properties. On the other hand, due to disconnection among fibers in the transverse direction, mechanical properties of mats cannot realize the real reinforcing effect of CNC in fibers. Consequently, aside from the composition and diameter of the fibers, the mechanical properties measured on fiber mats can be strongly influenced by fiber orientation within the mat, besides bonding between fibers, and their slippage on each other (M. Wang et al. 2004). Consequently, mechanical properties of a single fiber were considered, and to do so, a few nanoscale mechanical testing methods were developed. Among them, the atomic force microscope (AFM) cantilever, or commercial nanotensile testing is the most common technique. In AFM, a single electrospun nanofiber, is bent using nanoindentation, and their mechanical properties can be evaluated by studying their bending behavior (M. Wang et al. 2004; Tan, Ng, and Lim 2005). For example, to examine the reinforcing effects of CNCs in electrospun PMMA nanofibers, nanoscale dynamic mechanical analysis (nano-DMA) was performed using nanoindentation (H. Dong et al. 2012).

Chapter 3

3. Electrospinning of polystyrene solution, and controlling of the process conditions

3.1. Introduction

The main objective of this chapter is the selection of solvent as well as experimental conditions for the production of the uniform polystyrene (PS) fibers with proper characteristics. As described in Chapter 1, the ultimate goal of this research is the improvement of the mechanical properties of PS electrospun fibers. Since beads can cause mechanical defects in the fiber structures, all attempts were made to eliminate the bead presence in the PS electrospun structures. To that end, firstly PS solution characteristics were taken into consideration, and an optimum PS electrospinning solution was selected. Subsequently, after finding the most suitable electrospinning solution of PS, working process parameters of electrospinning were manipulated to obtain the best electrospinning conditions.

Regarding the electrospinning of PS, it was proven that polymer molecular weight, type of solvent (Wannatong, Sirivat, and Supaphol 2004; Eda and Shivkumar 2007; Jarusuwannapoom et al. 2005; Uyar and Besenbacher 2008), polymer concentration, solution viscosity (Casper and Stephens 2004; Shenoy et al. 2005a; C. Wang, Hsu, and Lin 2006), and solution conductivity (Fallahi et al. 2008; T. Lin et al. 2004) are main solution characteristics which can significantly influence the final morphology of the PS electrospun fibers. Consequently, the PS solution properties which can be electrospinnable was the first main objective of this chapter.

Polymer concentration in a selected solvent was found the first factor to control the transition of the bead-to-fiber structure (Gupta et al. 2005; McKee, Elkins, and Long 2004). Two concentrations of the entanglement concentration (Ce) and the chain overlap concentration (C*) were introduced as critical hydrodynamic concentrations. The entanglement concentration (Ce) is usually several times of the overlap concentration, and suitable electrospinning concentration can vary based on the polymer type and its molecular weight. The higher the molecular weight, the lower the proportion of C* is needed to obtain a good electrospinning solution(Gupta et al. 2005).

Solvent as a carrier of a particular polymer in electrospinning process has significant roles on the final properties of electrospun structures, and the solvent type can also determine the minimum electrospinning concentration (Gupta et al. 2005). Despite considerable efforts on the solvent selection (Uyar and Besenbacher 2008; Wannatong, Sirivat, and Supaphol 2004; Jarusuwannapoom et al. 2005; Eda and Shivkumar 2007), the electrospinnable polymer solutions were mostly chosen based on PS molecular weight, concentration and viscosity of PS solution, and almost no general and convincing explanation is presented based on the viscoelastic properties in these studies to discuss what makes a polymer solvent, a good electrospinning solvent. More importantly, no clear standard was established for judging whether a solvent of high solubility for a polymer will produce a good solution for electrospinning (Wannatong, Sirivat, and Supaphol 2004; C. Wang, Hsu, and Lin 2006; Uyar and Besenbacher 2008; Koski, Yim, and Shivkumar 2004; Shenoy et al. 2005b). Therefore, different solvents were considered in this study to have a closer look into the involved forces during electrospinning, and consequently on the final properties of the fibers. Five main solvents (Dichloromethane (DCM), Tetrahydrofuran (THF), Chloroform (CF), Dimethyl formaldehyde (DMF) and Toluene) were considered for PS electrospinning. These solvents are different in terms of density (d), boiling point (T_b), enthalpy of solution (ΔH_s), solubility parameters (δ_d, δ_p, and δ_h), dielectric constant, conductivity (K), and surface tension (γ) (Table 3.1 and Table 3.2).

In electrospinning, based on the Newton's Second Law of motion, different forces causes the motion of polymeric solution jet toward the collector (Seeram Ramakrishna, Kazutoshi Fujihara, Wee-Eong Teo, Teik-Cheng Lim 2005).

Table 3. 1:Properties of solvents used for PS electrospinning (Smallwood 1997)

Solvents	Chemical structures	Dipole	Absolute µ (mPa.s) @ 25 °	Dielectric constant @ 20 °	ɣ (mj/m2)	K (µs/m)	T_b (c°)
DMF	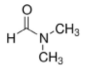	3.8	0.82	38.25	34.4	6	153
THF		1.75	0.55	7.52	26.7	9	65
CF	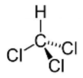	1.1	0.57	4.81	26.7	$1 * 10^{-2}$	61.2
DCM	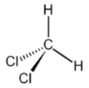	1.8	0.44	9.1	27.8	$4.3*10^{-9}$	39.6
Toluene	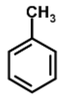	0.4	0.59	2.38	27.9	$4*10^{-2}$	110.6

F_T=Fc +Fe +Fv +Fs +Fd +Fg +Fa=ma Equation 3. 1

Where m, a, and F are equivalent mass, acceleration, and force respectively. The summation of forces can be corresponded to the summation of coulombic, electric field, viscoelastic, surface tension, air drag and gravitational forces individually. The different PS solvents have different columbic forces, surface tensions, volatilities and more importantly viscoelastic forces, when all the working parameters are kept constant. A comprehensive criteria of the solvent selection based on these factors are presented in this chapter.

As a final point, each electrospinning setup has its own optimum conditions based on its location, influenced by the humidity, air drag, and so on. Therefore, it is needed to manipulate working parameters, (flowrate, voltage and working distance) to obtain the best working conditions of a particular electrospinning system. Consequently, after picking the best electrospinning solution, working parameters, flowrate and voltage, were finally adjusted to the optimum electrospinning conditions.

3.2. Experimental details

3.2.1 Materials

Dichloromethane (DCM), Tetrahydrofuran (THF), Chloroform (CF), Dimethyl formaldehyde (DMF), and Toluene as solvents, and Polystyrene (PS) (MW = 280,000 g/mole, Tg = 100 °C) as fiber material used in this project were all purchased from Sigma Aldrich, Inc. All materials were used without further purification. The chemical structures and physical properties of the solvents are presented in Table 3.1.

3.2.2 PS fiber preparation

PS was dissolved in various organic solvents with concentrations of 20 % (w/v), in closed glass vials, under gentle stirring and at room temperature for 5 hours. Subsequently, the polymer solution was loaded in a 10 ml plastic syringe with a blunted metal needle. Electrospinning was performed with different flow rates (5, 10, 15, and 20 µl/min), a working distance (nozzle-to-collector distance) of 17 cm, and various voltages (5, 10, 15, 20, 25 kV) for all the PS solutions in this study. All electrospinning experiments were carried out under fume hood, and both temperature (T) and relative humidity (RH) were controlled at 23°C and 24%, respectively. A schematic representation of electrospinning system is shown in Figure 2.1.

3.2.3. SEM analysis

Both surface morphology and structures of fibers as well as their diameters were analyzed using a scanning electron microscope (SEM) (Vega-3 (Tescan) equipped with an EDXS detector (Oxford Instruments) at an acceleration voltage of 20 kV. SEM analysis of the samples was performed without coating. To determine the average diameter of each fiber sample, five different spots on each specimen were randomly selected for SEM analysis.

3.2.4. Rhelogical test

To investigate the effects of rheological properties on electrospinning, the AR-G2 rheometer was used to measure the rheological parameters of polymer solutions. The experiments were conducted in a laboratory at constant temperature.

3.3. Result and discussions

3.3.1. Solvent selections criteria.

In electrospun fiber productions, concentration of electrospinning polymer solution is among the most influential factors, and a critical minimum concentration, known as entanglement concentration Ce, is required. This concentration determines the onset of polymer chains entanglements and the transition from electro-spraying to electrospinning (McKee, Elkins, and Long 2004; Gupta et al. 2005). Polymer solutions with concentrations below Ce just produce droplets; while, solutions with concentrations above Ce can result in bead-on-string structures to flawless fibers by increasing concentration. However, finding an optimum concentration is out of the scope of this research, and several researches worked on this issue (Eda and Shivkumar 2007; C. Wang, Hsu, and Lin 2006; Jarusuwannapoom et al. 2005). Accordingly, 20% w/v was chosen based on the effective reported results and the fact that this concentration is several times larger than the Ce for PS in most of the solvents(G.-T. Kim et al. 2005; Jarusuwannapoom et al. 2005) which will be described thoroughly later.

As described previously, solvent as a carrier of a particular polymer in electrospinning has significant roles on the final properties of the electrospun structures, and several factors should be taken into consideration in order to select an electrospinning solvent. Here, factors such as polymer/solvent interaction, viscoelastic behaviour, surface tension, volatility and their electrical properties of PS were considered in selected solvents to not only find the best solvent, but also take a closer look into the impact of these effective factors on the final electrospinning products. Correspondingly, solvents with different physical properties were selected. These five solvents were dichloromethane (DCM), tetrahydrofuran (THF), chloroform (CF), dimethyl formaldehyde (DMF) and toluene.

3.3.1.1.Polymer solvent interaction

Based on the previous discussion, the degree of polymer-solvent interactions can determine the amount of the viscous and elastic forces (viscoelasticity), and they can be evaluated by means of solubility parameters. The higher polymer-solvent interaction can lead to a lower overlap, C^* and entanglement concentration Ce, hence higher elastic behaviour. A favorable interaction between polymer and solvent means a larger radius of gyration, or larger configurations of polymer chains in solvent. This can lead to the smaller entanglement concentration which is initiating elastic behaviour of the polymer solution, (Ferry 1948). This phenomenon is schematically shown in Figure 3.1.

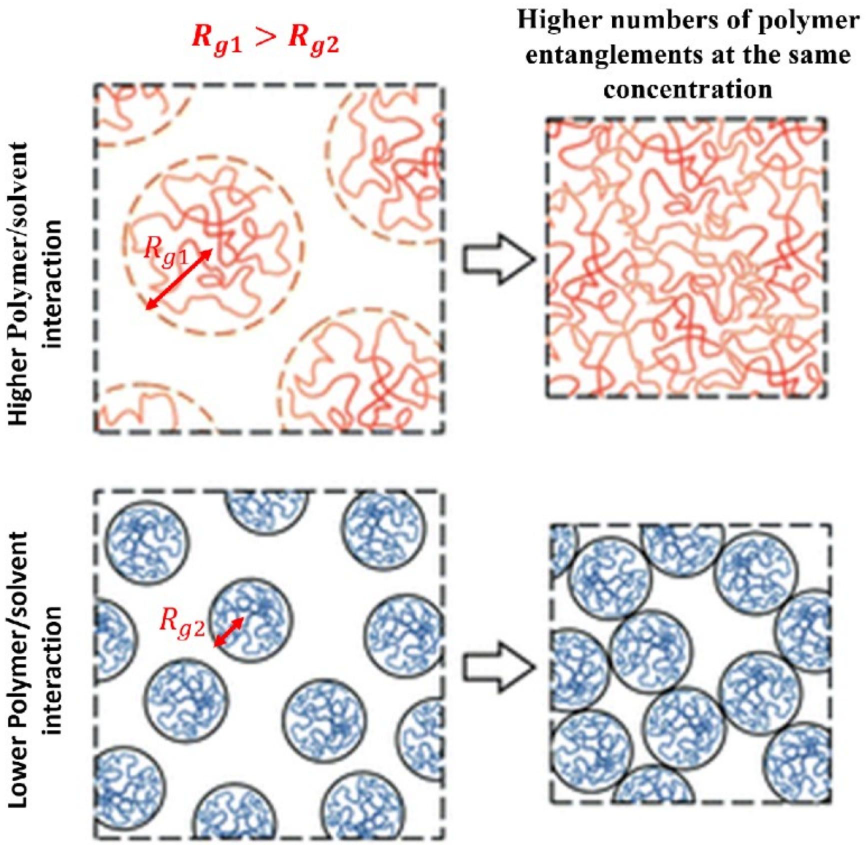

Figure 3. 1: Comparison of the polymer Radiuses of gyration in high and low polymer/solvent interaction (adopted by (Gupta et al. 2005))

Polymer/Solvent interaction can be evaluated by consideration of Gibbs free energy for polymer solution, presented in Equation 3.2.

$$\Delta G_m = \Delta H_m - T\Delta S_m \qquad \text{Equation 3.2}$$

Where ΔH_m , T and ΔS_m are enthalpy, temperature, and entropy of the mixing of the solution, respectively. Considering, Equation 3.2, the entropy term ($T\Delta S_m$) of the polymer solution is always positive, $\Delta H_m < T\Delta S_m$ has to be factor of the instantaneous solution. Hence ΔH_mhas to be as low as possible. The enthalpy of a solution can be calculated based on Equation 3.3.

$$\Delta H = \chi\varphi_s\varphi_p \qquad \text{Equation 3.3}$$

In Equation 3.3, χ is the polymer-solvent interaction parameter and φ is the volume fractions of the polymer or the solvent. The value of the interaction parameter can also be estimated from the Hildebrand solubility parameters δ_s (solvent) and δ_p (polymer) in Equation 3.4. Hildebrand solubility parameters are presented in Table 3.2.

$$\chi = \frac{V_r}{RT}(\delta_s - \delta_p)^2 \qquad \text{Equation 3.4}$$

where V_r, R and T are molar volume of solvent, gas constant and absolute temperature, respectively. Thus, enthalpy of solution can be presented in Equation 3.5.

$$\Delta H = \frac{V_r}{RT}(\delta_s - \delta_p)^2\varphi_s\varphi_p \qquad \text{Equation 3.5}$$

The values of χ between PS and selected solvents were compiled from the literature (Hansen 2013), and were used to calculate enthalpies of solution (Table 3.2). In addition, solubility parameters of solvents and polymers are presented in Table 3.2. Among the chosen solvents, DMF has the largest difference of solvent-polymer solubility parameters, and the highest enthalpy consequently which make DMF less thermodynamically favourable to dissolve PS. Accordingly, PS solution in DMF has the lowest viscosity among the other solvents. In contrast, CF with closest solubility parameters (δ_s) to the PS (δ_p) produces the lowest enthalpy among the other solvents. However, this solvent did not result in the highest viscosity, and DCM/PS has the highest viscosity in contrast. Therefore, only the similarity of the solubility parameters of polymer and solvent cannot independently describe the viscosity of solution.

Table 3. 2: Properties of 20% (w/v) PS solution in various solvents (Jarusuwannapoom et al. 2005)

Solvents	ɣ (mj/m2)	μ (mPas)	K (μs/m)	χ	ΔH Kj/mol
DMF	36.5	210	67	0.432	0.23
THF	22.6	297	6	0.286	0.15
CF	20.0	239	0.2	0.085	0.05
DCM	24.9	398	0.01	0.286	0.15
Toluene	30.2	236	0.3	0.37	0.17

In addition, Hanson's approach was considered to evaluate PS solubility in solvents. Hanson separated the solubility parameters into the dispersion, hydrogen, dipolar intermolecular components. These three fractions can be chosen as co-ordinates for a specific point in the Hansen space. The nearer two molecules are in this three-dimensional space, the more likely they are to dissolve into each other. To determine if a solvent and a polymer are soluble, a value called interaction radius (R0) is given to the polymer being dissolved. This value determines the radius of the sphere in Hansen space and its center is the three Hansen parameters. Equation 3.6 can be used to calculate the distance (Ra) between Hansen parameters in Hansen space.

$$R_a^2 = 4(\delta_{ds} - \delta_{dp})^2 + (\delta_{ps} - \delta_{pp})^2 + (\delta_{hs} - \delta_{hp})^2 \qquad \text{Equation 3.6}$$

The magnitudes of these fractioned solubility parameters of the solvents and PS are presented in Table 3.3.

Table 3. 3: Fractionated solubility parameters and fractional corresponding cohesion parameters (Hansen 2013)

Solvents	δ ($MPa^{1/2}$)	δ_d	δ_p	δ_h	$100F_d$	100Fp	100Fh
DMF	24.83	17.42	13.70	11.25	41.12	32.34	26.54
THF	19.43	16.79	5.66	8.00	55.14	18.60	26.26
CF	18.83	17.69	3.07	5.73	66.80	11.58	21.62
DCM	20.25	18.20	6.30	6.09	59.49	20.59	19.92
Toluene	18.20	18.04	1.43	2.05	83.84	6.65	9.51
PS	18.67	21.27	5.73	4.29	67.97	18.30	13.73

The R_as of the solvents were calculated based on Equation 3.6, and presented in Table 3.4. Dividing the R_a by the interaction radius of polymer gives the relative energy difference (RED) of the system.

$$RED = \frac{R_a}{R_0} \qquad \text{Equation 3.7}$$

If the RED is lower than 1, the polymer can dissolve into the solvents (Hansen 2013). Using Equation 3.7 and knowing R_0 of PS which is equal to 25.92 (j/cm3)-2 (Hansen 2000), RED of the chosen solvents were calculated and presented in Table 3.4. This evaluation technique seems more reliable in comparison with the previous one. Except THF case with RED of 0.36 and viscosity of 297 cp, an increasing trend in RED resulted in a decreasing trend in the viscosities of PS solution. For instance, DMF with the highest RED magnitude has the lowest viscosity.

Table 3. 4: Interaction radius and relative energy difference (RED) of the solvents

Solvents	Ra	RED
DMF	5.72	0.92
THF	4.58	0.36
CF	3.83	0.30
DCM	3.16	0.25
Toluene	3.65	0.29

Besides, a Teas graph based on a ternary solubility diagram helps compare these solvents in a 2D diagram rather than in 3D diagram (in case of RED factor). This issue helps analysis all three solubility parameters more straightforwardly. Moreover, due to the unique and firm location of the solvents and a particular polymer, solubility region of that particular polymer can be defined on the graph in case all variables such as concentration, temperature, etc. are constant (Stefanis and Panayiotou 2008). This type of graph is also studied in other electrospinning researches (Luo, Nangrejo, and Edirisinghe 2010; D. Xu et al. 2007; Ago et al. 2012; Luo, Stride, and Edirisinghe 2012) to compare the solubility and spinability of the electrospinning solvents. However, the suitable solvents based on Teas graph were not always good electrospinning solvents, and it was shown that solvents with lower solubility were better electrospinning solvents (Luo, Nangrejo, and Edirisinghe 2010; Z. Chen, Mo, and Qing 2007; Shenoy et al. 2005a; Fong et al. 1999).

In this graph, fractional cohesion parameters F_d, F_p, and F_h were introduce which are actually derived mathematically from dispersion force component δ_d, δ_p and δ_h based on Equation 3.8 to 3.10 (Stefanis and Panayiotou 2008).

$$F_d = \frac{\delta_{\mathrm{d}}}{\delta_{\mathrm{d}}+\delta_{\mathrm{p}}+\delta_{\mathrm{h}}} \qquad \text{Equation 3.8}$$

$$F_p = \frac{\delta_{\mathrm{p}}}{\delta_{\mathrm{d}}+\delta_{\mathrm{p}}+\delta_{\mathrm{h}}} \qquad \text{Equation 3.9}$$

$$F_d = \frac{\delta_{\mathrm{h}}}{\delta_{\mathrm{h}}+\delta_{\mathrm{p}}+\delta_{\mathrm{h}}} \qquad \text{Equation 3.10}$$

These information were also presented in Table 3.3, and their location were compared with PS in Figure 3.2. Here, it is attempted to pick solvent from different solubility region of PS (DMF and Toluene with partial solubility, and CF, DCM, and THF with complete solubility) in order to elucidate the correlation of the electospinnability of the PS solutions based on the solubility parameters of the solvents.

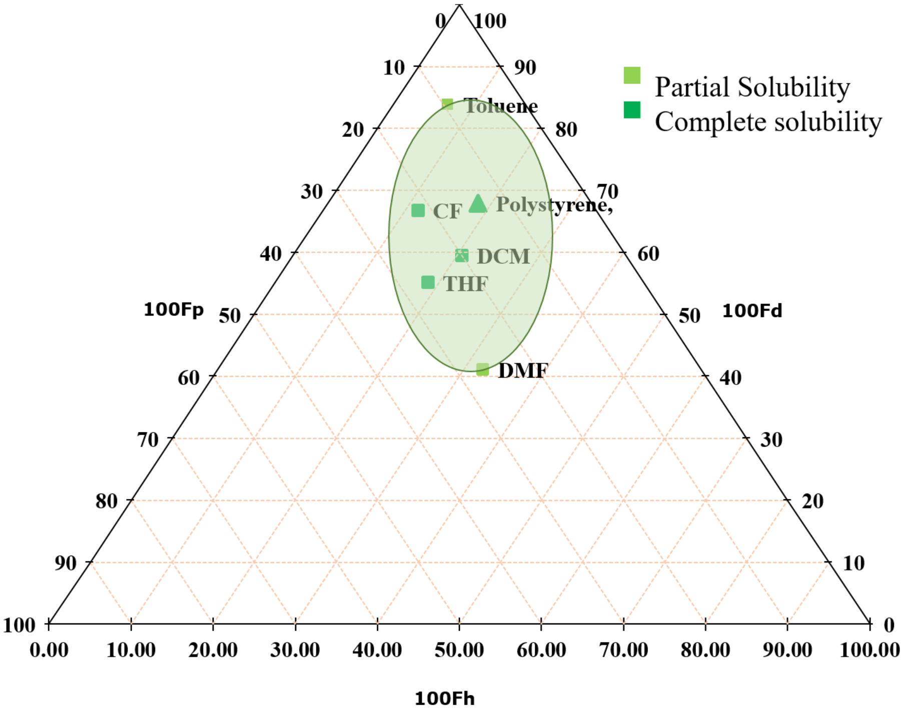

Figure 3. 2: Solubility of PS based on the ternary fractional parameters solubility diagram (The Oval-shape area is an assumption of PS solubility area)

3.3.1.2.Viscoelasticity of polymer solution

As described previously, according to the polymer/solvent interaction, a viscoelastic behaviour can be expected of a polymer solution. Several viscoelastic models were proposed to model the viscoelastic behaviour of polymer solutions. A viscoelastic material can exhibit combined elastic and viscose response by means of two types of elements: the dashpot element describing the viscose behaviour, and the spring element describing the elastic behaviour. Viscoelastic models can be developed using different combinations of these elements. The common schematic viscoelastic models are shown in Figure 3.3. Models are classified according to solid-like or fluid-like behavior of the fluids. The most famous models are parallel (Kelvin-Voigt solid) and series (Maxwell fluid) models. . However, complex viscoelastic models are composed of several dashpots and spring elements based on these two models.

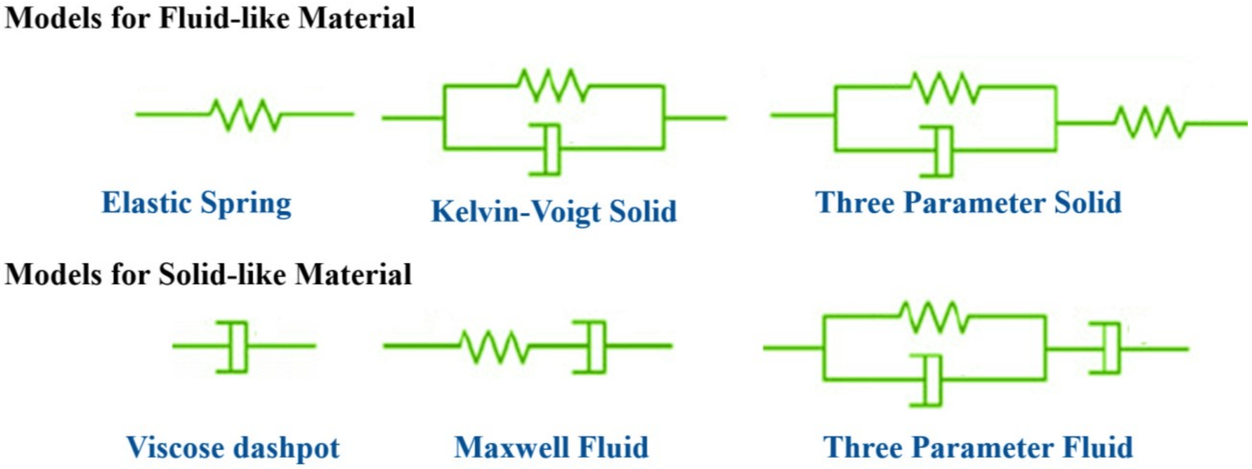

Figure 3. 3: Common viscoelastic models for viscoelastic substances (Adopted from (Mohammadi et al. 2010))

It should be highlighted that the Maxwell fluid model can sufficiently describe the rheological behavior of the concentrated polymeric systems in strong uniaxial elongation, which is the case in the electrospinning (Darrell H. Reneker et al. 2000). Equation 3.11 presents the viscoelastic forces change driven based on Maxwell model.

$$= G\frac{dl}{ldt} - \frac{G}{\eta}\sigma_v \qquad \text{Equation 3.11}$$

Where t is time, G and η are the elastic modulus and viscosity, respectively, and l is the filament length. By integration of Equation 3.11, stress relaxation can be driven, Equation 3.12.

$$\sigma(t) = \sigma_0 e^{(-\frac{t}{\lambda})} \qquad \text{Equation 3.12}$$

Where λ is the stress relaxation constant that can be calculated by Equation 3.13.

$$ʎ = \frac{\eta}{G} \qquad \text{Equation3.13}$$

Considering Equation 3.13, both shear and elongtional viscosities should be considered in electrospinning. Therefore, it is needed to discuss the acceptable range of viscosity for electrospinning.

As discussed in last section, the viscosity amount of a polymer solution can be related on the polymer molecular weight, polymer/solvent interaction, and temperature. Both higher molecular weight and polymer/solvent interaction can induce higher reduce of gyration of a polymer in solvent, resulting in the higher viscosity. Mark-Howinks equation can describe how higher molecular weight can increase the intrinsic viscosity.

$$[\eta] = K_m M^{a_m} \qquad \text{Equation 3.14}$$

Where $[\eta]$ and M are intrinsic viscosity and molecular weight of polymer. The K_m and a_m are the values of the Mark–Houwink parameters.

Constant a_m is a good representative factor of gyration radius. For solvents, a value of a=0.5 is an indicative of a theta solvent. A value of a=0.8 is typical for good solvents. For most flexible polymers, constant a_m between 0.5 and 0.8 distinguishes polymer solubility in solvent. These two Mark–Houwink parameters were presented for various solvents/PS systems in Table 3-4, and intrinsic viscosities were calculated based on them.

By means of $[\eta]$, the critical chain overlap concentration (C *) can be calculated using the Equation 3.15 (Krause, Bellomo, and Colby 2001).

$(C^* \sim 1/ [\eta])$ Equation 3.15

This concentration is an important factor determining a good electrospinning concentration for each polymer-solvent system. Gupta and his co-workers found three different solution regimes for poly methylmetacrylate in DMF, dilute ($c/c^*<1$), semidilute unentangled ($1<c/c^*<3$) and semidilute entangled ($c/c^*>3$). The crossover between semidilute unentangled and semidilute entangled regimes in their research occurred at $c/c^* \sim 3$ (Gupta et al. 2005). Therefore, it was defined as the onset of the critical chain entanglement concentration, (Ce) according to the procedure applied by Colby and co-workers (Colby et al. 1994). This critical chain entanglement concentration can be marked as the onset of electrospinning concentration. For instance, Gupta obtained smooth PMMA fiber at $c/c^* \sim 6\text{-}10$ for various molecular weight (see Figure 3.4). The higher molecular weight, the lower of this proportion was needed to obtain a good electrospinning (Gupta et al. 2005). Considering low molecular weight of PMMA used in this research (12470-

205800 g/mol), we expect lower magnitude of c/c* needed for a proper electrospinning of PS (Mw = 280000 g/mol). According to the Table 3.4, the amounts C/C* for 20% (w/v) PS in all solvent were larger than 10. Therefore, concentration of 20% (w/v) PS is sufficient for all solvents. Therefore, this concentration was considered for the electrospinning of PS in these solvents. However, the presence of entanglements is a sufficient but not a necessary condition for the polymer fluid to demonstrate strong elastic properties. The elastic response can also be achieved at lower polymer concentration if the relaxation time of the fluid is longer than the time of extensional deformation. This kind of elastic behavior is typical of Boger fluids that show high elasticity at concentrations well below c*(Boger and Nguyen 1978; Dontula, Macosko, and Scriven 1998).

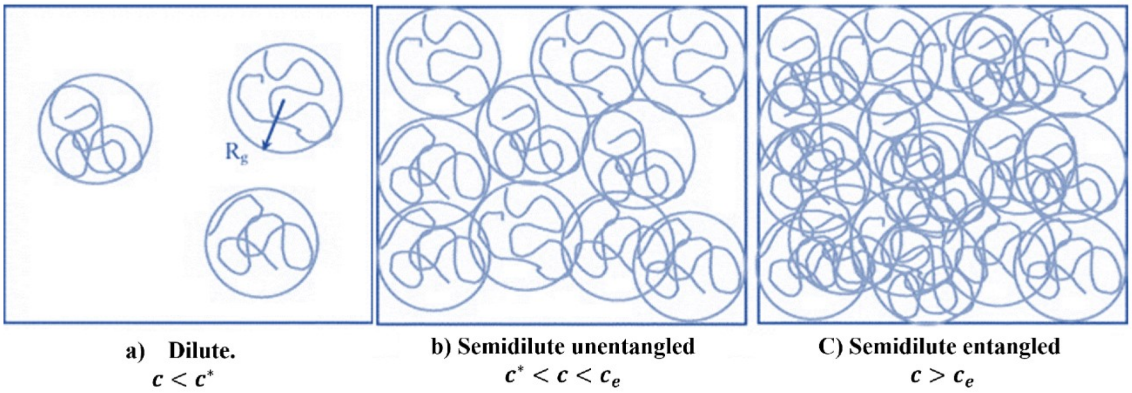

Figure 3. 4: Schematic pictures of the three polymer solution regimes, (a) dilute, (b) semidilute unentangled and (c) semidilute entangled (Adopted from (Gupta et al. 2005))

Table 3. 5: The values of the Mark–Houwink parameters for PS in different solvents (Spychal, Lath, and Berek 1979; Wagner 1985)

Solvent	K_m (cm3/g)	a_m	Calculated [η] (cm3/g)	C* (g/cm3%)	C/C* 20% (w/v)
THF	0.014	0.7	91.020	0.011	18.204
DMF	0.024	0.63	64.852	0.015	12.970
Toluene	0.011	0.725	97.855	0.010	19.571
DCM	0.021	0.68	106.240	0.009	21.248
Chloroform	0.0049	0.79	98.503	0.010	19.701

The other main factor is how the polymer/solvent interaction can influence the viscoelastic behaviour of the electrospinning jet. As described before, usually, stronger interaction between solvent and polymer results in a better solubility, extended chains, and consequently more viscose polymer solution. Though, it does not support the polymer-polymer self-interaction necessarily (Hiemenz 1984). Additionally, polymer-solvent interaction coupled with flow conditions make viscoelastic behavior of the electrospinning jet stream more complex than explainable with just the amount of viscosity.

In the case of PS, not only electrospinning but also solution rheology was widely studied. However, previous literature abundantly suggested that a solvent may dissolve a polymer of interest well, but whether the resulted solution could be fabricated into fibres by electrospinning cannot be guaranteed (Wannatong, Sirivat, and Supaphol 2004; C. Wang, Hsu, and Lin 2006; Uyar and Besenbacher 2008; Eda and Shivkumar 2007). Since the extensional component of the velocity gradient dominates the shear component in the elongational flow in the electrospinning jets, they must be very effective in stretching the polymer chains. Polymer chains coil up in theta or poor solvents due to the entropy contribution to the free energy. A strong elongational flow due to electromechanical stress (EMS) is able to stretch polymer chains resulting in coil–stretch transition (Gennes 2017). In this case, viscous forces exerted by the flow due to EMS overbear the entropic elasticity of polymer chains. The strength of the flow in electrospinning is characterized by the elongational strain rate. The response of the molecular chains to the flow field depends on the viscosity, concentration, and elasticity relaxation time, which characterizes entropic elasticity of macromolecular chains. The product of the strain rate and the relaxation time determines whether stretching or relaxation will dominate in the elongation process (Gennes 2017). If the flow is weak and molecular chains are able to return to their original conformation in a short time, the product of strain rate and relaxation time will be small and relaxation dominates. Thus, the coiled conformations prevail. If the flow is strong and polymer chains need a long time to come back to their original conformation, the product of strain rate and relaxation time will be large. Molecular chains have no time to rearrange in the flow field. Deformation is stored and added up. In this case, a coil-stretch transition occurs and the coil quickly reaches a stretched state. Consequently, a solution with enough large relaxation time can produce smooth fibers. Viscoelastic forces help the jet overcome the Rayleigh instability (Yu, Fridrikh, and Rutledge 2006), and an enough long stress relaxations help polymer chains keep their coil–stretch conformations. To evaluate the relaxation time, the variation of both shear and elongtional viscosities should be considered in electrospinning. (Equation 3.12 and Equation 3.13) The higher viscosity or the lower compliance, the slower stress relaxation resulting in the higher viscoelastic forces.

As a result of solvent evaporation and solidification, both shear and elongational viscosities will increase tremendously during electrospinning (Yarin, Koombhongse, and Reneker 2002). However, their increasing rates are not necessary similar. Moreover, factors such as dielectric constant or boiling points can have retardant effects in increasing rates of these two viscosities. Specifically elongation viscosity probably increases in a slower rate due to the stronger normal forces in electrospinning. For instance, the elongational viscosity of DMF with the higher boiling point, and dielectric constant can increase in a slower manner compared to THF with the lower boiling point and dielectric constant. Moreover, as shear viscosity results shows in Figure 3. 5, the shear viscosity of PS solution in DMF is more shear thinning than the viscosity of PS solution in THF. These results can apply to the elongational viscosity of PS solution in DMF as well. Consequently, evaluation of polymer solutions based on just their viscosity in electrospinning is not possible.

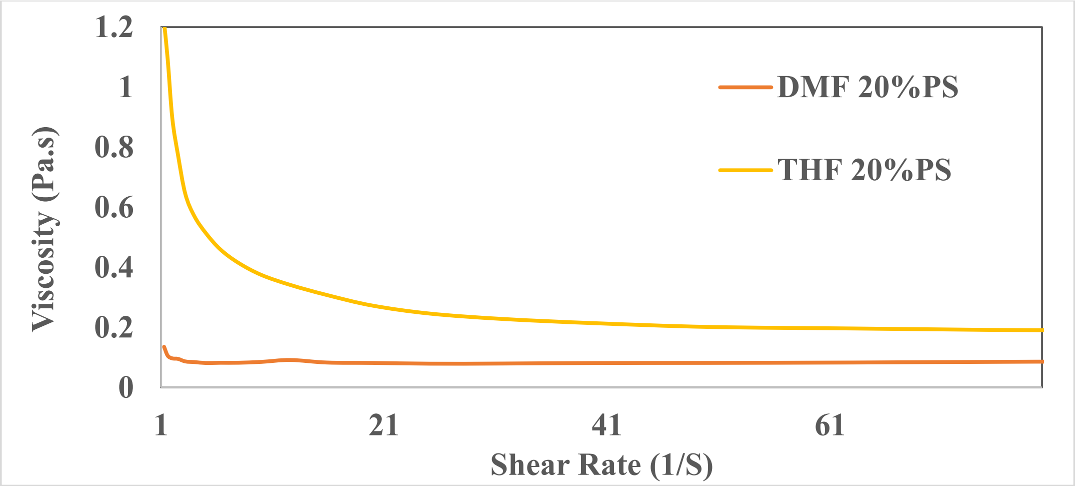

Figure 3. 5: Viscosity changes of PS solutions in DMF and THF by shear rate

3.3.1.3. Surface tension

Surface tension forces is one of the forces influencing negatively on electrospinning process. Surface tension has the decreasing effect on the surface area per unit mass of a fluid. In electrospinning case, when there is a high concentration of free solvent molecules (low polymer/solvent interaction), there is a greater tendency for the solvent molecules to collect and form a spherical shape due to surface tension. This deformation of the electrospinning jet is a kind of Rayleigh instability. Moreover, while the electrical charge repulsion and fluid elasticity drives non-axisymmetric instability, Rayleigh instability cause instability in axial direction and try to break the jet stream into droplets due to capillary action of surface tension. Therefore, morphology of electrospun polymer ranges from droplets (in the case of electrospraying) to bead on strings and smooth fibers. For a uniform fibre diameter, the Rayleigh instability must be suppressed by the viscous forces within the jet. Therefore, the higher surface tensions force is attributed with the higher Rayleigh instability resulting in jet breakage and bead formation in electrospinning. Solution with higher surface tension has a lower tendency to be electrospun (Hohman et al. 2001a). Surface tension force can be defined by

$$F_s \sim \gamma . d \qquad \text{Equation 3. 1}$$

Where Fs, γ and d are force applied on the electrospinning solution, surface tension of the solution and length where the force acts respectively (Bush 2004). According to this Equation, increasing both surface tension and length of the jet can result in the higher surface tension force in electrospinning. Table 3.1 and 3.3 show the surface tensions of the selected PS solvents and 20% (w/v) PS solutions respectively. As Table 3.1 shows, the surface tension of DMF is noticeably larger than the other solvents with almost the same amounts of surface tension which can be attributed to the more polar chemical structure of this solvent (with the highest Dipole magnitude of 3.8). However, 20% (w/v) PS solutions list has a wider range of the surface tensions which interestingly dropped or increased according to the higher or lower polymer/solvent interaction respectively, which determines the amount of free solvent volume in the polymer solution. This issue can be useful to evaluate this prominent factor on the final electrospun structures.

3.3.1.4. Conductivities and dielectric constants effect

Conductivity and dielectric constant of the solutions are two key factors of electrospinning solutions and highly depend on the solvent chemical structures (Z. Sun et al. 2012). The comprehensive effect of conductivity and dielectric constant are the other main objectives of this project.

A material's ability to conduct an electric current can be measured by electrical conductivity (κ (kappa) with the SI unit of siemens per metre (S/m) or CGSE unit of reciprocal second (s−1)). On the other hand, the dielectric constant also known as relative permittivity of a material is expressed as a ratio relative to the permittivity of vacuum. This property of materials affects the Coulomb force between two point charges in the material. Considering a material as a dielectric of a capacitor, dielectric constant is the ratio of the capacitance of a capacitor of that material to a similar capacitor with vacuum as its dielectric (Brown 1953).

It is usually assumed that conductivity of solution can be an influential factor in electrospinning, and higher conductivity can bring about higher excess charge. However, the electrical charge in a polymeric jet are the excess charges, which are not canceled out by the nearby counter ions at long distance under the electrical fields of electrospinning. In a charged fluid, the positive and negative ions incline to move in the opposite electrodes. The excess charge is simply the difference between the number of the positive and negative ions in a certain length of jet. Higher conductivity of solvent can increase the number of ions per unit of volume and shorten the time required for the excess charge to move through the jet. However, it cannot increase the amount of the excess charge (Darrell H. Reneker et al. 2000). Consequently, the conductivity of the solvent may not have a sufficient influence on the formation of smooth fibers.

Unlike conductivity, dielectric constant value can be a good representation of the jet functionality under an electrical field. Solvents with higher dielectric constant are able to store higher electrical energy in an electric field, and this may facilitate the formation of a continuous jet from the Taylor cone to the collector. In other words, the electromechanical stress (EMS) is stronger in a solvent with higher dielectric constant. Therefore, these forces can prevail the coiled conformation of polymer chains, and elongate them toward the fiber axis. Higher elongation of polymer chains can decrease the rate of bead formation. As presented in Table 3.1, the amount of dielectric constant of solvents increases by their dipole magnitudes. Therefore, there is a direct correlation between polarity of the solvent, and dielectric constant. However, PS as a polymer with low polarity is not mostly interested to dissolve in a very polar solvent, like DMF and, PS dissolves partially in it.

3.3.2. Resultant electrospun fibers

Electrospinning of 20% w/v PS solution in various solvents was performed under the same working parameter conditions. Figure 3.6 shows electrospun PS fibers obtained from different solvents. As it is shown in Figure 3.6, DMF resulted in the most suitable fibers with smooth and narrow structures; while, the PS solutions in the other solvents turned out to either droplets structure (in the case of toluene), or to bead on strings structure (in the case of DCM, CF, and THF). Fibers obtained from DCM has the largest structure. In the case of the beaded structures, CF and toluene resulted in almost round shape beads, but THF and DCM samples have drawn shape beads.

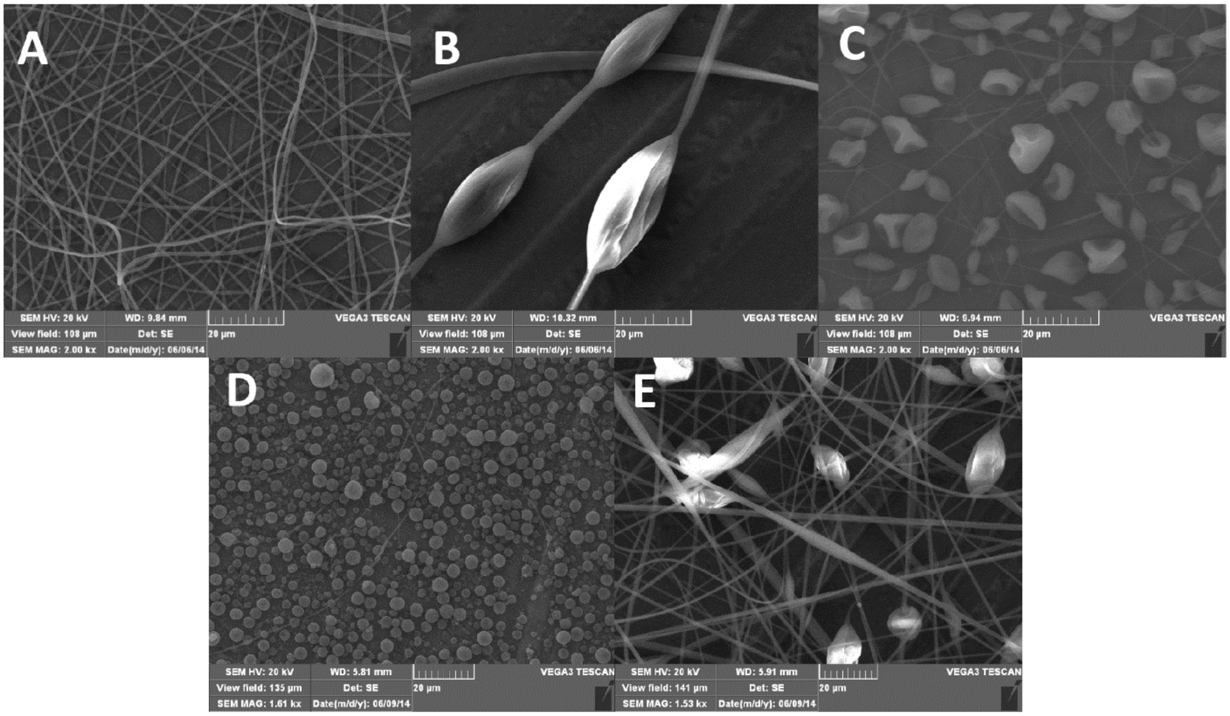

Figure 3. 6: Electrospun PS fibers obtained from different solvents: A) DMF, B) DCM, C) THF, D) Toluene, and E) CF

Among the chosen solvents, DMF has the lowest Polymer/solvent interaction and viscosity, and the other solvents are better thermodynamic solvents of PS. Despite the lowest interaction of DMF among the chosen solvents, the most suitable fibers were electrospun of the DMF solution. This contradictory result can be explained by the evaluation of viscoelastic behaviour changes during electrospinning. In spite of the low viscosity of PS solution in DMF, the compliance or elongational viscosity of this solution could increase in a slower manner compared with the shear viscosity during electrospinning due to the high dielectric constant, and high boiling point of DMF solution. Consequently, considering Equation 3.13, this viscoelastic behaviour can increase the stress relaxation time which can help coil-stretch conformation prevails, and smooth fibers form. Thinner PS fiber can be attributed to the supposition that solutions with higher boiling points have more time to elongate in electrospinning (H. et al. 2006); while, other researches did not report a significant difference as a result of boiling point variations(Luo, Nangrejo, and Edirisinghe 2010).

However, in case of the other solvents with higher polymer/solvent interactions (DCM, THF, and CF), the bead on string structures were observed. This can be explained by either high surface tension, or low relaxation time. Probably the amount of the elongational viscosity did increased as rapidly as the shear viscosity due to the fast solidification and low dielectric constant. Consequently, the relaxation times of these solution were not enough large to fix the elongated configuration of polymers chains.

Moreover, larger viscosity can spark larger structures. For instance, the highest viscosity of DCM (398 cp) resulted in the largest structures. In case of surface tension, these three solutions has a lower magnitudes which can be attributed to their high solvent/polymer interaction, so this beads on strings can be hardly related to their surface tensions. The same structures were obtained for THF/PS solutions (Eda and Shivkumar 2007; Wannatong, Sirivat, and Supaphol 2004; Huan, Liu, et al. 2015).

On the other hand, DMF and toluene solutions have the highest magnitudes of the surface tensions in both solvent and solution cases. In the toluene solution, electrospraying has almost occurred due to the high surface tension and low viscosity of toluene solution. The high surface tension of toluene solution increases the Rayleigh instability during the electrospinning, and low viscose jet can easily break before perturbation of the jet. This issue results in the electrospraying of the PS solution rather than electrospinning, and collecting of beads rather than fibers. The same results were also reported on the electrospinning of toluene-PS solution, and surface tension was also found the main problem of this solvent (Jarusuwannapoom et al. 2005). Besides toluene, DMF also has a large surface tension in both solvents and solution cases. Despite high surface tension of DMF, its viscoelastic behaviour and dielectric constant can compensates the Rayleigh instability forces.

Finally, dielectric constants of these solvents influenced on the electrospun structures. As presented in Table 3.1, the amount of DMF dielectric constant is noticeably higher than the other solvents. Besides proper viscosity of DMF solution, this characteristic can ease and accelerate the electrospinning procedure. Other researchers mostly pointed out both high conductivity and dielectric constant of DMF for its best functionality in electrospinning (Jarusuwannapoom et al. 2005; Wannatong, Sirivat, and Supaphol 2004; Huan, Liu, et al. 2015). Moreover, Luo and his colleague have obtained beaded or thick poly-caprolactone fibers with solvent with dielectric constant lower than 19 (Luo, Stride, and Edirisinghe 2012). In another research, dielectric constant was found the main reasons for thinner electrospun structures (Luo, Nangrejo, and Edirisinghe 2010).

In case of beaded structures, more drawn structures can be attributed to the solutions with higher dielectric constant (DCM samples with drawn shape beads in comparison with toluene samples with rounded shape beads). In addition, higher surface tensions are attributed to the more spherical bead structures.

Considering all of the factors, although DMF is not the best solvent for the PS in thermodynamic points of view, this solvent can be one of the best option in electrospinning. Consequently, DMF was chosen as the main solvent to evaluate the other factors.

3.3.3. Optimization of the electrospinning parameters

As explained before, each electrospinning setup has its own optimum conditions based on its location, influenced by the humidity, temperature, air drag, and so on. Therefore, it is not possible to choose the best working parameters by just reviewing the other researches. Consequently, after picking the best electrospinning solution, working parameters, flowrate and voltage were finally manipulated to obtain the optimum electrospinning conditions.

3.3.3.1.Voltage adjustment

In order to find the best working parameters, some initial values were considered for voltage, working distance, and feeding rate based on the literature (Jarusuwannapoom et al. 2005). Firstly, the maximum possible working distance of this electrospinning system, 17 cm, was chosen for the best working distance due to the high boiling point of DMF, and the fact that the longer the working distance, the longer the time for DMF evaporation.

Subsequently, to find the optimal voltage, electrospinning of PS solutions was performed under different voltages of 7 kV, 10 kV, 15kV, 20 kV, and 25 kV. The flowrate was the first assumption, and was set to 10 µl/min. As shown in Figure 3.7, fibers obtained from voltages under 20 kV are beaded, because higher electrical field power is needed to form a smooth fiber (Eda and Shivkumar 2007). Therefore, the higher voltage resulted in the smoother and narrower fibers because of the increase of the electrostatic repulsive force on the charged jet (see Figure 3.7) (Yuan et al. 2004). Figure 3.8 shows the change of fiber diameters by applied voltage.

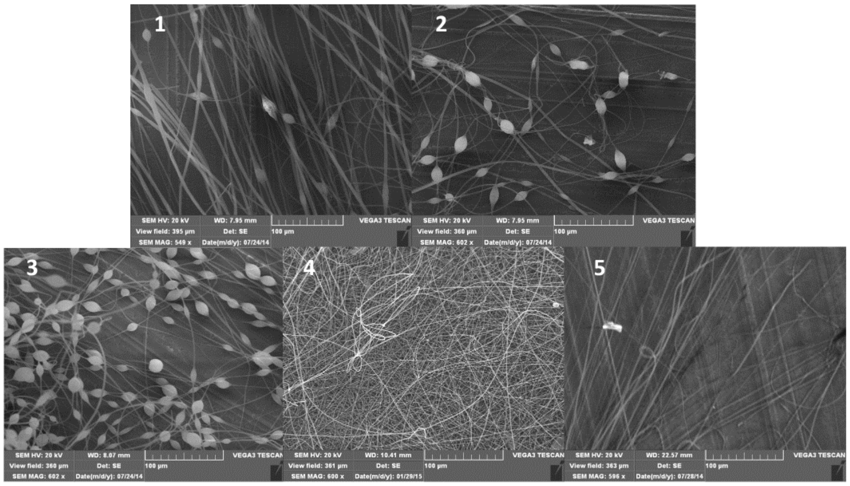

Figure 3. 7: Electrospun fibers obtained at different voltage 1) 7kV 2) 10kV 3) 15kV 4) 20 kV 5) 25 kV

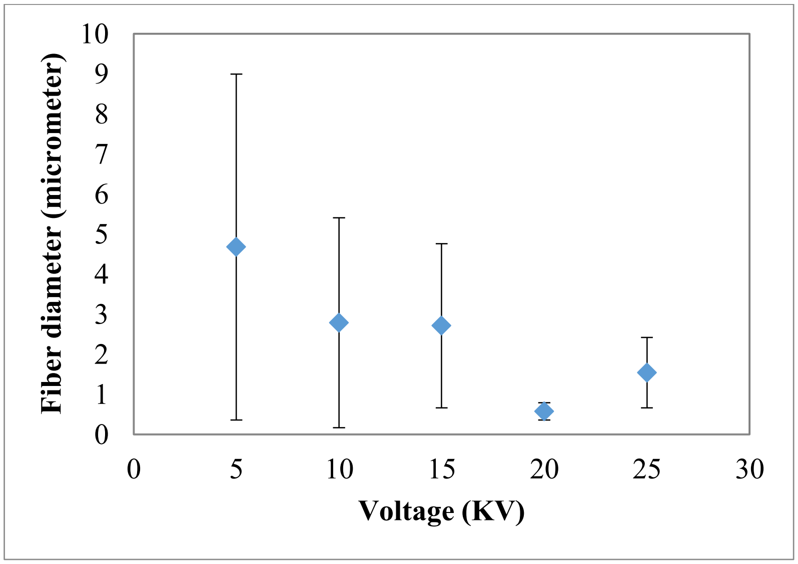

Figure 3. 8: Nano fiber diameter versus voltage on the flowrate of 10 microliter per minute

Wang and his collogue found that either increasing voltage or working distance produced a slightly thinner jet and smaller fiber, but the effects were not significant due to the limited processing range available for the stable initial Taylor cone, the cone observed in electrospinning before the formation of the jet (C. Wang, Hsu, and Lin 2006). Here, also no huge difference on the fiber diameters can be seen by the voltage change. However, voltages higher than the optimal amount resulted in thicker fibers and low productivity of the process. This issue can be explained by the fact that the electrostatic repulsive forces were higher than the amount that the solution jet can tolerate, therefore a particularly high voltage can result in breakage of the jet before reaching the collector.

3.3.3.2 Flowrate adjustment

Finding the best electrospinning voltage to be 20 kV, flowrate was manipulated to check the best possible flowrate for electrospinning. As shown in Figure 3.9, at very low (5 microliter per minute) and very high (20 microliter per minute) flowrates, the productivity of the process is very low. This result can be related to the different sizes of the Taylor cones. Therefore, 20 kV can disrupt the cone before jet formation, in case of small size and low flowrates. Alternatively, this amount of voltage is not high enough to overcome the large Taylor cone and form a jet in case of high flow rates. Consequently, flowrates of 10 and 15 microliters resulted in smooth and uniform fibers.

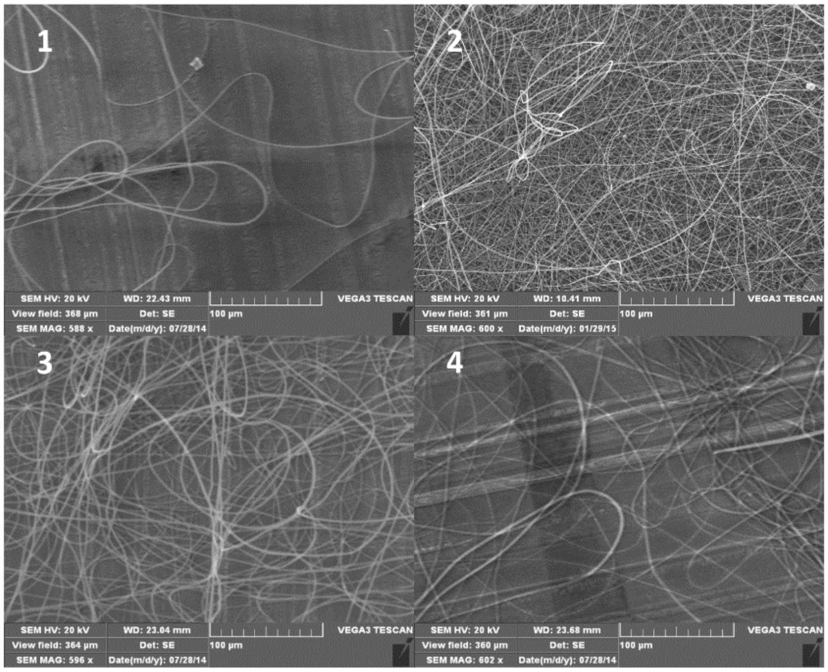

Figure 3. 9: Electrospun PS fibers obtained at different flowrates 1) 5μL/min 2) 10μL/min 3) 15μL/min 4)20μL/min.

In the other points of view, higher flow rates means higher magnitude of term m in Equation 3.1. Therefore, to have equilibrium on this equation, higher forces should be applied. In this specific case that the PS solution characteristic does not change, electrical field and columbic forces can be amplified by application of higher voltage. Totally, flowrates of 10 microliter per minute was found as the best flowrate because of the higher productivity and narrower fibers (see Figure 3.9). In an theoretical effort, Wang and his colleagues also estimated the PS fibers diameter as a function of the processing variables, i.e., solution flow-rate (Q), applied voltage (V) and working distance (H), with a power law model (C. Wang, Hsu, and Lin 2006).

$$d_f = m(\eta_0 k \gamma) d_j \qquad \text{Equation 3.16}$$

Where, η_0, k, γ and d_j are zero shear rate viscosity, conductivity, solvent surface tension, and initial jet diameter respectively, and m is a prefactor related with the solution properties (such as cinductivity, viscosity, and etc.) only. The value of m is lower for the solutions with lower viscosity and/or higher conductivity, and were successfully scaled to be as follows:

$$m \sim \eta_0^{0.38} k^{-0.12} \qquad \text{Equation 3.17}$$

They also found that Q was the dominant factor in determining the fiber diameter and the Q dependences of d_j and d_f were approximately scaled with: dj $\sim Q^{0.5}$ and df $\sim Q^{0.25}$. As Figure 3.10 shows, the experimental results are almost following the scale suggested by Wang.

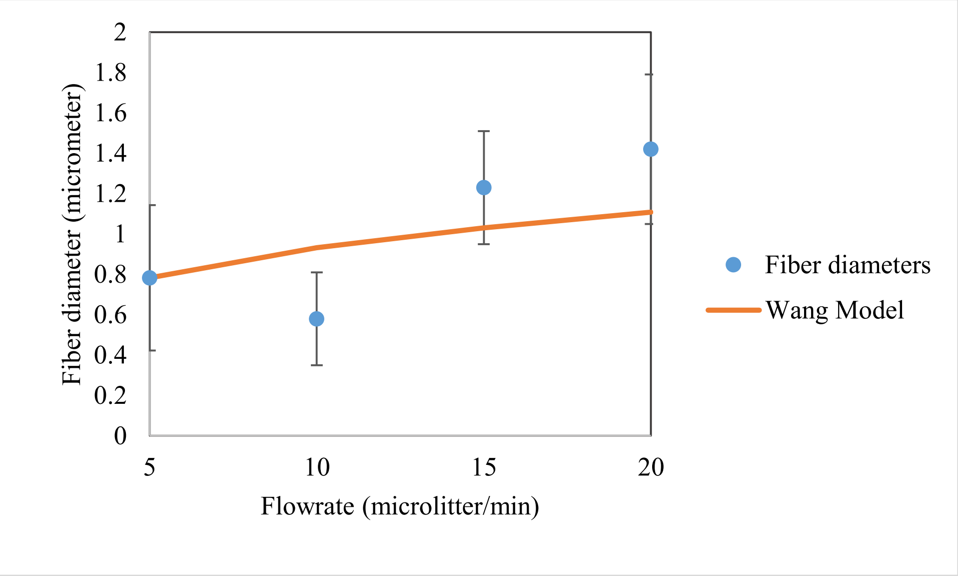

Figure 3. 10: Nano fiber diameter versus flowrate on the voltage of 20 kV.

3.3 Conclusion

Electrospinning of PS were optimized in this chapter. Firstly, PS solutions in various solvent were electrospun to find the best electrospinning solvent of PS. Bead-free and narrower fibers was obtained using DMF; while, the electrospinning of the PS solutions in the other solvents turned out to either droplets structure (in the case of toluene), or bead on strings structure (in cases of DCM, CF, and THF). Consequently, Dimethyl Formaldehyde (DMF) was found the best electrospinning solvent due to the higher conductivity and proper viscosity of the PS solution in this solvent. These results suggested that a thermodynamically good solvent is not necessarily a proper solvent for electrospinning. After PS solvent collection, working parameters were also manipulated to obtain the best electrospinning condition of PS solution in DMF. 10 µl/min of flow rate and 20 KV of voltage were found as optimum working parameters.

Chapter 4

4. Morphology and mechanical properties of the Non-oriented CNC/PS fibers Webs

4.1 Introduction

In Chapter 3, the production of the electrospinning of PS were discussed where optimum electrospinning solution and working parameters were obtained. The main objective of this chapter is mechanical characterization of the electrospun PS fibers and their webs. As described previously, mechanical properties are the most deficient part of PS electrospun fibers. Brittleness and relatively low mechanical characteristics of PS limits its broader use. Previously, modulus and maximum tensile strength of neat PS nanofibrous mats were reported as 1.2 MPa and 0.15 MPa, respectively (Huan, Bai, et al. 2015; Rojas and Habibi 2009). Consequently, incorporation of nano-sized fillers, such as multiwalled carbon nanotubes (Worzakowska 2015), into the PS fibers has attracted great interest.

An alternative to the aforementioned particles is cellulose nanocrystals (CNC). CNC is a wood or plant-based novel nano-material that offers an attractive combination of properties such as biocompatibility, high mechanical stiffness and high strength (Kargarzadeh et al. 2015). These characteristics make it favorable in composites applications (Klemm et al. 2011) to improve mechanical properties of polymeric materials (Habibi, Lucia, and Rojas 2010) For the mechanical improvement purposes, incorporation of 1-15% wt. were reported (H. Dong et al. 2012; C. Sun, Boluk, and Ayranci 2015; Cacciotti et al. 2014; C. Zhou et al. 2013). However, considering percolation of CNC, lower concentration can result in more influential mechanical improvements, and addition further CNC won't have the initial effects (Takayanagi, Uemura, and Minami 1964).

Despite of all suitable characteristics of this nanomaterial, it may not be applicable for all polymer matrices. Due to the existence of surface hydroxyl groups, CNC is basically a hydrophilic material. Therefore, the strong hydrophilicity of CNC is a disadvantage in terms of their reinforcement capacity in hydrophobic matrices such as PS. Moreover, CNCs have a great tendency towards self-aggregation in continuous phase. This stems from their nanoscale dimensions and large surface area (N. Lin and Dufresne 2014). This problem can lead to aggregation or nonhomogeneous dispersion of CNC particles into nonpolar PS continuous matrix. To benefit from its nano-dimension and mechanical properties, a homogeneous dispersion of CNCs in the polymer matrix needs to be obtained (N. Lin and Dufresne 2013).

Adding amphipathic surfactant is an effective method to disperse CNCs homogeneously and to enhance their interfacial compatibility with nonpolar PS (Bercea and Navard 2000). PS and CNCs can be well mixed by adding a proper surfactant. However, the properties of PS/CNC nanocomposite materials may still deteriorate, due to the dynamic phase separation that can be induced by external stimuli during fiber preparation (e.g. temperature and evaporation rate) (Bercea and Navard 2000).

Surface modification or chemical functionalization of CNCs is the other possible route to improve their compatibility in nanocomposites. This technique is especially more suitable for combination with nonpolar or hydrophobic matrices. It helps to obtain better colloidal dispersion by tuning the surface characteristics of CNCs. Abundance of hydroxyl groups on the surface of cellulose makes it possible to do many different chemical modifications based on the type of polymeric matrix (Habibi, Lucia, and Rojas 2010). Considering the above-mentioned problems of surfactant application, modification of CNCs seems a more reasonable method to improve the interfacial interaction between CNC and polymeric matrix.

In this chapter, an investigation into the production of CNC reinforced PS fiber mats is outlined. To that end, several surface modifications of the CNC particles were considered to improve the compatibility of CNC with both PS and the solvent, (Heux, Chauve, and Bonini 2000), dimethyl formaldehyde (DMF). Improvement of the compatibility of CNC and DMF can result in a better CNC dispersion in the electrospinning solution. Furthermore, improvement of CNC and PS compatibility can allow to have stronger interfacial interaction between nanoparticles and polymeric matrix. These two factors help enhance the final mechanical properties of fibers.

For this work, fibers containing unmodified CNCs and modified CNCs were produced to show the effect of CNC modification. Afterwards, to determine the optimal amount of CNC needed for fiber reinforcement, several mats with various percentages were produced and, their tensile properties as well as their dynamic mechanical properties were compared.

4.2. Experimental details

4.2.1. Materials

Rod-shaped cellulose nanocrystal (CNC) particles that were prepared by sulfuric acid hydrolysis of kraft pulp and subsequently neutralized by NaOH in Innotech Alberta's CNC pilot plant were used in this study. The width (w) (or diameter) of rod shaped CNC particles were uniform and measured as 8+2 nm from STEM pictures. The length of CNC particles was calculated as 214 nm, by assuming the shape of CNC particles was cylindrical and measuring the translational diffusion coefficient (Dt) from DLS and particle diameter from STEM pictures (Boluk and Danumah 2014; Oguzlu and Boluk 2017). Sodium hydroxide, 4-Bromoaniline, 4-Nitroaniline, 4-(Trifluoromethyl)aniline, Styrene, Tetrafluoroboric acid solution (48 wt. % in H2O), L-asacorbic acid, Acetonitrile, Diethyl ether, Dichloromethane (DCM), Tetrahydrofuran (THF), Chloroform (CF), Dimethyl formaldehyde (DMF)as solvent, and Polystyrene (PS) (MW = 280,000 g/mole, Tg = 100 °C) as fiber material used in this project were all purchased from Sigma Aldrich, Inc. All materials were used without further purification.

4.2.2. Precursor diazonium salt synthesis

The diazonium salts were synthesized according to a published procedure (Solak et al. 2003). Firstly, an appropriate aniline solution of 4-bromoaniline, 4-nitroanailine, or 4-trifluoromethyl (0.1 M) was prepared and mixed to 50 ml floroboric acid (48 wt. %). Afterward, the solution was cooled in an ice water bath to 0 ºC, and sodium nitrite solution in DI water (50% w/v) was added drop by drop with stirring. The reaction mixture was further cooled in an ice water bath and stirred for another hour. The resultant precipitate was finally filtered in a Buchner funnel and washed with cold anhydrous Diethyl ether. Figure 4.1 shows this chemical reaction, schematically.

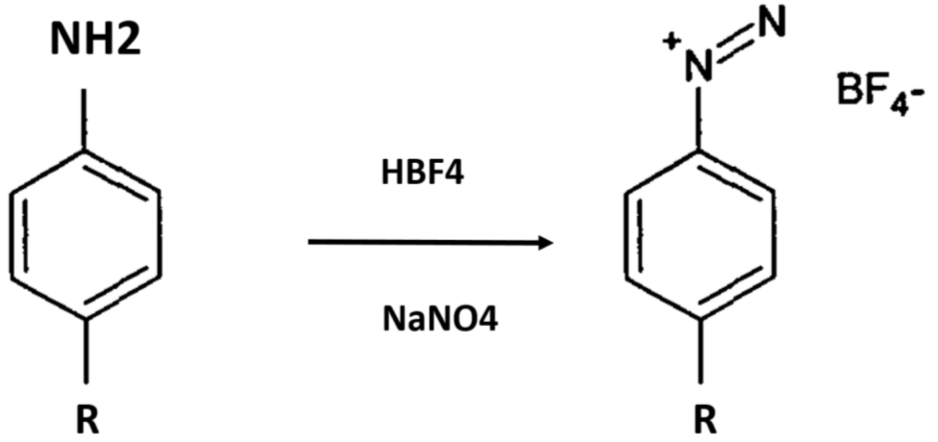

Figure 4. 1: Chemical reaction of the precursor diazonium salt (where R can be bromo (Br), nitro (NO2), or trifluoromethyl (CF3) functional groups)

4.2.3. Synthesis of Nitrobenzene modified CNC (CNC-1) and Trifluoromethyl benzene CNC(CNC-2)

1.0 wt. % CNC suspension was prepared by dispersing CNC in DI water using an ultrasonic treatment in an ultrasonic cleaner (CREST Ultrasonics Corp., model-275T) for 5 min. After that, 0.01 mole of prepared diazonium salts (4-nitrobenzenediazonium tetrafluoroborate or 4-(trifluoromethyl) benzenediazonium tetrafluoroborate) were added and dispersed in 200ml 1.0 wt. % CNC suspension under sonication treatment for 5 min. Then 20 ml of L-ascorbic acid solution (0.05 M) was added to the mixture and kept under sonication for 1 h. The resulting suspension mixtures were then transferred to a centrifugal filter unit (10,000 molecular weight cut-off, Amicon Ultra-4) to collect modified CNC from solution. The modified CNCs were further cleaned by rinsing with acetonitrile and centrifuging three times. Finally, the product was re-dispersed in DI water and freeze-dried using a FreeZone 4.5 Plus apparatus from Labconco Corporation (Kansas

City, Missouri). Figure 4.2 shows the chemical reactions taken place on the CNC-1and CNC-2 productions.

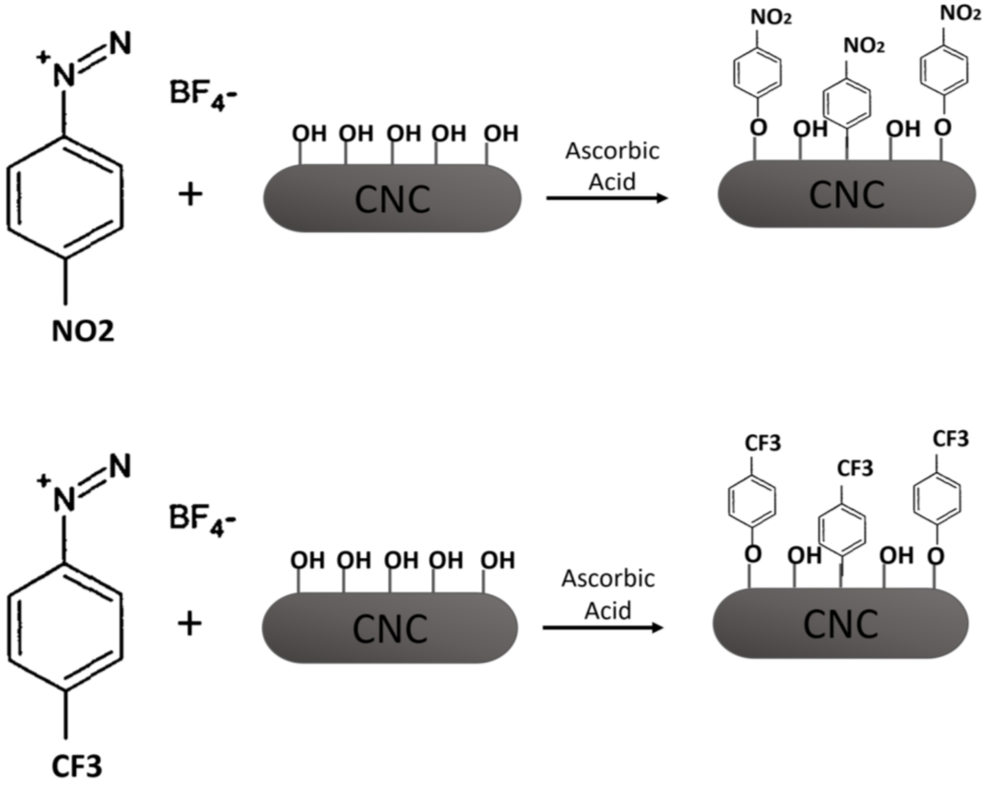

Figure 4. 2: Chemical reactions of the CNC-1 and CNC-2 productions

4.2.4. Synthesis of grafted PS CNC(CNC-g)

To modify the CNC surface with PS grafted chains, atomic transfer radical surface polymerization were used in which the initial radicals are created on the CNC surface first, and the styrene monomer add to them (Morandi, Heath, and Thielemans 2009). The procedures of this polymerization technique was performed as follow:

Firstly. 0.005 mole of 4-bromobenzenediazonium tetrafluoroborate was added and dispersed in 100 ml of 1 wt. % CNC suspension under ultrasonic treatment for 5 min. Afterward, 10 ml of L-ascorbic acid aqueous solution (0.05 M) was added to the mixture, and the resultant mixture was again kept under ultrasonic treatment (or stirring) for another hour. Subsequently, 0.5 g of styrene (NaOH treated) was sonicated in ~150 ml H2O. The generated Styrene/water emulsion was then mixed with the CNC /Diazonium dispersion in a beaker and kept stirring for an extra hour. In between, another 0.005 moles of 4-bromobenzenediazonium tetrafluoroborate and 10 ml of 0.05 M aqueous l-ascorbic acid were added to the mixture. The final mixture kept under stirring overnight. The grafted CNC was then centrifuged with a centrifugal filter unit, rinsed with acetonitrile, and re-dispersed in water. Finally, it was freeze-dried as the procedure described previously in section 4.3. Figure 4.3 shows the chemical reactions of the PS grafting on the CNC surface.

It should be noted all of these chemical reactions were performed following the methodology described by Dr.Rongbing Du (Chemistry Department at University of Alberta) - details of which is not published yet.

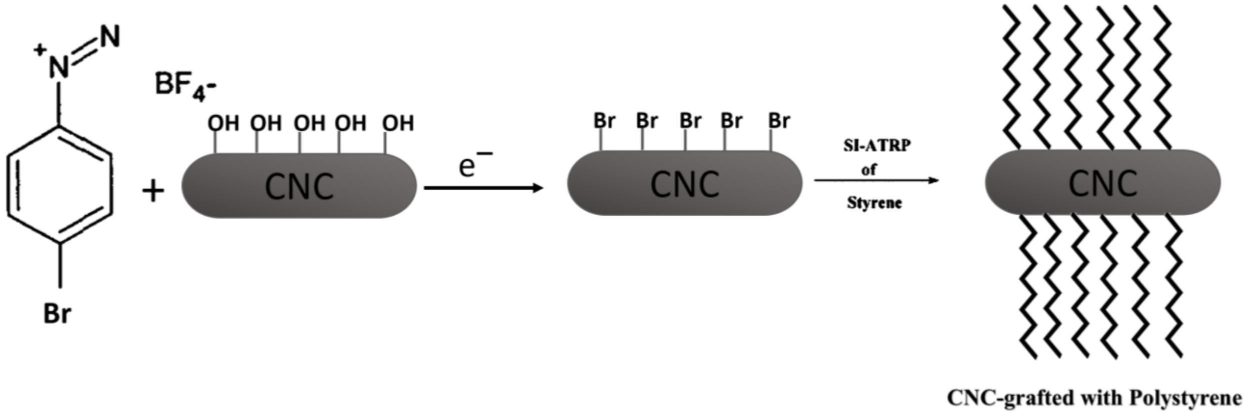

Figure 4. 3: The PS polymerization on the CNC surface

4.2.5. PS fiber preparation

Electrospinning solutions were prepared with 20% (w/v) PS and various concentrations of the three prepared modified CNCs in DMF (Table 4.1).

Electrospinning was performed with a constant flow rate of 10 μL/min, constant voltage of 20KV and with a working distance (nuzzle-to-collector distance) of 17 cm for all the solution systems in this research. Table 4.1 shows the details and characteristics of the polymer solutions applied for electrospinning.

Table 4. 1: Characteristics of electrospinning solutions containing modified or unmodified CNCs (CNC-R) as well as 20% PS in DMF

Sample	Chemical Structure of modified CNC	PS concentration (w/v%)	CNC concentration of PS (w/w %)	CNC concentration in solution (w/v %)	Conductivity (µs/m)	Viscosity (Pa.S)
		20	0	0	67	0.21
CNC-1	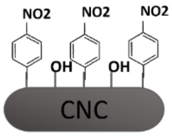	20	0.5	0. 1	283	-
		20	1	0. 2	765	-
		20	1.5	0. 3	1278	-
		20	2	0. 4	1423	0.23
CNC-2	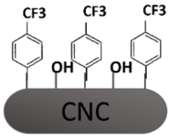	20	0.5	0. 1	560	-
		20	1	0. 2	1412	-
		20	1.5	0. 3	2043	-
		20	2	0. 4	2260	0.23
CNC-g PS-grafted CNC	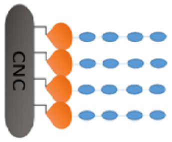	20	0.5	0. 1	276	-
		20	1	0. 2	952	-
		20	1.5	0. 3	1832	-
		20	2	0. 4	2117	0.23
CNC-R Unmodified CNCs	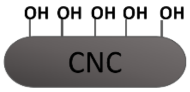	20	0.5	0. 1	87	-
		20	1	0. 2	92	-
		20	1.5	0. 3	98	-
		20	2	0. 4	112.4	0.22

4.2.6. Fourier Transform infra-red spectroscopy (FT-IR)

FT-IR spectra were attained to evaluate the surface modifications of CNCs, and they were attained on a Varian FT-IR spectrophotometer (FTS-7000) by means of KBr pellets of freeze-dried samples of modified and unmodified CNC at room temperature under continuous nitrogen purging. Spectra in the range of 3700–700 cm^{-1} were obtained.

4.2.7. Turbidity analysis

As a guide to the electrospinning polymer solution stability (aggregation and distribution of modified CNC), the turbidity of solution were analyzed based on the measurement of backscattering and transmission using a Turbiscan Lab system (Formulaction Co., France). In this system as Figure 2.1 shows, the suspensions are placed in flat-bottomed cylindrical cells (25 mm diameter, 55 mm height), and a pulse near-infrared light source (A = 850 nm) emits to the suspension sample. Then, two detectors at different positions of the suspension collect the average intensity of transmitted or backscattered lights from 0 mm to 20 mm height of the sample cell. In this study, DMF solutions containing 1% (w/v) of the various modified CNC and 5 % (w/v) of PS were prepared. Both transmission and backscattering were measured immediately after preparation of solutions, and the changes of their intensities were reported during 120 minutes.

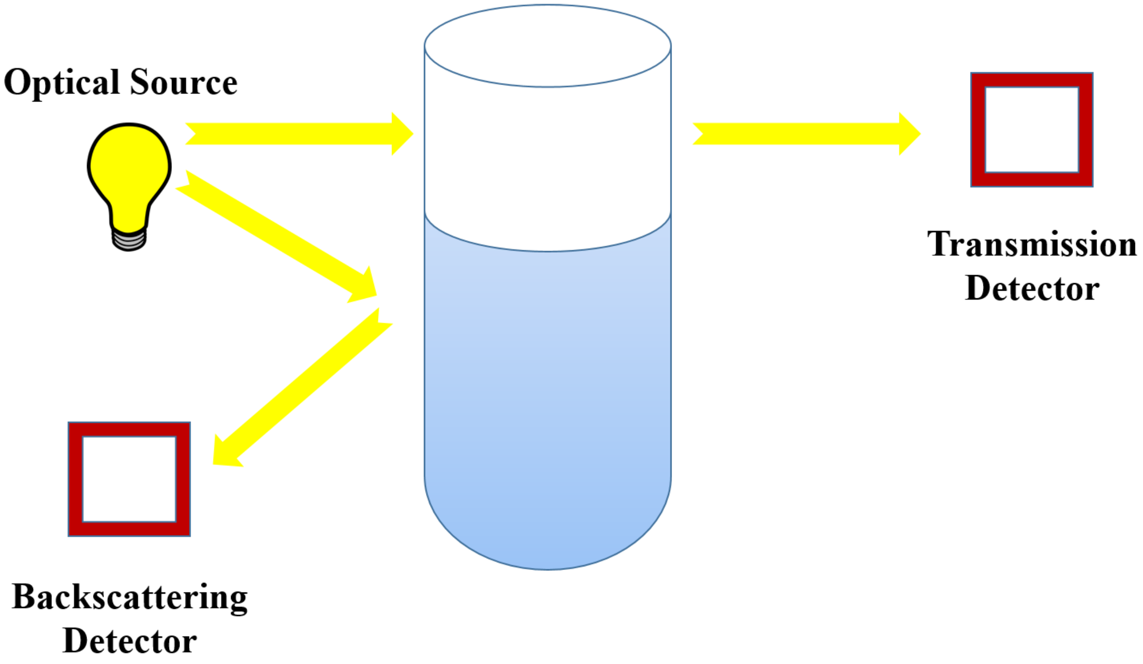

Figure 4. 4: Mechanism of turbidity analysis

4.2.8. Rheological test

The AR-G2 rheometer were used to measure the rheological parameters of polymer solutions. The experiments were conducted in a laboratory at constant temperature.

4.2.9. Solution conductivity measurement

The conductivity of both PS (w/v) 20% solution and CNC/PS solutions were measured by using a conductivity meter (Isteck Model 455C) at 25 °C. The CNC/PS solutions contained 2 wt. % (To PS content) of the modified CNCs.

4.2.10. SEM analysis

Both surface morphology and structures of fibers and their diameters were analyzed using a scanning electron microscope (SEM) (Vega-3 (Tescan) equipped with an EDXS detector (Oxford Instruments) at an acceleration voltage of 20 kV. SEM analyses of samples were performed without coating. To determine the average diameter of each fiber sample, a total of 100 fibers were randomly measured from five different spots for each specimen by means of ImageJ software.

4.2.11. Tensile test

By means of tensile test, deformation of electrospun PS and PS/CNC fiber mats were compared according three mechanical properties, namely: elastic modulus (E), ultimate tensile stress (σ uts), and the strain at UTS (ε uts). Mechanical properties of a porous mesh (which is the case of the electrospun web) are influenced by many factors, such as individual fiber morphology, porosity, and their orientation in mat. Moreover, the bonding between fibers and the slipping of fibers over each other plays important roles in mechanical properties (M. Wang et al. 2004; C. Zhou and Wu 2012). So, it is need to take porosity, and fibrous structure into account by specific stress calculation. Specific stress in N/Tex was calculated by means of the Equation 4.1.

σ (N/Tex) = (F (N)/ D (mm))/(da (g/m2))   (Ko and Wan 2014)   Equation 4.1

Where:

F= Force, D= specimen width, and da= Areal density

The areal density is simply calculated by using the weight (g) of the nonwoven samples divided by their area. The stress in N/Tex was converted to GPa by multiplying it by the density of PS, taken as 1.05 g/cm^3 (Lynwood 2018).

σ (Gpa) = σ(N/Tex)* Density (g/cm3)   (Ko and Wan 2014)   Equation 4.2

The strain was calculated by dividing the displacement by the gauge length (Ko and Wan 2014). In this Project, the tensile properties of the electrospun nanocomposites were measured with a BOSE tensile tester (model Electroforce 3200) with a 250 g load cell at ambient conditions. Tensile properties (Young’s modulus, tensile strength) were determined using samples cut from electrospun mashes (50 mm long and 10 mm wide). The tests were conducted at a constant crosshead speed of 10 mm/min. In order to prevent the grips from direct contact with the mashes, end-tabs were used. At least 10 samples were tested for each condition.

4.2.12. Dynamic mechanical analysis (DMA)

A Dynamic Mechanical Analyzer (DMA 2980 from TA Instruments) was used to evaluate the thermomechanical properties of the neat and CNC reinforced fibers under tension as a function of temperature. The samples were cut into 5-mm wide strips from the fibers mats. All the tests were performed at 20 Hz frequency and with 1% strain. The sample gap distance was adjusted at 20 mm for all samples. The temperature range was room temperature to 150°C with a heating rate of 2°C/min.

4.3. Results and Discussions:

4.3.1. Chemical modification of CNC for higher compatibility with PS

Three modified CNCs, CNC-1, CNC-2, and CNC-g were considered for incorporation in PS fibers. Table 4.1 shows their chemical structure. The successful modifications of the CNC samples were verified by the FT-IR spectroscopy shown in Figure 4.5. Unlike unmodified CNC, the CNC-1 samples display a new FT-IR peaks at about 1350 cm^{-1} and 1516 cm^{-1} due to the stretching of N-O bands belonging to the nitro group. Moreover, peaks at 1590 cm^{-1} proves the existence of C=C bands of benzyl groups. In the case of the CNC-2 spectrum, in addition to the peaks related to the aromatic C=C, a peak at 1320 cm-1 can be observed. This pick is related to the stretching of C-F bands proving the existence of the CF3 group. PS grafted CNC samples shows several new FT-IR peaks at about 760 cm-1, 1490 cm-1 and 3020 cm-1 for aromatic C-H stretch as well as aromatic C=C at 1590 cm-1, which confirm successful PS grafting.

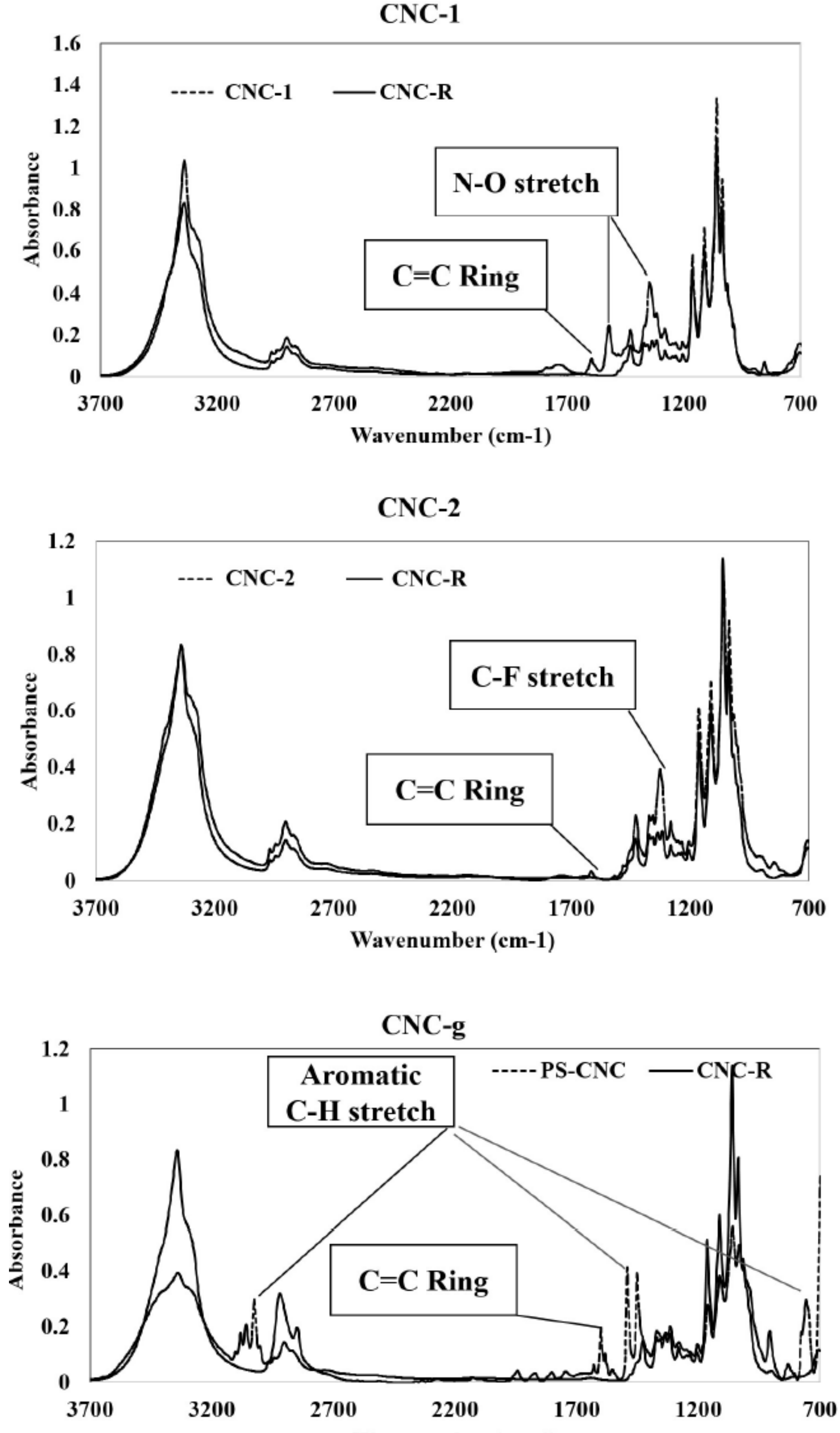

Figure 4. 5: FT_IR spectra of modified CNCs

4.3.2. The effect of the chemical modifications on the suspension properties

4.3.2.1. Evaluation of the chemical modifications based on Visual observation of the modified CNCs suspentions

Since the electrospinning of PS is carried out in DMF solutions in this study, the dispersion of CNC particles in DMF solvent is expected to be crucial for the electrospinning of CNC suspensions in PS/DMF solutions. Therefore, the effect of modification of CNC on the stability of the suspensions in DMF was studied. The sedimentation behavior of 1.0% suspensions of CNC-R (unmodified) along with surface modified CNC-1, CNC-2 and CNC-g in DMF at zero and 120 minutes later allowed to observe visually the dispersion stability of CNC (Figure 4.6). A good dispersion of CNC particles in DMF requires first wetting of dry CNC agglomerates by DMF, then breaking them up to individual CNC particles, finally spreading individual CNC particles throughout DMF medium by mixing. The individual CNC particles formed should be maintained in the dispersed state; otherwise, in cases of accumulation and sedimentation, two phases can form, supernatant at top, and sediment at bottom. These kinds of destabilization phenomena are called clarification (Tadros 1996). In all columns, two phases can be distinguished at 120 min of settling: a supernatant at the top and sediment at the bottom. Their formation characteristics seem to be influenced by the type of CNC modification. In the case of CNC-R, the supernatant is clear and separated from the sediment with a sharp boundary called “clarification front,” not only at 120 min but at 0 min. This issue illustrates the lack of miscibility of unmodified CNC with DMF. In the case of various types of modified CNC, all were mixed with DMF spontaneously which shows their initial miscibility. However, after 120 minutes, two distinguishable phases, a supernatant at the top and sediment at the bottom, were formed in all cases. Note that in the column containing CNC-2 and CNC-g, height of the supernatants are shorter than CNC-1 and CNC-R. This shows the higher compatibility of these two types of modified CNC in comparison with CNC-1 and CNC-R. Furthermore, in the case of CNC-2, the supernatant is hazier than the other columns, suggesting higher compatibility of this modified CNC compared with the other ones. These first observations allowed to highlight the compatibility in DMF depending on the type of CNC modification.

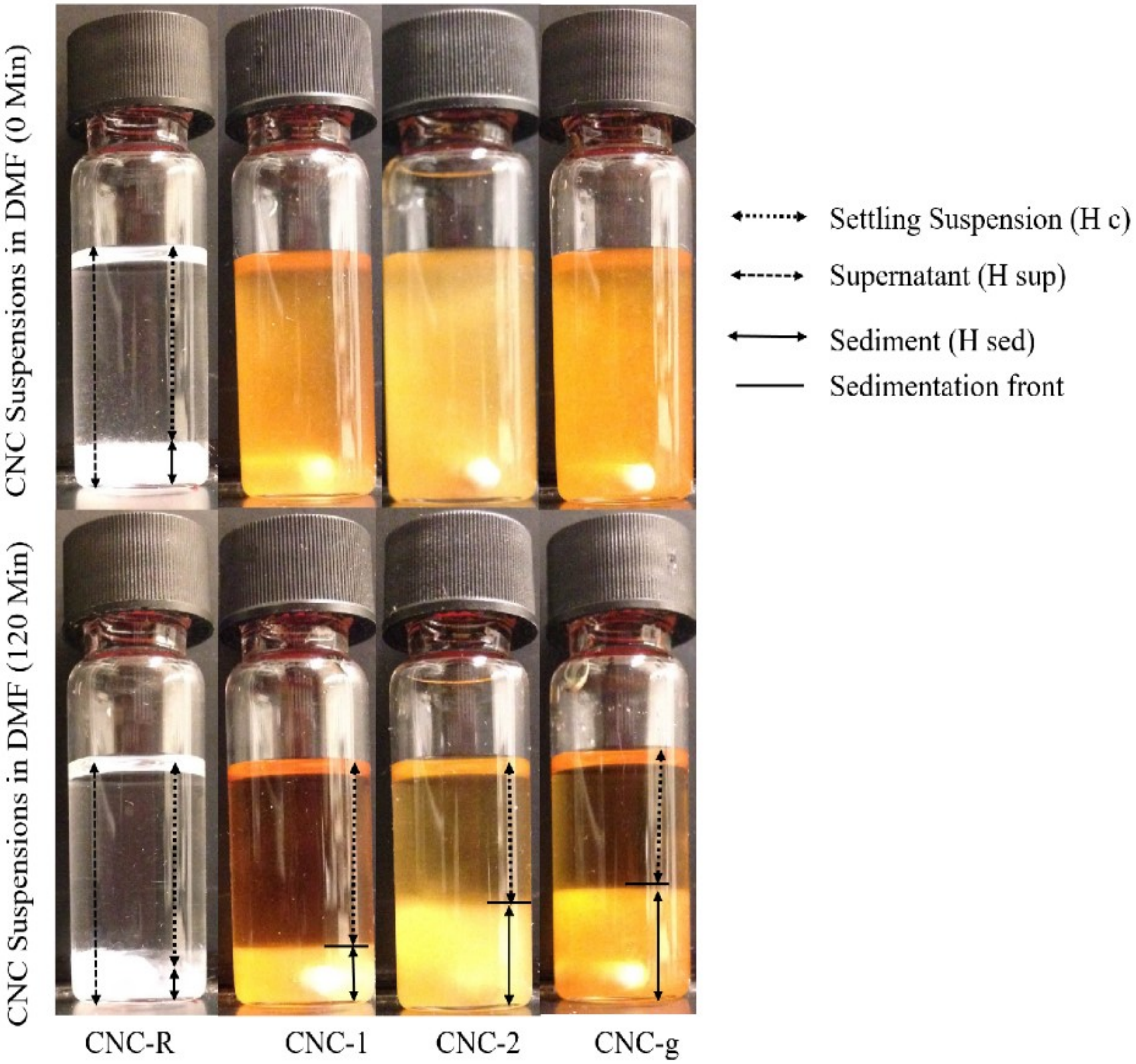

Figure 4. 6: Visual observation of sedimentation suspensions containing various type of CNCs.

The settling velocities and times of CNC samples were influenced by the size of agglomerates. Terminal settling velocity, V_t of particles can be calculated by using Stokes law:

$$V_t = \frac{gd(\rho_p - \rho_m)}{18\mu} \qquad \text{Equation 4.3}$$

where g is acceleration of gravity (981 m/s2), d is agglomerate diameter, ρp is density of CNC particle ρp (1500 kg/m3) ρm is density of DMF (920 kg/m3) and μ is the viscosity of DMF (0.92 mPa.s). Hence it can be seen that an individually dispersed 100 nm CNC particles can travel only 0.22 mm as opposed to a 2 μm size agglomerates which can travel 86.6 mm during the observation time of 120 minutes.

4.3.2.2.Evaluation of the chemical modifications using turbidity measurements of the modified CNCs suspensions

In order to develop a quantitative approach, the stability of the CNC suspensions were examined using a Turbiscan, model MA 2000 (Formulaction, L'Union, France). The Transmission (T) detector receives the light which passes through the sample (at 180 degrees from the incident beam), whereas the Back Scattering (BS) detector detects the light scattered backward from the sample (at 45◦ of the incident beam). The detection section scans the sample through its entire height (0 to 50mm), and obtains T and BS data every minute for 2h. The variation of the reginal particle concentration (migration) or diameter (coalescence), will result in a variation of BS and T signals, so the measurement of these signals is based on this principle (Lemarchand et al. 2003). In this study, variation of transmission signals are presented at two different heights of 10 and 20 mm. Figure 4.7 shows the turbidity results (Transmission) of suspensions containing various types of modified CNC in pure DMF in the absence of PS. As these results illustrate, CNC-

R was settled almost instantenously and resulted very high level of light transmission at both 10 and 20 mm heights. In the case of CNC-1, one can say that sedimentation was much slower and the change of the opacity of the supernatant with time was almost identical both at 10 and 20 mm heights. A thereshold time was observed for the start of clarification process in CNC-2 and CNC-g suspensions. The thereshold time was longer in the case of CNC-2 than CNC-g. As these results showed, CNC-2 was the most compatible sample in DMF followed by CNC-g, CNC-1, and finally non compatible CNC-R. Knowing DMF as an electron pair donating solvent, both CNC-1 and CNC-2 are more likely to be dispersed in DMF due to the existence of strong electron pair acceptor functional groups of –NO2 and –CF3 on them respectively (Reichardt and Welton 2010). In the case of CNC-g, protruding PS chains from the CNC surfaces sterically stabilized it. On the other side, CNC-R with hydroxyl groups and weaker electron withdrawing characteristics made it less favorably dispersed in DMF.

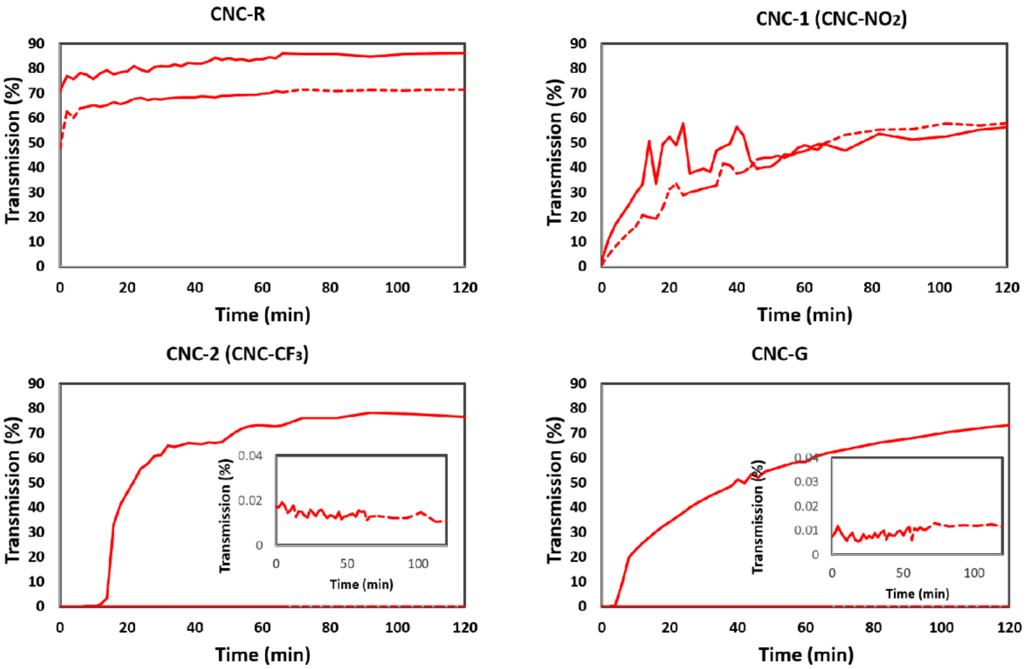

Figure 4. 7: Turbidity results (Transmission) of suspensions of various modified CNCs in DMF (Filled Lines (20 mm) and Dotted Lines (10 mm))

In addition, turbidity of CNC samples in DMF solvent after sonication were monitored during the 120 minutes time frame at 10 mm and 20 mm heights in the turbiscan cell. Since there was a significant difference in dispersion characteristics between stirring and ultrasonic mixing of CNC-R in DMF solvent, it is worth to comment here. Figure 4. 8 shows side by side the dispersion of 1.0% CNC-R in DMF after stirring and sonication. Unlike quick settling after mechanical stirring, sonication resulted in stable dispersion of CNC-R in DMF. The release of water residues (~ 4-5%) from freeze dried CNC-R sample, during the sonication might be the reason for the dispersion stability of the CNC-R suspensions in a polar aprotic solvent DMF (Viet, Beck-Candanedo, and Gray 2007). In contrast to CNC-R, mechanical stirring and sonication did not produce different dispersion results in the cases of CNC-1, CNC-2 and CNC-g. It is believed that, the chemical surface modification procedures eliminated residual moisture on CNC surfaces, hence turbidity data of stirred and sonicated dispersions of CNC-1 and CNC-2 and CNC-g behaved similarly.

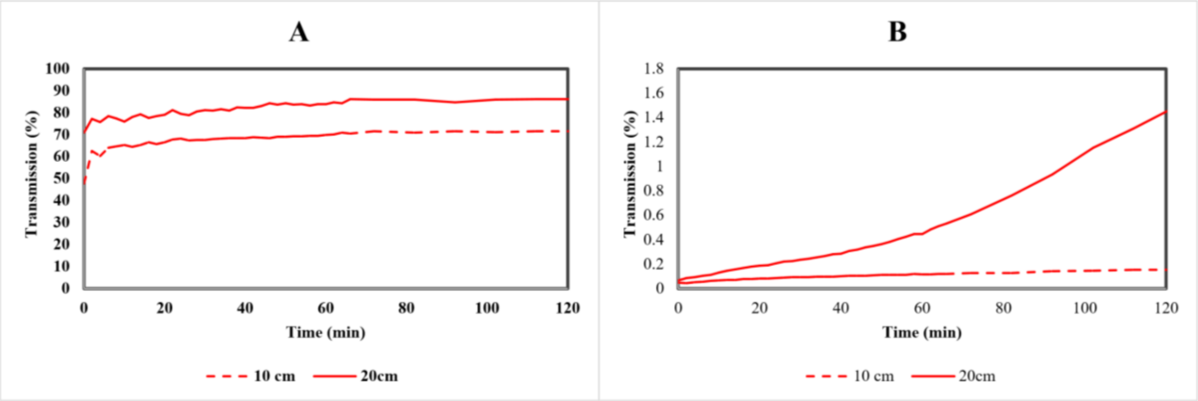

Figure 4. 8: Turbidity results of 1.0% CNC-R suspensions in DMF: A) after stirring B) sonication

Figure 4. 9 shows turbidity results of 1.0% CNC samples in DMF solutions after sonication at 10 mm and 20 mm heights as a function of time. As discussed before, the excellent stability of

CNC-R both in DMF solvent and 5.0% PS DMF solution was due to the presence of residual moisture on CNC-R flakes. In the case of CNC-1 the light transmission through the cell increased continuously from time zero due to the increase in sedimentation with time. The change of the opacity of the supernatant with time was almost identical both at 10 and 20 mm heights. Unlike CNC-1, threshold times were observed for the start of clarification process both in CNC-2 and CNC-g suspensions. The threshold time was longer in the case of CNC-2 than CNC-g, similar to the results before sonication.

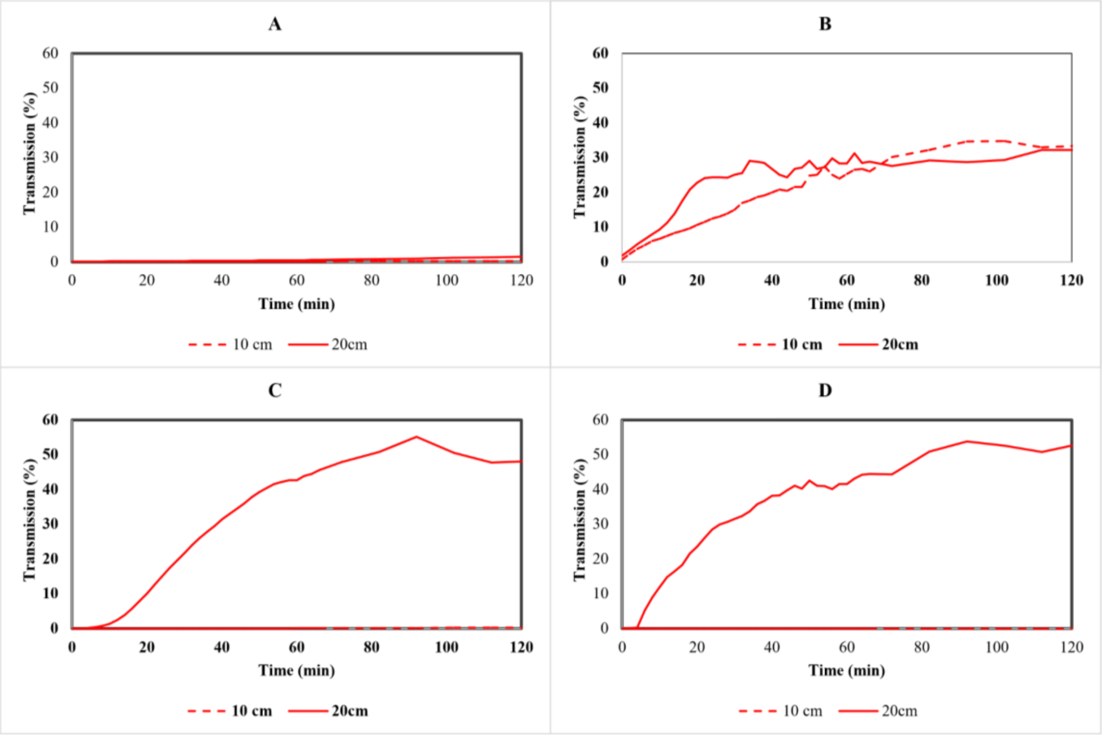

Figure 4. 9: Turbidity results of 1.0% CNC suspensions in DMF after sonication of the samples: A) CNC-R, B) CNC-1, C) CNC-2 D) CNC-g

The lack of sonication influence on the modified CNCs can be explained by to their hydrophobicity. Therefore, water absorption does not increase their miscibility. However, in the case of CNC-1, sonication can improve the suspension behaviour of this sample to some extent, due to the hydrophilicity of the NO2 functional groups. Figure 4. 10 shows the different CNC suspensions in DMF before and after sonication schematically.

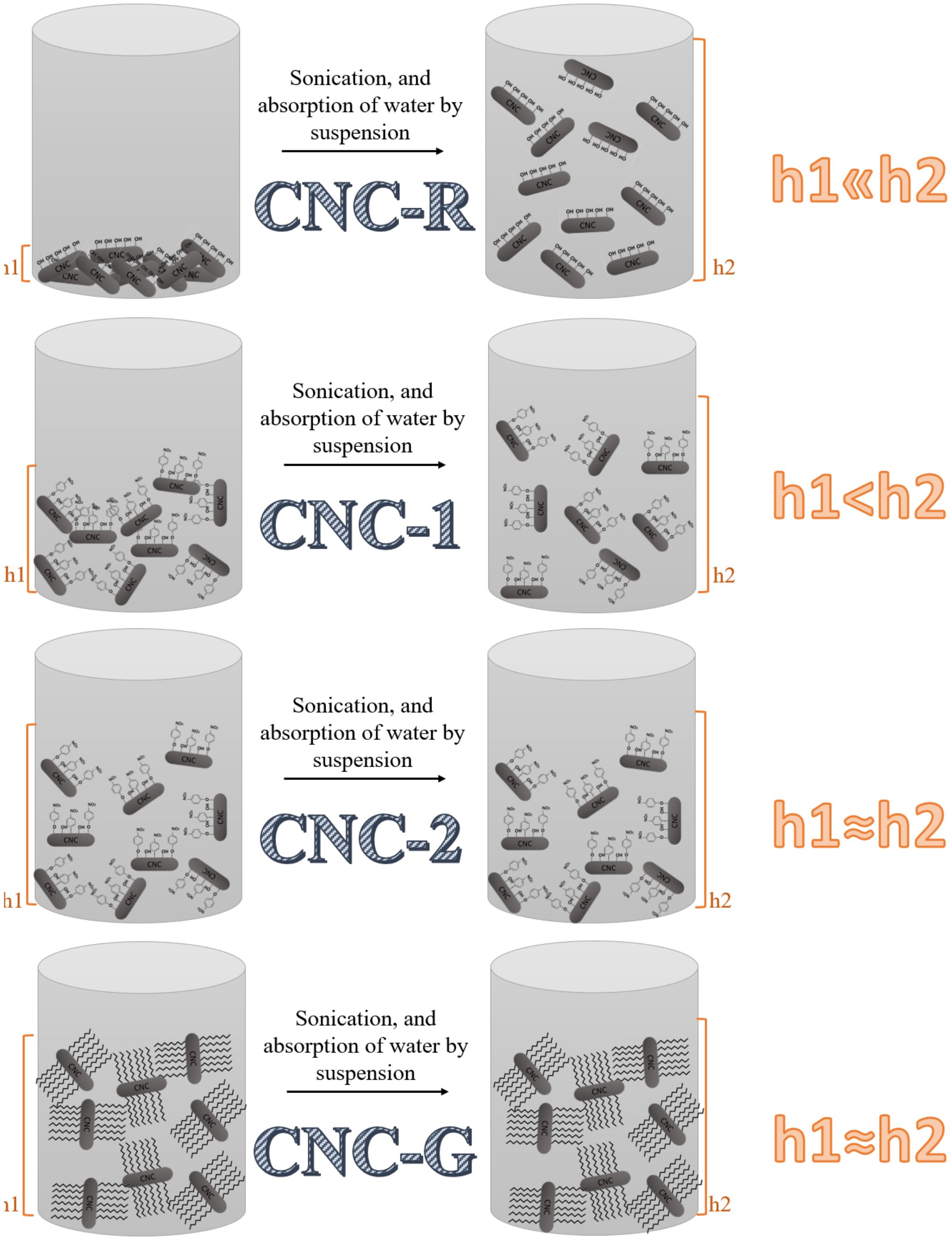

Figure 4. 10: Schematic images of CNC suspentions in DMF before and after sonication

4.3.2.3. Evaluation of the chemical modifications based on the work of adhesion of the modified CNCs

These results can be evaluated from two different points of view. The first point of view is calculation of the work of adhesion between various types of CNC and DMF, which is defined as the amount of energy needed to wet CNCs with DMF. According to Figure 4.11, there are three surface tensions involved in work of adhesion of the DMF by CNC, so it can be calculated by Equation 4.4.

$$W_A = \gamma_{CNC} + \gamma_{DMF} - \gamma_{CNC/DMF} \qquad \text{Equation 4.4}$$

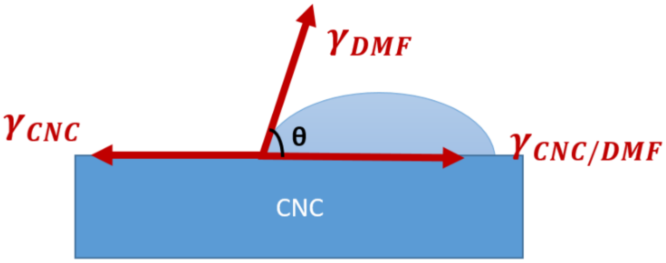

Figure 4. 11: Surface tensions involved in working adhesion of DMF on the CNC surface

Where γ_{CNC} , γ_{DMF} and $\gamma_{CNC-DMF}$ are the surface tension of CNC, the surface tension of DMF and interfacial tension between CNC and DMF. The last term can be calculated by Equation 4. 5

$$\gamma_{CNC-DMF} = \gamma_{CNC} + \gamma_{DMF} - (2\left(\gamma_{CNC}^{d}\gamma_{DMF}^{d}\right)^{0.5} + 2\left(\gamma_{CNC}^{p}\gamma_{DMF}^{p}\right)^{0.5}) \qquad \text{Equation 4.5}$$

Where γ^d and γ^p are the dispersive and polar parts of surface tension of each component. Their summation is equal to the total surface tension. By substitution Equation 4.4 in Equation 4.5 work of adhesion can be calculated by Equation 4.6.

$$W_A = 2\left(\gamma_{CNC}^{d}\gamma_{DMF}^{d}\right)^{0.5} + 2\left(\gamma_{CNC}^{p}\gamma_{DMF}^{p}\right)^{0.5} \qquad \text{Equation 4.6}$$

Therefore, knowing dispersive and polar parts of each CNC and DMF, work of adhesion of various CNCs can be calculated. These data were found for CNC-R, CNC-1, and CNC-g from literature, and using Equation 4.6, their work of adhesions were compared in Table 4.2.

As shown in Table 4.2, the lowest work of adhesion belongs to the CNC-g with higher stability compared with CNC-1, and CNC-R. Unfortunately, the dispersive and polar surface tensions of CNC-2 could not be found in literature, so the higher stability of CNC-2 suspension in DMF was evaluated by the other point of view, solubility parameters of different types of CNC.

Table 4. 2: Work of Adhesion of various modified CNCs

CNC Type	γ^d (mJ/m2)	γ^p (mJ/m2)	Reference	Wa(mJ/m2)	Note
CNC-R	27.5	41	(Dankovich and Gray 2011)	92.92	Dispersive and Polar components of surface energy were obtained for CNC
CNC-1	40.24	11	(Victor M. Starov, Manuel G. Velarde 2007)	87.19	Dispersive and Polar components of surface energy were obtained by means of knowing contact angle of water and diodomethan on nitrocellulose (DS:1-2)
CNC-2	N.A	N.A	N.A	N.A	
CNC-g	38	0.1	(Botaro and Ã 1998)	68.19	Dispersive and Polar components of surface energy were obtained for cellulosic film grafted with PS
DMF	29	8.1	(Hansen 2000)	-	

4.3.2.4. Evaluation of the chemical modifications based on the solubility parameters of the modified CNCs

To make a comparison between various types of CNC, their solubility parameters were calculated according to the group contribution method given by Small and Hoy (Small 1953; Hoy 1970). To use this method, the molar attractive constants of chemical groups (Fi) composing a polymer unit should be considered. Finally solubility parameter can be easily calculated by Equation 4.7.

$$\delta = \frac{d\Sigma\, Fi}{M} \qquad \text{Equation 4.7}$$

Where d is the density of polymer and M is molecular weight of repeating unit.

Table 4.3 presents the molar attractive constants of chemical groups existing in CNC-R, CNC-1, and CNC-2. Using these constants and the above mentioned equation, the solubility parameters of each type of CNC were calculated and presented in Table 4.4. It should be noted that the degree of substitution of hydroxyl group with the newly modified chemical group was considered 0.5. It means that just one of the six hydroxyl groups was substituted with nitro aryl and three flouro aryl groups in CNC-1 and CNC-2 respectively as shown in Figure 4.12.

Table 4. 3: Molar attractive constants of chemical groups exciting in CNCs

		cellulose	cellulose-CF3	cellulose-NO2
-OH	Number of functional groups in a polymer unit	6	5	5
	Molar Attractive Constant (Small)	226	226	226
	molecular weight of the chemical group	17	17	17
-O-	Number of functional groups in a polymer unit	4	5	5
	Molar Attractive Constant (Small)	115	115	115
	molecular weight of the chemical group	16	16	16
-CH-	Number of functional groups in a polymer unit	10	10	10
	Molar Attractive Constant (Small)	86	86	86
	molecular weight of the chemical group	13	13	13
-CH2-	Number of functional groups in a polymer unit	2	2	2
	Molar Attractive Constant (Small)	133	133	133
	molecular weight of the chemical group	14	14	14
-Phenyl-	Number of functional groups in a polymer unit	0	1	1
	Molar Attractive Constant (Small)	658	658	658
	molecular weight of the chemical group	76	76	76
-CF3	Number of functional groups in a polymer unit	0	1	0
	Molar Attractive Constant (Small)	274	275	276
	molecular weight of the chemical group	63	63	63
-NO2	Number of functional groups in a polymer unit	0	0	1
	Molar Attractive Constant (Small)	440	440	440
	molecular weight of the chemical group	38	38	38

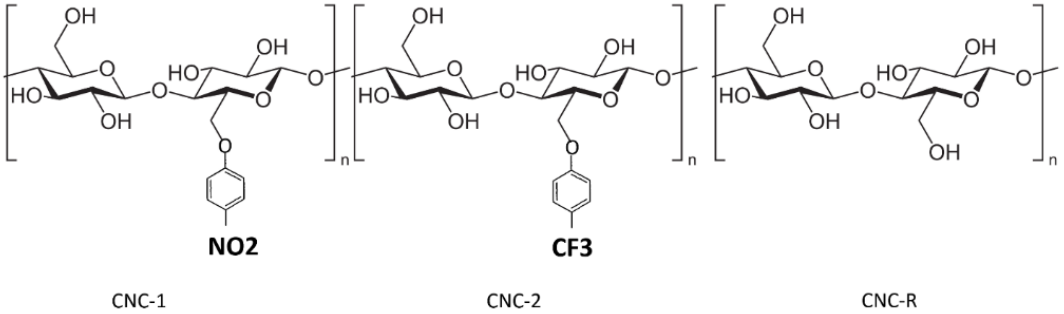

Figure 4. 12: Modified CNCs with Degree of Substitution of 0.5

Table 4. 4: Solubility parameters calculated using Small and Hoy method

	Cellulose	cellulose-CF3 (CNC-2)	cellulose-NO2 (CNC-1)	DMF
Solubility Parameter ($MPa^{1/2}$)	27.85	24.99	27.58	24.83

As presented in Table 4.4, the closest solubility parameter belongs to CNC-2 which showed the best miscibility in Figure 4.7 following by CNC-1, and CNC-R respectively. It should be noted because of our lack of knowledge about the chain length of PS grafted on CNCs, exact molecular weight of this modified CNC is not distinguishable so we could not calculate solubility parameter for this type of CNC.

On the other side, the behaviours of CNC suspensions in 5% PS solution were totally different. Unexpectedly, suspension containing regular CNC has the highest stability due to their different level of electron acceptors of functional groups belonging to various modified CNCs compared to unmodified CNC. As it is shown in Figure 4.13, there is almost no changes but possibly insignificant enlargement of particles by time for CNC-R sample. This is the result of agglomeration especially in lower levels demonstrated by a slight increase of T signals at the higher heights, and a decrease of BS signals at the lower heights. Because there was less attraction among regular CNC and PS due to their different hydrophilicity, they less attracted to each other. Consequently, PS chains just acted as a stabilizer in suspension and prohibit CNC from sedimentation due to the increased viscose forces.

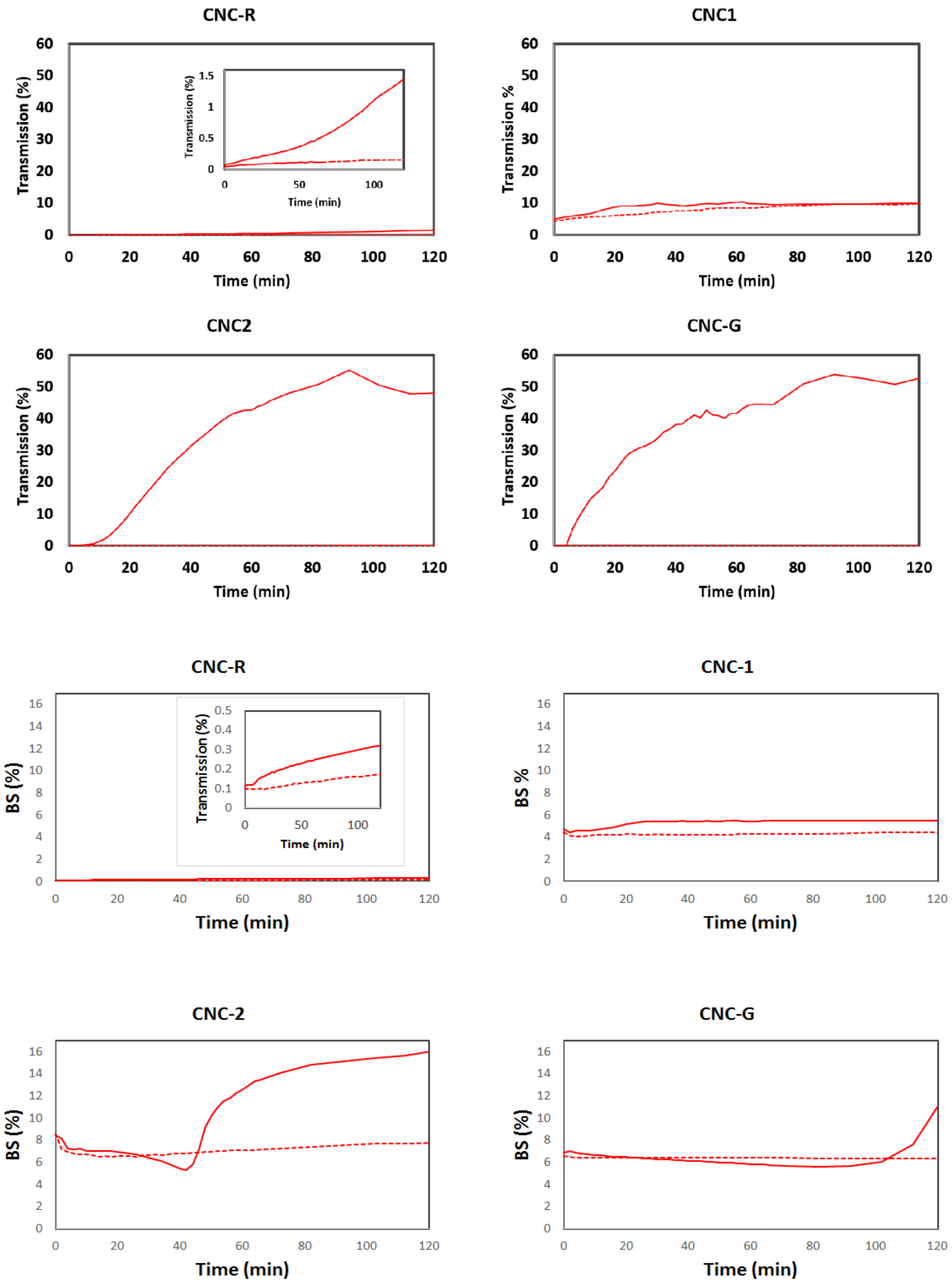

Figure 4. 13: Turbidity results of suspensions of various modified CNCs in DMF containing 5% (w/v) PS: 1) delta Transmission 2) Delta backscattering.

Samples containing CNC-1 demonstrated sharper changes by the time. It shows a higher instability compared to the former case. Sharp increases on both T and BS signals can describe a quick displacement of large and small particles and their arrangement based on their size in the bottle as a result of initial poor dispersion. About CNC-2 sample, there was no significant change in T signal for 40 minutes; consequently, BS signal should be studied during this period of time. Decreasing BS signal at 20 mm of height can show agglomeration of CNCs especially at 20 mm of height and their partial sedimentation. Due to the constant trend of both T and BS signals at 10 mm of height, changes in suspension took place between 10 and 20 mm, even after 40 minutes of measurement when a sudden sedimentation happened. These changes in suspension could attribute to a gradual agglomeration and consequently a clarification at higher heights. Compared to DMF, the benzene rings in PS are stronger source of electron. Therefore, it is likely that the electron withdrawing functional groups of CNC-1 or CNC-2 could be attracted toward PS chains instead of DMF. This attraction could finally result in the agglomeration of PS chains around the modified CNCs leading to instability of the suspension.

Finally, in the case of CNC-g, the partial sedimentation took place at 110 min. It shows the similar behaviour of CNC-g and CNC-2 samples. However, CNC-g sample was more sustainable than the CNC-2 sample. It could be due to the free PS chains being attracted toward the grafted PS chains on CNC particles with a slower pace. Due to the fact that DMF is not a good solvent for PS, these PS grafted CNCs could act as a nucleus of agglomeration for free PS chains around themselves. This process took longer than electrostatic attraction taking place in the cases of CNC-1 or CNC-2, so sedimentation of CNC-g in PS/DMF system occurred in a slower pace. Figure 4. 14 shows the influence of PS addition into the CNC suspensions in DMF, schematically.

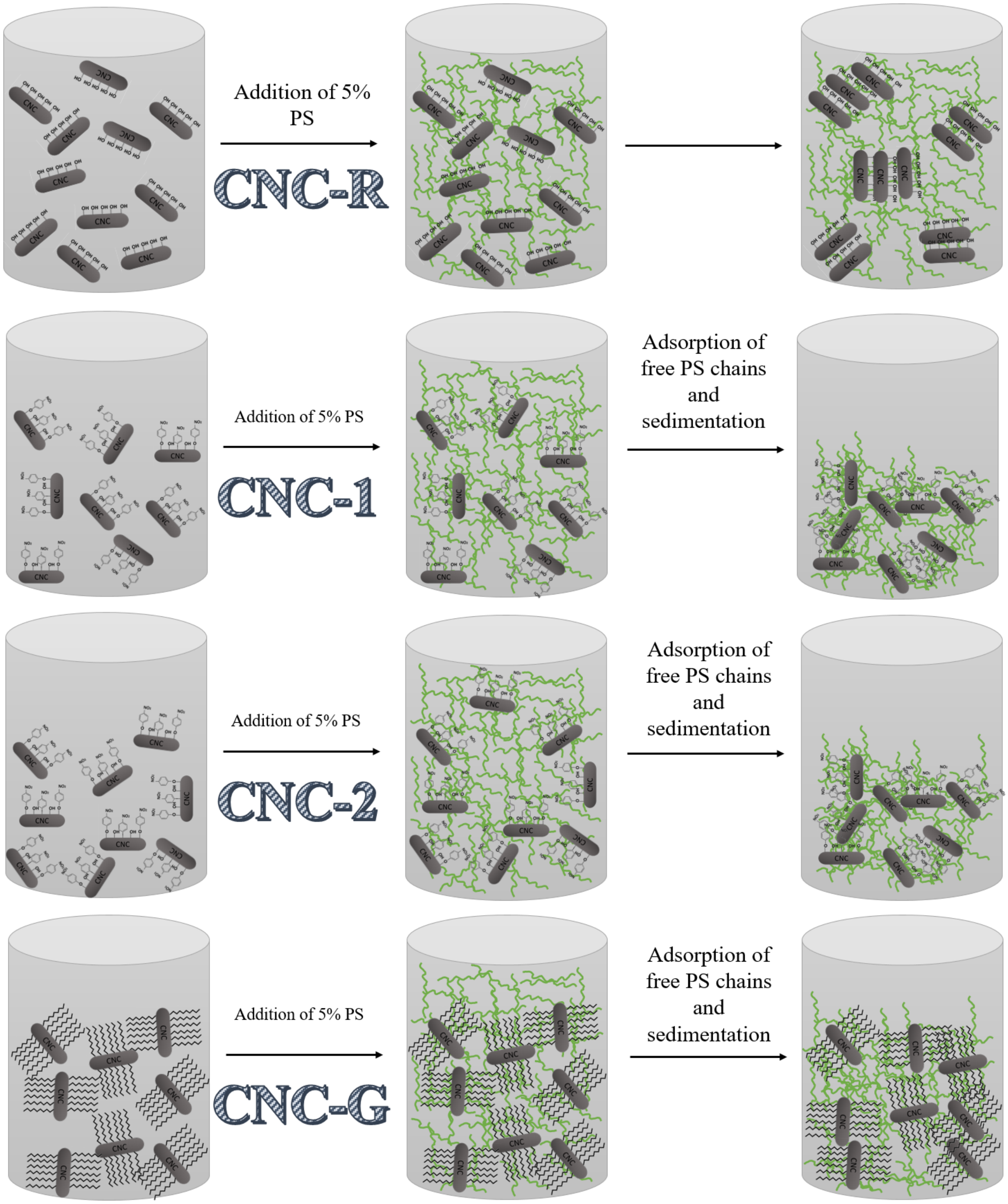

Figure 4. 14: the schematic images of the influences of PS addition into the CNC suspensions in DMF

4.3.3. Impact of chemical modification on the morphology of fibers

The effects of CNC modifications in electrospun fibers were studied and compared with unmodified CNC. To that end, four types of electrospun fiber samples containing 1 wt. % regular and modified CNCs were prepared. Figure 4.15 shows the SEM images of these four types of mats. Surface modified CNC-1 and CNC-2 resulted in bead-free and smooth fiber because of their good dispersion in DMF and consequently in PS matrix after evaporation of DMF. As it was expected, poor dispersion of unmodified CNC in DMF resulted in beaded electrospun fibers. The beaded morphology of CNC-R electrospun fibers can be explained by nonuniform extensional stretching capacity of PS toward the fiber axis under the electrical field due to the presence of aggregated CNC-R particles. CNC-g sample with grafted PS brushes resulted in beaded structures which was rather unexpected. This issue can result in entanglements of the short grafted PS chains with free PS Chains and with each other in case of higher concentration. Consequently, after a specific concentration, agglomeration of CNC-g can cause beaded structures in fibers as shown in Figure 4.16.

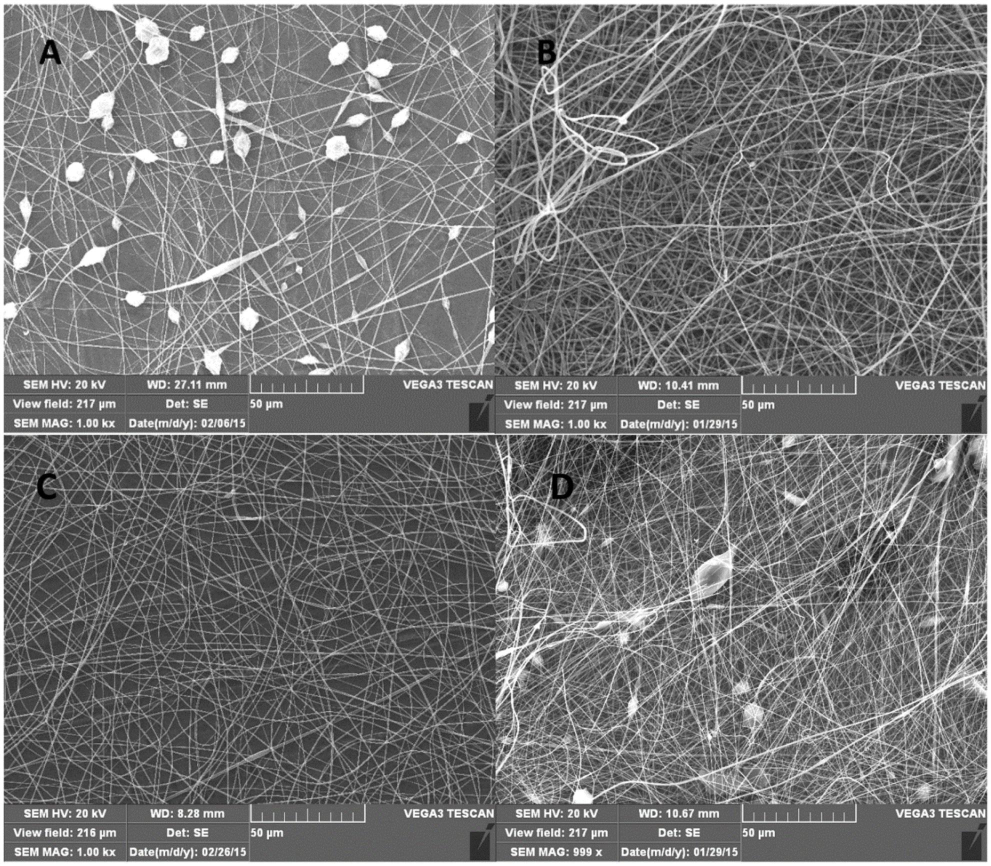

Figure 4. 15: SEM images of PS fibers containing: A) 1wt. % regular CNC; B) 1wt. % CNC-1 C) 1wt. % CNC-2 D) 1wt. % CNC-g

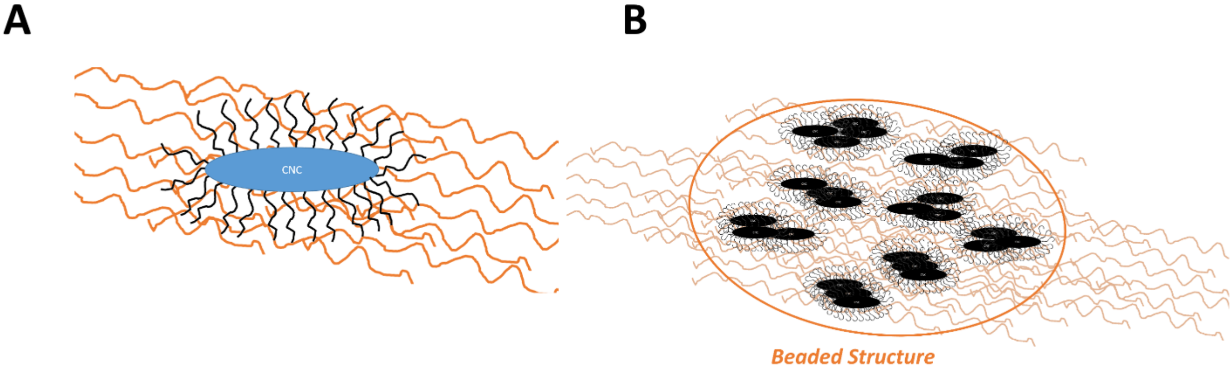

Figure 4. 16: Proposed mechanism for beaded structures A) entanglement of PS short grafted chains with free PS chains B) entanglement of PS short grafted chains with each other, and bead formation.

To investigate the possible reasons for these beaded structures, Energy-dispersive X-ray spectroscopy (EDX) was performed on both beaded and fiber areas contributing to fibers containing CNC-R and CNC-g. As shown in Figure 4.17, both spectra related to beaded areas are illustrating the existence of Oxygen in them compared to the spectra related to the fibers area. Oxygen as an element exclusive to the cellulose in this composite can illustrate the accumulation of CNCs in the beaded areas. The quantitative percentages of elements are reported in Table 4.5.

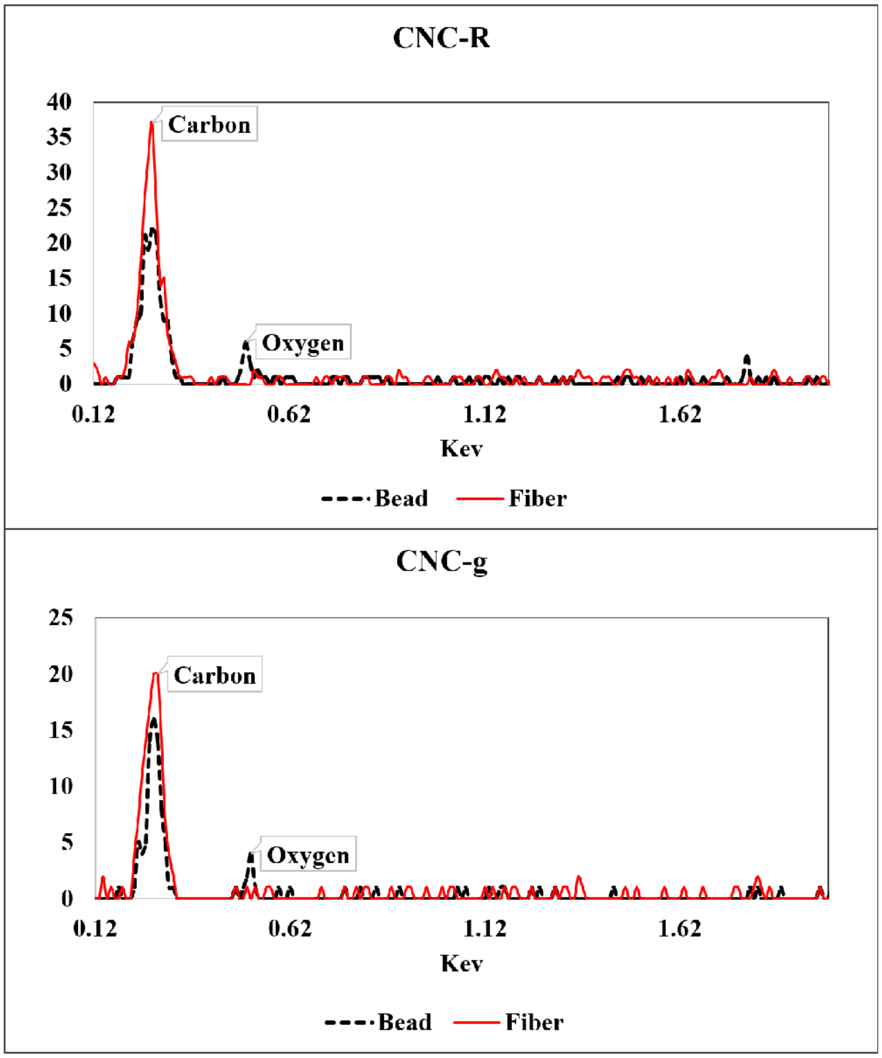

Figure 4. 17: Energy-dispersive X-ray spectroscopy (EDX)

Table 4. 5: EDX analysis of CNC NFs Containing CNC-g and CNC-R on both bead and fibers areas.

Elements (wt. %)	CNC-R		CNC-G	
	Fiber	Bead	Fiber	Bead
C	99.9	96.78	99.8	98.54
O	-	3.21	-	1.45
S	-	-	-	-

To investigate the possible reasons for the beaded structures in CNC-g/PS fibers and to compare with other surface modified CNC-1 and CNC-2 in PS samples, PS with different concentrations of modified CNCs was produced. Representative SEM pictures can be seen in Figure 4.18, 4.19, and 4.20 for fibers containing CNC-1, CNC-2, and CNC-g respectively. The increase amount of modified CNCs resulted in the contradictory results (see Figure 4.21). The average diameters were found to be 0.58, 0.66, 0.67, 0.86, and 1.11 micrometer for 0, 0.5, 1, 1.5, and 2 w.t% of CNC-1 loadings, respectively. For samples containing CNC-2, the average diameters were measured to be 0.58, 0.5, 0.6, 0.68, and 0.78 micrometer at the same concentrations of CNC-2, respectively.

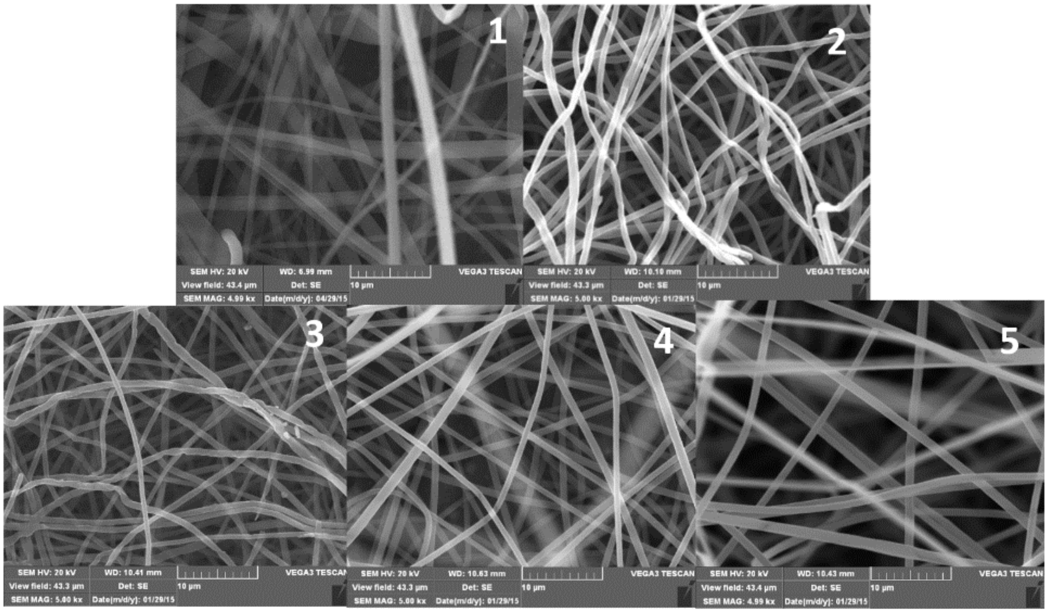

Figure 4. 18: SEM images of the PS fiber containing CNC-1 with concentrations of (1) 0 wt. % (2) 0.5 wt. % (3) 1wt. % (4) 1.5 wt. % (5) 2 wt. % CNC.

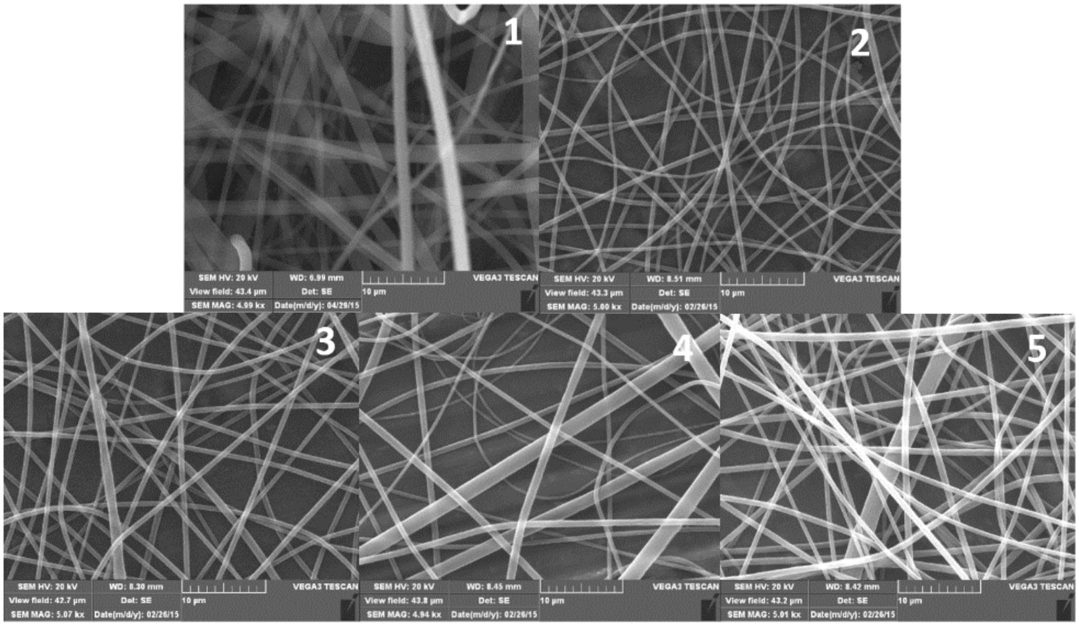

Figure 4. 19: SEM images of the PS fiber containing CNC-2 with concentrations of (1) 0 wt. % (2) 0.5 wt. % (3) 1wt. % (4) 1.5 wt. % (5) 2 wt. % CNC

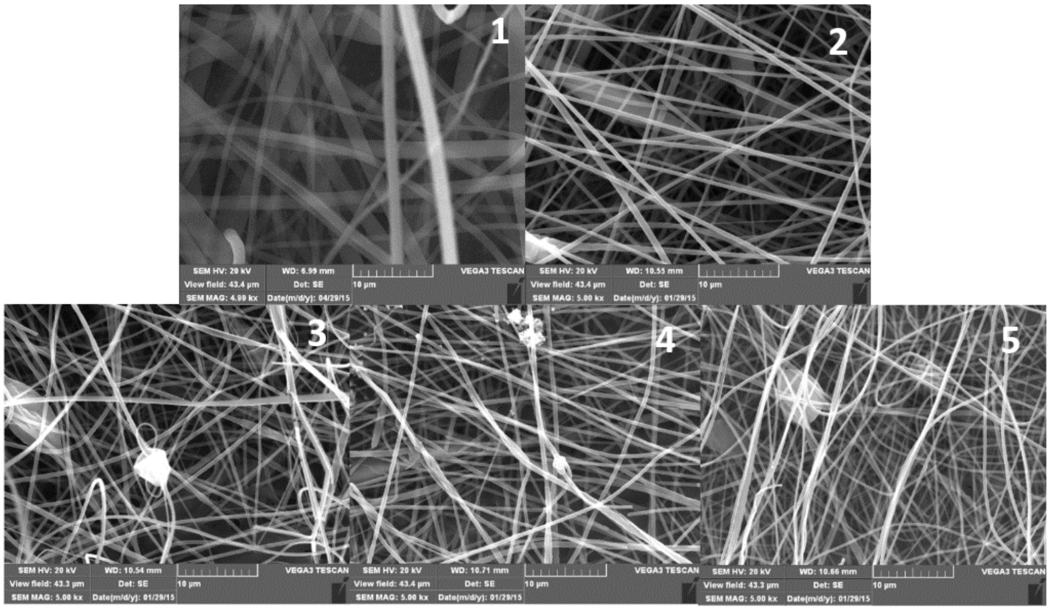

Figure 4. 20: SEM images of the PS fiber containing CNC-g with concentrations of (1) 0 wt. % (2) 0.5 wt. % (3) 1wt % (4) 1.5 wt. % (5) 2 wt. % CNC

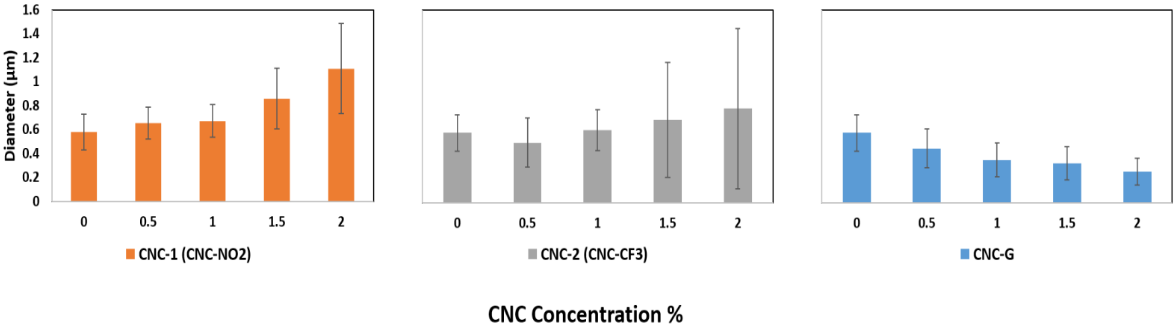

Figure 4. 21: Changes of the fiber diameters with different concentrations of the modified CNCs

This slight increase of the fiber diameters may be due to the PS solution viscosity change, and the presence of CNC particles. It was reported that the diameter of fibers increased by increase of viscosity (Rošic et al. 2012) and as measured previously, adding more CNC could bring about higher viscosity after specific concentration of CNC (Boluk et al. 2011; Q. Wu et al. 2014). However, viscosity magnitudes, shown in Table 4.1, did not change tremendously by adding CNC due to their low contents. Moreover, CNC inclusion resulted in higher solution conductivity, and as the Wang’s model (C. Wang, Hsu, and Lin 2006) describes the conductivity of solutions can decrease dimeters of electrospun fibers. Equation 4.8 presents Wang’s model.

$$df \sim k^\wedge(-0.12) \qquad \text{Equation 4. 8}$$

Where, df and K are the average fibers diameters and the conductivity respectively. As Figure 4.22 shows, only sample containing CNC-g follows this model. Nevertheless, since above CNC-g fibers contained beads, their diameter measurements were not reliable.

On the other side, inclusions of CNC-1 and CNC-2 resulted in larger electrospun fibers. These result can be attributed to the stress relaxation of the semi-dried fibers collected on stationary collector. As a result of these forces, the free PS chains get elongated toward the jet axis. At the same time, modified CNCs are absorbed by the PS chains because of the chemical affinity between them, and a dilute continues phase is left behind. Moreover incomplete evaporation of solvent takes place simultaneously. However, these longitudinal forces are cut when the semi-dried fibers reach to the stationary collectors. Subsequently, elongated free PS chains start relaxing the longitudinal forces. As a result of these stress relaxation before complete evaporation of DMF, their radius of gyration start decreasing which finally results in the thicker fiber (see Figure 4.23). It should be noted that diluter continues phase helps stress relaxations happen more easily and quickly. However, as shown in Figure 4.24, in the case of CNC-g the stress relaxations take place in a slower manner because of the possible entanglements between the short grafted PS chains on CNC and the free PS Chains. Consequently, DMF evaporates completely before a complete stress relaxations, and thinner fibers are left behind.

Moreover, although the shear viscosities of the PS solutions were not affected by the additions of small amounts of CNC-1 or CNC-2, the changes in the fiber diameters can be explained by their contribution to the increase of the elongational viscosities of PS/DMF solutions.

As the jet formation in the electrospinning process is mostly an elongational flow, the fiber diameter can be more fundamentally related more to the elongational viscosity. Since the elongational and the shear viscosities are related by the Trouton ratio, the shear viscosity can only be used for the correlations of electrospinning behavior, if the Trouton ratio remains constant over the rates of extension experienced during electrospinning. However, at higher strain rates, when elongational rate is higher than inverse of the polymer stretch relaxation time, the extensional viscosity increases, giving rise to the extensional thickening behavior. For monodisperse polymers, the relaxation time is related to the number of entanglements per chain. However, the presence of rigid nanoparticles at very low concentration range also modify the entanglement density of polymer chains. This may explain that although no change in the zero-shear viscosity of the CNC/PS/DM solutions, the presence of variety of CNC suspensions exhibited different extensional thickening behavior and fiber diameter. If this argument is valid, it can be said that very low concentrations of chemically surface modified CNC-1 and CNC-2 effected the entanglement density of PS/DMF solutions and fiber diameter.

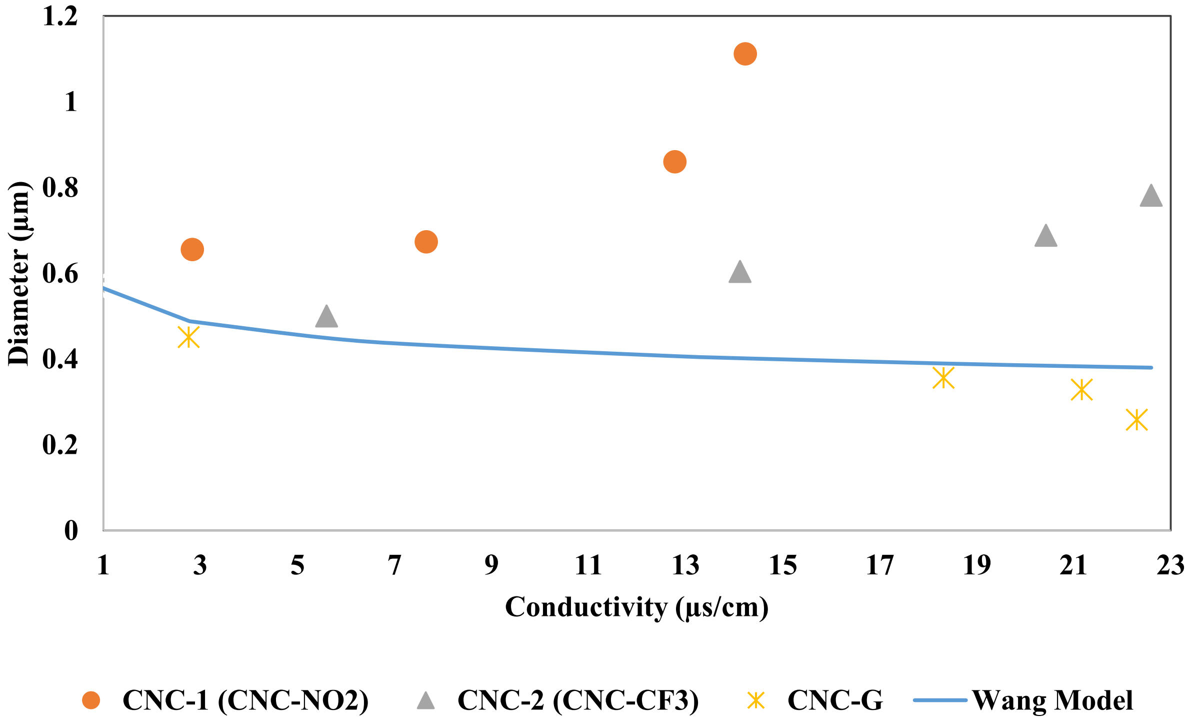

Figure 4. 22: Changes of the fiber diameters by conductivity of electrospinning solution.

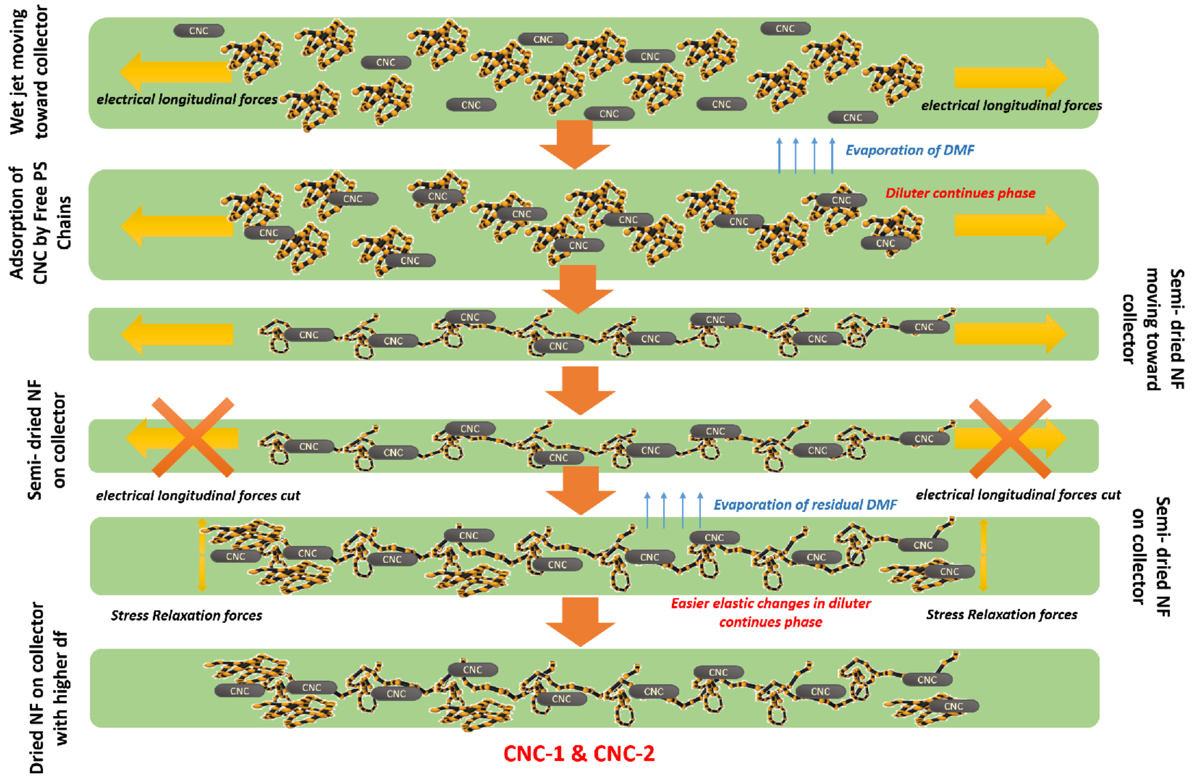

Figure 4. 23: Proposed mechanism of the stress relaxations in the electrospun fibers containing CNC-1 and CNC-2

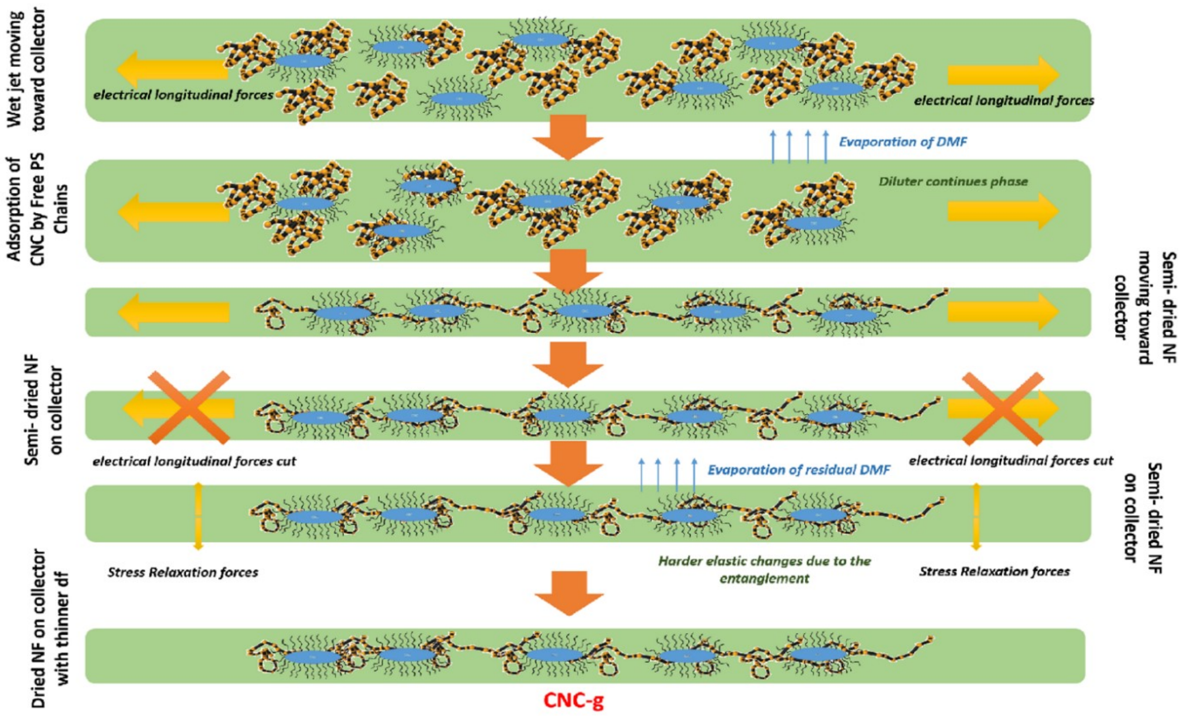

Figure 4. 24: Proposed mechanism of the stress relaxations in the electrospun fibers containing CNC-g.

4.3.4. Impact of the chemical modifications of CNC on the tensile properties of the PS/CNC electrospun webs

In this study, several tensile tests were performed on nonwoven meshes formed of fibers. Mechanical properties of a nonwoven mesh are influenced by many factors, such as individual fiber morphology, porosity, and the fiber orientation in the mat. Moreover, the bonding between fibers and the slipping of fibers over each other play important roles in the mat mechanical properties (M. Wang et al. 2004; C. Zhou and Wu 2012).

Figure 4.25 shows the typical stress-strain curves of PS nonwoven mesh containing various percentages of different CNCs. As shown in Figure 4.26, the strain at ultimate tensile stress (ε at UTS) of the nonwoven PS mats was about 0.2%; while it is around 0.15% for electrospun samples with CNC The presence of rigid fillers (CNC) decreased the elasticity of the PS in the specimen, and resulted in smaller ε at UTS. Ultimate strain values of CNC incorporated PS fibers also showed a trend similar to their ε at UTS values.

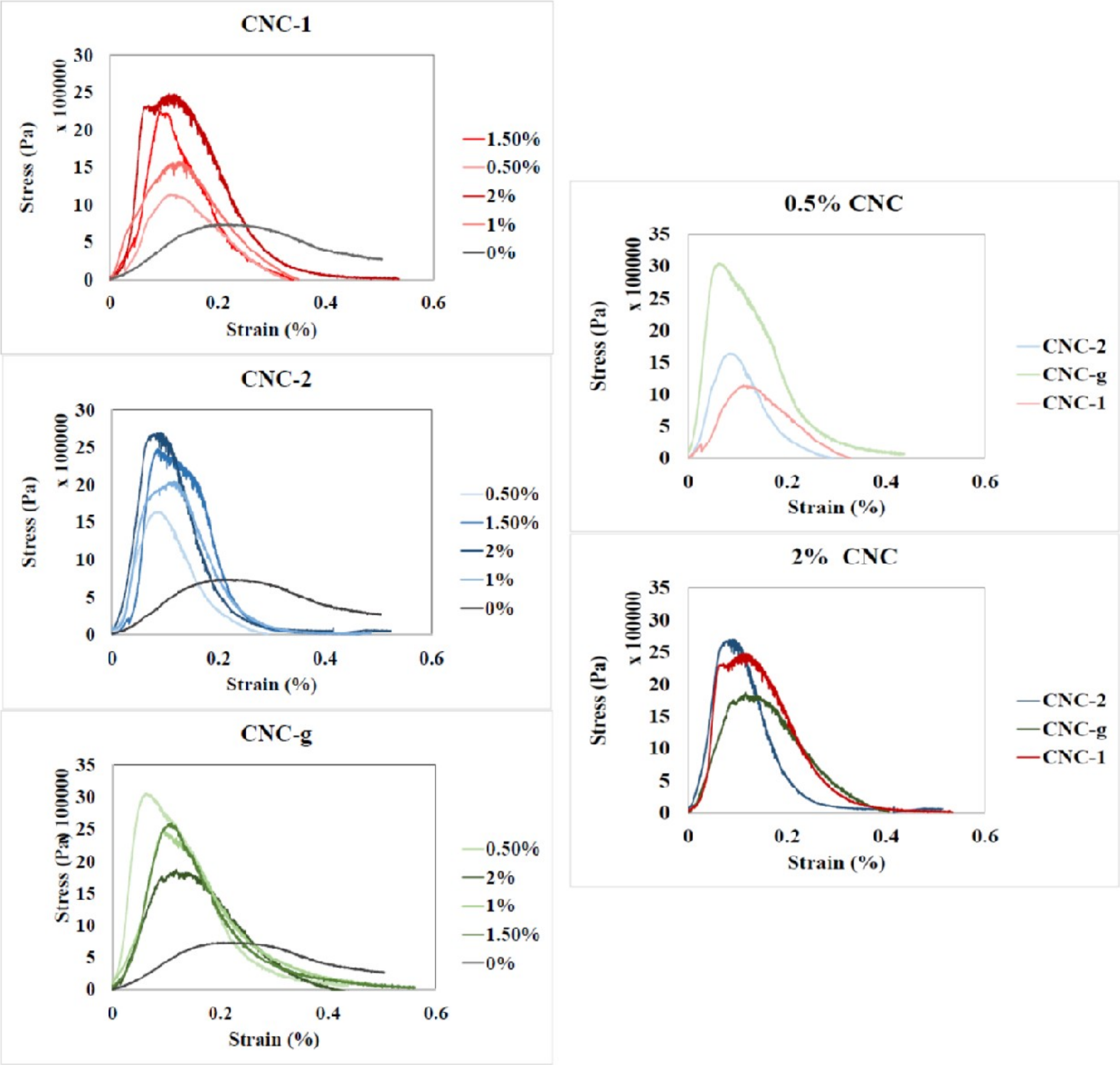

Figure 4. 25: the typical stress-strain curves of PS nonwoven mesh containing various percentages of different CNCs

Figure 4.26 shows the reinforcing effect of CNCs on electrospun PS fiber mat. The average Young's modulus value of the fiber mats increased 340% with the addition of 0.5 wt. % CNC-1. Similarly, the addition of 1 wt. %, 1.5 wt. %, and 2 wt. % of CNC-1 resulted in an increase of 458%, 682%, and 781% in Young's modulus, respectively. The average strength values of the pure fiber mats increased 21% by adding 0.5 wt. % CNC-1. By adding 1 wt. %, 1.5 wt. %, and 2 wt. % CNC, an increase of 76%, 107%, and 120%, were achieved in average strength, respectively. Moreover, by inclusion of 0.5 wt. % CNC-1, the strain of the fiber mats decreased 66% in comparison with the non-reinforced mats. In a similar trend, increasing CNC-1 by 1 wt. %, 1.5 wt. %, and 2 wt. % resulted in an additional decrease of -71%, -78%, and -80%, in the fibers strain, respectively.

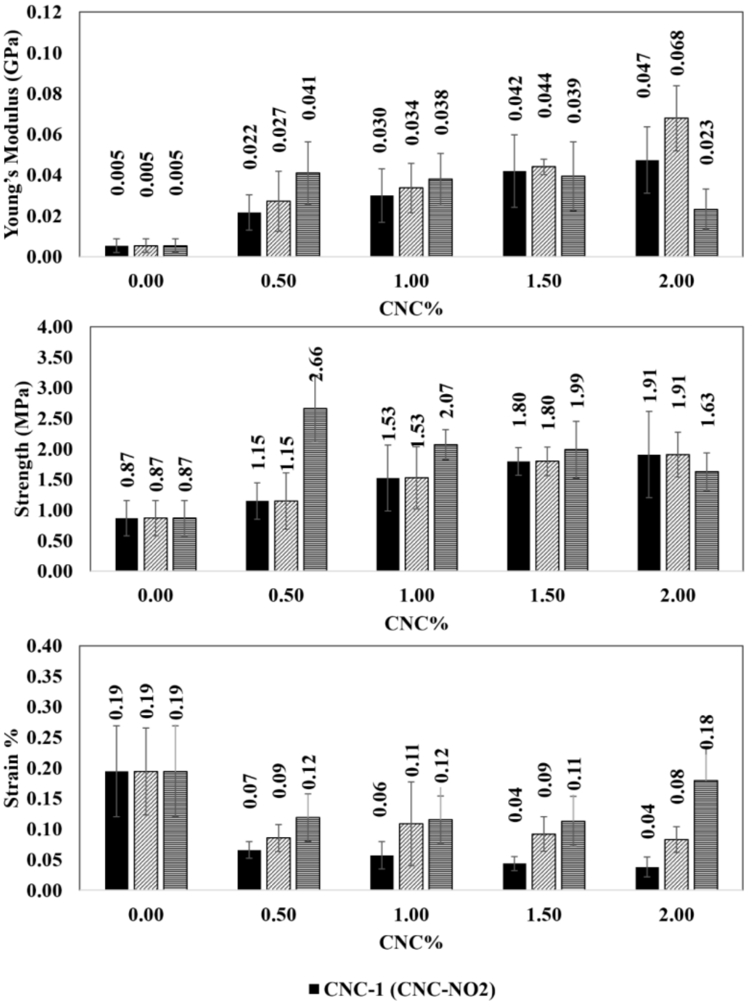

Figure 4. 26: Young's modulus, Strength, and strain at highest strength with different concentrations of modified CNCs

Regarding CNC-2, the average Young's modulus value of the fiber mats increased 440% with the addition of 0.5 wt. % CNC-1. Similarly, the addition of 1 wt. %, 1.5 wt. %, and 2 wt. % of CNC-2 resulted in increases of 527%, 720%, and 1162% in Young's modulus, respectively. The average strength values of the fiber mats increased 43% by adding 0.5 wt. % CNC. By adding 1 wt. %, 1.5 wt. %, and 2 wt. % CNC, we obtained additional changes in average strength of 73%, 100%, and 157%, respectively. By adding 0.5 wt. % CNC, the strain of the fiber mats decreased

55%. In the same way, increasing CNC by 1 wt. %, 1.5 wt. %, and 2 wt. % resulted in additional changes of -44%, -52%, and -57%, in the strain of fibers, respectively.

Finally in the case of CNC-g, the average Young's modulus value of the fiber mats increased 665% with the addition of 0.5 wt. % CNC-g. However, the addition of 1 wt. %, 1.5 wt. %, and 2 wt. % of CNC resulted in just increases of 606%, 633%, and 332% in Young's modulus, respectively. The average strength values of the fiber mats increased 206% by adding 0.5 wt. % CNC compared to that of non-reinforced mats. In contrast, by addition of 1 wt. %, 1.5 wt. %, and 2 wt. % CNC, a decreasing trend was observed in the average strength, and lower increases of 138%, 129%, and 88% were obtained respectively. By adding 0.5 wt. % CNC, the strain of the fiber mats decreased only 39% in comparison with the non-reinforced mats. However, increasing CNC by 1 wt. %, 1.5 wt. %, and 2 wt. % resulted in a fluctuating trend of -40%, -41%, and -8%, in the strain of fibers, respectively.

Such high increase in both Young's modulus and yield strength was reported for higher contents of CNC. For instance, by adding 20% of CNC to polyethylene oxide (PEO) electrospun fibers, a 282% increase in Young's modulus and 232% increase in the strength were obtained (C. Zhou et al. 2011). In the other case, PVA fibers showed 240% of stiffness improvement by adding 6.6% of CNC (Medeiros et al. 2008). These results can prove the significant effect of surface modification of CNCs on mechanical improvement of PS fibers. Due to the possible chemical interaction between modified CNCs and PS matrix, higher mechanical performance was obtained by just adding low amount of CNCs. The effect of possible chemical interaction between CNCs and polymeric matrix was shown for poly acrylic acid. By adding 20% of CNC to PAA, astonishing results were reported. The Young's modulus and tensile strength were significantly improved up to 35-fold and 16-fold, respectively (P. Lu and Hsieh 2009). This results can be related to possible chemical reaction between hydroxyl groups of CNCs and carboxyl groups of polymer matrix.

4.3.5. Impact of the chemical modifications of CNC on the mechanical properties of fibers web by Dynamic Mechanical Analysis (DMA)

DMA analysis were performed to obtain the resultant storage modulus (E'), loss modulus (E") and damping factor (tanδ) of the CNC reinforced samples. The storage modulus is roughly an approximation of the Young or elastic moduli. The loss modulus is a magnitude of the energy absorbed as result of a relaxation, and it is useful in describing the mechanisms of internal motions. The damping factor (tanδ) shows the relative contributions of the viscous and elastic components of a viscoelastic material. In case of a thermoplastic material like linear atactic PS, both storage and loss modulus change with temperature due to the changes in the molecular mobility. The storage modulus of a polymer decreases rapidly while the loss modulus and tan δ show a maximum when the material temperature approaches to the glass transition (Tg). Mobility of the amorphous regions causes reduction in the storage modulus. However, the material still exhibits solid-state properties before reaching melting temperature (Menard 1999; Sepe 1998).

The storage modulus and loss modulus of electrospun neat PS and PS/CNC sample are presented in Figure 4.27 and Figure 4.28, respectively. Unexpectedly, all of the storage moduli of the electrospun samples had increasing trend and reached to a maximum around 110 degree. This increasing trends of storage muduli can be explained by the fiber fusing and the immediate densification of the electropsun samples (Blaker et al. 2005). As expected, the CNC reinforced electrospun samples exhibit much higher storage modulus than pure PS, especially at low temperatures, given the reinforcing effect of CNC on the electrospun samples (see Figure 4.30). The resultant storage moduli are comparable with the resultant stiffness at Figure 4.26. However, higher storage moduli obtained at higher temperatures. As the temperature increased during DMA test, the randomly oriented fibrous structure formed some fuzzed points (resulting in interconnection between fibers). Finally at higher points by densification of the whole structure, the fibrous structure turn into a continuous structure like film. This structure can represent a higher storage modulus of CNC/PS composites. At 110°C, the addition of 2 wt. % of CNC-1 and CNC-2 to PS fibers results in a 288% and 364% increases in storage moduli of these electrospun samples respectively. This also shows that CNC-2 has a better interfacial interaction with PS in comparison with CNC-1. Moreover, samples contains CNC-g shown a storage modulus trend similar to the stiffness trends. Lower concentrations of CNC-g resulted in a better mechanical performance. At 110°C, addition of 0.5 wt. %, 1wt. %, 1.5 wt. %, and 2% of CNC-g resulted in 180%, 320%, 58%, 68% increases in storage moduli of these samples. Eventually, with the increase of temperature to melting temperature, the storage modulus tends to converge to that of pure PS, indicating that at high temperature, the modulus of the composites were dominated by the matrix intrinsic modulus.

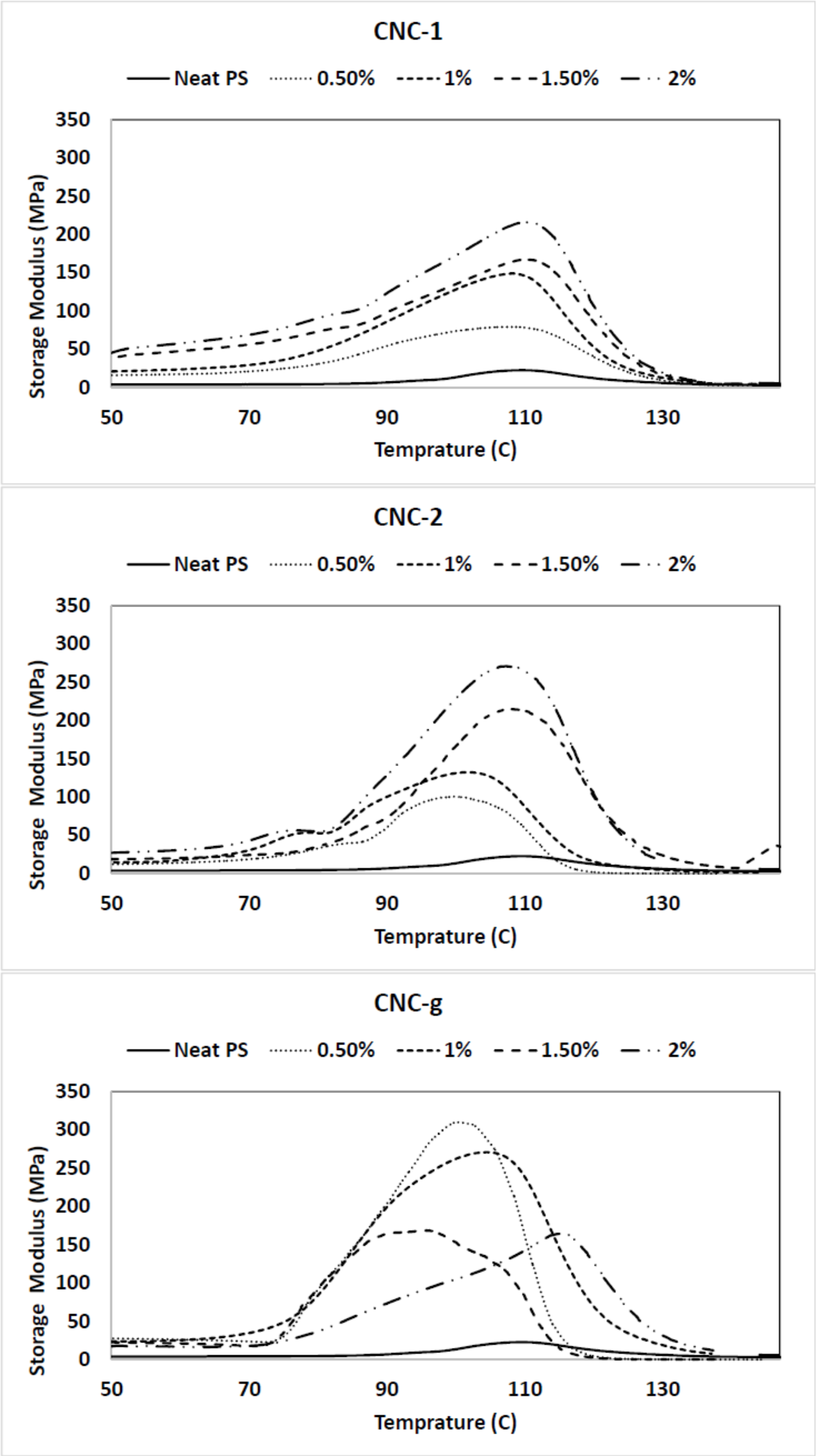

Figure 4. 27: Storage moduli of non-oriented PS fibrous mats containing different CNCs

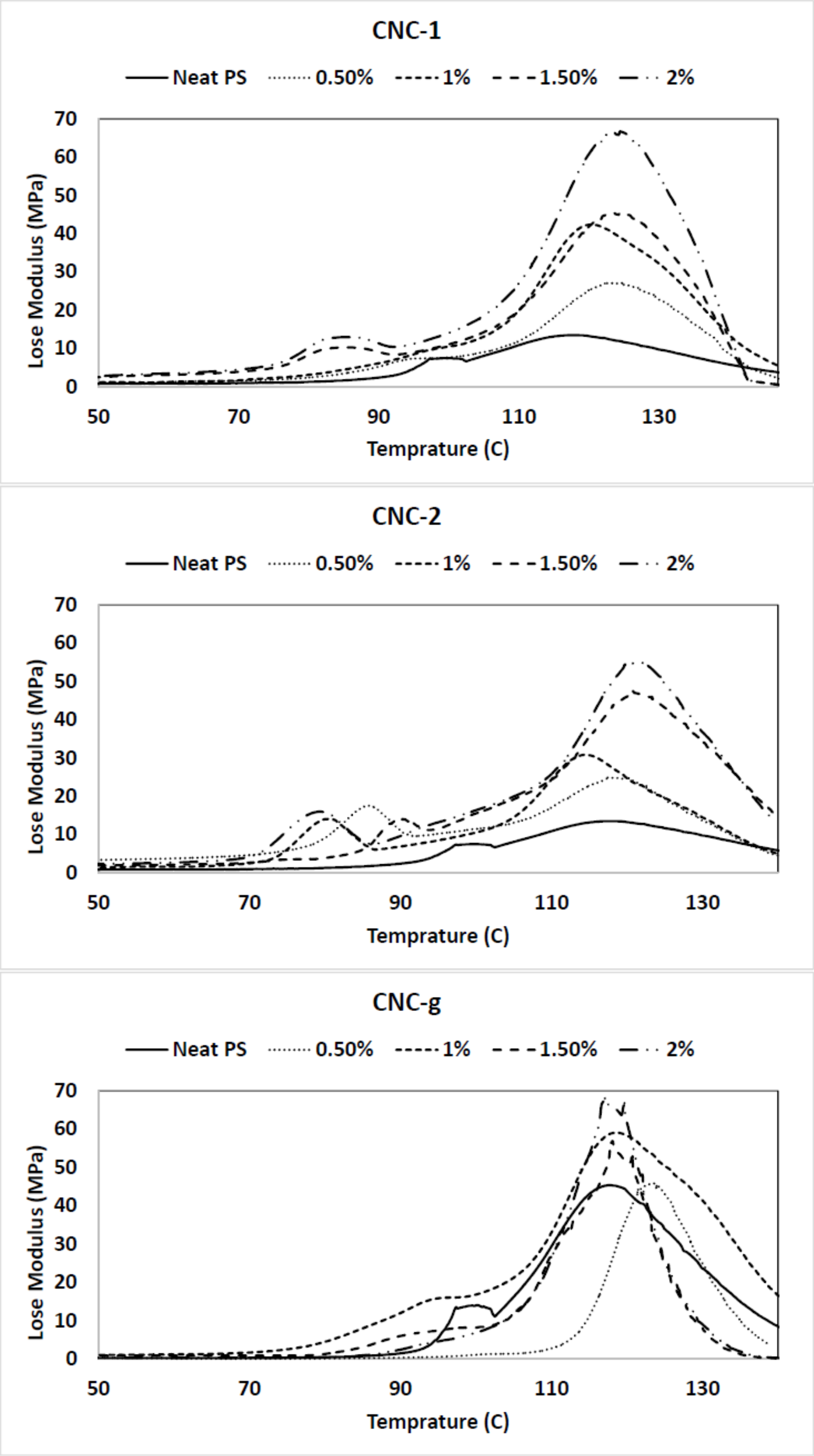

Figure 4. 28: Loss moduli of non-oriented PS fibrous mats containing different CNCs

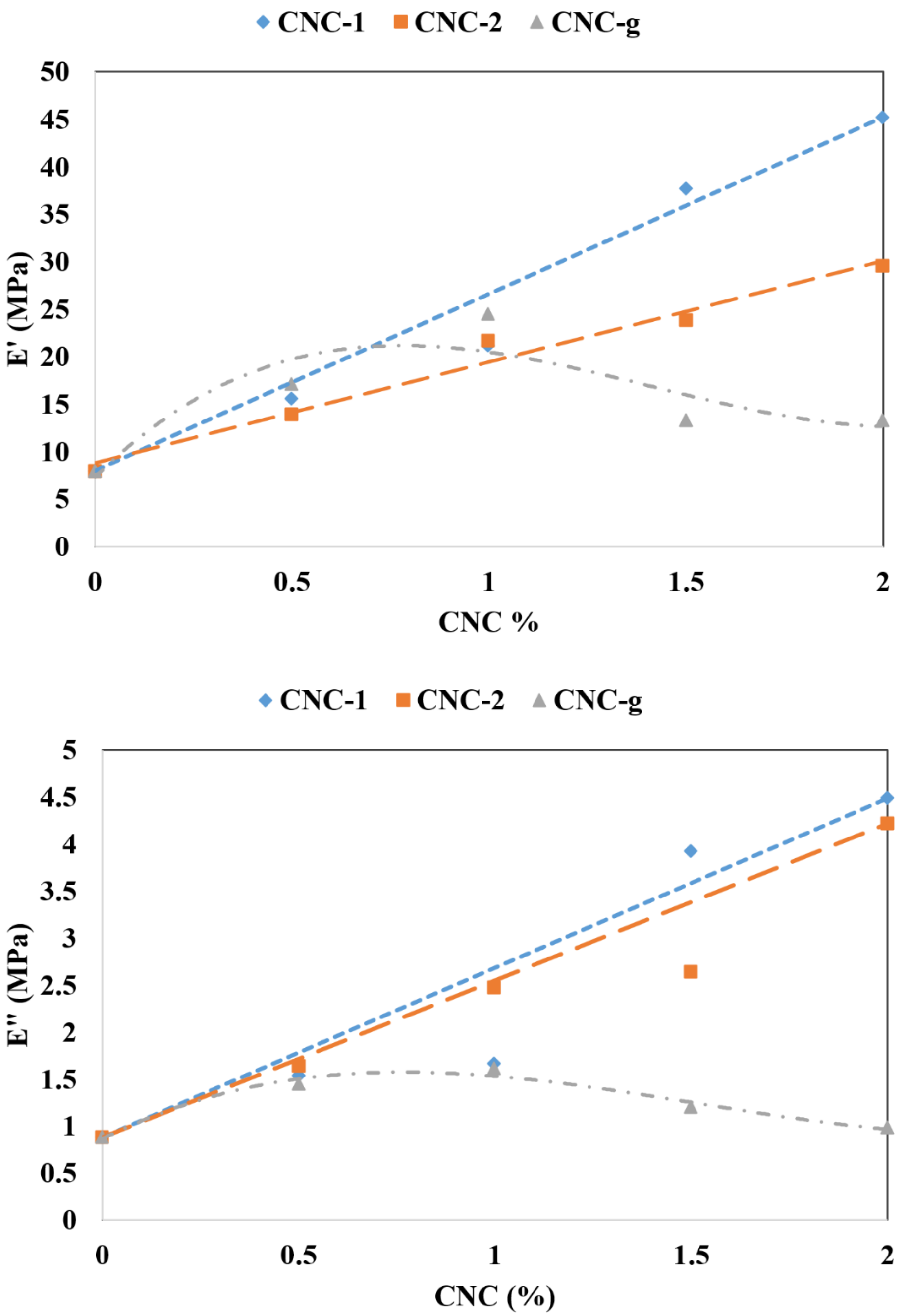

Randomly Oriented

Figure 4. 29: Storage and loss moduli of the CNC/PS electrospun samples at 70º C

The loss modulus was also observed to increase along with the inclusion of CNC, as shown in Figure 4.28. When the composites were subjected to external stress, energy was dissipated by frictions between CNC–PS interactions. The inclusion of CNC showed some transition peak in loss moduli, which indicates that the inclusion of CNC affect the relaxation behavior of PS significantly. The relaxation transition peak shown in E″ around 110-130 °C is thought to be related to a complex multi-relaxation process which is mainly concerned with their different dimensions of fibers and packing density in electrospun structures. This can influence on the densification rate of the samples as well as glass transition points of the samples (Akabori et al. 2005).

The damping factor or tan δ is the ratio of the loss modulus to the storage modulus. Figure 4.30 presents the tan δ curves of the CNC/PS and neat PS electrospun samples. It was found that the CNC/PS samples showed a slightly lower damping than neat PS sample, owing to the higher fiber–PS interaction (Boluk and Schreiber H 1986). Considering Figure 4.30 and Table 4.6, it is also obvious that the inclusion of CNC-1 or CNC-2 increased the peak position of tan δ. This reflects the restriction effects of CNC to the relaxation of the PS chains as well as lower packing densities of samples containing CNC due to their larger fibers. The same results were reported for the nylone electrospun samples. Tg shifted to higher temperatures with inclusion of CNT (Baji, Mai, Wong, Abtahi, and Du 2010). In another research, incorporation of nano-hydroxyapatite also increase the Tg of poly(D,L-lactide-co-glycolide) (Jose et al. 2009). The same Tg changes were observed for the other randomly oriented electrospun samples with CNC contents and, Tg in the PMMA electrospun samples increased from 119ºC to 123ºC with 5 wt. % CNC content (H. Dong et al. 2012). However, there were cases that Tg decreased by CNC inclusion. Peresin et al. showed a decrease of 15 degree in Tg as result of 5 wt. % inclusion of CNC in PVA (M. S. Peresin et al.

2014). Finally, it can be also seen that inclusion of CNC-g has a negligible influence in Tg transition in comparison with CNC-1 or CNC-2. This can explain by higher flexibility of grafted PS chains with CNC in comparison with small modified pendant groups of NO2 and CF3 in the cases of CNC-1 and CNC-2 respectively. However, samples containing 2 wt. % CNC-g shows an increase in Tg which can be explained by agglomeration of CNC and bead formation. Existence of the beads or thicker fibers can result in the lower packing density. It is hypothesised that samples with lower packing densities have higher air content acting as the heat insulation, making heat transfer difficult through the sample, and increasing the Tg (for instance Tg of PS films were around 90°C).

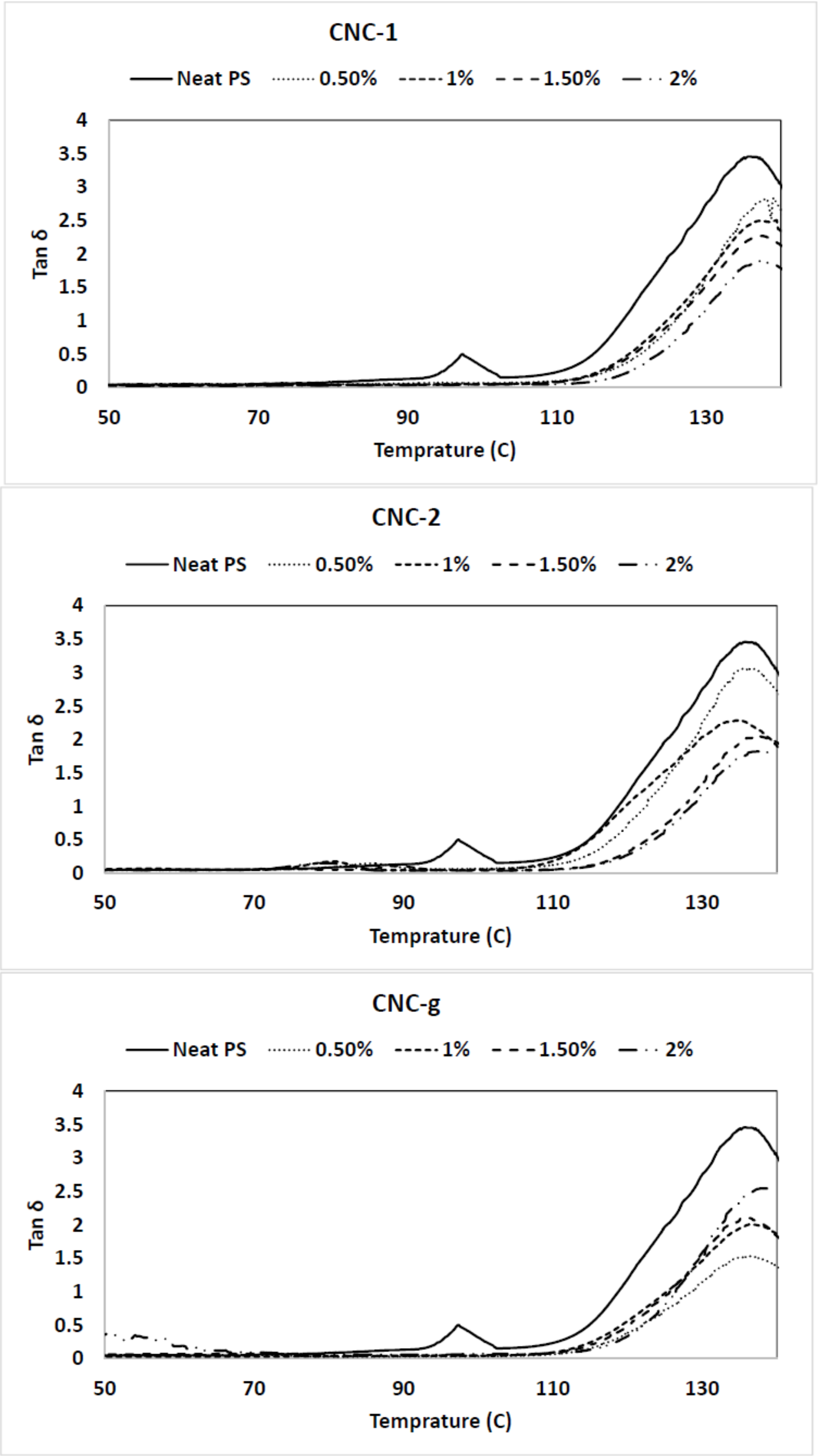

Figure 4. 30: Tan δ results of non-oriented PS fibrous mats containing different CNCs

Table 4. 6: Tan δ and Tg of electrospun samples containing various types of CNCs

CNC Type	Percentage	Tan δ	Tg
Neat PS		3.45	135.32
CNC-1	0.50 wt. %	2.87	138.22
	1 wt. %	2.49	137.73
	1.50 wt. %	2.26	137.97
	2 wt. %	1.89	137.27
CNC-2	0.50 wt. %	3.06	136.49
	1 wt. %	2.28	134.99
	1.50 wt. %	2.05	137.45
	2 wt. %	1.82	137.52
CNC-g	0.50 wt. %	1.53	136.63
	1 wt. %	2	136.07
	1.50 wt. %	2.1	136.7
	2 wt. %	2.58	137.57

4.4. Conclusion

In this chapter, we investigated the production of CNC reinforced PS fiber mats. To improve the interfacial interaction of CNC with PS matrix, CNC nanoparticles were first modified by different functional chemical groups. In this work, three different types of modified CNC were used. The modifications included replacement of hydroxyl groups through substitutive reactions with the para nitro benzene, three fluorocarbon benzene, and grafted PS chains. Then, these modified CNCs were used to reinforce PS fibers that were produced using electrospinning technique. Five different loading levels of CNC (0, 0.5, 1, 1.5, 2 wt. % in solid fiber corresponding to 0, 0.01, 0.02, 0.03, 0.04 w/v % CNC dispersion in PS solution) were investigated. Solutions were prepared using DMF as the solvent (20 wt. % of PS (Mn= 250000) was dissolved in DMF). The effects of modifications on the fiber morphologies were studied through SEM images. Subsequently, results obtained from SEM images were also evaluated by turbidity, conductivity and viscosity of electrospinning solutions. Fibers were initially analyzed for morphological properties. The CNC modified with para nitro benzene and para three fluorocarbon benzene resulted in smoother fibers structure and an increase in fibers diameter. On the other hand, beaded fibers, with smaller diameters, were obtained by adding CNC grafted with PS. Finally, mechanical properties of the produced electrospun mats of these fibers were studied by means of tensile tests, and DMA. The reinforcing effects of CNC on the elastic modulus, strength and maximum strain of the electrospun mats were investigated. The nonwoven PS mats with 0.5 wt. % CNC grafted with PS resulted in the best mechanical gain. The elastic modulus (E) and strength increased 820% and 337%, respectively; however, maximum strain decreased 36% compared to the non-reinforced mats. DMA results shown the similar trends to tensile results. CNC inclusion decreased Tanδ magnitudes, shifted the glass temperature to the higher temperature. These resulted were explained with interfacial interaction of modified CNC with PS matrix.

Chapter 5

5. Production and mechanical properties of oriented CNC/PS nano fibrous mats

5.1 Introduction

The main objective of this chapter is the fiber collection in an oriented / alligned pattern to improve the final mechanical behaviour of the electrospun PS webs. As discussed previously, improvement of the mechanical properties in the electrospun PS structures is the main objective of this project, so production of homogenous or beads free fibers, and incorporation of cellulose nanocrystals (CNC) were performed to do so. Besides, orientation of the fibers was considered in this chapter as an additional influence on the improvement of the final mechanical properties of the electrospun PS product, similar to (Mathew et al. 2006; J. Lee and Deng 2012). To that end, an electrospinning technique with a rotating drum was replaced with the stationary collector, used in the chapter 4. Figure 5.1 shows a schematic image of this system.

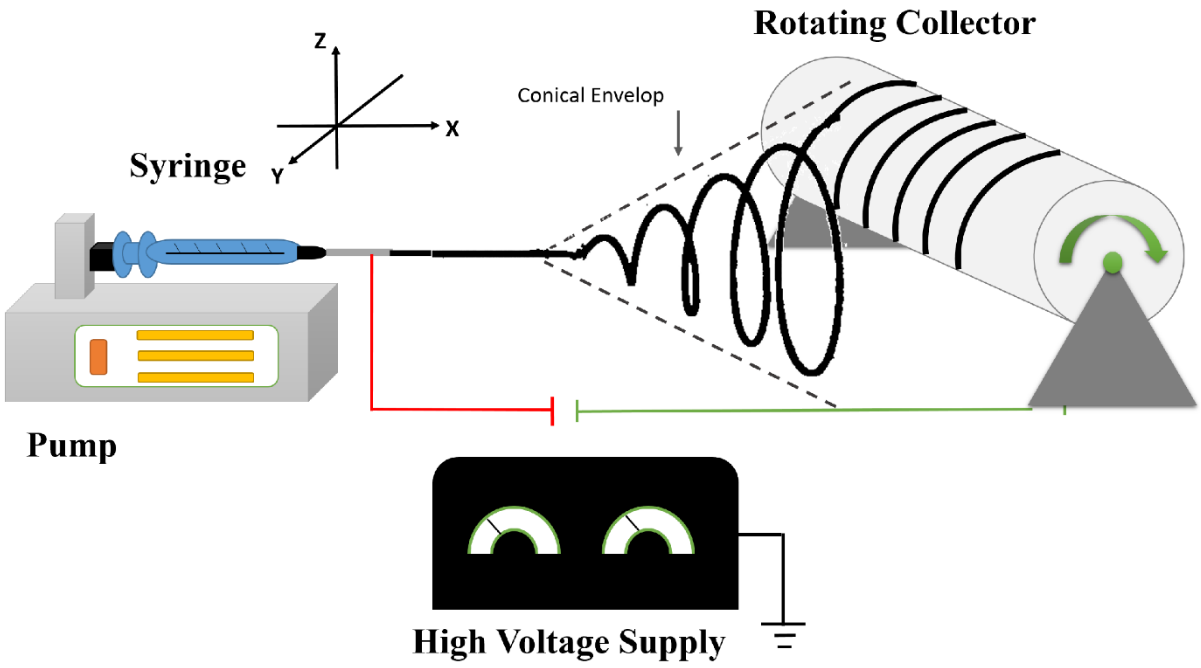

Figure 5. 1: Electrospinning system equipped with rotating drum

The major objectives of this chapter are the following: a) to discuss the mechanism behind the electrospinning system equipped with a rotating drum, and to demonstrate the potential of the rotating drum technique in producing fibers with aligned structures; b) to address experimental effects of rotating drum speed on the final morphology of the electrospun fibers; c) to assess the influences of the fiber alignment on the final tensile mechanical properties; and d) to evaluate the dynamic mechanical properties of the electrospun samples.

Three dimensional arrangements of fibers can improve the functionality of the electrospun products in various application. Hence, it is necessary to devise new techniques that make the fabrication of the desired fibre assemblies, possible (Teo and Ramakrishna 2006; Baji, Mai, Wong, Abtahi, and Chen 2010). Among several possible assemblies for electrospun fibers, aligned fibrous structure is the most common assembly for various purposes, such as bacteria cultivation (C. Xu et al. 2004), nanowires (Bashouti et al. 2006) and mechanical improvement (Mathew et al. 2006;

J. Lee and Deng 2012). As Table 2.1 shows techniques like rotating drum (Mathew et al. 2006; Wannatong, Sirivat, and Supaphol 2004; J. Lee and Deng 2012), parallel electrodes (D. Li, Wang, and Xia 2003), rotating wire drum collector (Katta et al. 2004), disc collector (Theron, Zussman, and Yarin 2001; C. Y. Xu et al. 2004), and array of counter-electrodes (D. Li and Xia 2004) that were all devised to create aligned structures in electrospun products.

Orientation inducing techniques can be divided into electrostatic and mechanical methods. In the first approach, collectors were designed in a way to induce electrostatics forces in specific directions, which is causing fiber depositions in a particular pattern. Dersch et al. produced oriented polyamide fibers on a metal frame as the collector. They attributed the orientation of the fibers to the polymer jet jumping from one side of the frame to the other side, obviously due to the electrostatic charging effects (Dersch et al. 2003). In another attempt, Zussman et al. achieved alignment in small regions by the use of a sharp needle, due to the same mechanism. However, the second (mechanical) approach or a combination of mechanical and electrostatic techniques are more convenient because larger and thicker samples can be made using these techniques (Teo and Ramakrishna 2006). Rotating drum is the most convenient mechanical technique to collect aligned fibers. In this technique, a substrate is rotated with a high speed (Sundaray et al. 2004). Speed of the rotor was found as the most effective factor on the fiber alignment. Matthews et al. demonstrated that just a random mix of collagen fibres was collected at a speed of less than 500 rpm. However, the collagen fibres showed significant alignment along the axis of rotation when the rotating speed of the mandrel was increased to 4500 rpm.

Rotating speed of the collector can effect the molecular orientation and crystallinity of the constitutive polymer or polymers of electrospun materials as well as fiber morphologies (Baji, Mai, Wong, Abtahi, and Chen 2010).

In electrospinning, the molecular orientation can be induced as result of the high elongation strains and shear forces during the process, and the macromolecular chains orientate along the fiber axis (Wong, Baji, and Leng 2008; K. Kim et al. 2004). It is also expected that crystallinity degree can be effected in case of rotating drum (Kongkhlang et al. 2008). Lower crystallinity in electrospun fibers is expected due to the rapid evaporation of the solvent, and less time for the realignment of the polymer chains in crystalline unites (Z. M. Huang et al. 2003). Contrarily, Lee (K. H. Lee et al. 2002), and Renker (D. H. Reneker et al. 2002) reported that the crystalline structure in fibers is developed in many polyesters and ductile materials at higher mandrel speeds. However, atactic PS cannot crystalline due to lack of packing ability for styrene pendant groups, so PS excluded from this influential case.

In points of fiber structure, fiber diameters commonly decreases at higher speeds of the mandrel; however after an optimum speed of the drum, thicker fiber can be obtained due to the fiber breakage at high speed (Thomas et al. 2006). Several papers reported the bead removal at higher velocity of the rotating drum which can be explained by an increasing elongational drawing force suppressing Rayleigh instability (Yu, Fridrikh, and Rutledge 2006; Wannatong, Sirivat, and Supaphol 2004).

Improvement of mechanical properties of electrospun mats as the other main influential factor of fiber orientation is aimed to discuss in this chapter. Uniaxial, oriented fibers have anisotropic tensile behaviours. Resulting in the higher tensile strength and modulus compared with the randomly oriented fibers (C. Huang et al. 2006). This issue can be explained by the equal distribution of the tensile force when the electrospun mats have oriented fiber in the loading direction. Moreover, the shear and elongation forces can intensify the alignment of the polymer chains in the fiber axis direction. Higher speed of the collector can also increase the stacking density of the fibers, and decrease the inter-fiber spacing. This can be also attributed to the thinner fiber obtained at higher speeds of drum. Furthermore, the fibers have more uniform diameter and morphology at higher rotational velocities. All of the above mentioned factors can contribute towards a better tensile performance of an electrospun samples (H. S. Kim et al. 2005).

Besides tensile properties, dynamic mechanical properties of the electrospun sample can be evaluated by means of dynamic mechanical analysis (DMA). This technique not only can examine the dynamic mechanical properties, but also can evaluate the interfacial interaction of the nanoparticles with polymer matrix.

Several researches reported the thermal and mechanical properties of the electrospun samples using this technique (Gonçalves et al. 2017; Ago, Jakes, and Rojas 2013; Shirole et al. 2016). This technique were used to investigate the influence of all types of nanoparticles incorporation in electrospun samples (Corcione and Frigione 2012; Elkhaldi, Guclu, and Koyuncu 2016; Koosha et al. 2015). There are also several papers reporting the mechanical improvement of CNC electrospun samples (Bellani et al. 2016; H. Dong 2015). The effects of CNC as a reinforcing agent were tested on the storage modulus of several nanocomposite fibers at temperatures either above or below Tg. For instance, the storage modulus of polycaprolactone fibers containing various percentages of CNCs was evaluated, and a significant increase in the storage modulus was reported in PCL fibers with 2.5 wt. % and 7.5 wt. % loadings of unmodified CNCs compared with the neat PCL. However, the reinforcement of the sample with 2.5 wt. % CNCs was not only attributed to the CNC but also to the smaller fiber diameters and higher inter-fiber bonding area. The higher storage modulus of the sample with 7.5 wt. % CNC was atributed to the reinforcing contribution of CNCs within the fiber, despite the larger diameter of the PCL fiber in this sample (Zoppe et al. 2009). In another research, electrospun mats with oriented fibers of PEO/CNC were prepared with different CNC contents (5 wt. %, 10 wt. %, and 15 wt. %). The reinforcement influences of CNCs on the PEO fiber storage moduli were 1.5–2 times greater than the neat PEO fiber sample. It should be noted that the effect of interfiber bonding on the mechanical properties of the oriented samples can be largely eliminated due to the disconnection among the fibers in the transverse direction (Changsarn et al. 2011).

The performance of composites materials is usally controlled by the properties of an interfacial region. To ensure the load transfer from matrix to reinforcement agent, a good interface bonding is a key requisite to benefit of reinforcing nanoparticles. Among many methods for interface characterization, dynamic mechanical analysis was the most frequent technique, because it offers two types of response to a low-strain periodic deformation, an elastic and a damping term. The damping term can show all types of molecular motions in a material. The interfacial molecular motions mostly contribute to the damping of the material aside from those of the nanoparticles and the matrix in a nanocomposite. Therfore, the magnitude of the damping at the interfaces will be an quantified estimation of the interface bonding (S. Dong and Gauvin 1993; Boluk and Schreiber H 1986). This evaluation method is usually considered for the composites with continous structure. However, for electrospun samples just few reserches used this technique as a evaluation method of interfacial interaction. Lin et al. evaluated the interfacial interaction of the PAN core–PMMA shell fibers with PAN matrix using DMA, and a decreasing damping term were considered as a demonstartion of the interfacial interaction (S. Lin et al. 2008).

Finally briefly describing, several objectives were covered in this chapter. Firstly, production of electrospun mats with oriented fibers was intended to improve the final mechanical properties, and a rotating mandrel was devised as a collector to do so. Afterward, the mechanism behind the alignments of fiber on the rotating drum was studied to estimate the exact rotational speed resulting in the maximum orientation of the fibers. To that end the impinging velocities of the jet were calculated, and the velocity of the drum was estimated accordingly. Moreover, as a new approach, the fiber morphological changes were explained based on the changes of the rheological properties of the electrospinning jet at different rotational speeds, and different modified CNC contents. Finally mechanical properties of the oriented electrospun were examined using both tensile test and DMA, and as a novel approach, DMA results were evaluated to estimate the interfacial interaction between the CNC and PS .

5.2. Experimental

5.2.1. Materials

Rod-shaped cellulose nanocrystal (CNC) particles, which were prepared by sulfuric acid hydrolysis of kraft pulp and subsequently neutralized by NaOH in Innotech Alberta's CNC pilot plant were used in this study. The width (w) of rod shaped CNC particles were uniform and measured easily as 8+2 nm from STEM pictures. The length of CNC particles was calculated as 214 nm, by assuming the shape of CNC particles was cylindrical and measuring the translational diffusion coefficient (Dt) from DLS and particle diameter from STEM pictures (Boluk and Danumah 2014; Oguzlu and Boluk 2017). Sodium hydroxide, 4-Bromoaniline, 4-Nitroaniline, 4-(Trifluoromethyl)aniline, Styrene, Tetrafluoroboric acid solution (48 wt. % in H2O), L-asacorbic acid, Acetonitrile, Diethyl ether, Dichloromethane (DCM), Tetrahydrofuran (THF), Chloroform (CF), Dimethyl formaldehyde (DMF)as solvent, and Polystyrene (PS) (MW = 280,000 g/mole, Tg = 100 °C) as fiber material used in this project were all purchased from Sigma Aldrich, Inc. All materials were used without further purification.

5.2.2. Precursor diazonium salt synthesis

The diazonium salts were synthesized according to a published procedure (Solak et al. 2003). Firstly, an appropriate aniline solution of 4-bromoaniline, 4-nitroanailine, or 4-trifluoromethyl (0.1 M) was prepared and mixed to 50 ml floroboric acid (48 wt. %). Afterward, the solution was cooled in an ice water bath to 0 ºC, and sodium nitrite solution in DI water (50% W/V) was added drop by drop with stirring. The reaction mixture was further cooled in an ice water bath and stirred for another hour. The resultant precipitate was finally filtered in a Buchner funnel and washed with cold anhydrous Diethyl ether.

5.2.3. Synthesis of Nitrobenzene modified CNC (CNC-1) and Trifluoromethyl benzene CNC(CNC-2)

1.0 wt. % CNC suspension was prepared by dispersing CNC in DI water using an ultrasonic treatment in an ultrasonic cleaner (CREST Ultrasonics Corp., model-275T) for 5 min. After that, 0.01 mole of prepared diazonium salts (4-nitrobenzenediazonium tetrafluoroborate or 4-(trifluoromethyl) benzenediazonium tetrafluoroborate) were added and dispersed in 200ml 1.0 wt. % CNC suspension under sonication treatment for 5 min. Then 20 ml of L-ascorbic acid solution (0.05 M) was added to the mixture and kept under sonication for 1 h. The resulting suspension mixtures were then transferred to a centrifugal filter unit (10,000 molecular weight cut-off, Amicon Ultra-4) to collect modified CNC from solution. The modified CNCs were further cleaned by rinsing with acetonitrile and centrifuging three times. Finally, the product was re-dispersed in DI water and freeze-dried using a FreeZone 4.5 Plus apparatus from Labconco Corporation (Kansas City, Missouri).

5.2.4. Synthesis of grafted PS CNC(CNC-g)

Firstly. 0.005 mole of 4-bromobenzenediazonium tetrafluoroborate was added and dispersed in 100 ml of 1 wt. % CNC suspension under ultrasonic treatment for 5 min. Afterward, 10 ml of L-ascorbic acid aqueous solution (0.05 M) was added to the mixture, and the resultant mixture was again kept under ultrasonic treatment (or stirring) for another hour. Subsequently, 0.5 g of styrene (NaOH treated) was sonicated in ~150 ml H2O. The generated Styrene/water emulsion was then mixed with the CNC /Diazonium dispersion in a beaker and kept stirring for extra hour.In between, another 0.005 moles of 4-bromobenzenediazonium tetrafluoroborate and 10 ml of 0.05 M aqueous l-ascorbic acid were added to the mixture. The final mixture kept under stirring overnight. The grafted CNC was then centrifuged with a centrifugal filter unit, rinsed with acetonitrile, and re-dispersed in water. Finally, it was freeze-dried as the procedure described previously in section 4.3. Chemical structure of modified CNC was depicted in Table 5.1.

Table 5. 1: Characteristics of electrospinning solutions containing modified or unmodified CNCs

Sample	Chemical Structure of modified CNC	PS concentration (w/v%)	CNC concentration of PS (wt. %)	CNC concentration in solution (w/v %)	Conductivity (µs/cm)	Viscosity (Pa.S)
Neat PS		20	0	0	0.67	0.21
Neat PS		30	0	0	0.67	0.65
CNC-1	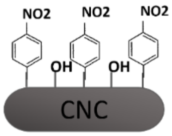	20	0.5	0. 1	2.83	-
		20	1	0. 2	7.65	-
		20	1.5	0. 3	12.78	-
		20	2	0. 4	14.23	0.23
CNC-2	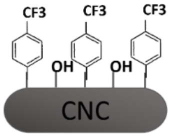	20	0.5	0. 1	5.6	-
		20	1	0. 2	14.12	-
		20	1.5	0. 3	20.43	-
		20	2	0. 4	22.6	0.23
CNC-g	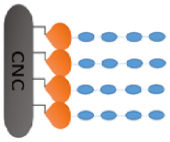	20	0.5	0. 1	2.76	-
		20	1	0. 2	9.52	-
		20	1.5	0. 3	18.32	-
		20	2	0. 4	21.17	0.23
CNC-R	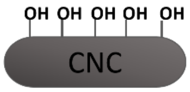	20	0.5	0. 1	0.87	-
		20	1	0. 2	0.92	-
		20	1.5	0. 3	0.98	-
		20	2	0. 4	1.124	0.22

5.2.5. Electrospinning process

Electrospinning solution was prepared with 20% or 30% (w/v) PS and various concentrations of modified CNCs in DMF. Table 5.1 shows a list of polymer solutions applied for electrospinning.

In the electrospinning system, a 10 ml BD plastic syringe were connected to a syringe pump via tubing and connectors. The syringe was attached to a mechanism that is on traversing belt (moving to the left and right) to collect more uniform fibrous mats. The inner diameter of the needle for this type of syringe is 0.05 mm, and the distance of needle to the collector were adjusted to 15 cm. Electrospinning was performed with constant flow rate of 10 μL/min. The tip of the needle was connected to a high voltage supply with constant voltage of 20 KV to generate the charge in polymer solution, and the collector was grounded, on the other side. As Figure 5.1 shows, the electrospinning system is equipped with a rotating drum. This rotating drum helps produce aligned fibers (Xu et al 2004). The rotating drum has a diameter of 10 cm and a length of 40 cm. Five constant speeds of 500 RPM, 1000 RPM, 1500 RPM, 2000 RPM and 3000 RPM where considered to evaluate the rotating drum speed (V_D) effects. According to the diameter of the drum and Equation 5.1, these drum speeds are equivalent to 2.62 m/s, 5.23 m/s, 7.85 m/s, 10.47 m/s, and 15.7 m/s, respectively.

$$V_D\left(\frac{m}{s}\right) = \frac{2\pi r W_D\,(RPM)}{60} \qquad \text{Equation 5. 1}$$

Where r is the radius of the drum, W_D is the frequency of rotation (Revolutions per minute (RPM)).

5.2.6. SEM analysis

Both surface morphology and structures of fibers and their diameters were analyzed using a scanning electron microscope (SEM) (Vega-3 (Tescan) with an EDXS detector (Oxford Instruments) at an acceleration voltage of 20 kV. SEM analyses of samples were performed without coating. To determine the average diameter of each fiber sample, five different spots on each specimen were selected for SEM analysis, and totally 100 fibers of each samples were measured to do so.

5.2.7. Solution conductivity measurement

The conductivity of both PS (20% or 30% wt.) solutions and CNC/PS solutions were measured by using a conductivity meter (Isteck Model 455C) at 25 °C. The CNC/PS solutions contained 2 wt. % (To PS content) of the modified CNCs.

5.2.8. Tensile properties evaluation

In this project, the tensile properties of the electrospun nanocomposites were measured with a BOSE tensile tester (model Electroforce 3200) with a 250 g load cell at ambient conditions. Tensile properties (Young's modulus, tensile strength) were determined using samples cut from electrospun mashes (50 mm long and 10 mm wide). The tests were conducted at a constant crosshead speed of 10 mm/min. In order to prevent the grips from direct contact with the mashes, end-tabs were used. At least 10 samples were tested for each condition.

5.2.9. Dynamic mechanical analysis

A Dynamic Mechanical Analyzer (DMA 2980 from TA Instruments) was applied to evaluate the thermomechanical properties of the neat and CNC reinforced fibers under tension as a function of temperature. The samples were cut into 5-mm width strips from the fibers mats collected on the rotating drum or stationary collector. All the tests were performed at 20 Hz frequency and with 1% strain. The sample gap distance was adjusted at 20 mm for all samples. The temperature range was room temperature to 150°C with a heating rate of 2°C/min.

5.3.Result and Discussions:

5.3.1. Evaluation of the morphology and the structure of aligned electrospun CNC/PS Fibers

5.3.1.1. Rotating speed and alignment of fibers

The alignment of the fibers were controlled using a rotating drum. If a loop of the electrospun fibers created in whipping area is picked up by a rotating drum with a certain amount of velocity, the loop can be pulled into straight, parallel segments aligned with the rotating direction of the drum (J.-S. Kim and Reneker 1999). Usually higher speeds are associated with higher alignments of fibers; however, at some point, the increasing drum speed can cause a negligible improvement or even a reverse outcome. Therefore, there is an optimum for rotor speed resulting in the maximum fiber alignments. Here, it is attempted to observe this optimum speed. Figures 5.2 and 5.3 show the neat PS fibers electrospun from 20% (w/v) PS and 30% (w/v) PS solutions in DMF, and collect at different velocities of drum. Similarly, electrospinning of samples containing 0.2% different types of CNC and 20% PS was performed at different rotor speed (see Figure 5.4-5.7). For all of these samples, higher speeds are associated with higher alignments of fibers, and as it can be seen in these Figures, more aligned fiber could be obtained at higher speeds. The whipping frequency of the jet is much higher than the rotation speed of cylinder and whipping jet is continuously impinging on the cylinder. Assuming DMF solvent is mostly evaporated, electrospun fiber impinges on the rotating cylinder at least in semi-rigid but deformable state. If the impingement speed of fiber jet is higher than linear surface speed of the drum, fibers will be randomly accumulated on the drum. As the RPM of the rotating drum is increased, the linear speed of drum exceeds the speed of incoming fiber jet and the electrospun fiber is taken up and drawn down by the rotating cylinder. Such a critical speed is called alignment speed.(Pavel Kiselev and Joan 2012; Z. M. Huang et al. 2003).

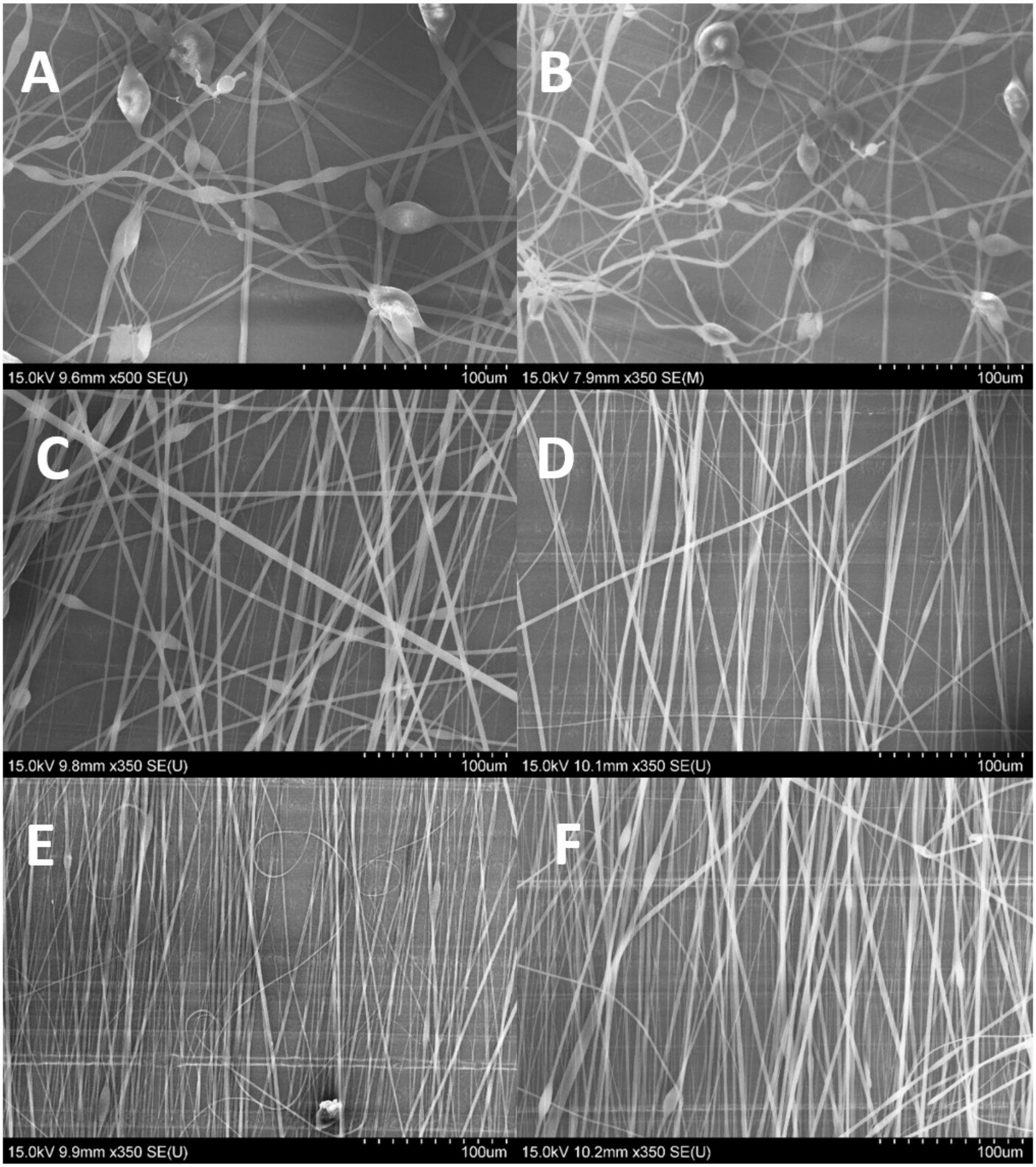

Figure 5. 2: Neat PS fibers electro-spun from 20% (w/v) PS solution in DMF, and at different RPM of rotating collector A) 0 RPM B) 500 RPM C) 1000 RPM D) 1500 RPM E) 2000 RPM

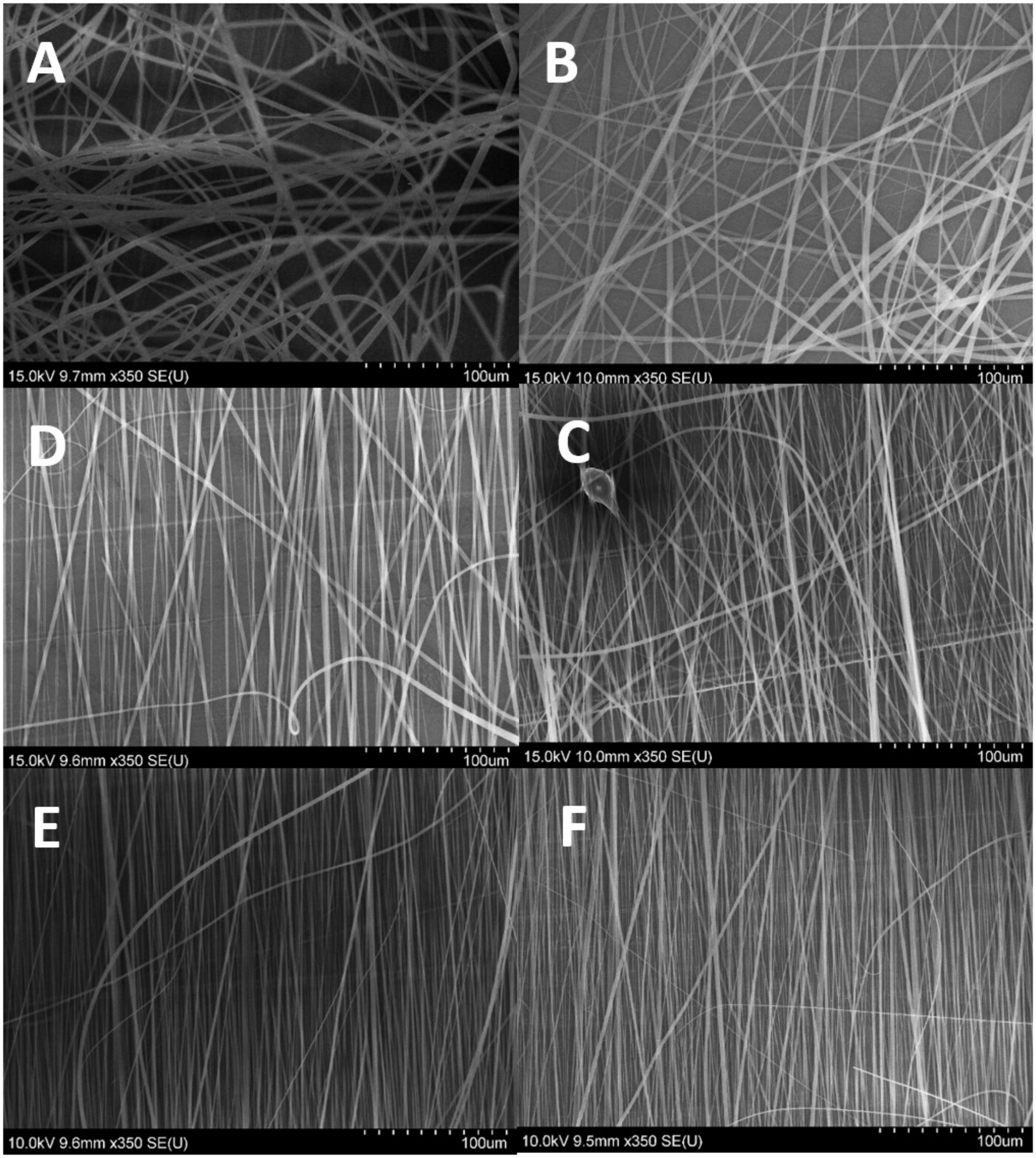

Figure 5. 3: Neat PS fibers electro-spun from 30% (w/v) PS solution in DMF, and at different RPM of rotating collector A) 0 RPM B) 500 RPM C) 1000 RPM D) 1500 RPM E) 2000 RPM

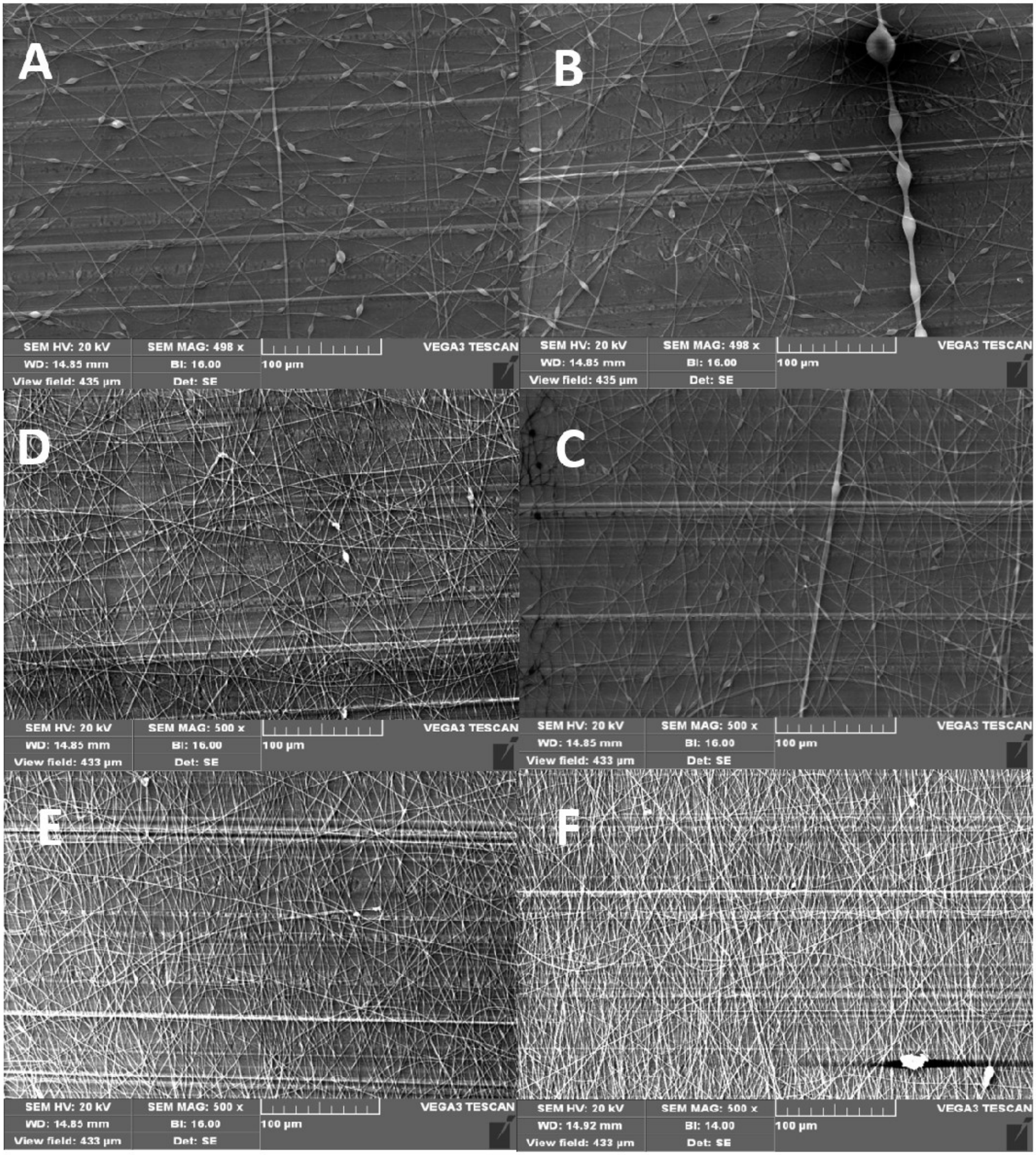

Figure 5. 4: PS fibers containing 1 wt. % CNC-1 electro-spun from 20% (w/v) PS solution in DMP, and at different RPM of rotating collector A) 0 RPM B) 500 RPM C) 1000 RPM D) 1500 RPM E) 2000 RPM

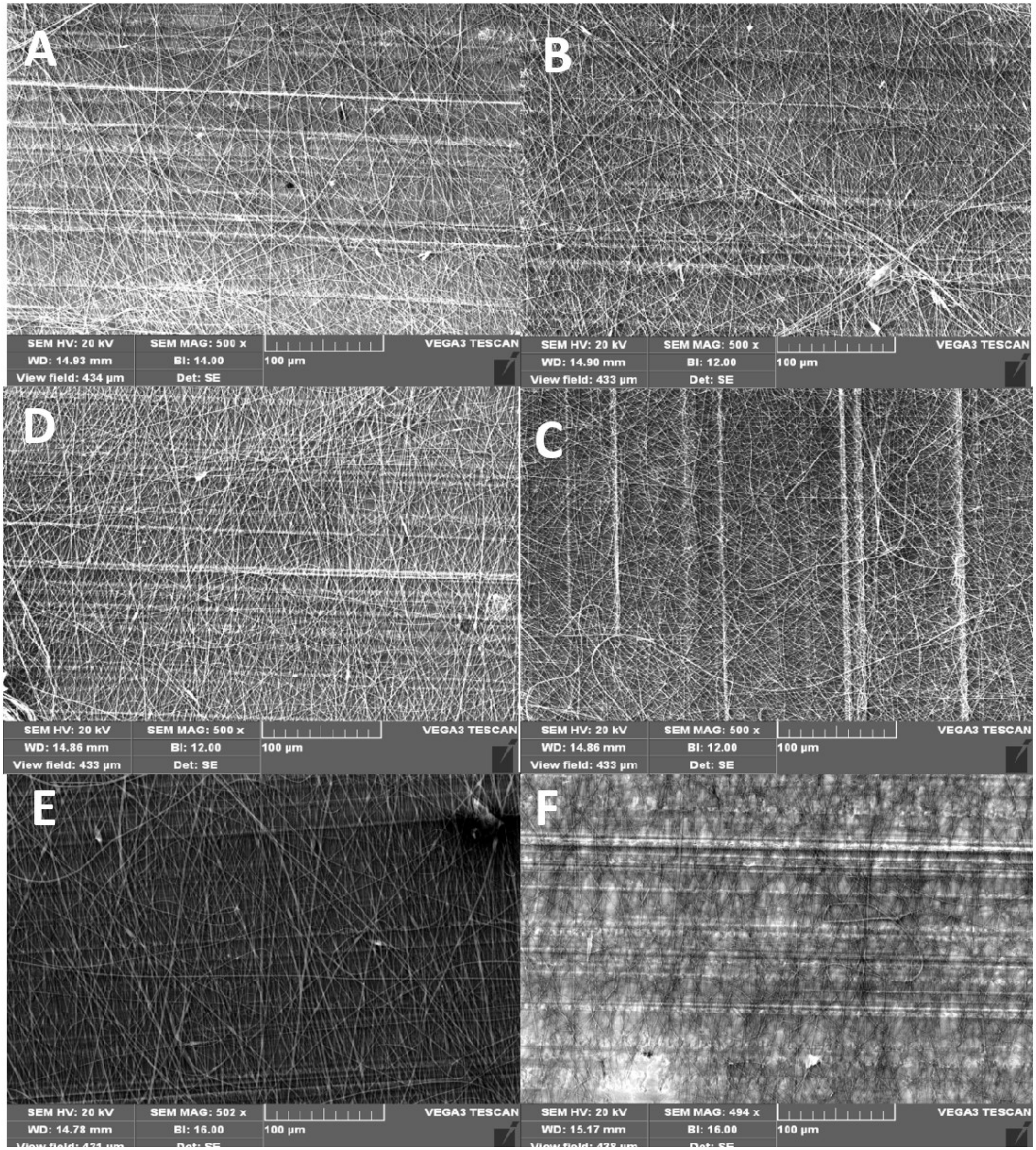

Figure 5. 5: PS fibers containing 1 wt. % CNC-2 electro-spun from 20% (w/v) PS solution in DMP, and at different RPM of rotating collector A) 0 RPM B) 500 RPM C) 1000 RPM D) 1500 RPM E) 2000 RPM

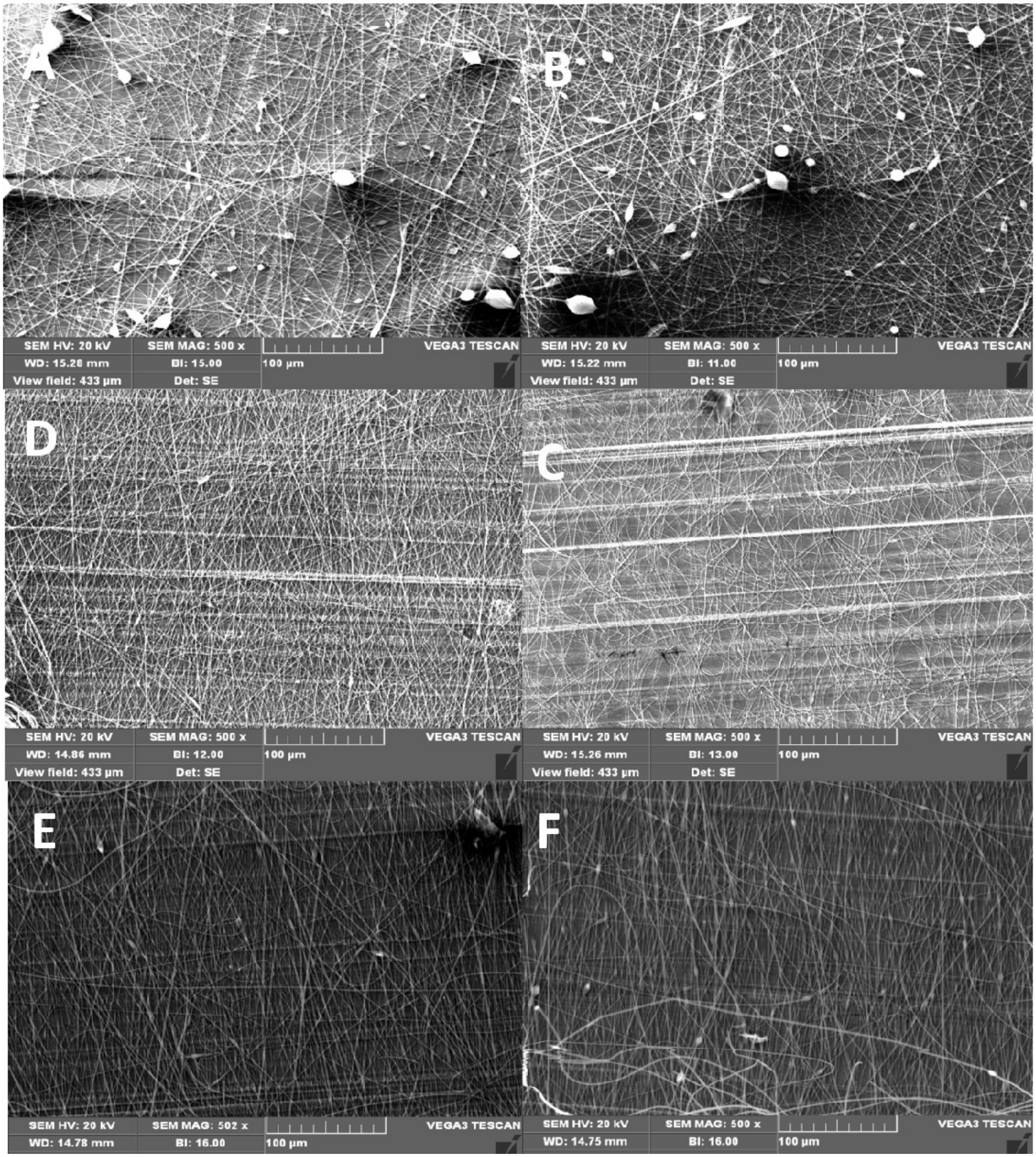

Figure 5. 6: PS fibers containing 1 wt. % CNC-g electro-spun from 20% (w/v) PS solution in DMF, and at different RPM of rotating collector A) 0 RPM B) 500 RPM C) 1000 RPM D) 1500 RPM E) 2000

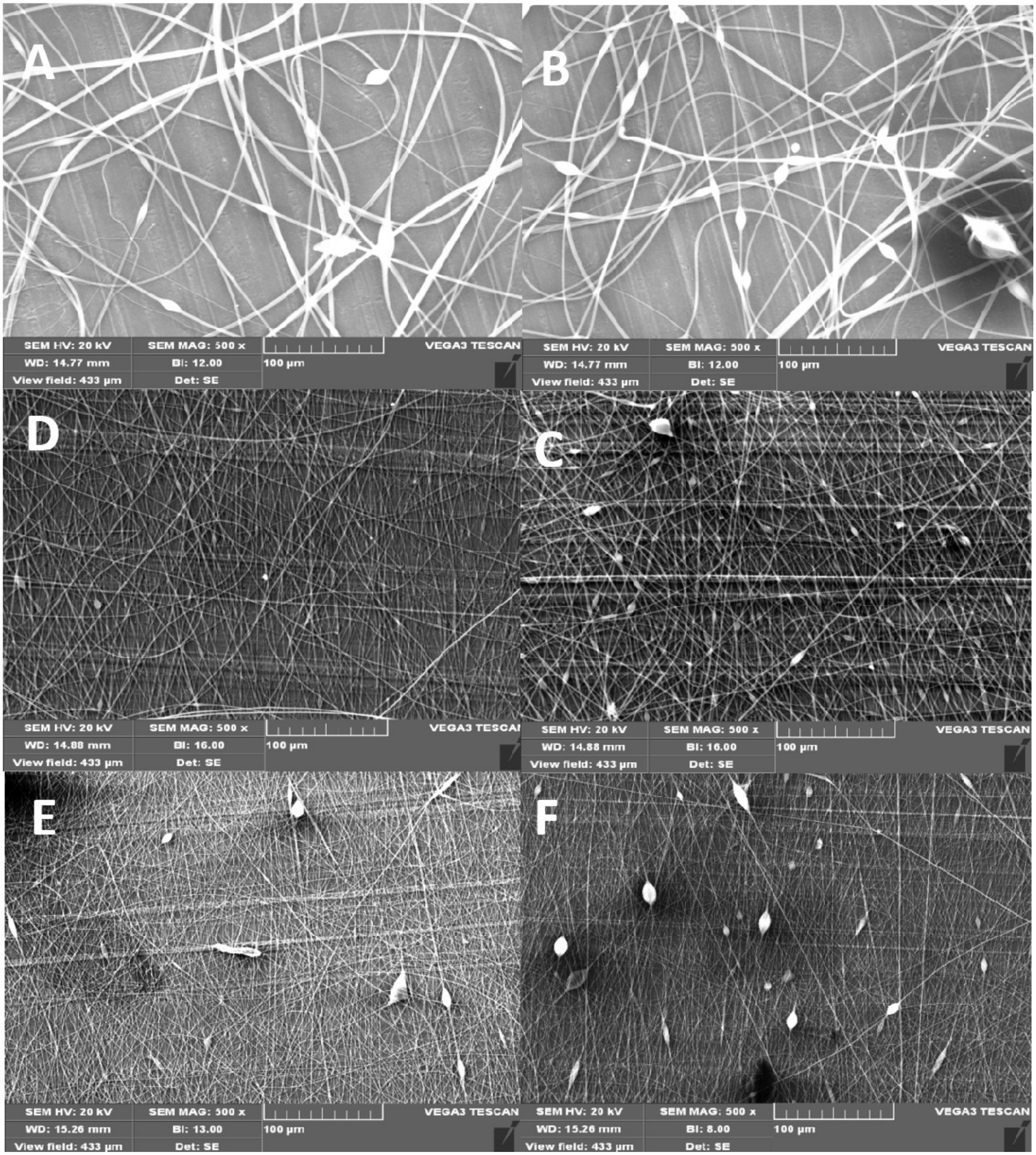

Figure 5. 7: PS fibers containing 1 wt. % CNC-R electro-spun from 20% (w/v) PS solution in DMF, and at different RPM of rotating collector A) 0 RPM B) 500 RPM C) 1000 RPM D) 1500 RPM E) 2000 RPM

Following the discussion on the rotating speed of drum and fiber pickup, the alignment of the collected fibers vs. the rotational speed of the drum was plotted for each sample set in Figure 5.8. The orientation of fibers on the drum in each sample set increased with the rotation speed and almost levelled of after alignment speed is reached. Maximum fiber orientation was reached with the rotation speed of 3000 rpm which corresponds linear speed of 15.7 m/s in the case of PS 20%, and PS 30% without any CNC and 20% PS with 0.2% CNC-R, CNC-1 in DMF solutions. On the other hand, in the case of 20% PS with 0.2% CNC-2 and CNC-g sample, the full linear alignment was not reached up at15.7 m/s. Hence approximately 16 m/s was called as the alignment speed for the 20% and 30% PS in DMF solutions without any CNC and 0.2% CNC-R and CNC-1 in 20% PS/DMF solutions. In the case of CNC-2/PS and CNC-g/PS fibers, the alignment speed was expected to be much higher than 16 m/s. In another electrospinning of PS in DMF, alignment speed of 6 m/s is reported (Pavel Kiselev and Joan 2012).

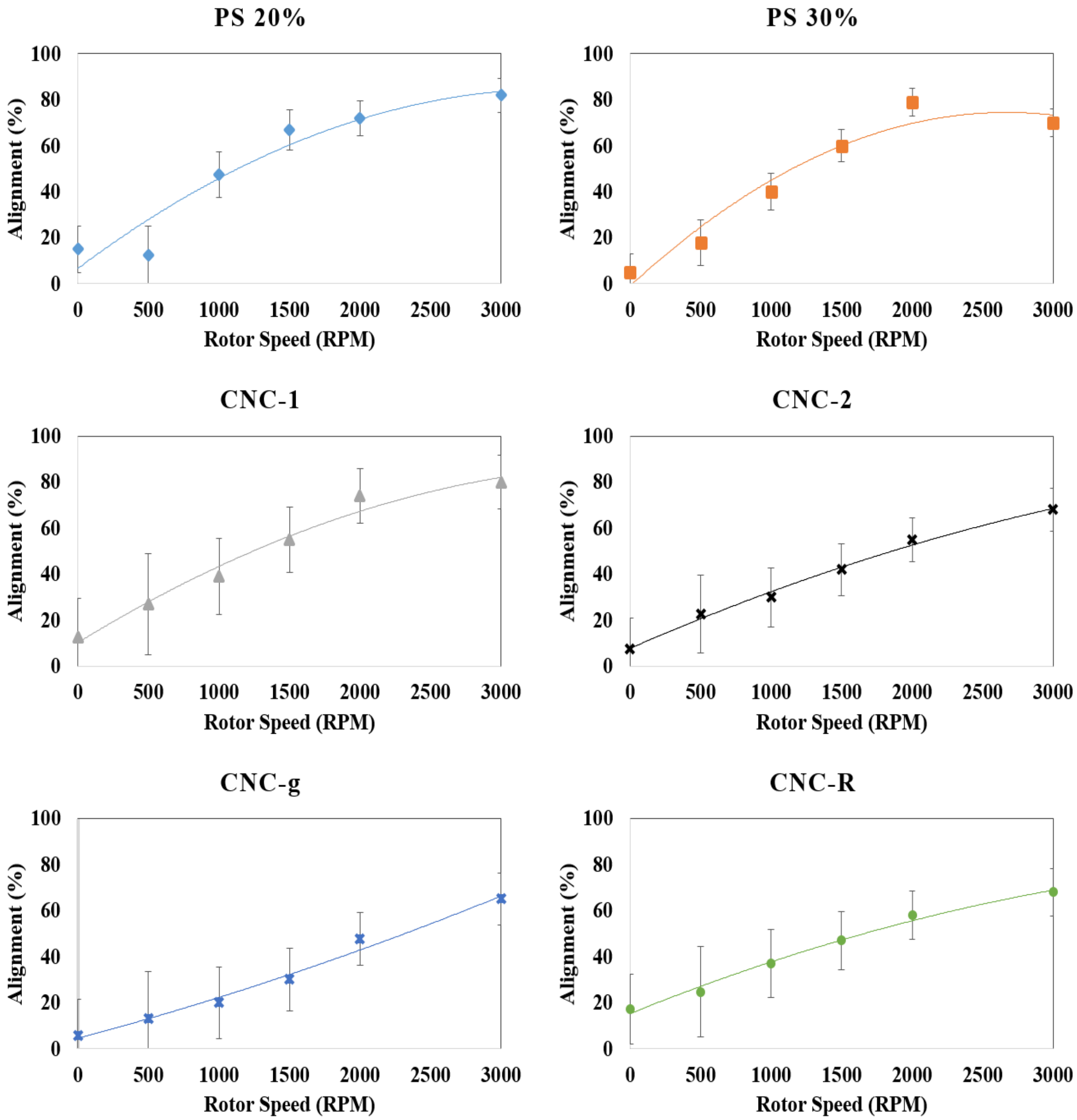

Figure 5. 8: Degree of alignment for the neat PS fibers and PS fibers containing 1 wt. % of differently modified CNCs at different RPM of rotating collector

Since CNC concentrations were very low (0.2%) in CNC/PS/DMF mixtures, it did not effect the shear viscosity of those samples, but caused big changes in the conductivities (Table 5.1). Therefore, the alignment speed can be discussed in terms of conductivity changes while the rest of electrospinning process parameter kept constant. As discussed before, the alignment speed was an indirect measurement of speed of fiber when it touches down onto the rotating drum. Hence, we can discuss the effect of conductivity of the PS/DMF and CNC/PS/DMF mixtures on the whipping velocity of fiber. As reported by Hohman et al., the current through the jet is proportional to the conductivity, therefore the surface charge on the jet increases linearly with the conductivity (Hohman et al. 2001a; Hohman et al. 2001b). Higher conductivity results in the suppression of the Rayleigh mode at lower field and increases the enhancement of the whipping instability. Among the measured samples, 0.2 % CNC-2 in 20% PS/DMF and 0.2% CNC-g in 20% PS/DMF mixtures had the highest conductivities (1412 µS/m and 952 µS/m respectively). Hence, we can argue that impinging speed on the substrate increases with an increase in the conductivity of electrospinning solutions when everything else is constant. However, our fiber impinging speed of around 15 m/s is an order of magnitude higher than the whipping jet's measured downward velocity of around 1.0 m/s and radial velocity of 0.5 m/s (Darrell H. Reneker et al. 2000). As these figures show, all beaded structures could be removed for some samples at some point of rotor speed. These results can be explained by an increasing elongational drawing force suppressing Rayleigh instability which is the main reasons of beads formation (Yu, Fridrikh, and Rutledge 2006). The same results were reported by Wannatong (Wannatong, Sirivat, and Supaphol 2004), and beaded structures disappeared at higher rotor speed.

5.3.1.2 Evaluation of the beaded structures

As it is shown in Figure 5. 2, samples prepared with 20% (w/v) concentration of PS in DMF are beaded when rotating drum is not applied. In comparison, the same concentration resulted in smooth structures in the system equipped with the stationary collector in chapter 4. As described previously, working distance in this new system can be maximum 15 cm which is less than 17 cm in the system with stationary collector. Lower working distance decrease the elongational forces needed to supress Rayleigh instabilities. Though, after some point of rotor speed, the beaded structures were removed due to the higher elongational force.

However, after some point of rotation speed, other forms of the beaded structure can be observed. In electrospinning process, to form an uniform filament in the absence of beads-on-a-string morphology, it is essential the relaxation time was enough long that elongated configuration of polymer chains can prevail (McKinley 2005). At higher rotor speed, elongational forces increase and their time of induction decrease, so elongated polymer chains prefer to restore their first polymer configuration as result of stress relaxation. Consequently, beads formed at very high rotor speeds can be mostly due to the stress relaxation; while, the first type of bead formation at lower rotor speeds can be mostly as a result of Rayleigh instability. Moreover necking can be another main reason of the bead formations in electrospinning. This phenomenon is usually explained by a strong stretching of solidified fibers by the tapered accumulating wheel, at very high rotation speed. In a study performed on electrospinning of PEO, necking showed for electrospun fibers collected on rotating collector; while it was not observed in the fibers collected on a grounded plate (Zussman, Rittel, and Yarin 2003)

Higher concentration of PS (30% (w/v)) resulted in smooth fibers. This can be describe by higher viscosity of polymer solution supressing Rayleigh instability (Yu, Fridrikh, and Rutledge 2006). Jarusuwannapoom and his team (Jarusuwannapoom et al. 2005) reported the same results at stationary collectors.

5.3.1.3 Fiber stretching and fiber radius

Figure 5.9 shows numerical measurements of the fibers diameters. Higher speeds of the drum are mostly associated with smaller diameters of fiber for all samples. These result can be explained by the higher elongational forces and consequently higher drawing ratio at higher speed of drum. However, at some point of the rotor speed, fiber diameters reach to a minimum value and did not decrease further with the additional rotor speed increase. We can define the fiber draw due to rotating drum as secondary draw (first one is during electrospinning process) and its draw ratio (DR) can be defined as the ratio of the collection rate to the feeding rate. Assuming no solvent evaporation, DR can be calculated according to $DR=(D_{initial}/D_{final})$ where D is the average diameter of fibers. According to the results in Figure 5.10 maximum DR ratio of 5 was reached. The fiber thickness change with rpm was more gradual in the case of pure 20%, pure 30% and 0.2% CNC-R in 20% PS/DMF solutions. However, 0.2% CNC-1, CNC-2 and CNC-g in 20% PS/DMF solutions gave more steep thickness drops with an increase in rotor speed and then levelled of.

In case of the 30% PS sample, an increase of fiber diameters can be observed at 3000 RPM which can be explained by possible jet breakages. The jet breakage can happen when a high rotor speed is applied due to the extremely high elongational forces. Therefore, thicker fibers can be collected on the drum. The other possibility can be explained by stress relaxation and bead formation, described previously. The same results was reported by Vinoy and his colleagues (Thomas et al. 2006) for polycaprolactone electrospun samples. However, they attributed their results to the increase of additional stretching of the polymer fiber besides the possibility of fiber breakages.

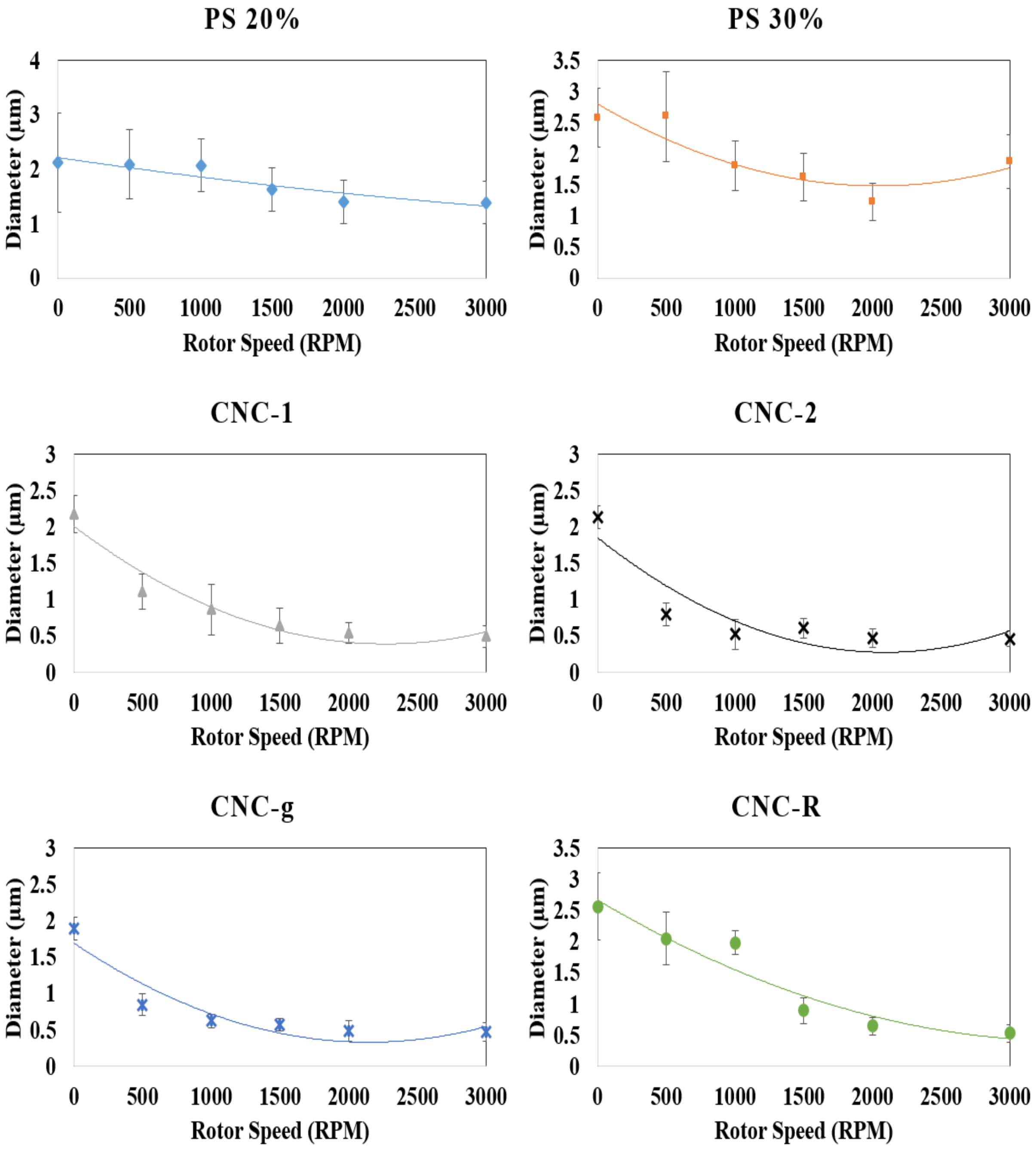

Figure 5. 9: Size of neat PS and PS fibers containing various types of modified CNCs collected at different speed of drum.

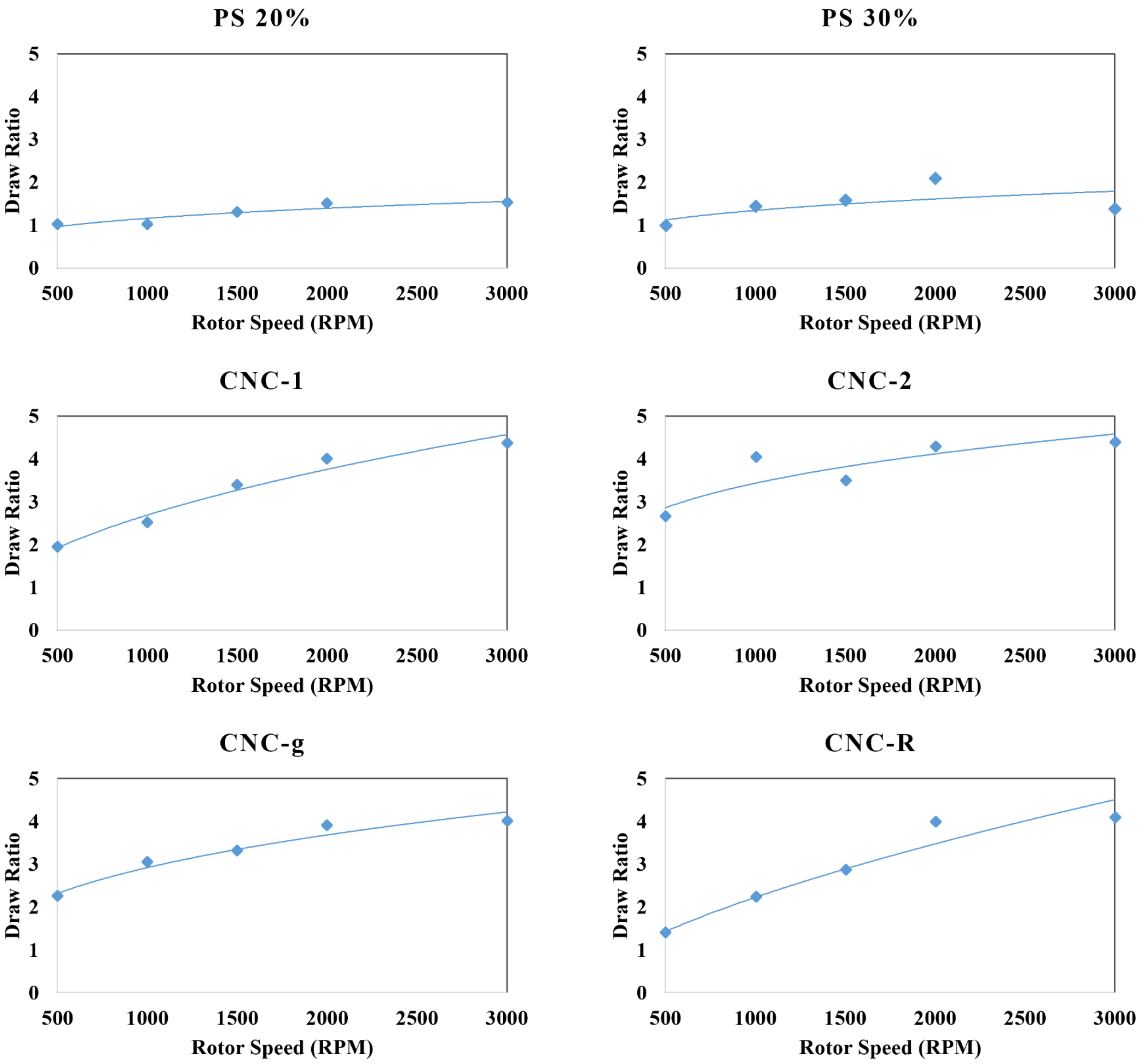

Figure 5. 10: Estimated drawing ratio based on fibers diameters

5.3.2. Evaluation of the conductivity of electrospinning solutions on the dimension of final electrospun fibers

As described in Chapter 4, the conductivity of the solution can influence on the final morphology and dimensions of the collected electrospun fibers. Stretching or drawing of the electrospinning jet is dependent on the ability of the solution to carry charges. Solutions with higher conductivity are able to carry more charges to some extent, so stronger stretching of the jet can take place in case of higher conductivity. In an attempt to estimate the diameter of the electrospun PS fibers as a function of conductivity, Wang scaled a power correlation presented in Equation 5.2 (C. Wang, Hsu, and Lin 2006).

$$df \sim K^{(-\alpha)} = FK^{(-\alpha)} \qquad \text{Equation 5. 2}$$

Where, df and K are the average fibers diameters and the conductivity respectively, and α and F are constant magnitudes. The magnitude of α was estimated around 12 for PS fibers collected on a stationary collectors (C. Wang, Hsu, and Lin 2006). However, it is expected that the magnitude of both α and F can change in case of rotating drum.

As described in the last chapter, this model could not describe the change of the CNC/PS fibers by the conductivity changes totally, when the stationary collector was applied. However, as shown in Figure 5.11, application of the rotating drum caused that changes in the fiber diameter fit this model. Increase of the rotation speed resulted in larger magnitudes of α, and smaller F amounts in the Wang's correlation (see Figure 5.12). It can be concluded that the rotor speed can intensify the effect of the solvent conductivity. However, at very high drum velocities, the increasing trend of α magnitudes in Wang's model reached to a plateau. This can explain that the effect of conductivity is not intensified after some points of the rotor speed, due to the fiber breakage, especially in case of very narrow electrospun fibers.

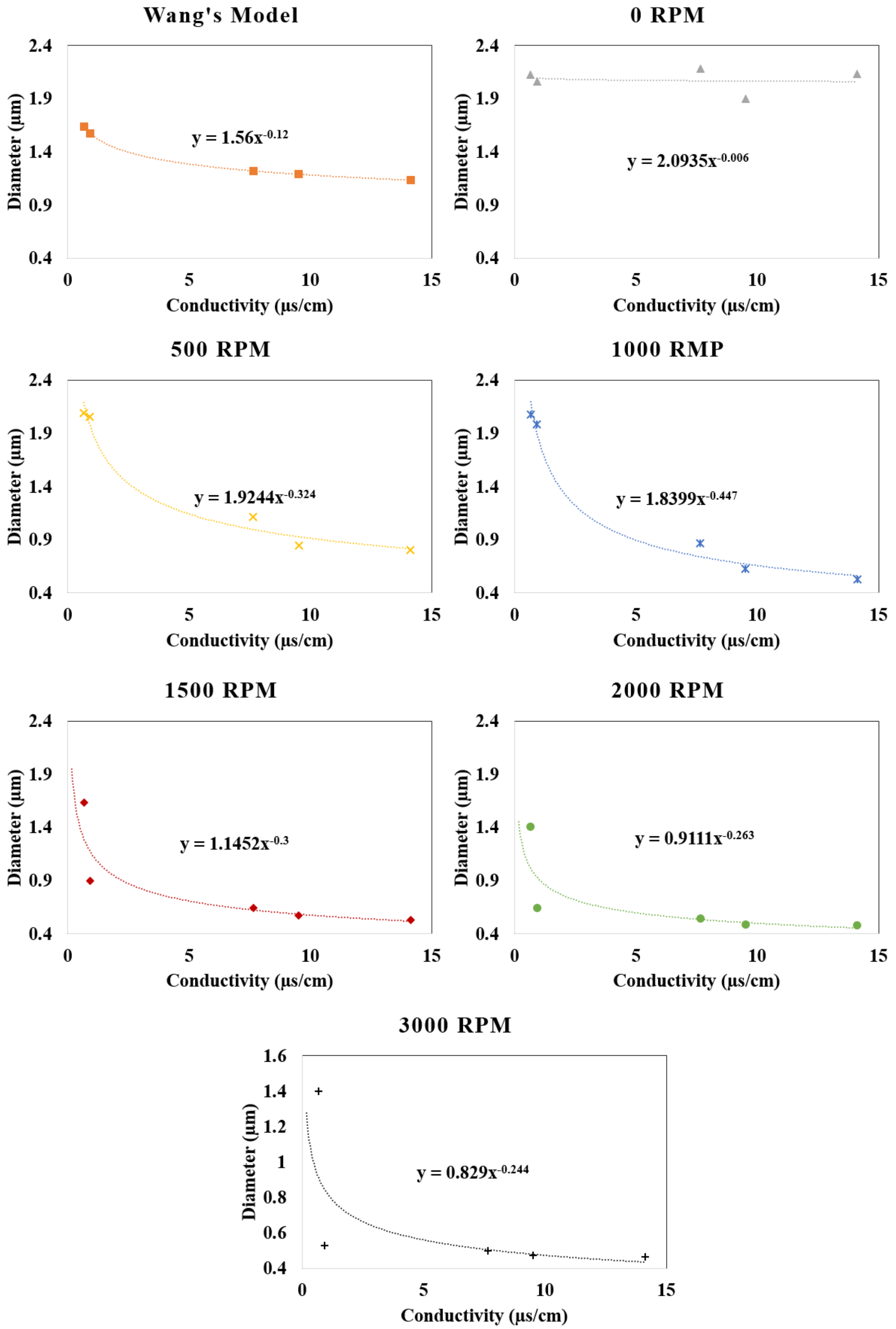

Figure 5. 11: Effect of the conductivity of electrospinning solution on the diameters of fibers, and comparison of empirical results with the Wang's model.

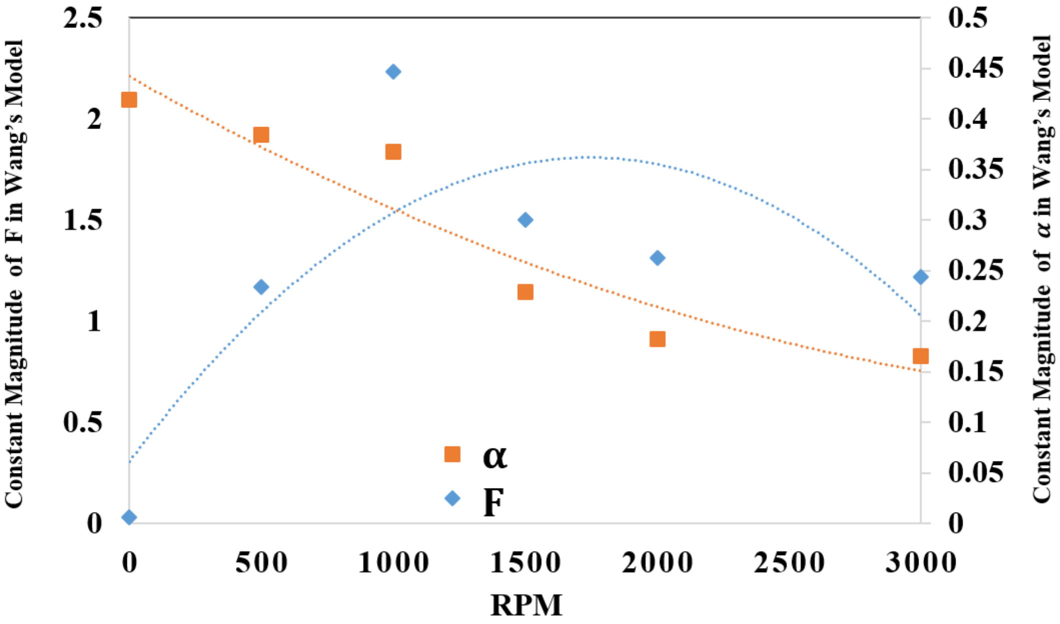

Figure 5. 12: Changes of the power and constant K magnitudes in the Wang model by the conductivity change (These dash-lines are depicted to guide eyes)

5.3.3. Tensile properties of PS nanofibrous web reinforced with modified CNC

5.3.3.1. Experimental tensile results of the oriented PS/CNC electrospun webs

Tensile tests were performed to measure both Young's modulus and strengths of the oriented fibrous webs, and the result were compared with those obtained for the non-oriented samples. Figure 5.13 shows the typical stress-strain curves of the PS aligned webs containing various percentages of the different modified CNCs. As can be seen in Figure 5.13, addition of CNCs resulted in the same trend as the non-oriented samples discussed previously. However, mechanical properties of the oriented fibers are noticeably higher than those of non-oriented samples.

The strains at ultimate tensile stress (ε at UTS) of nonwoven PS mats are about 2-6% which are higher than the value previously reported by Hasan and Boyce for maximum Hookean deformation of PS cylindrical specimen (Hasan and Boyce 1993). In the case of non-oriented samples, the low value of 0.2% for ε uts implies the engagement of a small percentage of fibers with the instrument clamps (see Figure 5.14). On the other hand, the increase in the ultimate strain of aligned mats can be attributed to the higher numbers of fiber engagements with the clamps of the tensile instrument. This can be rooted in the orientation of the fibers. In other words, in the case of aligned mats most of the fibers are oriented toward the force direction and strain up to their individual UTS. However, in the non-oriented mats the breakage of few fibers can result into the entire rapture of the electospun sample, so smaller UTS can be obtained for the non-oriented samples.

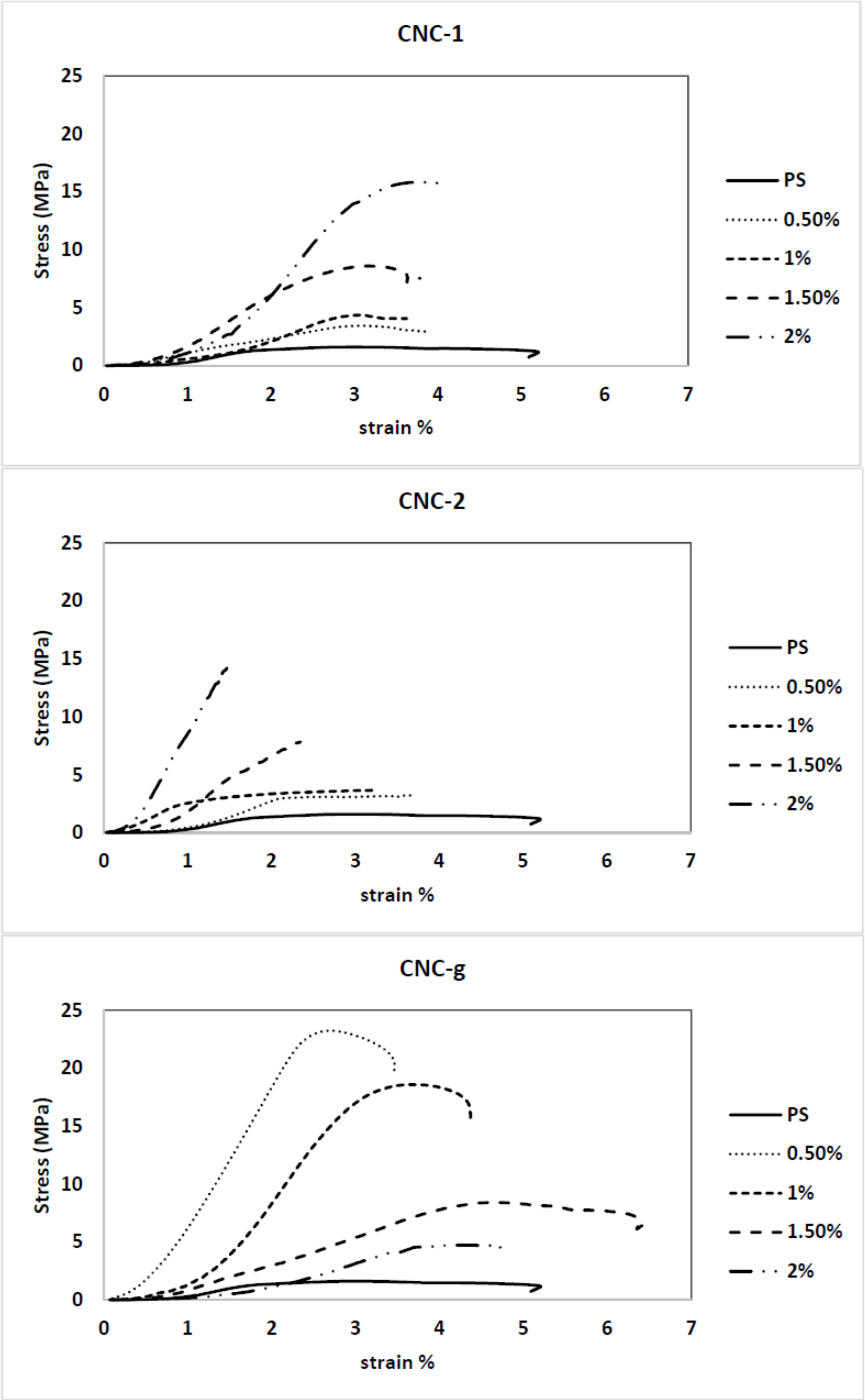

Figure 5. 13: The typical stress-strain curves of aligned PS nonwoven mesh containing various percentages of different CNCs

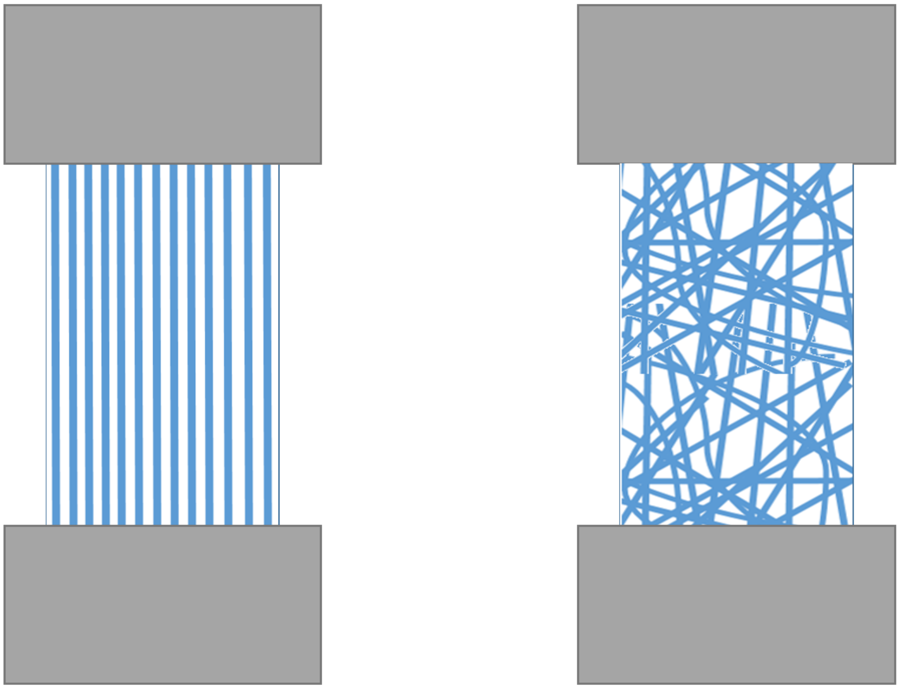

Figure 5. 14: Conditions of differently oriented samples during tensile test

Figure 5.15 compares the averages of the Young's moduli and the strengths of the CNC-reinforced samples with non-oriented and oriented fibrous structures. The alignment of fibers was resulted in 8x increment of stiffness for the neat PS sample, and 3.6x, 4.7x, and 9.5x improvements for 1 wt. % inclusions of CNC-1, CNC-2, and CNC-g samples, respectively. These results are comparable with the results reported for the poly-caprolactone electrospun samples, 10X increase of stiffness due to the alignment of fibers (Thomas et al. 2006). In another similar research, a 5X improvement of modulus was observed which was owing to the arrangements of fibers in electrospun samples of Poly (p-Phenylene Biphenyltetracarboximide) (C. Huang et al. 2006). However, Lee and Deng could just increase the stiffness of vinyl alcohol fibrous samples as low as 40% by using fibers alignment (J. Lee and Deng 2012). These results noticeable increases in stiffness can be attributed not only to the fiber orientations but also to the CNC alignments in fiber structure. Moreover, as can be seen in Figure 5.9, both CNC inclusion and higher rotor speed can decrease the fibers diameter. Electrospun samples with smaller fibers showed exponentially improved mechanical behaviour due to the orientation of polymer macro molecules in the fiber structure (Arinstein et al. 2007) and the higher density of fibrous structures (Wong, Baji, and Leng 2008).

Non-oriented Fibers

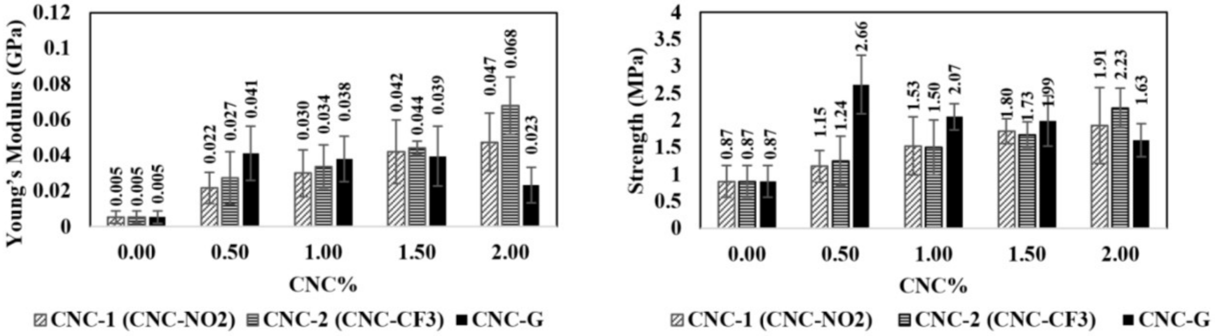

Oriented Fibers

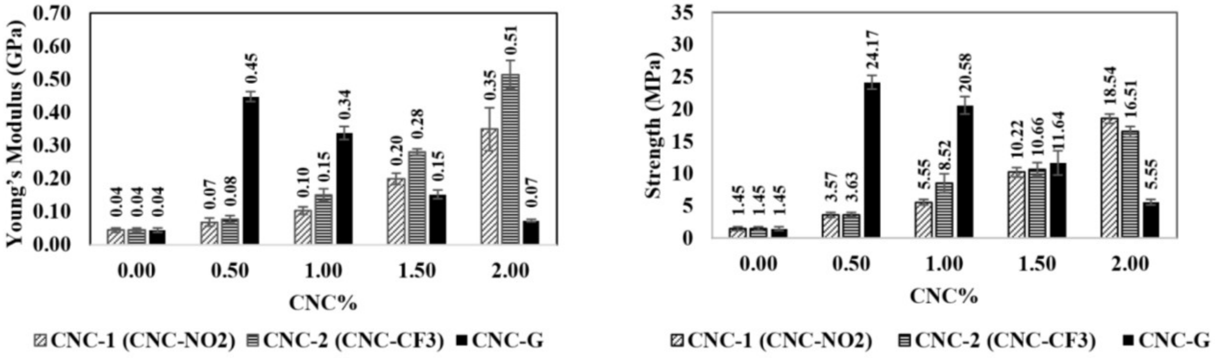

Figure 5. 15: Young's modulus and strength, of aligned PS nano-fibrous web with different concentrations of modified CNCs

As Figure 5.15 illustrates, tensile strength of fibers also improved as a result of fibers' alignment. The alignment of fibers can lead to 1.6x raise in the strength of the neat PS sample. Besides, samples with 5.5x, 5.6x, and 7.7x higher strength were obtained when CNC-1, CNC-2, and CNC-g were incorporated into the fibers. These results are comparable with the results reported for the polycaprolactone electrospun samples which two increases of 1.5X and 4X increases of strength were reported for the alignment of the fibers collected at 3000 RPM and 6000 RPM drum speeds, respectively (Thomas et al. 2006). In another similar research, a 2-5X stronger fibers were obtained by the arrangements of fibers in electrospun samples of Poly (p-Phenylene Biphenyltetracarboximide) (C. Huang et al. 2006). However, Lee and Deng could just increase the strength of vinyl alcohol fibrous samples as low as 20% by alignment of the fibers (J. Lee and Deng 2012). These noticeable results of the strength improvements can also be attributed to the alignment of both fibers and CNCs. Furthermore, the thinner fibers which were obtained as result of CNC inclusion and higher drum speed (Arinstein et al. 2007; Wong, Baji, and Leng 2008).

5.3.3.2. Evaluation of the experimental tensile results based on existing models

In an effort to evaluate the obtained tensile results based on the existing mechanical models for nanoparticles-reinforced matrices, a comparison was made between the experimental results and these models (Ahmed and Jones 1990; Counto 1964; Sato and Furukawa 1963; Nielsen 1967). Figure 5.16 presents Young's modulus improvement of CNC rienforecd PS matrix based on these models. In this image, Young's modulus of matrix (E_m) and Young's modulus of nanoparticles (Ep) were considered 0.04 GPa (Young's modulus of neat PS electrospun sample) and 150 GPa (Young's modulus of CNC from literature (Kargarzadeh et al. 2015)), to calculate the Young's modulus of composites (E_C). φ is the volume fractions of nanoparticles in these models which are

0.0033, 0.0066, 0.0099, and 0.0133 corresponded to the 0.5 wt. %, 1 wt. %, 1.5 wt. % and 2 wt. % of CNC in PS, respectively. However, according to the Figure 5.16, these models are all failed to verify the experimental result. This can be explained by different structures of electrospun samples in comparison with continuous composite structures. As reported in section 5.3.2, the conductivities of electrospinning solution increased by the CNC content, this issues can result in drastic changes in electrospun structures. Structure and geometry of electrospun mats play significant rules in final mechanical performance (Arinstein et al. 2007). For instance, smaller fibers or denser structure (Wong, Baji, and Leng 2008), or stronger fiber-fiber nodes all can bring about higher mechanical performance. Therefore, to estimate the mechanical improvements of electrospun mats, the structural changes in fibrous network of samples should be taken into consideration in the mechanical model.

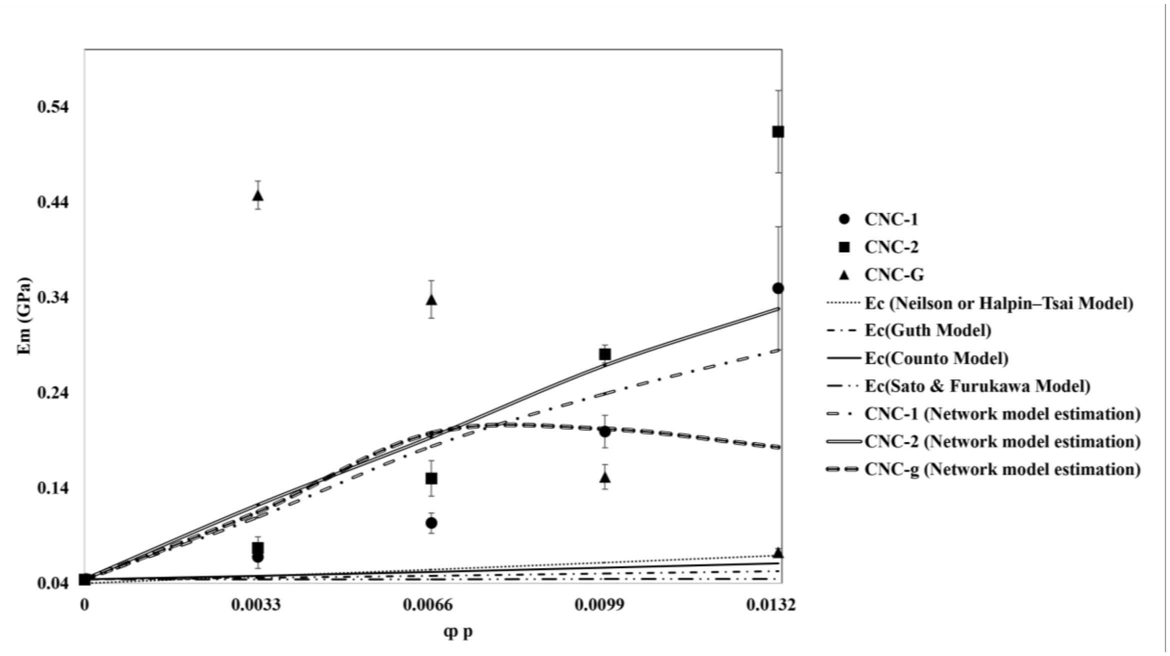

Figure 5. 16: Experimental Young’s moduli VS particulate nanocomposite models

In order to consider the changes in fibrous network, two models can be combined. These models are micromechanics model, and network models (Goodsell et al. 2014). Figure 5.17 shows a brief description of these models. In micromechanics model, each single fiber was considered as a particulate composite with continuous matrix. This model estimates the storage modulus of a CNC/PS single fiber as a function of CNC and PS characteristics as well as CNC volume fraction (Affdl and Kardos 1976). Network model is constructed of a 2D networks representing of an array of fibers. In this model, elastic modulus of network can be estimated by geometry of network, single fiber properties, and fiber/fiber joint (node) properties (Goodsell et al. 2014).

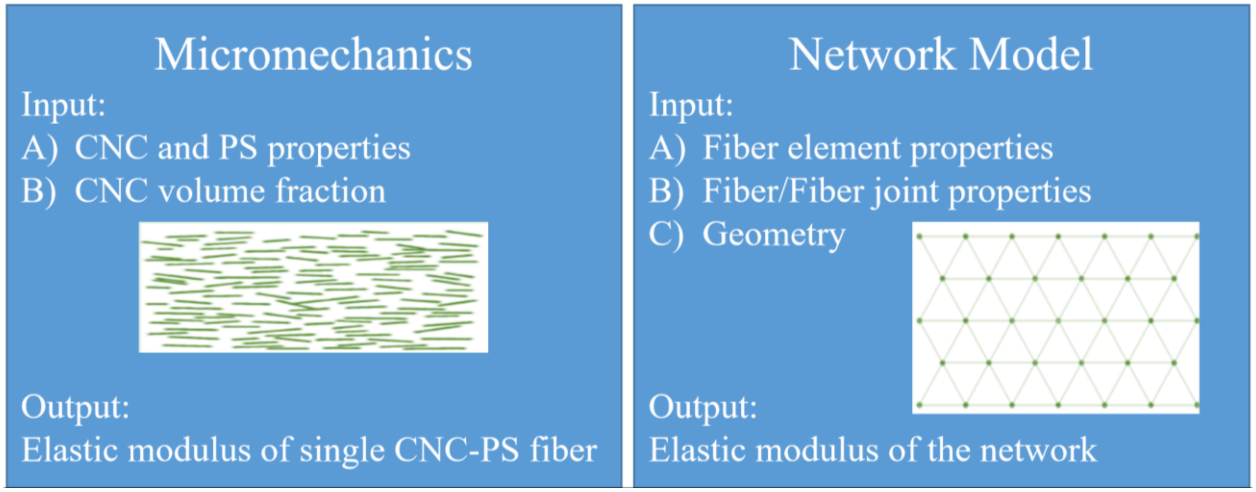

Figure 5. 17: brief descriptions of micromechanics and network models

Firstly, the young modulus of single PS were estimated by means of any micromechanics models presented in Figure 5.17. Here, Neilsen or modified Halpin-Tsai model (Equation 5.3) was considered.

$$E_c = E_{PS}\left(\frac{1+A\eta V_{CNC}}{1-\eta\psi V_{CNC}}\right)$$ Equation 5.3

Where

$$\psi = 1 + \left(\frac{1-\phi_{max}}{\phi_{max}}\right)V_{CNC}$$ Equation 5.4

$$A = K - 1 = 2l/d$$ Equation 5.5

$$K = 1 + 2l/d$$ Equation 5.6

$$\eta = \frac{\frac{E_{CNC}}{E_{PS}}-1}{\frac{E_{CNC}}{E_{PS}}+A} \quad \text{Equation 5.7}$$

Where E and V are the corresponding elastic modulus and volume fractions of CNC and PS, respectively, and l/d is the aspect ratio of CNC which is considered 216/8. Eps, and E_{CNC} were considered 3 GPa and 150 GPa respectively. ϕ_{max} is the maximum packing fraction of the reinforcement which is equal to 0.82 for random packing of fibers (Politechnika Warszawska. Instytut Techniki Cieplnej. and Wiśniewski 2011). Accordingly, the elastic moduli of fibers containing different amounts of CNC were calculated, and presented in Table 5.2.

Table 5. 2: Estimated elastic moduli of single fibers containing different percentages of CNC

V (CNC)	E $_{\text{fiber}}$
0	3
0.003	3.259545981
0.006	3.519918488
0.009	3.781123244
0.012	4.043166024

Subsequently, using the network model, a 2-D network constructed as an array of fiber were considered. This isotropic network is assumed a unit-cell geometry where the fibers in the network form equilateral triangles, representing an array of fiber oriented at 0/60 degrees (for oriented samples was considered 25 degree).

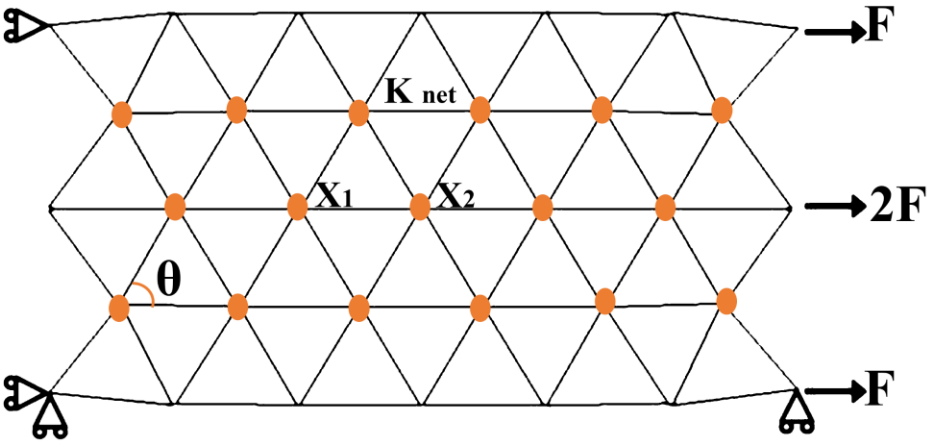

Figure 5. 18: Schematics of network model

The network elastic modulus, E (net) was calculated for neat PS fiber networks and fiber networks in which the individual fibers were reinforced with CNC. Calculation of the young's moduli was made by applying a uniaxial stress (F) to the network through horizontal nodal points fixing the network. Nodal displacements were used to determine the E net.

$$E_{net} = \frac{2F}{(\delta_{x2} - \delta_{x1}) D_{fiber} \mathrm{Sin}\theta} \qquad \text{Equation 5.8}$$

Where $\delta_{x2} - \delta_{x1}$ is the displacements of the nodes, D $_{\text{fiber}}$ is the average diameters of the fibers in the net. Considering this equation, the mechanical properties of a net can be a function of several factors including single fiber stiffness, fiber alignment, fiber diameters, and the strength of cross-over points or nods (which can be altered by the friction between fibers, and amount of solvent content after fiber depositions. High solvent content or semidried fibers can result in fiber fusing in net structures, and stronger nodes).

$$E_{net} = f(E_{fiber}, D_{fiber},\ \alpha, \sigma_{nods}, d) \qquad \text{Equation 5.9}$$

In E_{net} equation, the term of $\frac{2F}{\delta_{x2}-\delta_{x1}}$ and D $_{\text{fiber}}$ can be replaced by $K_{net}E_{fiber}$ and D $_{\text{relative}}$, a dimensionless diameter representing the relative changes of fiber after CNC inclusion.

$$E_{net} = \frac{K_{net}E_{fiber}}{D_{Relative}\text{Sin}\theta} \qquad \text{Equation 5.10}$$

Where K_{net} can be characterized by the density of the net, and σ_{nods}. This two items were unknown for all of the CNC reinforced electrospun samples. Due to the low concentration of CNC, K_{net} can be considered the same for the whole electrospun samples. To obtain an estimation of K_{net}, the term of $\frac{E_{fiber}}{D_{Relative}\text{Sin}\theta}$ were obtained for neat PS samples (at θ=25), and the results were compared with the experimental results of this sample, and the amounts of 3.16 was obtained for K_{net}. Considering magnitudes of K_{net}, D_{relative} (measured based on SEM images), *and* E $_{\text{fiber}}$ for different percentage of CNC contents, E net can be estimated for each CNC/PS electrospun samples (Figure 5.16)

This model could estimate the stiffness improvement of the samples to some extent. Consideration of geometrical changes of the fibrous structure, and fiber diameter changes in this model helps a better estimation of stiffness improvement obtained for CNC/PS electrospun samples. This model could also estimate the drop of the mechanical behaviour of CNC-g due to the thicker fiber in the beaded structures, or fiber breakages. However, in this model the aggregation of particles were not considered, so the amount of stiffness drop in CNC-g were not estimated perfectly.

In a numerical effort to estimate the angular dependence of Young's modulus theoretically, a classical equation was considered (Equation 5. 11). Originally, this equation was used for the prediction of angular dependence of tensile modulus in the case of short fiber-reinforced rubber composites (Coran, Boustany, and Hamed 1971). However, this Equation can be considered for electrospun samples as well (Mathew et al. 2006).

$$\frac{1}{E} = \frac{Cos\theta^2}{E_0} + \frac{Sin\theta^2}{E_{90}} \qquad \text{Equation 5. 11}$$

Where E is the modulus of composite with fibers deviating from the direction of tensile test by an angle θ, E_0 is the longitudinal composite modulus at $\theta = 0°$ and E_{90} is the transverse composite modulus at $\theta = 90°$. Both E_0 and E_{90} were estimated by extrapolation of experimental data, which already measured for the oriented and non-oriented fibrous samples and presented in Table 5.3. Young's modulus of the randomly oriented samples were considered as E_{45} and according to the alignment degree for different samples (see Figure 5.8) their Young's moduli were considered at an average alignment of 75 degree. It should be noted because just two Young's moduli for each sample is measured, just a linear correlation were considered between the Young's modulus and the fiber alignment degree. Then, linear extrapolations were done to estimate E_0 and E_{90} for each sample individually which are also presented in Table 5.3. Finally knowing E_0 and E_{90} and according to Equation 5.11, an estimation of E75 was calculated for each sample, and the calculated results were compared with experimental results of stiffness obtained for the aligned CNC/PS in Figure 5.19. As this Figure shows, the experimental results are mostly higher than the predicted values of the presented model; while, they are following almost the same trends. The lack of compatibility between the experimental and the model-estimation values can attributed to the tremendous reduction of fiber dimensions due to the drawing forces at rotating drum. Although the reported results for the Poly(butylene terephthalate) electrospun samples were matched with this model (Mathew et al. 2006), the dimensions of the fibers were not changed at higher rotation speed of drum, which is not the case in this research.

Table 5. 3: calculation of Young’s modulus of electorspun based on the model describing angular dependence of Young’s modulus

CNC%	CNC-1				
	E_{45} experimental	E_{75} experimental	E_0 extrapolated	E_{90} extrapolated	E_{75} calculated based on the model
0	0.005	0.132	0.146	0.004	0.074
0.5	0.022	0.204	0.224	0.017	0.166
1	0.030	0.310	0.341	0.023	0.245
1.5	0.042	0.598	0.658	0.033	0.426
2	0.047	1.048	1.153	0.037	0.621
CNC%	**CNC-2**				
	E_{45} experimental	E_{75} experimental	E_0 extrapolated	E_{90} extrapolated	E_{75} calculated based on the model
0	0.005	0.132	0.146	0.004	0.074
0.5	0.027	0.232	0.255	0.021	0.193
1	0.034	0.450	0.495	0.026	0.328
1.5	0.044	0.841	0.925	0.034	0.533
2	0.068	1.541	1.695	0.053	0.902
CNC%	**CNC-g**				
	E_{45} experimental	E_{75} experimental	E_0 extrapolated	E_{90} extrapolated	E_{75} calculated based on the model
0	0.005	0.132	0.004	0.146	0.074
0.5	0.041	1.342	0.032	1.476	0.649
1	0.038	1.014	0.030	1.115	0.548
1.5	0.039	0.455	0.030	0.500	0.348
2	0.023	0.217	0.018	0.239	0.177

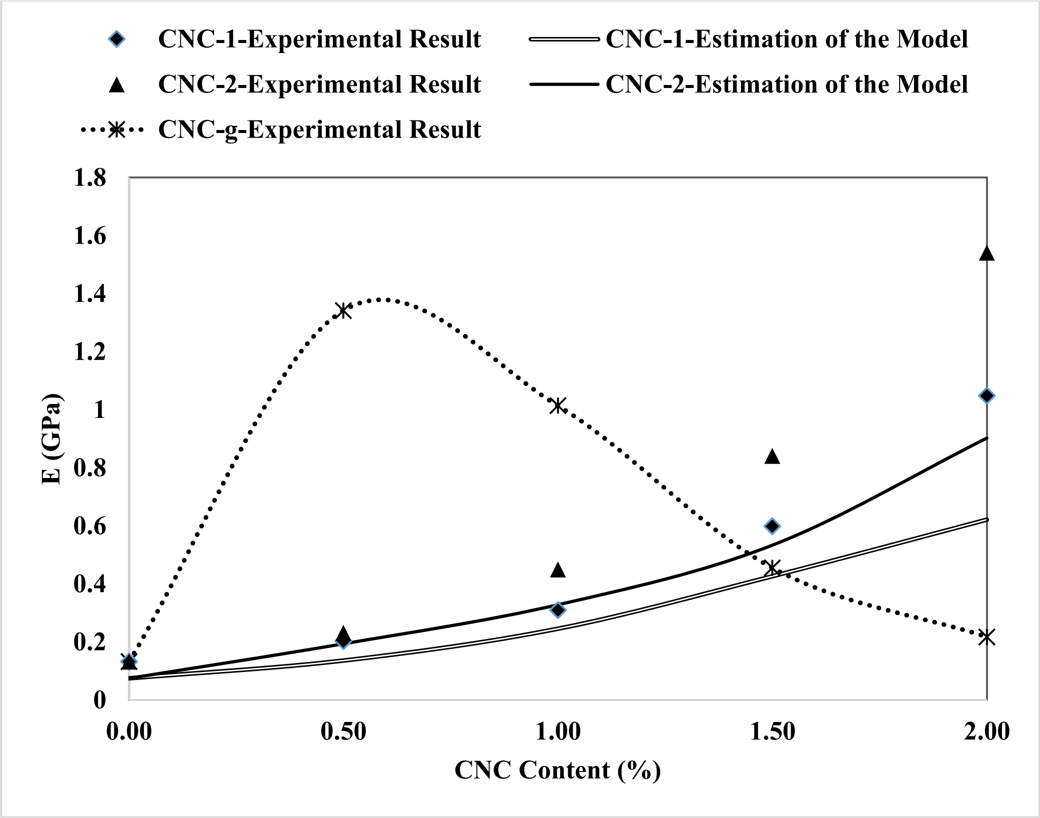

Figure 5. 19: comparisons between experimental quantities and the model estimation of stiffness (The dash-line is depicted to guide eyes)

As described previously, some fiber breakages occurred at the high rotor speeds (3000 RPM). Mechanical properties of a single fiber can be estimated based on these breakages. Longitudinal strains at breakage of a single fiber can be assessed by means of the transverse strain obtained from the fiber diameter changes (see Figure 5.9) and the Poisson's ratio of PS (0.4). Figure 5.20 shows the estimated longitudinal strains of a single fiber based on the transvers ones. Due to the breakage of fibers at the drum speed of 3000 RPM, the largest longitudinal strain obtained at the drum speed of 2000 RPM (1.3%) was used in this analysis. By assuming a 100% alignments of CNC in the fiber structure, the magnitude of this estimated strain can be attributed to all samples. Therefore, an estimation of ultimate tensile strength of a single fiber can be calculated based on the above mentioned strain. Figure 5.21 compares the calculated strength for single fibers and the actual strength obtained from the tensile tests at Figure 5.15. As can be seen, the trend of the results for both calculated single fiber strength and the actual strength is very similar. However, the predicted results based on the strains of a single fiber are generally lower than those of tensile test. This can be due to the fact that the single fiber strain is calculated based on the samples prepared at 2000 RPM; however, the actual threshold breakage speed is somewhere between 2000 RPM and 3000 RPM. Clearly, the samples that would be prepared at that threshold speed will have a larger ultimate strain and consequently a higher predicted strength.

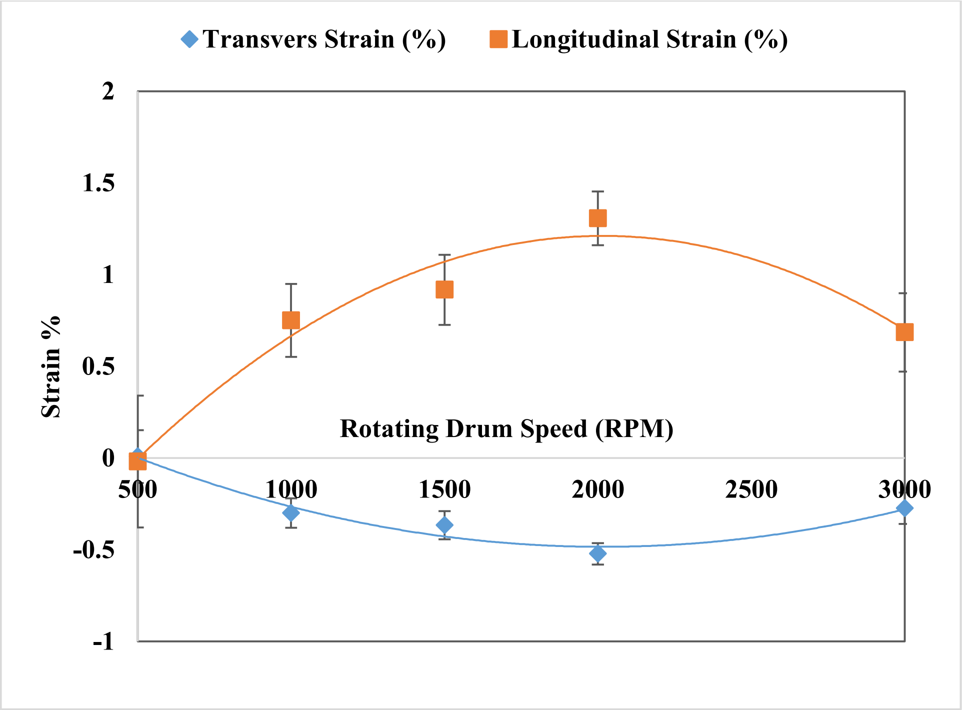

Figure 5. 20: the estimated longitudinal strains of a single fiber based on the transvers strains

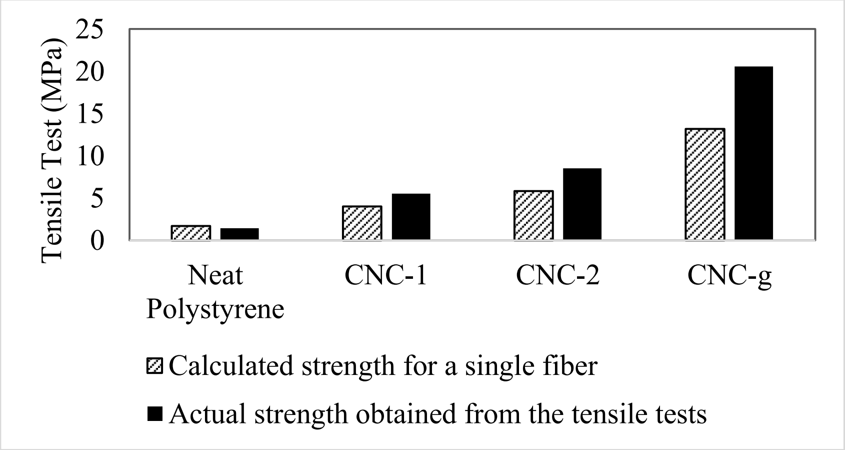

Figure 5. 21: A comparison of the calculated strength for single fibers and the actual strength obtained from the tensile tests

5.3.4. Dynamic mechanical properties of PS nanofibrous web reinforced with modified CNC

DMA analysis was performed to obtain the storage modulus (E’), loss modulus (E”), and damping factor (tanδ) of the CNC reinforced electrospun samples with oriented structures. The storage modulus is roughly an approximation of the Young’s or elastic modulus, or stiffness. The loss modulus is a magnitude of the energy absorbed as result of a relaxation and is useful in describing the mechanisms of internal motions. The damping factor (tanδ) shows the relative contributions of the viscous and elastic components of a viscoelastic material. In case of a thermoplastic material like linear atactic PS, both storage and loss moduli change with temperature due to the changes in the molecular mobility. The storage modulus of a polymer decreases rapidly while the loss modulus and tan δ show a maximum when the material temperature approaches to the glass transition (Tg). Mobility of the amorphous regions causes a reduction in the storage modulus. However, the material still exhibits solid-state properties before reaching melting temperature (Menard 1999; Sepe 1998).

5.3.4.1. A comparison between DMA of PS electrospun web and film

DMA results of the neat PS electrospun fibers were compared with the DMA results of the PS film in Figure 5. 22. As this figure shows, PS film shows the storage and loss moduli several times larger than the electrospun sample which are in confirmation with the results reported in literatures for PS film (Kontou and Anthoulis 2007), and electrospun mats (Rojas and Habibi 2009). This issue can be explained by the uniformity and confinement of the film structure versus electrospun sample with porous and disunited structure. The α transition peak of pure PS oriented-electrospun fiber in Figure 5.22 corresponds to the segmental motions at glass transition temperature (Tg) of 115°C which was higher than 90°C for the solvent cast PS film. Glass transition temperature of thin polymer films with free surfaces decreases linearly only if the film thickness is less than 70 nm (Sharp and Forrest 2003). However, diameters of electrospun fibers in this study were always higher than 500 nm. Similar results were reported for other polymers. Similar increases in glass transition temperature were also reported for electrospun fibers of other polymers.The glass transition temperature of electrospun Nylon 6-6 fibers is 80°C as opposed to 50°C of the polymer (Baji, Mai, Wong, Abtahi, and Chen 2010). For electrospun polylactic acid, T_g value is increased around 10°C compared to a film sample (Cacciotti et al. 2014). Again in the case of electrospun polymethyl methacrylate fiber, T_g is around 120°C, compared to the film T_g of 105°C (H. Dong et al. 2012). The increase in the glass transition temperature of electrospun PS fibers can be explained by the difficulties of heat transfer during the dynamic mechanical analysis. Samples with lower packing densities have higher air content which act as heat insulation (FRANCL and KINGERY 1954). Moreover, a larger magnitude of tan δ was observed for electrospun sample implicating more drastic structural change at Tg.

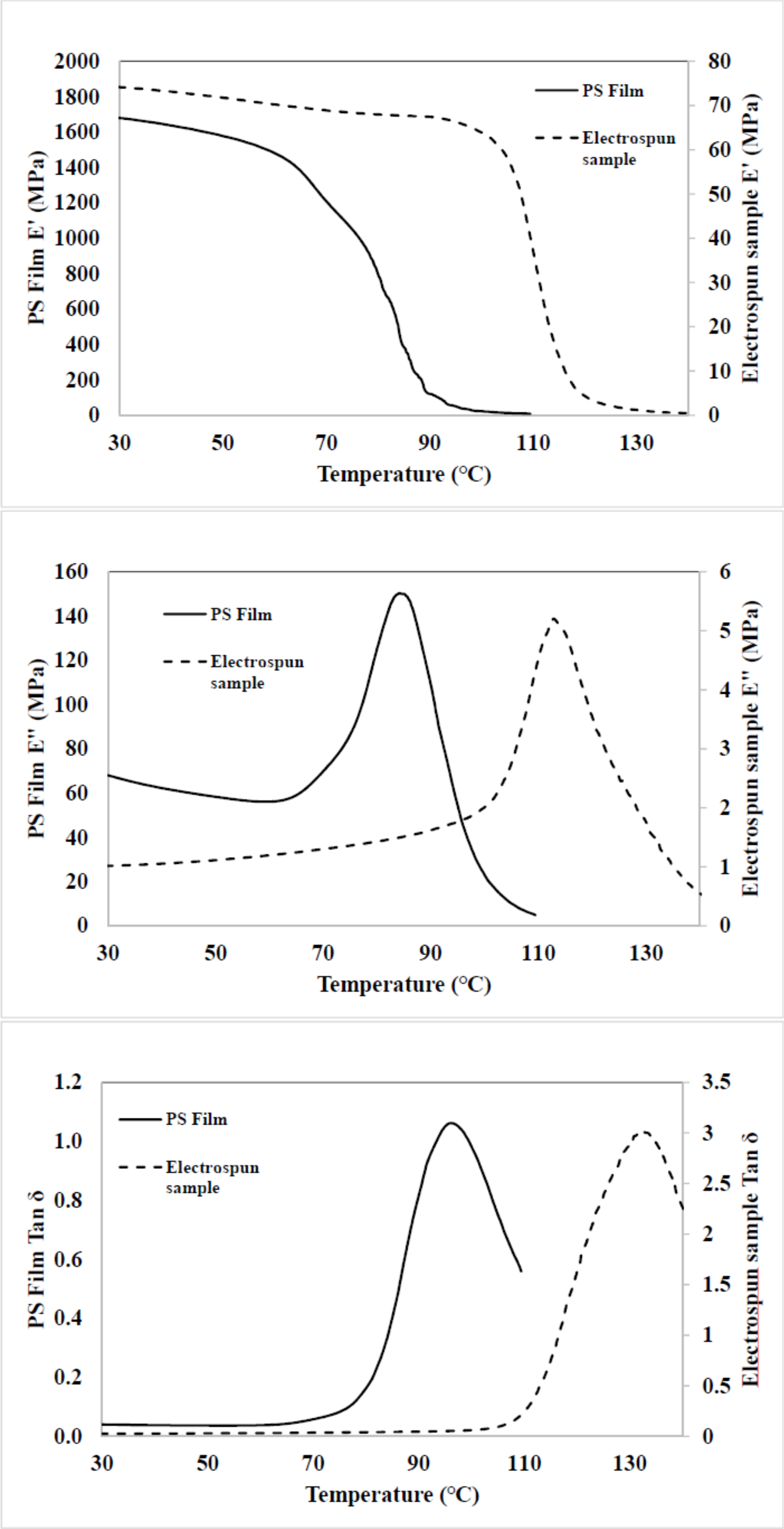

Figure 5. 22: DMA results of PS Film versus electrospun neat PS web with oriented structure.

5.3.4.2. Storage and Loss moduli of the oriented CNC/PS electrospun samples

The storage and loss moduli of the oriented electrospun neat PS and PS/CNC sample are presented in Figure 5.23 and Figure 5.24, respectively. As expected, samples with the CNC inclusions exhibit much larger storage moduli than neat PS electrospun samples. For these electrospun samples, at 70°C the addition of 2 wt. % of CNC-1 and CNC-2 to PS fibers resulted in a 257% and 382% increases in storage modulus, respectively. The storage modulus of the samples containing CNC-g showed a trend similar to that observed for the stiffness. In general, lower concentrations of CNC-g led to a better mechanical performance. At 70°C, addition of 0.5 wt. %, 1wt. %, 1.5 wt. %, and 2 wt. % of CNC-g resulted in 350%, 249%, 196%, and 104% increases in storage moduli of these samples, respectively. These results are comparable with the results of cellulose acetate (CA) electrospun samples containing 1 wt. % CNC with storage modulus of 10 times larger than neat CA electrospun samples (Herrera et al. 2011). In this study, the decrease in the plateau storage modulus at higher CNC-g concentrations suggests the more favorable interactions among grafted PS brushes on CNC-g particles than the PS brushes and PS chains in the continuous phase.

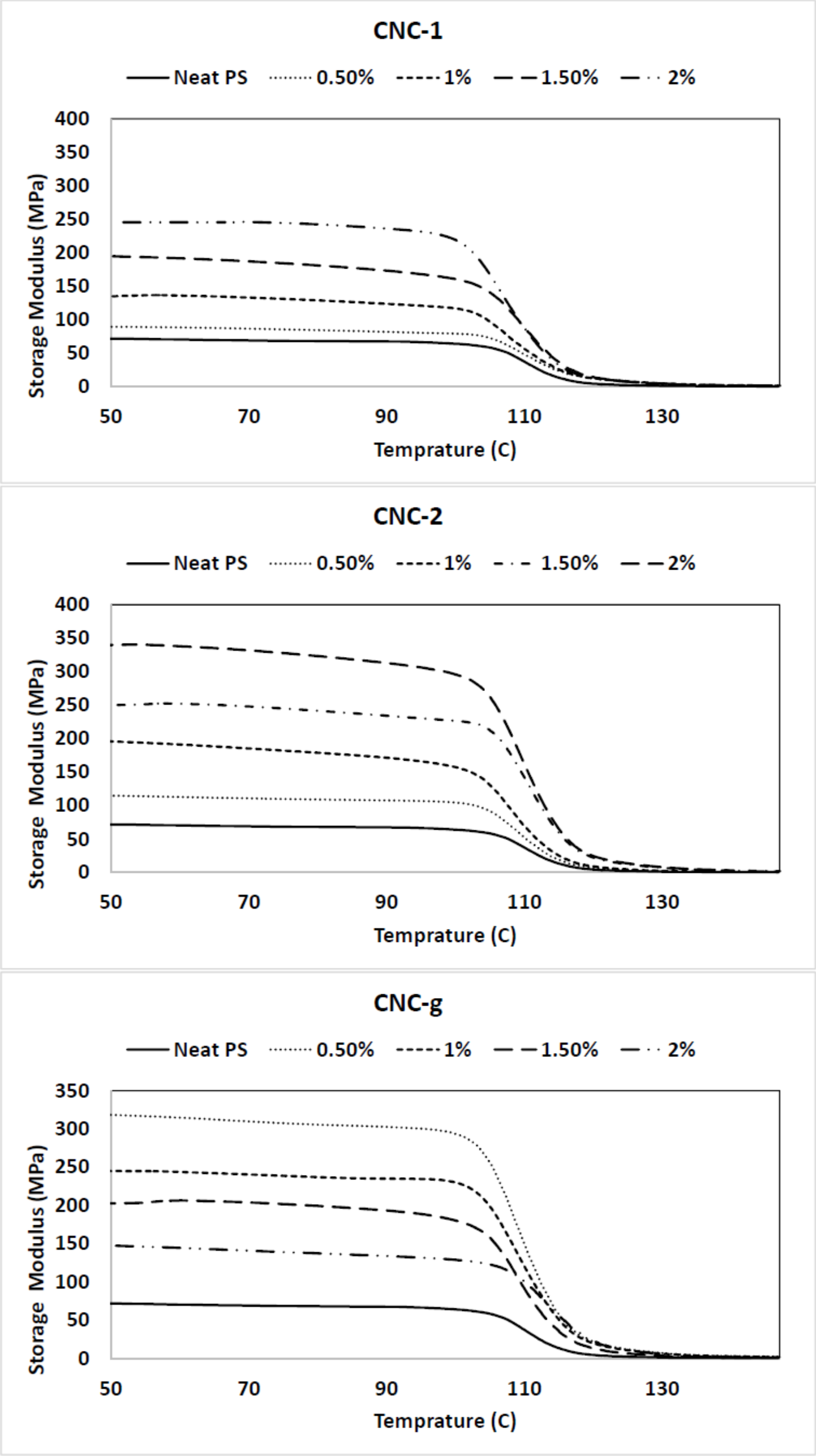

Figure 5. 23: Storage moduli of oriented PS fibrous mats containing different CNCs

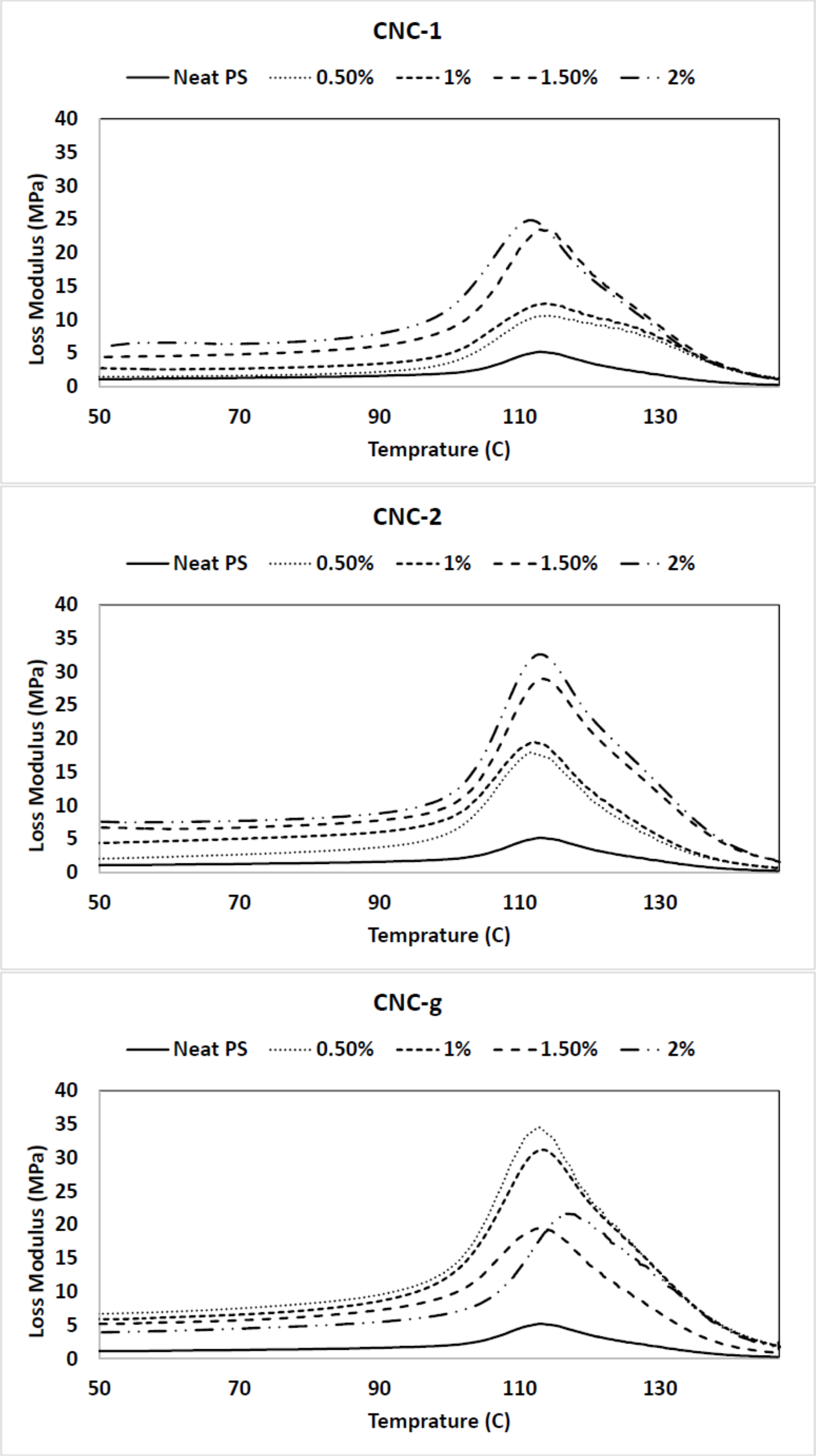

Figure 5. 24: Loss moduli of oriented PS fibrous mats containing different CNCs

However, the storage moduli values obtained in the present study are mostly higher than the results reported in the similar researches for the other polymers. With inclusions of 5 wt. % CNC, only a 210% increase in storage modulus were reported for poly (ε-caprolactone) fibers (Zoppe et al. 2009). In another study, with incorporation of 15 wt. % CNW into the poly ethylene oxide fibers, the storage modulus increased 100% compared with the neat PEO fibers (Changsarn et al. 2011). More importantly, in a similar study for PS with non-oriented structure (Rojas and Habibi 2009), with inclusion of 9 wt. % CNW, the storage modulus increase 400% which is nearly as high as the value obtained in the present research for incorporation of 2 wt. % of CNC-1 or CNC-2 and only 0.5 wt. % of CNC-g in this study. These striking improvements in storage moduli can be attributed to the smooth fiber structure, proper CNC dispersion, stronger CNC/PS interfacial interaction, and more uniformly oriented fibers of electrospun structures.

5.3.4.3. Effect of orientation on the loss and storage moduli

The presence of oriented structures also enables the electrospun samples to sustain a higher modulus value compared with randomly oriented samples (See Figure 5.25 and Figure 5.26). By alignments of the samples containing 2 wt. % CNC-1, CNC-2, and CNC-g, storage moduli incremented by 250%, 360%, and 105%, respectively. These results can be attributed not only to the fiber orientations but also to the CNC alignments in the structure of the electrospun mats. Besides, the packing densities of the oriented samples are higher than non-oriented samples due to their ordered structures and smaller fibers, which makes them stronger (Arinstein et al. 2007; Wong, Baji, and Leng 2008). Moreover, in the case of non-oriented samples, fiber slippery can influence mechanical properties of the samples. It is noteworthy that at higher temperatures (i.e., 110 °C), the magnitudes of the storage moduli of the oriented samples get closer to those of the non-oriented samples which can attributed to the deformation of the fibrous structures. The slightly higher storage moduli of the oriented electrospun samples at this temperature can be explained by the rotating drum causing the post drawn effect (Arinstein et al. 2007). The post-drawn after electrospinning does improve the mechanical properties of CNC reinforced fibers by giving the orientation to the CNCs and the polymer chains. Eventually, with the increase of temperature to melting temperature, the storage modulus tends to converge to that of pure PS, indicating that at high temperature, the moduli of the composites were dominated by the matrix intrinsic modulus.

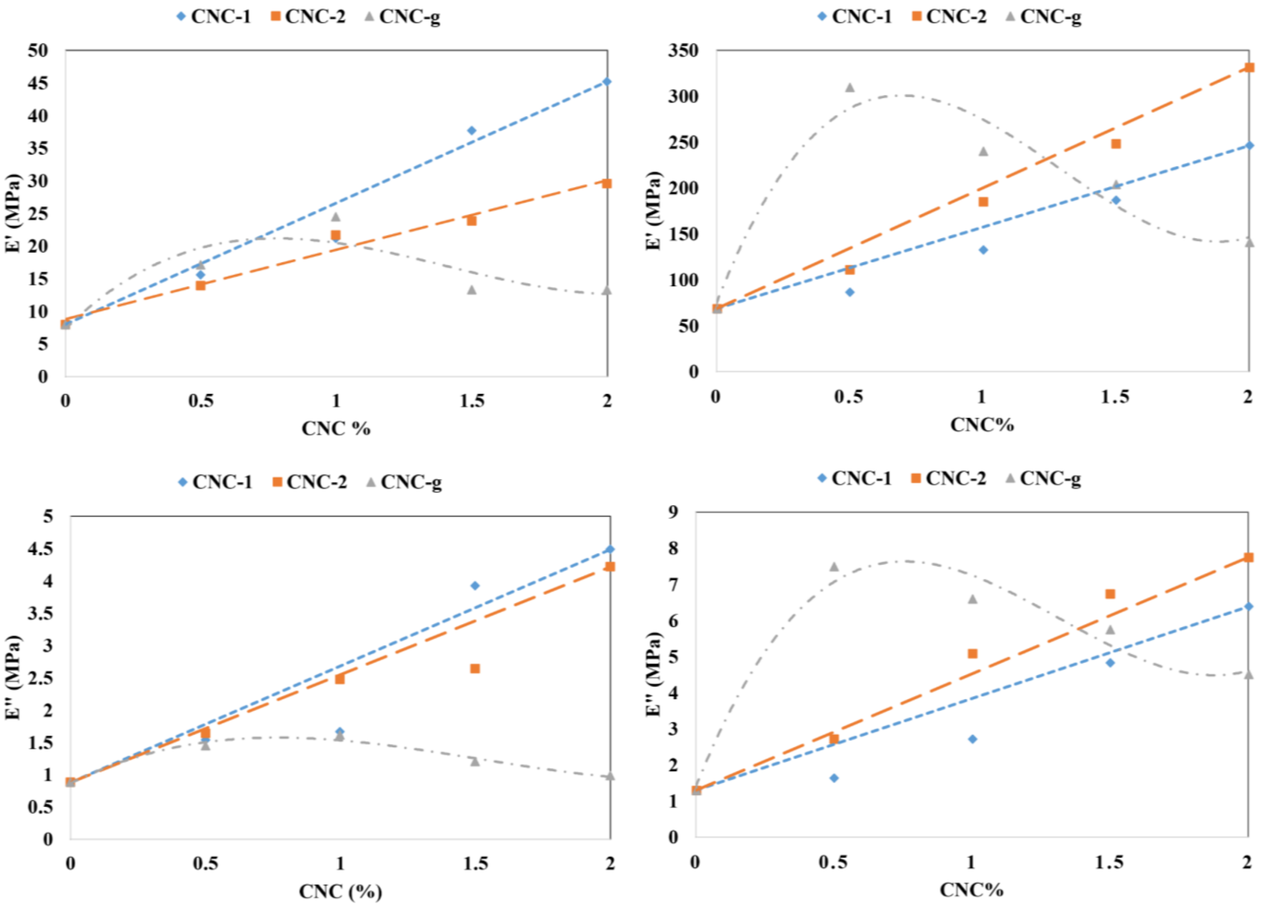

Randomly Oriented

Oriented

Figure 5. 25: loss and storage moduli results of non-oriented CNC/PS fibrous mats (left) and oriented CNC/Fibrous webs (right)

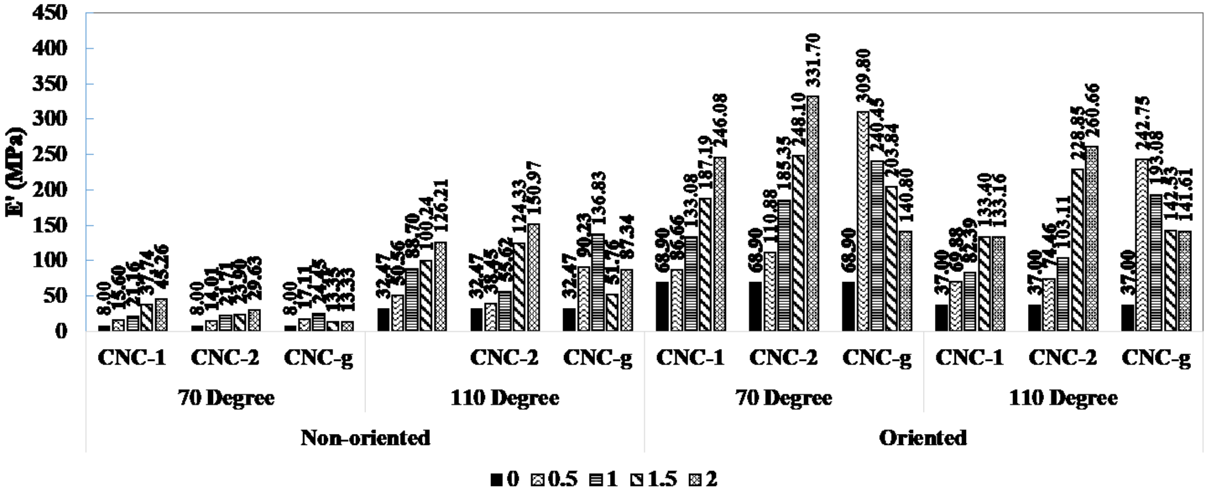

Figure 5. 26: Comparison of storages moduli in oriented and non-oriented PS/CNC electrospun samples at 70 and 110 degrees

Finally, the addition of the same amount of CNCs to both oriented and non-oriented samples resulted in a roughly same percentages of storage modulus improvements in both samples. At 70°C, the addition of 2 wt. % of CNC-1 and CNC-2 to PS fibers resulted in 257% and 382% increase in the storage moduli of the oriented samples, respectively. Similarly, at the same temperature, and the same concentration of CNC-1 and CNC-2, 270 % and 450% growth were observed in the storage moduli of the non-oriented sample, respectively. Slightly higher storage increase ratios in the non-oriented samples can be explained by severe morphological changes in non-oriented electrospun structure by CNC inclusions. In oriented samples, morphological changes by CNC incorporation are negligible, so mechanical improvement can be related mostly to the CNC reinforcing factor.

The loss modulus was also observed to increase along with the inclusion of CNC (see Figure 5.24). When the composites were subjected to external stress, energy was dissipated by the frictions between CNC–PS interactions. The inclusion of CNC showed some transition peak in loss moduli, which indicates that the inclusion of CNC affect the relaxation behavior of PS significantly. The relaxation transition peak shown in E″ around 110-130 °C is thought to be related to a complex multi-relaxation process which is mainly concerned with their different dimensions of fibers and their packing density in electrospun structures. This can influence on the densification rate of the samples as well as glass transition points of the samples. It is expected samples with smaller fibers have lower Tg compared with the samples with larger fibers (Akabori et al. 2005) which can be evaluated by Tan δ graphs in Figure 5.29 better. Unlike storage moduli, the orientation of electrospun samples did not influence on the loss moduli tremendously, which can be explained by the same rates of energy dissipation for all electospun samples regardless of their structures.

5.3.4.4. Evaluation of the reinforcing mechanism of modified CNCs on the storage moduli

The reinforcing mechanisms of grafted and surface modified CNC on the storage moduli of the oriented PS fibers were judged by visiting Halpin-Kardos semi-empirical model (Affdl and Kardos 1976)based on mean-field approach and Ouali's percolation modified series−parallel model of Takayanagi (Takayanagi, Uemura, and Minami 1964).

As discussed previously, Halpin-Kardos semi-empirical model is based on mean-field approach and was proposed to estimate the modulus of randomly oriented short fiber nanocomposites. It can be summarized as:

$$E_{\parallel} = E_m \frac{1+\eta_{\parallel}\zeta\varphi_f}{1-\eta_{\parallel}\varphi_f} \qquad \text{Equation 5.12}$$

$$E_{\perp} = E_m \frac{1+2\eta_{\perp}\varphi_f}{1-\eta_{\perp}\varphi_f} \qquad \text{Equation 5.13}$$

and

$$\eta_{\parallel} = \frac{\frac{E_f}{E_m}-1}{\frac{E_f}{E_m}+\zeta}$$ Equation 5.14

$$\eta_{\perp} = \frac{\frac{E_f}{E_m}-1}{\frac{E_f}{E_m}+2}$$ Equation 5.15

where $E_{//}$ and $E_{\perp}$ are longitudinal and transverse direction elastic modulus of the composite, φ_f is the volume fraction of CNC particles, E_m is the elastic modulus of the PS matrix, E_f is the elastic modulus of the CNC particle filler, and ζ is the shape factor of CNC which depends on its length (L), width (w) and orientation. ζ= L/2w is used here as suggested for short fibers (Dalmas et al. 2007) and used for CNC whiskers (X. Xu et al. 2013). Elastic moduli (E_c) of isotropic filled CNC-PS composite fibers can be calculated by using the laminate theory (Van Es et al. 2001).

$$E_c = 0.18E_{\parallel} + 0.816E_{\perp}$$ Equation 5.16

In these calculations width (w) and length (L) of CNC particles were taken as 8 nm and 214 nm respectively based on a previous characterization (Oguzlu and Boluk 2017). The elastic modulus of PS *(E_m)* was taken as 68 MPa based on the storage modulus of unfilled electrospun-oriented PS fiber data. E_f of CNC was taken as 145 GPa following the justification given by Xu et al (X. Xu et al. 2013).

The model for percolated network of rod shaped particles in a polymer matrix was also used to investigate the reinforcing mechanism of the CNC whickers in PS. Ouali et al. modified the Takayanagi's (Takayanagi, Uemura, and Minami 1964) series-parallel model. Accordingly, the elastic modulus is expressed by the following equation:

$$E_C = \frac{(1-2\psi+\psi\varphi_f)E_mE_f+(1-\varphi_f)\psi E_f^2}{(1-\varphi_f)E_f+(\varphi_f-\psi)E_m}$$ Equation 5.17

Where, φ_f, E_f, E_m, are the volume fraction of CNC particles, the elastic modulus of the CNC particles, the elastic modulus of the PS matrix. Ψ is the volume fraction of CNC network which is active in transferring stress from one particle to another and can be estimated as follow:

$$\psi = 0 \ \varphi_f \leq \varphi_{fc} \qquad \text{Equation 5.18}$$

$$\psi = \varphi_f (\frac{\varphi_f - \varphi_c}{1-\varphi_c})^b \varphi_f > \varphi_c \qquad \text{Equation 5.19}$$

where, b is the percolation exponent and taken as 0.4 (Favier et al. 1997) φ_c is the critical volume fraction which is also called as the percolation threshold and needed to reach the geometrical percolation of rod shaped CNC particles. As summarized by Favier et al. percolation threshold is the function of aspect ratio and orientation distribution of particles and taken as 0.08% for CNC whickers which was also used in our calculations (Favier et al. 1997).

Figure 5.27 shows the experimental moduli results of chemically modified CNC-1, CNC-2 and PS grafted CNC-g filled electrospun and oriented PS fibers along with Halpin-Kardos and Ouali's percolation models. Since Halpin-Kardos model is built on a single short fiber enclosed in a cylindrical volume of continuous phase and does not consider interactions among fibers, it gave very low values compared to all of our experimental results. On the other side, percolation model with E_f values of 120 GPa and 80 GPa for the network forming CNC described the behavior of CNC-1 and CNC-2 filled PS fibers extremely well. Ouali's phenomenological percolation model is based on Takayanagi's series-parallel representation of crystalline-amorphous polymer phases. Original Takayanagi's model is extended by including parallel part of percolating particles into the series part which includes a continuous polymer phase and fillers with no percolation. The agreement of experimental results of CNC-1 and CNC-2 filled PS fibers with percolation model showed the CNC-CNC interactions and percolated network formation even at the very low CNC concentrations. It is worth to note that the transitions from dilute to semi dilute and from semi dilute to concentrated regimes in CNC suspensions occur at volume fractions of $\varphi^* \simeq (w/L)^2$ and $\varphi^{**} \simeq w/L$ respectively based on rigid rod approximation. Those equations suggest that, CNC particles with the width of 8 nm and length of 214 nm as investigated in this work, φ^* shall be 0.16% and φ^{**} shall be 3.7 vol.%. Hence the CNC suspension concentrations investigated in our study were within the semi dilute concentration range where particles contact each other. The experimental results of PS grafted CNC-g in PS showed totally different modulus vs. concentration trend. CNC-g at 0.33 vol. % (0.5 % by weight) concentration lead to higher composite modulus than CNC-1 and CNC-2 and prediction of percolation model. Nevertheless, the effectiveness of CNC-g reduced at higher concentration levels. This is mainly due to the strong slowing down of the chain motions of free PS chains near the PS grafted CNC particles. According to the molecular simulation study on the PS grafted silica surfaces in a PS matrix, the dynamics of polymer chains of the PS matrix within the radius of gyration distance from the PS grafted silica surfaces reduced by several orders of magnitude (Ndoro, Böhm, and Müller-Plathe 2012). Strong and thicker immobilized polymer chains at low concentrations result a strong polymer-CNC interactions and very high elastic modulus. However, at higher CNC concentrations immobilized polymer chains acted like stickers among CNC particles and caused agglomerates with entrapped free PS from the matrix hence caused a decrease in the elastic modulus.

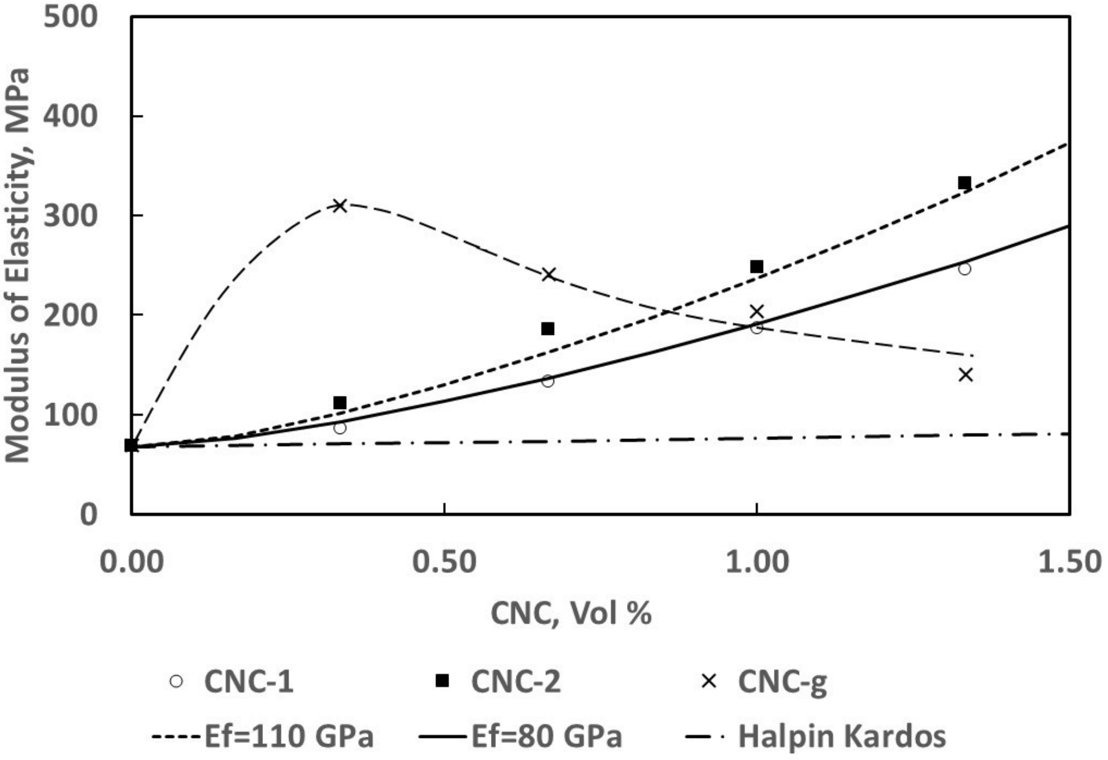

Figure 5. 27: Comparison of experimental modulus of elasticity data with Ouali's percolation (with E_f=110 GPa and E_f= 80 GPa) and Halpin-Kardos mean-field (E_f= 145 GPa) models. (The curve passing through CNC-g data points was drawn only to guide the eye.)

Figure 5.28 highlights the differences in the behavior of chemically modified CNC and polymer grafted CNC in PS matrix. Depending on wetting characteristics, chemically modified CNC (CNC-1 or CNC-2) caused some limited increase in $T_{g.}$, however a respectable increase in elastic modulus with concentration increases. The increase in storage moduli with concentration was due to the filler-filler interactions and formation of percolated CNC network. On the other hand, immobilized polymer layers around polymer grafted CNC particles caused a respectable increase in T_g with particle concentration. Immobilized polymer layers with polymer grafted CNC particles resulted very high increase in storage modulus at low concentrations. However, grafted polymer chains behaved like stickers and caused agglomeration of particles at higher CNC concentrations. Those findings agreed with the results on PS grafted silica in PS nanocomposites (Chevigny et al. 2011).

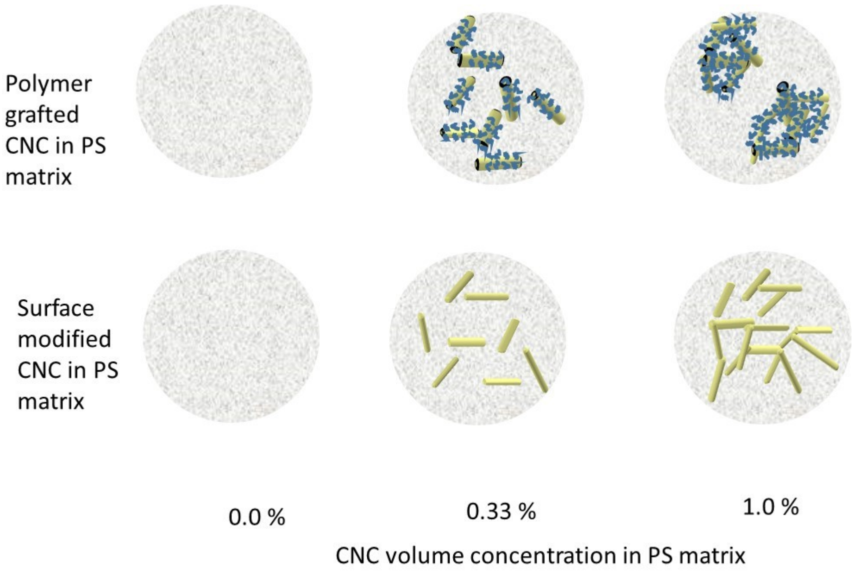

Figure 5. 28: Behaviors of chemically modified and PS grafted CNC in PS

5.3.4.5. Damping factor (tan δ) of the oriented CNC/PS electrospun samples

The damping factor or tan δ is the ratio of the loss modulus to the storage modulus. Figure 5.29 presents the tan δ curves of the CNC/PS and neat PS electrospun samples with the oriented structures. It was found that the CNC/PS samples showed a slightly lower damping than the neat PS sample, owing to the higher fiber–PS interaction (Boluk and Schreiber H 1986). Addition of CNC particles also shifted glass transition temperature higher. Moreover, the loss tangent curves of CNC incorporated electrospun PS fibers were broadened due to the presence of rigid CNC particles.

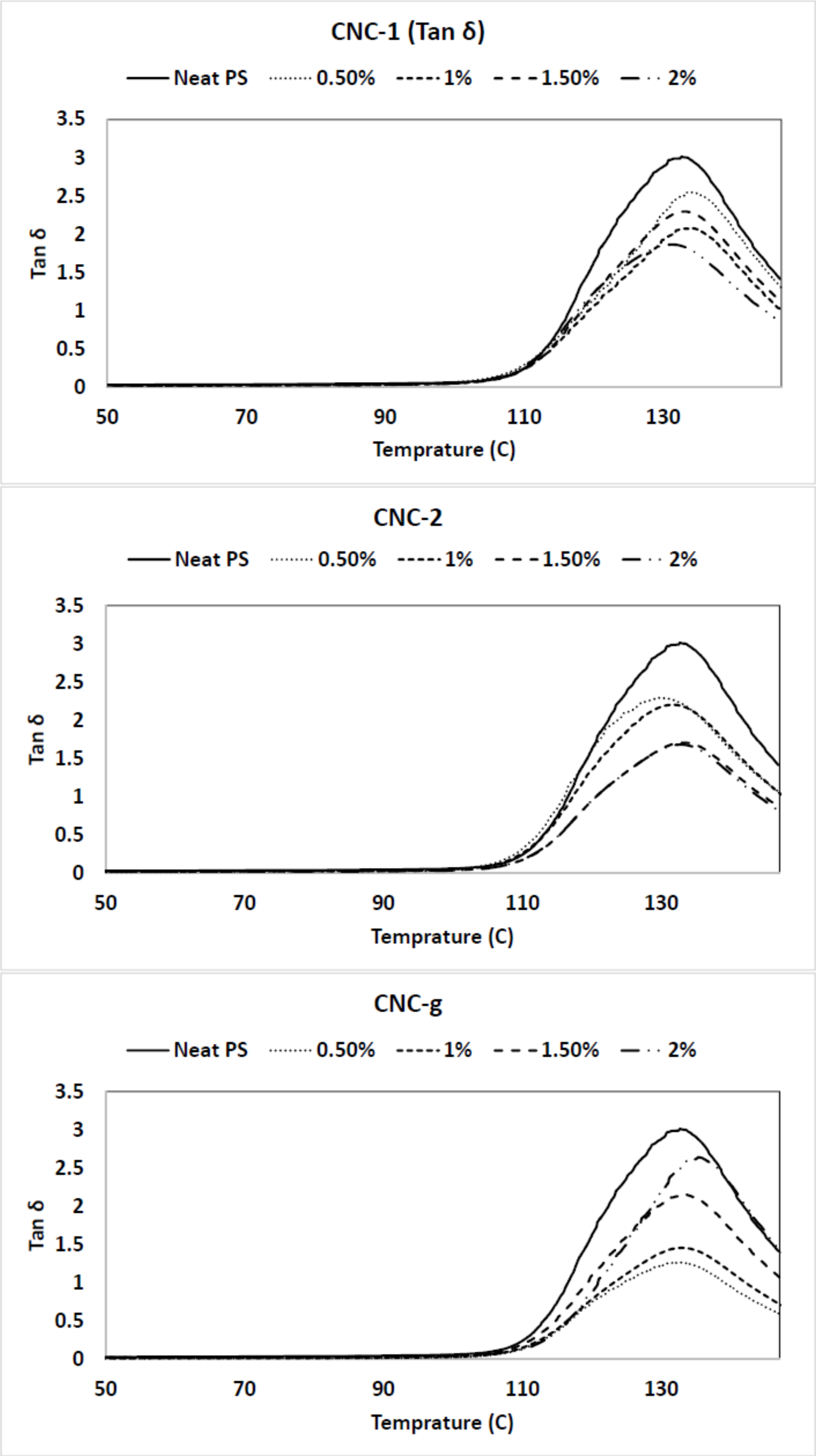

Figure 5. 29: Tan δ results of oriented PS fibrous mats

The effects of CNC presence on Tg can be discussed based on mixing rules:

$$T_{comp} = \frac{V_P T_P + V_{int} T_{int}}{V_P + V_{int}} \qquad \text{Equation 5.20}$$

Where T_{comp}, T_p, T_{int}, are the glass transition temperatures of CNC filled PS fibers, pure PS fibers and immobilized interfacial layers around CNC particles respectively. Again, V_{comp}, V_p, V_{int}, are the volume fractions of the CNC filled PS fibers, pure PS fibers and immobilized interfacial layers around CNC particles respectively. To calculate the interfacial volume fraction (V_{int}), Equation 1 was rearranged by following Mortezaei et.al. as follows (Mortezaei, Famili, and Kokabi 2011):

$$(T_{comp} - T_P)/(T_{int} - T_P) = \frac{V_{int}}{V_{CNC}}(V_{CNC}/(1 - V_{CNC})) \qquad \text{Equation 5.21}$$

Where V_{CNC} is the volume fraction of CNC in PS fibers and in our results it was calculated based on the CNC density of 1.560 g/cm^3 and PS density of 1.065 g/cm^3. Figure 5.30 shows the plots of $(T_{comp} - T_P)/(T_{int} - T_P)$ vs. $(V_{CNC}/(1 - V_{CNC}))$ for CNC-1, CNC-2 and CNC-g samples in oriented electrospun PS fibers by assuming that immobilized PS layers around CNC increased the glass transition temperature about 25^{0}C which was reported by others (Mortezaei, Famili, and Kokabi 2011; J. Berriot et al. 2002; Julien Berriot et al. 2002; Montes, Lequeux, and Berriot 2003). Among three surface modified samples, CNC-1 in PS electrospun fibers showed the smallest change in T_g. There was even a decrease in T_g after reaching a maximum at 1.5% wt. (1.0% vol) nanoparticles concentration. In contrast, CNC-g and CNC-2 in PS electrospun fiber composites resulted steady increases in Tg along with increases in CNC nanoparticles concentration. The weak response of electrospun PS fiber T_g with the addition of nitrobenzene modified CNC-1 can be explained by weak wetting of CNC-1 nanoparticle surfaces with PS molecules. In the case of CNC-g, strong interactions exist among the interpenetration of grafted PS chains on CNC-g surfaces and free PS chains within the PS matrix. In a lesser extent, the inclusion of trifluoromethyl benzene modified CNC-2 also resulted in a steady increase in T_g with CNC-2 concentration. It is due to a good wetting and adhesion at PS- CNC-2 interfaces which leads to reductions in cooperative segmental mobility in the PS matrix. Those results are qualitatively in agreement with the turbidity measurements of the PS grafted CNC particles and their electrospinning in PS/N,N dimethylformamide solutions in Chapter 4. The behavior of glass transition in the supported thin polymer films is the field of extensive research. The results reported in the literature showed the presence of two contrasting effects: the effect of the free surface at the interfaces accelerates the segmental motion and reduces T_g, whereas strong interfacial interactions produce the opposite effect and increases T_g (Forrest and Dalnoki-Veress 2001; Ndoro, Böhm, and Müller-Plathe 2012; Akabori et al. 2005; Karatrantos, Clarke, and Krouger 2016).

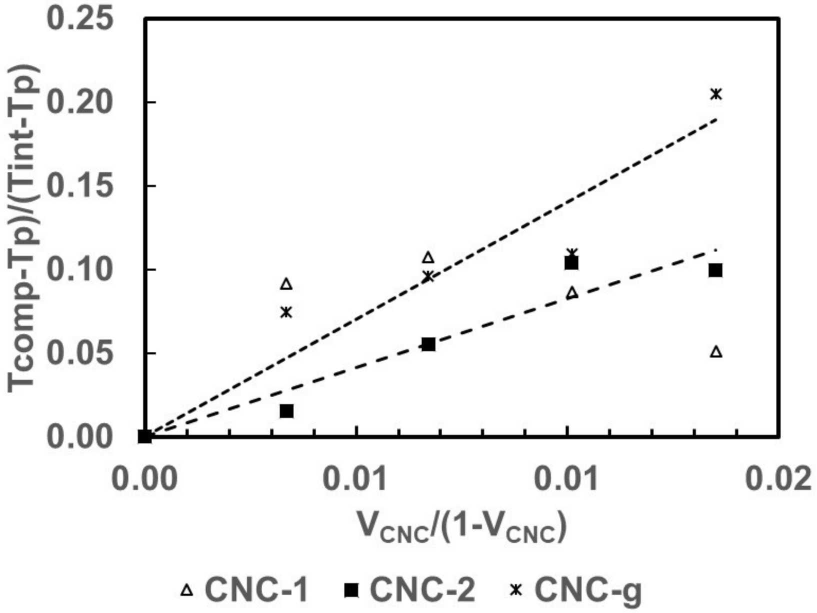

Figure 5. 30: $(T_{comp} - T_P)/(T_{int} - T_P)$ vs. $(V_{CNC}/(1 - V_{CNC})$ for CNC-1, CNC-2 and CNC-g samples in oriented electrospun PS fibers by assuming that T_{int}=25^{0}C. Obtained slopes for CNC-2: 8.266; CNC-g: 13.991.

The slopes of the plots for oriented electrospun PS fibers filled with CNC-2 and CNC-g were used to calculate the volume fractions of immobilized PS thickness around CNC-2 and CNC-g particles.

The thickness of the immobilized polymer films around CNC particles (Δ) can be calculated based on a geometry of CNC particles:

$$\Delta = (\frac{d}{2})(\sqrt[3]{\frac{V_{int}}{V_{CNC}} + 1} - V_{CNC} \qquad \text{Equation 5.22}$$

Where d is the diameter of CNC particles which was taken as 8 nm. By using Equation 5.22, the immobilized interfacial layer thicknesses (Δ) were calculated as 4 and 6 nm for trifluoromethyl benzene modified CNC-2 and PS grafted CNC-g respectively. According to a dynamic study on the interface and interphase dynamics of free PS chains near PS grafted silica nanoparticles, the presence of a surface has a significant influence on the dynamics of the surrounding polymer chains within 1-3 radii of gyration of the bulk PS molecules in the interfacial region (Ndoro, Böhm, and Müller-Plathe 2012).

5.3.4.6. Effect of the fiber orientation on the damping factor

In non-oriented samples (Table 5. 4), the Tg did not change by CNC-g inclusion. In these samples, higher flexibility of grafted PS chains, or smaller fibers structures caused that Tg remain almost constant. However, samples containing 2 wt. % CNC-g shows an increase in Tg which can be explained by agglomeration of CNC and bead formation. Existence of the beads causing the lack of structural uniformities can lead to the lower packing density. Samples with lower packing densities have higher air content acting as heat insulation, and making heat transfer difficult through the sample. Therefore, Tg of the porous structures are usually higher than continues structures. For instance, Tg of PS film is around 90°C. Similarly, the CNC-1 and CNC-2 inclusions cause a positive shift in Tg. This can reflect the possible restriction effects of CNC to the relaxation of the PS chains or lower packing densities of CNC-2/PS and CNC-1/PS electrospun samples with larger fibers. The same results reported for the other randomly oriented electrospun samples with CNC contents. For instance, Tg in the PMMA electrospun samples increased from 119°C to 123°C with 5 wt. % CNC content (H. Dong et al. 2012). However, there were cases that Tg decreased by CNC inclusion. Peresin et al. showed a decrease of 15 degree in Tg for 5 wt. % CNC inclusion in PVA (M. S. Peresin et al. 2014). On the other hand, according to the Figure 5.29 and Table 5.5, the inclusion of CNC did not change the peak position of tan δ obviously for the oriented samples. In oriented samples, the electrospun structures are all almost the same and uniform. Moreover, fiber diameters in most of the samples are the same, so the Tg did not change due to the similar electrospun structure. These results were confirmed by a similar research worked on the CNC/cellulose acetate electrospun fibers with oriented structures (Herrera et al. 2011). Considering the CNC incorporation, it was reported that the addition of CNC lower than 3 wt. % cannot change the Tg tremendously (Sullivan, Moon, and Kalaitzidou 2015), so the Tg changes in the non-oriented samples seems to be mostly because of the different electrospun structures.

Considering the effect of the fiber orientation on the damping amounts, the Tan δ magnitudes for the oriented samples are slightly lower than non-oriented samples. This can prove that the influence of CNC additions in oriented samples were more influential than the non-oriented ones. Finally the oriented structures resulted in the Tg transition to the lower temperatures. This also can be explained by smaller diameter of fibers in the oriented samples (Akabori et al. 2005), and higher packing density. Similar to the non-oriented samples, by inclusion of 2 wt. % CNC-g, an obvious positive in Tg is reported. This can be a reflection of the beaded structure of this sample. Besides, the agglomeration of CNC in this sample could result in the restriction of the PS chains movement.

Table 5. 4: Tan δ and Tg of electrospun samples containing various types of CNCs

CNC Type	Percentage	Tan δ	Tg	Tan δ	Tg
		Oriented		Non-Oriented	
Neat PS		2.98	132.07	3.45	135.32
CNC-1	0.50 wt. %	2.54	133.29	2.87	138.22
	1 wt. %	2.29	133.69	2.49	137.73
	1.50 wt. %	2.08	133.16	2.26	137.97
	2 wt. %	1.85	132.28	1.89	137.27
CNC-2	0.50 wt. %	2.28	131.38	3.06	136.49
	1 wt. %	2.19	132.38	2.28	134.99
	1.50 wt. %	1.52	133.6	2.05	137.45
	2 wt. %	1.47	133.49	1.82	137.52
CNC-g	0.50 wt. %	1.26	132.87	1.53	135.63
	1 wt. %	1.45	133.4	2	135.07
	1.50 wt. %	2.14	133.74	2.1	135.7
	2 wt. %	2.62	136.12	2.58	137.57

5.4.Conclusion

In this chapter, we investigated the production of CNC reinforced PS fiber webs with oriented structures. A rotating drum was considered as a collector in order to induce orientated structures in electrospun products. Likewise to the chapter 4, three types of modified CNC with stronger PS/CNC interfacial interactions were used to reinforce these oriented electrospun products. The modifications included replacement of hydroxyl groups through substitutive reactions with the para nitro benzene, three fluorocarbon benzene, and grafted PS. Electrospinning solutions were prepared using DMF as a solvent, 20 wt. % of PS (Mn= 250000) as a polymer matrix, and five different loading levels of CNC (0, 0.5, 1, 1.5, 2 wt. % in solid fiber corresponding to 0, 0.01, 0.02, 0.03, 0.04 w/v % CNC dispersion in PS solution). The optimum orientation were obtained for the neat PS samples (20%) firstly. To that end, five constant speeds of 500 RPM, 1000 RPM, 1500 RPM, 2000 RPM and 3000 RPM were considered to evaluate the effects of the rotating drum speed. Then, the inclusion effects of the different CNCs on the fiber morphologies, and alignments were studied through SEM images. Subsequently, the results obtained from SEM images were compared by those of the corresponding non-oriented samples. Higher PS concentrations resulted in the smoother and thicker electrospun fibers collected on the rotating drum, and thinner fibers obtained at higher rotating drum speeds. Furthermore, the rotating drum speed of 2000 RPM resulted in the best alignment of fibrous structures. Thus, this speed was applied for the preparation of the CNC/PS samples as well. Addition of the CNC modified with para nitro benzene and para three fluorocarbon benzene to the fiber resulted in a smooth fiber structure. Alternatively, beaded fibers, were obtained by using regular CNC and CNC grafted with PS for higher concentrations. However, the best rotor speeds to obtain optimum fiber alignments were slightly different for the CNC reinforced fiber and the neat PS fibers. Finally, the effects of CNC inclusion and fiber alignments on the elastic modulus, strength and maximum strain of the fiber mats were investigated by conducting tensile tests. Besides, storage moduli, loss moduli, and damping factors of the electrospun samples were measured and compared by means of Dynamic Mechanical Anlysis (DMA). The oriented PS mats with 0.5 wt. % CNC grafted with PS showed the best mechanical gain. The elastic modulus (E) and storage modulus (E') of this samples increased 910% and 250%, respectively. Finally, alignments of the electrospun fibers led to 450% improvement in stiffness, and 250% increment in storage modulus with inclusion of 2 wt. % of different CNC.

Chapter 6

6. Electrospun PS Fibers as a Novel Approach to Produce Super hydrophobic Surface

6.1. Introduction

The present Chapter aims to study the surface properties of produced electrospun as well as to maximize their hydrophobicity.

Superhydrophobic surfaces can result in non-adhesive and non-wetting properties in multifunctional materials. Some instances of such properties are including self-cleaning, anti-corrosion, anti-icing, and low hydrodynamic friction. Therefore, production of materials with such surface properties recently attracted tremendous attentions (Ma et al. 2007; Sas et al. 2012; Y. Li, Lee, and Cho 2007; Nuraje et al. 2013; Feng et al. 2002; Y. Li et al. 2005; Ma, Hill, et al. 2005). Not only superhydrophobic surfaces exhibit extremely high-contact angles (i.e., >150 ^{o}), but also they have low contact-angle hysteresis between advancing and receding contact angles, normally less than 5^{o}. There are several examples of these phenomenal surfaces in nature, such as the wings of insects or the lotus leaves which are superhydrophobic due to their surface structure and chemistry (Ma et al. 2007; Sas et al. 2012).

The superhydrophobic property of a surface is mainly controlled by two key surface parameters namely, the surface energy and surface roughness (Michielsen and Lee 2007; Ma et al. 2007; Ma, Mao, et al. 2005). Hence, a superhydrophobic surface can be actually fabricated and modified by increasing the roughness of a low energy surface or reducing the surface energy of a rough surface (Ma, Mao, et al. 2005; Zhai et al. 2004).

Thus far, numerous techniques were effectively designed to create rough textures on surfaces, such as inverse opal surface, plasma polymerization or etching, layer-by-layer process, phase separation, and sol–gel process (Y. Li et al. 2005; Lim et al. 2007; Shang et al. 2005). Among these techniques, electrospinning was mainly employed to produce continuous nano-/micro-fibers of a large range of materials, including natural and synthetic polymers, polymer derived carbon, metals, metal oxides, ceramics, etc. (Gopal et al. 2007; M. Wang et al. 2004; D. Li and Xia 2004; D. Chen et al. 2009; Bellani et al. 2016; Seeram Ramakrishna, Kazutoshi Fujihara, Wee-Eong Teo, Teik-Cheng Lim 2005). This technique is a low-cost, continuous, and scalable nano-manufacturing procedure. Moreover, the surface morphology of electrospun fibers can be easily tailored by changing the parameters of electrospinning process or the solution properties. The solution properties that can be manipulated are including the solution conductivity, polymer molecular weight and concentration, applied electrical field, working parameter, inner diameter of needle, flow rate, etc. (Theron, Zussman, and Yarin 2001; Gopal et al. 2007; Mohammadian and Haghi 2014; X. F. Wu and Yarin 2013; Z. Zhou et al. 2014; Z. Zhou et al. 2011).

6.1.1. Theory of superhydrophobicity

In a theoretical attempt, Young tried to quantify the contact angle (θ) by measuring the forces acting on a droplets enclosed by air molecules (Nuraje et al. 2013). There are four categories of surface in term of hydrophobicity as following: superhydrophilic, hydrophilic, hydrophobic, and superhydrophobic surfaces. Figure 6.1 illustrates a schematic of these four categories.

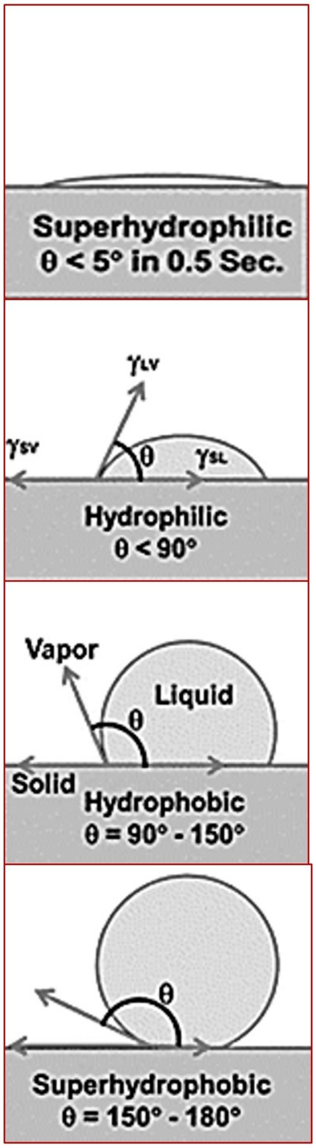

Figure 6. 1:The schematic of four different types of surface in term of hydrophobicity (Adopted by (Sas et al. 2012))

Based on the Young's equation (Equation 6.1), the contact angle θ_c of a water droplet on a flat solid surface can be calculated by the interfacial surface tensions of γ_{sv}, γ_{sl}, and γ_{lv} where S, L, and V stand for solid, liquid, and vapor, respectively.

$\mathbf{Cos}(\boldsymbol{\theta}_\mathbf{c}) = \frac{\gamma_{sv}-\gamma_{sl}}{\gamma_{lv}}$ (Ma et al. 2007) Equation 6. 1

According to this equation, the term of cos θ_c of a specific droplet on a specific surface is a proportion of the difference of interfacial forces of solid–vapor and solid–liquid interfaces per unit length to the interfacial forces of the liquid–vapor interface, at equilibrium (Sas et al. 2012).

To discuss the dynamic behavior of water droplets, a tilted surface is usually considered. A three-phase contact line is the main parameter used to predict the dynamic behavior of a droplet on the surface of a solid (Nuraje et al. 2013; Öner and McCarthy 2000). Throughout the droplet motion, water molecules result in a three-phase contact line forming a specific solid and air interface (Sas et al. 2012). At equilibrium stage, this contact line stays mostly in balance, and other energy barriers for the advancing and receding of the contact line can cause hysteresis (Sas et al. 2012). When the contact line is destabilized, it forms a lower hysteresis. At lower hysteresis, the droplet can move by the gravity (Sas et al. 2012). The dynamic behavior of a droplet on a tilted surface is shown in Figure 6.2. The average of the different angles on each side of the droplet determines the overall contact angle values of the droplet on a sloped surface.

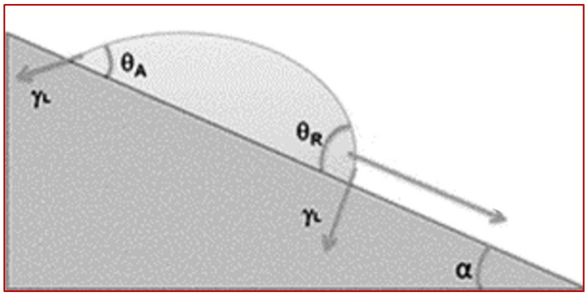

Figure 6. 2: the dynamic behavior of a droplet on a sloped surface

As described before, the surface roughness is the other significant factor that can change the surface hydrophobicity, thus this factor can also affect the water contact angle values. Two models were suggested to evaluate the effect of roughness on the water contact angle. The first model was proposed by Wenzel (Equation 6.2). In this model, water is in intimate contact with the surface, and it can fill all its microstructures. Accordingly, the water contact angle can be altered (Sas et al. 2012).

$\mathrm{Cos}\ \theta_w = r\mathrm{Cos}\theta_c$ Equation 6. 2

where $\cos \theta_w$ is the Wenzel contact angle, and r is the surface roughness factor. If the surface roughness factor is equal to one, the Equation 6.2 turns into Equation 6.1. Since the water penetrates into the cavities on the surface (see Figure 6.3), the roughness factor is always greater than unity, resulting in an increase in contact angle on a hydrophobic surfaces and a decrease in contact angle on a hydrophilic surfaces (Sas et al. 2012).

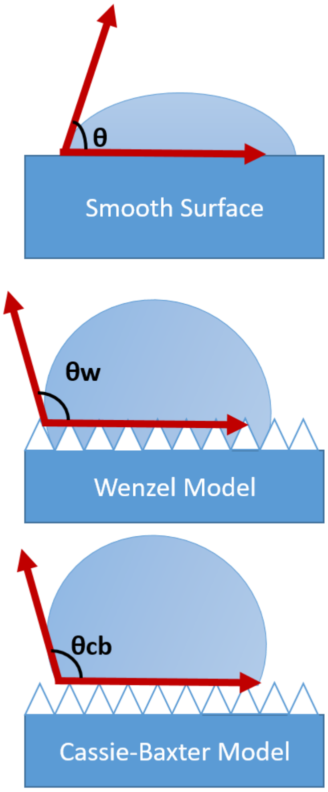

Figure 6. 3: Water droplets on flat solid surface (left), Wenzel state (middle), and Cassie–Baxter state (right) (Adopted by (Nuraje et al. 2013))

The second model describing the effect of roughness on the water contact angle was proposed by Cassie and Baxter (Equation 6.3). This model was developed based on the heterogeneous wetting state, whereby air is entrapped by water in the surface microstructures (Sas et al. 2012). Based on this assumption, the contact area between the solid and water is minimized, while the area between the air and water is maximized, thereby allowing water to create spherical droplets (Sas et al. 2012).

$$\mathbf{Cos\theta_c = r_f f Cos\theta_\gamma + f - 1} \qquad \text{Equation 6. 3}$$

where f defines the ratio of the solid–liquid contact area to the area of projection of the droplet, and r_f is the roughness ratio (Sas et al. 2012). Therefore, when f drops due to the more entrapped air, both surface roughness and contact angle can significantly increase.

Both of these models are successful to describe how the contact angle increases by surface roughness, and predict a high contact angle on rough hydrophobic surfaces. However, they do not consider the dynamic behavior of a droplet when it moves on a surface, so the resultant contact-angle hysteresis can be entirely different in both cases.

In the Wenzel model, the liquid phase fills all the cavities and pours of the surface, so it is strongly attached to the surface, resulting in relatively high-contact-angle values. Therefore, a higher force is needed to replace the attached droplet on the surface. Based on this model, a higher surface roughness will lead to a larger surface area. This can increase hydrophobicity because water fills microstructures on the rough surface resulting in a stronger pinning, and such a surface shows a high hysteresis as well (Sas et al. 2012).

When the roughness factor is higher than a certain value, water droplets cannot permeate to all voids and cavities of the surface. Subsequently, a transition from the Wenzel model to the Cassie–Baxter model happens, (Sas et al. 2012; Nakajima, Hashimoto, and Watanabe 2001).

6.1.2. Rose petal effect

A suitable combination of surface roughness and surface chemistry can be considered to create surfaces with superhydrophobic features. Tus far, different types of superhydrophobic surfaces were studied theoretically and also fabricated artificially as discussed previously. There are also another superhydrophobic surface that not only shows a large contact angle but represents a high contact angle hysteresis. On this type of surfaces, water droplets demonstrations strong adhesion to the surface despite of large contact angles. Rose petal or gecko's foot are some natural examples of these phenomenal surfaces, and they are so-called surfaces with rose petal effect. In addition to red roses, Chinese kaffir lily (Clivia miniata) and sunflower (Helianthus anuus) also show the same effect. This characteristic can be explained by the hierarchical structure of these rough surfaces constructed of micro- and nanoscale roughness (Bhushan and Nosonovsky 2010).

There are some researches conducted on the production of surfaces with rose petal effect. Jin and his colleagues reported a superhydrophobic PS aligned nanotubes layer with high adhesive force (Jin et al. 2005). They reported that this material can be successfully used for a no-lost reversible transport of microliter-sized liquid droplets (Hong, Gao, and Jiang 2007).

Both Wenzel and Cassie–Baxter models can be considered to describe the behaviour of the surfaces with rose petal effect (see Figure 6.4). Water can fill either the micro- or nano-structure, or both. Moreover, these structures can be permeated by water or air. Table 6.1 comprehensively describes the possibility of each regime, and the consequent behaviour of the surface (Bhushan and Nosonovsky 2010).

Based on the hydrophobicity of PS, and the high roughness of electrospun samples, it is expected that the CNC/PS electrospun samples prepared in the present study show one of the hydrophobicity regime described above. To evaluate the samples surface properties, water contact measurement and roughness measurement were performed. The results show a high contact angle, as large as 150 degree, along with high water adhesion, which can be attributed to the hierarchical roughness of the electrospun samples (Bhushan and Nosonovsky 2010).

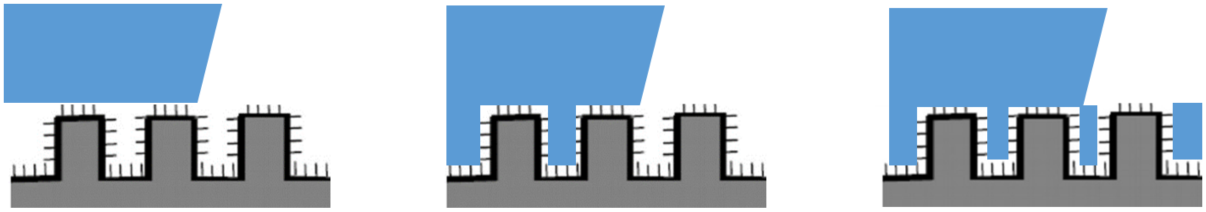

Lotus **Rose** **Rose Filled Microstructures**

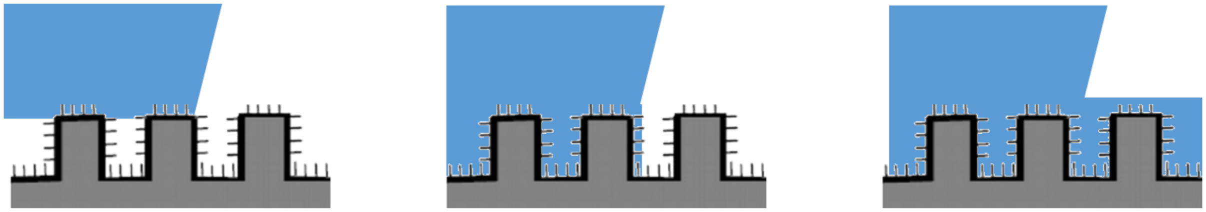

Cassie **Wenzel** **Wenzel Filled Microstructures**

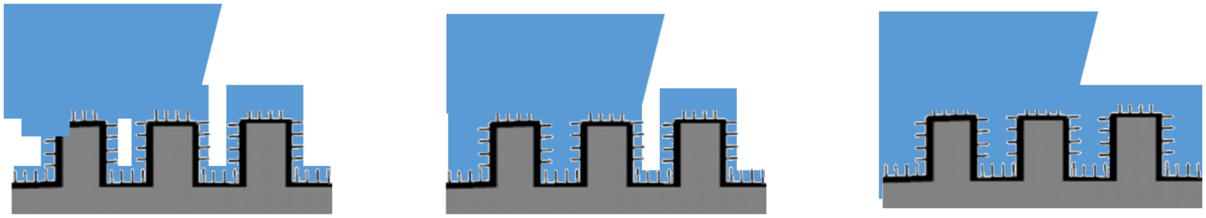

Cassie Filled nanostructures **Wenzel Filled nanostructures** **Wenzel Filled Micro/nanostructures**

Figure 6. 4: Schematic of nine wetting situations for a hierarchical rough surface (Adopted by (Bhushan and Nosonovsky 2010))

Table 6. 1: Different systems of wetting for a dual rough surface (Bhushan and Nosonovsky 2010).

	Microstructure filled with air	Just microstructure in contact with droplet filled with water	water fills the whole microstructure
Nanostructure filled with air	lotus, high CA, low CA hysteresis	rose, high CA, high CA hysteresis	rose filled microstructure
Just nanostructure in contact with droplet filled with water	Cassie (air-filled microstructure, water in nanostructure), high CA, low CA hysteresis	Wenzel (water in micro- and nanostructure), high CA, high or low CA hysteresis	Wenzel filled microstructure
water fills the whole nanostructure	Cassie filled nanostructure	Wenzel filled nanostructure	Wenzel filled micro- and nanostructure

6.2. Experimental

6.2.1. Materials

Tetrahydrofuran (THF), Dimethyl formaldehyde (DMF), and Toluene as solvents, and Polystyrene (PS) (MW = 280,000 g/mole, Tg = 100 °C) as fiber material used in this project were all purchased from Sigma Aldrich, Inc. All materials were used without further purification. The chemical structures and physical properties of the solvents are presented in Table 3.1.

6.2.2. PS nano rough surface preparation

PS was dissolved in various organic solvents or mixtures of them with concentrations of 20 w/v% under gentle stirring at room temperature for 5 hours. Subsequently, the polymer solution was loaded in a 10 ml plastic syringe with a blunted metal needle. The electrospinning sections were performed with 10 µl/min of flowrate, a working distance (nuzzle-to-collector distance) of 17 cm, and 20 KV of voltage for all the solution systems in this research. All the electrospinning experiments were carried out under fume hood, and both temperature (T) and relative humidity (RH) were controlled at 23°C and 24%, respectively. Electrospinning were performed at different periods of time including 5 minutes, 20 minutes, 40 minutes, 1 hour, 2 hours, and 3 hours.

The solvents that were used to form various electrospun structures selected based on the results obtained in Chapter 3.

6.2.3. SEM analysis

Both the surface morphology and structures of fibers and their diameters were studied using a scanning electron microscope (SEM) (Vega-3 (Tescan) with an EDXS detector, Oxford Instruments) at an acceleration voltage of 20 kV. SEM analyses of samples were performed without coating. To determine the average diameter of each fiber sample, five different spots on each specimen were randomly selected for the SEM analysis.

6.2.4. Contact angle measurement

Contact angles were measured by using a contact angle system (FTA-200, FTA Co., USA) at ambient temperature. Water droplets (2.0 μL) were released carefully onto the surface of the samples. The average contact angle was obtained by measuring at five different positions of every sample.

6.2.5. Laser scanning Confocal Microscopy

A confocal laser scanning microscopy (CLSM) was used to measure the roughness of the electrospun products. In this optical imaging technique, a spatial pinhole is used to block out-of-focus light beams in image formation for increasing optical resolution and contrast of a micrograph (see Figure 6.5). A three-dimensional structures can be obtained by capturing several two-dimensional images at different depths in an electrospun sample (Pawley 2006).

Confocal micrograph of the CNC/PS fiber mesh were obtained by a laser scanning confocal microscope (Olympus OLS-3000) both with excitation at 480 nm and emission at 540 nm.

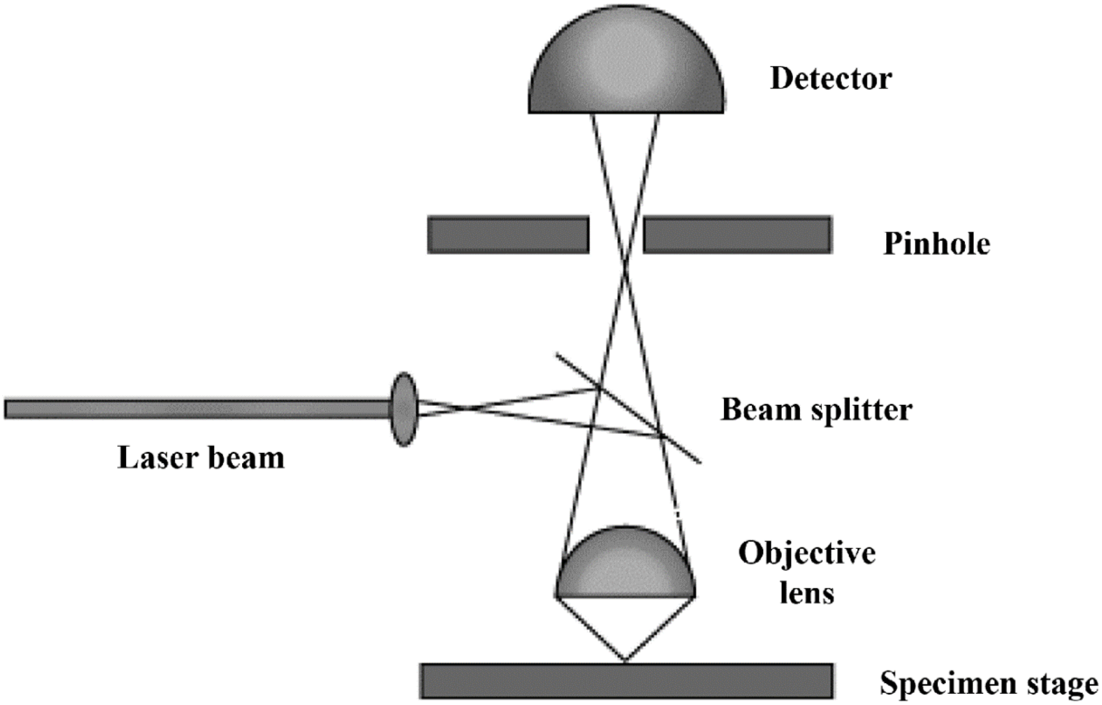

Figure 6. 5: construction of a confocal laser scanning microscopy (Adopted by (Pawley 2006)).

The numerical roughness measurements were conducted and reported according to Equation 6.4.

$$\boldsymbol{R_q = \sqrt{\frac{1}{n}\sum_{i=1}^{n} h_i^2}} \qquad \text{Equation 6. 4}$$

where R_q is the root mean squared of the linear roughness and h_i is the vertical distance from the mean line to the i^{th} data point. The mean line, and h_i were shown in Figure 6.6.

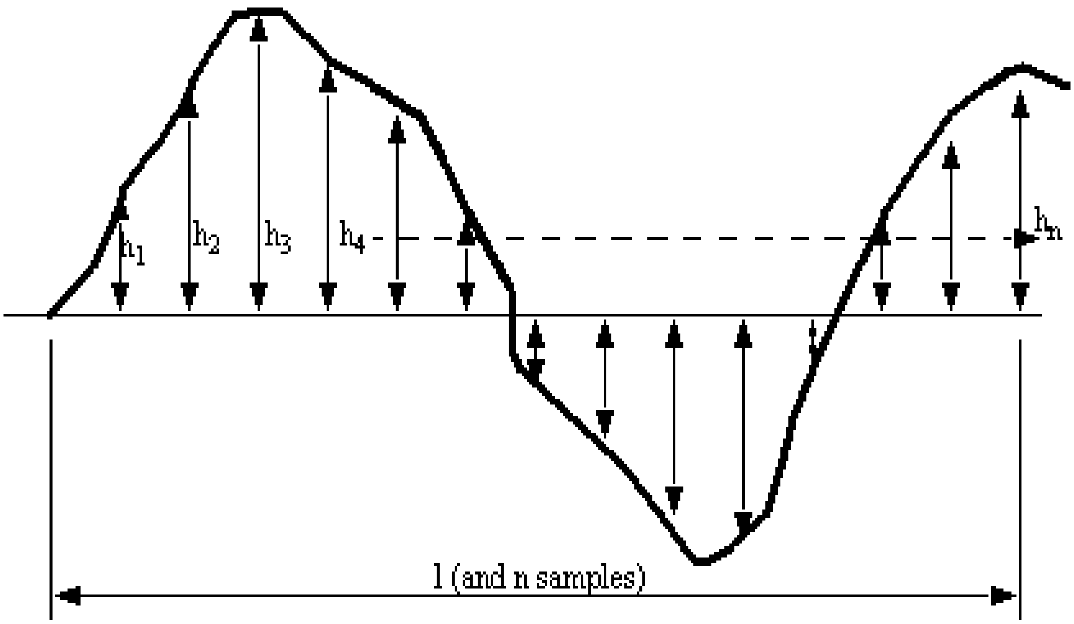

Figure 6. 6: The mean line, and hi of a rough surface

6.3. Results and Discussions

6.3.1. Evaluation of the morphology effects on the hydrophobicity of nanofibrous Webs

Three different morphologies such as smooth fibers, beaded fibers, and electrosprayed beads were considered to obtain the best hydrophobicity. These structures were produced by electrospinning of PS solution in various solvents based on the results obtained in Chapter 3. The smooth fibers and electrosprayed beads were obtained by means of PS/DMF and PS/Toluene solution, respectively. To produce beaded fibrous structures with the same fiber size, a 50% DMF-50% THF combination was used as the electrospinning solvent. Figure 6.7 shows the SEM images of these electrospun products.

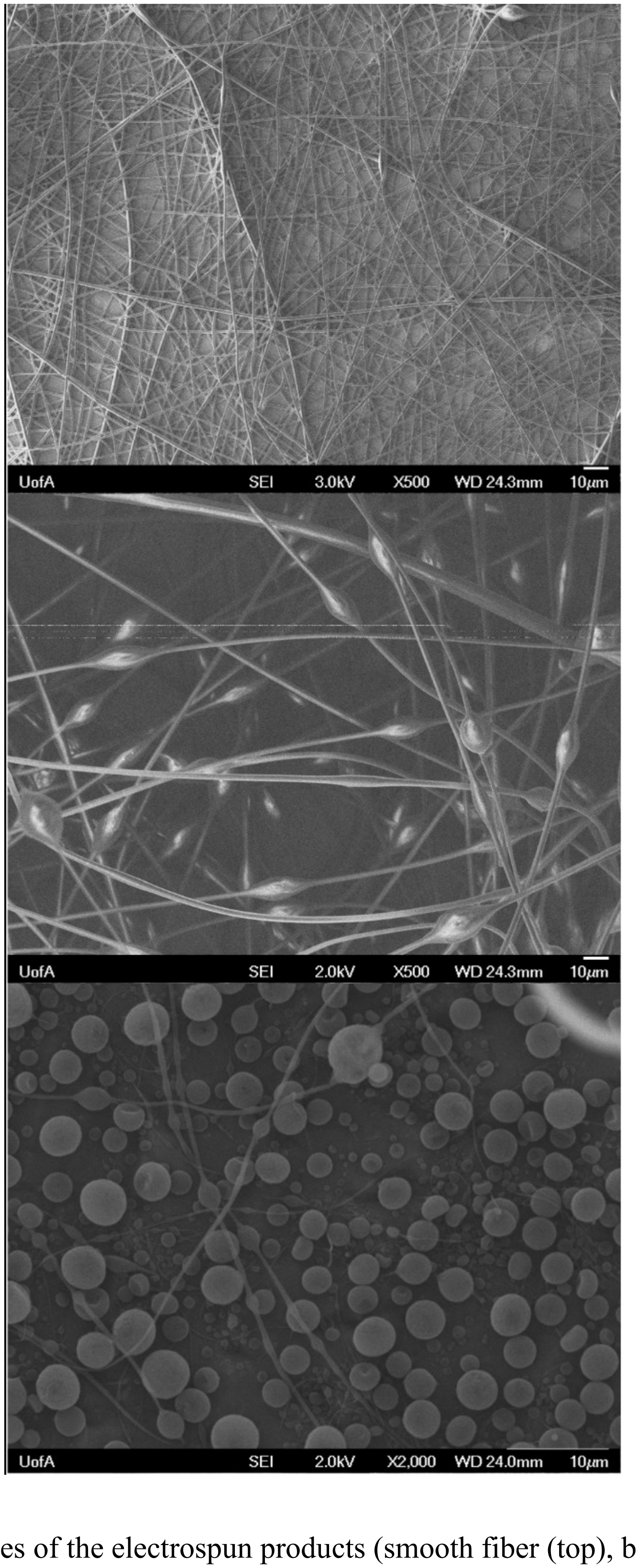

Figure 6. 7: SEM images of the electrospun products (smooth fiber (top), beaded fibers (middle), and electrosprayed beads (down)).

As described previously, the hydrophobicity of the electrospun samples were evaluated using the water contact angle measurement. Figures 6.8, 6.9, and 6.10 depict the change in the water contact angle corresponding to various durations of the electrospinning for smooth fibers, beaded fibers, and electrosprayed beads, respectively. For the sake of easier comparison, these results are also presented in a graph in Figure 9.11. As can be seen, 30-60 min of electrospinning will result in the highest contact angle for smooth fibers and beaded fibers. On the other hand, for electrosprayed beads a continuous growth in contact angle was observed with increase in electrospinning time. This trend can be explained by the fact that the productivity of the elctrosprayed beads was too low, and smaller amounts of beads can be collected during an specific time in comparisons with the electrospun products. In electrospun samples, the conductivity of the solvents are higher than the toluene because of the existence of DMF. Higher conductivity of the electrospinning solvent can lead to a higher productivity. Accordingly, more material were collected on the aluminium foil after a particular time, and these material are not necessarily increased the roughness. Sometime, collection of a thick layer of nonwoven fibers can lead to larger void which in water can penetrate easily. This issue can describe the decreasing trends of contact angle after a particular time of electrospinning.

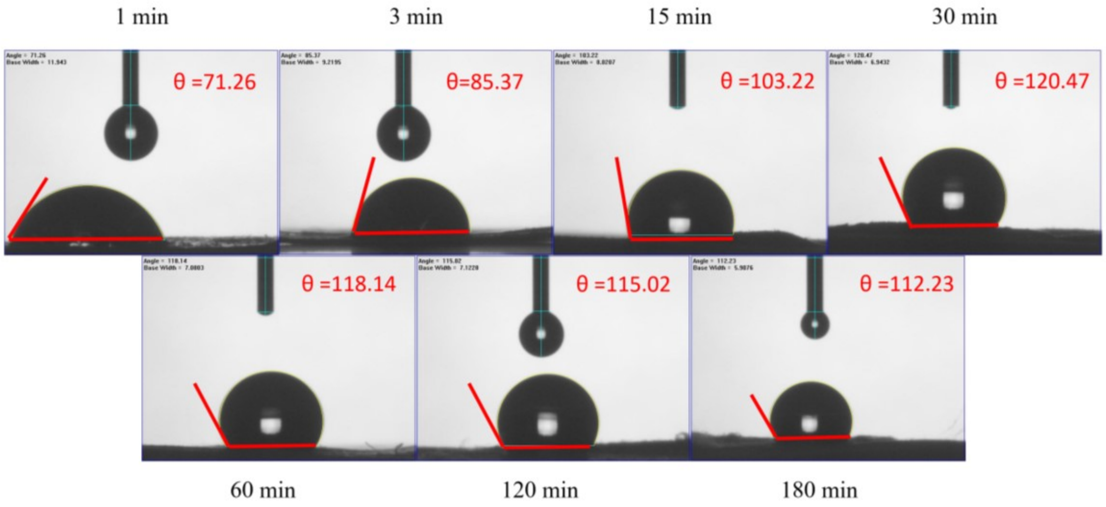

Figure 6. 8: Water contact angles of the electrospun PS smooth fiber at different time of the electrospinning

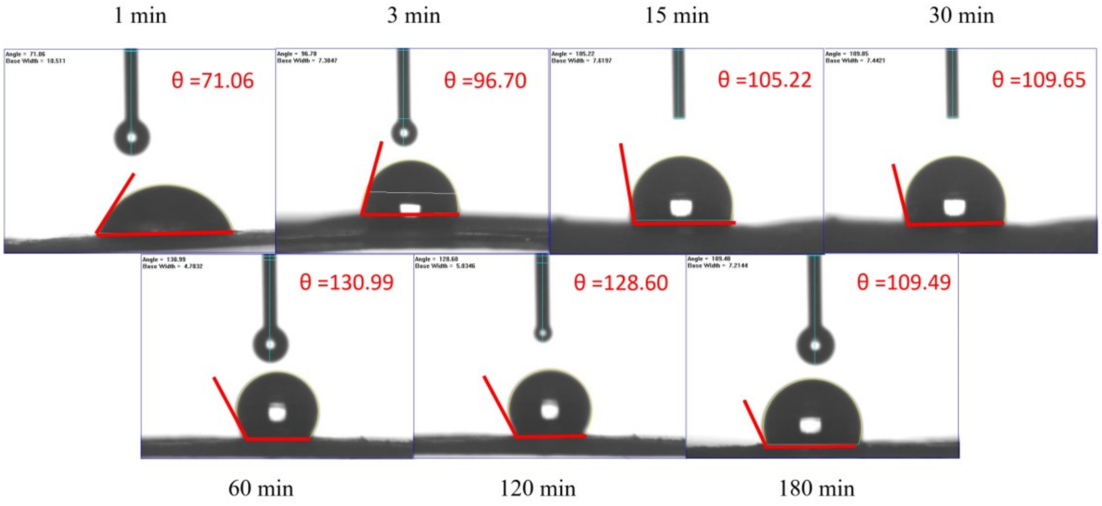

Figure 6. 9: Water contact angles of the electrospun PS beaded fiber at different time of the electrospinning

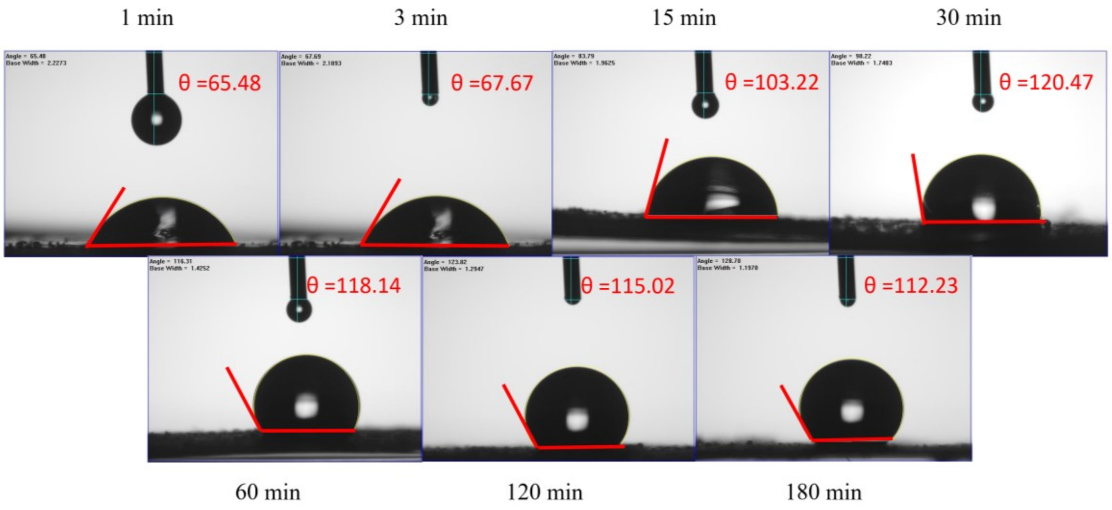

Figure 6. 10: Water contact angles of the electrosprayed PS beads at different time of the procedure

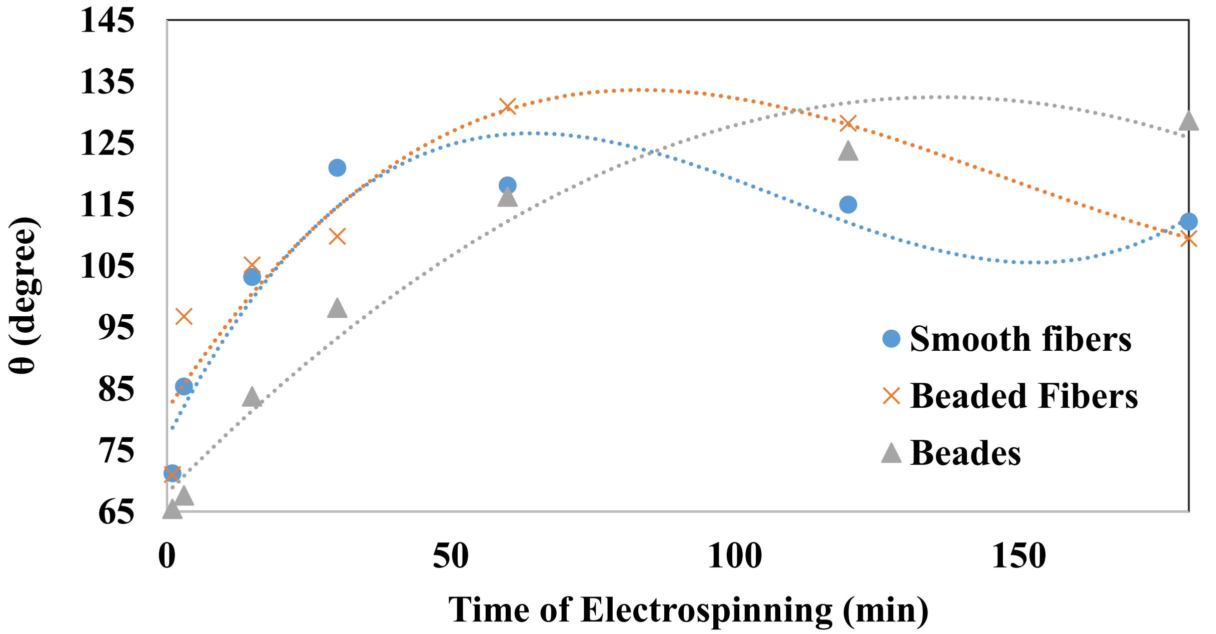

Figure 6. 11: The water contact angles for different samples versus the electrospinning duration

Moreover, the sample of the smooth fibers resulted in the contact angles around 120° which shows a notable increase in hydrophobicity in comparison with the PS film with contact angle of 95° (Jin et al. 2005). This can be explained by the higher roughness of electrospun samples (Sas et al. 2012). Similar trend was observed in other studies as well where higher contact angles were reported for electrospun samples compared with the smooth films of the same polymers. For instance, while the contact angle of gelatin is around 45° (Yasuda, Okuno, and Yasuda 1994)a contact angle of 76 ° was reported for the electrospun product of this polymer (Zhang et al. 2005). Likewise, despite of the low contact angle of 82° observed for polycaprolactone film, a high contact angle of 128° was reported for PCL electrospun fibers (Can-Herrera et al. 2016).

The samples of beaded structures showed a contact angle as high as 135° which can be attributed to their larger structures of the formed beads. According to Huang et al. (F. L. Huang et al. 2010), the thicker fibers resulted in the larger contact angles. They attributed these results to the higher roughness of the larger fibers. Finally, the samples of the electrosprayed beads with higher roughness resulted in a contact angle of 130 ° after 3 hours of the electrospinning. These results indicate the potential of the PS electrospraying as a technique for the production of materials with superhydrophobic surfaces.

6.3.2. Evaluation of the roughness of nanofibrous structures

Roughness measurements were carried out by means of laser confocal microscopy, and the numerical magnitudes of the samples were presented in the root mean squared of the linear roughness in Figure 6.12. Higher roughness was obtained for the samples with higher contact angle which agrees with the predictions of the Wenzel's model. In order to evaluate the accuracy of this model, firstly, the surface roughness factor was calculated. For surfaces with low contact angle, the aluminum foil was considered as the reference surface, and for surfaces with contact angles close to the 95 degree (The contact angle of PS film), a combination of both aluminum foil and PS film were considered as the reference surface. Table 6.2 shows the evaluation steps of the surface roughness based on this model. For surfaces with the contact angles larger than 95 degree, just PS film were considered as the reference surface. The calculated surface roughness factors are presented in Figure 6.13. As can be seen, these results show a good agreement with the experimental results obtained for the roughness.

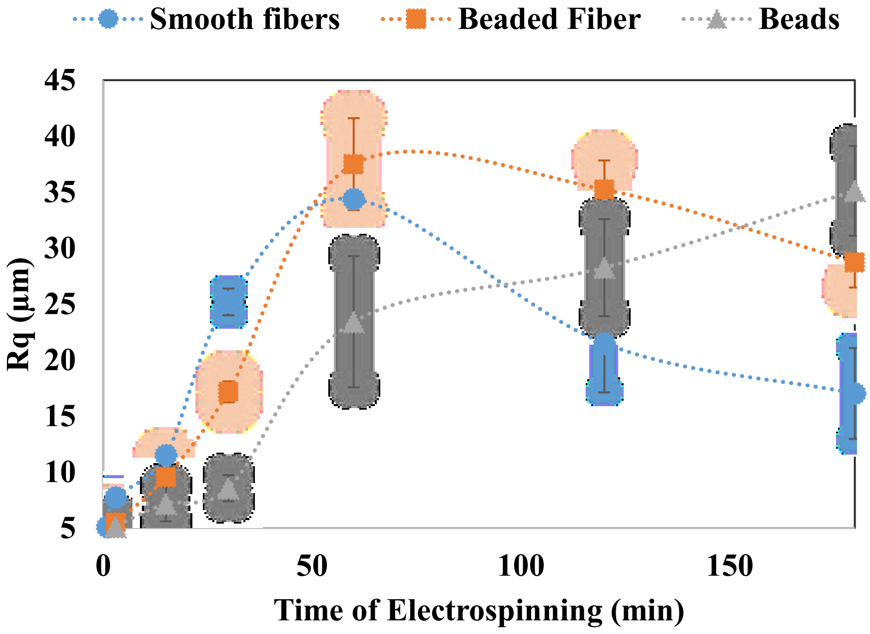

Figure 6. 12: The root mean squared of the linear roughness of different samples

(In this chart lines are illustrated to guide the eyes)

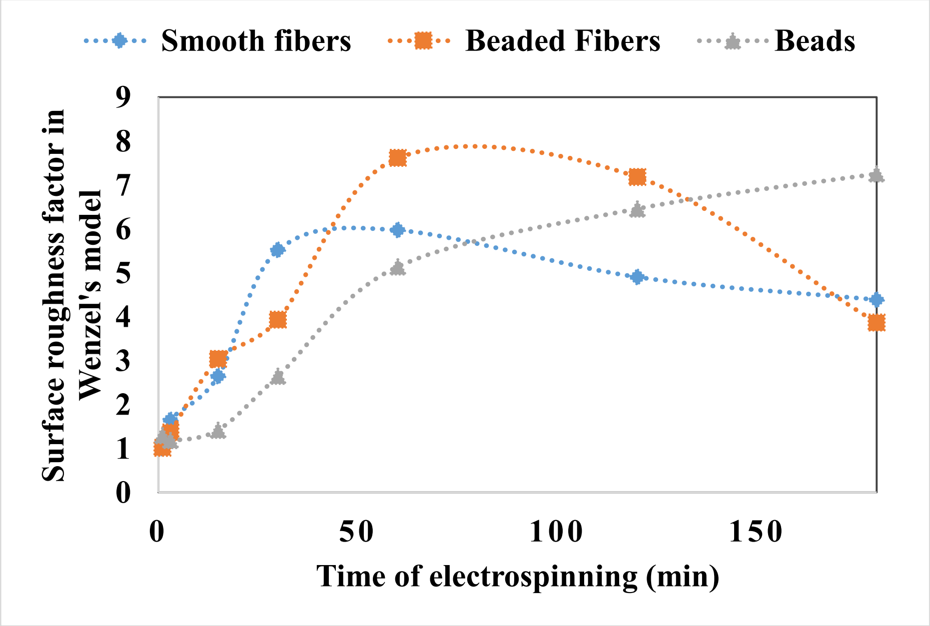

Figure 6. 13: The surface roughness factor of Wenzel’s model for different samples

(In this chart lines are illustrated to guide the eyes)

Table 6. 2: Evaluation steps of the surface roughness based on the Wenzel's model

Product	Time of procedure	Contact Angle	Cos(θw)	Surface type	Cos(θc)	r	Rq	Rq/r
Smooth fibers	1.00	71.26	0.32	Aluminium foil	0.32	1.01	5.12	5.09
	3.00	85.37	0.08	Aluminium foil/PS	0.06	1.65	7.73	4.68
	15.00	103.22	-0.23	PS	-0.09	2.65	11.50	4.34
	30.00	118.40	-0.47	PS	-0.09	5.52	25.20	4.57
	60.00	120.97	-0.51	PS	-0.09	5.97	34.37	5.75
	120.00	115.02	-0.42	PS	-0.09	4.91	21.50	4.38
	180.00	112.23	-0.38	PS	-0.09	4.39	17.02	3.88
Beaded Fibers	1.00	71.06	0.33	Aluminium foil	0.32	1.02	4.56	4.49
	3.00	96.78	-0.12	PS	-0.09	1.36	5.49	4.03
	15.00	105.22	-0.26	PS	-0.09	3.04	9.54	3.14
	30.00	109.85	-0.34	PS	-0.09	3.94	17.17	4.36
	60.00	130.99	-0.66	PS	-0.09	7.62	37.50	4.92
	120.00	128.22	-0.62	PS	-0.09	7.18	35.23	4.90
	180.00	109.48	-0.33	PS	-0.09	3.87	28.73	5.43
Beads	1.00	65.48	0.42	Aluminium foil	0.32	1.30	4.16	3.20
	3.00	67.69	0.38	Aluminium foil	0.32	1.19	5.12	4.31
	15.00	83.79	0.11	Aluminium foil/PS	0.06	1.77	7.17	4.06
	30.00	98.22	-0.14	Aluminium foil/PS	0.06	2.65	8.56	3.23
	60.00	116.31	-0.44	PS	-0.09	5.14	23.43	4.56
	120.00	123.82	-0.56	PS	-0.09	6.46	28.26	4.37
	180.00	128.70	-0.62	PS	-0.09	7.26	35.12	4.84

Figure 6.14 illustrates the change in ratio of the R_q values over the surface roughness factor of Wenzel's model for each sample. As demonstrated in these graphs, this ratio is fairly constant and is fluctuating in a small range for all samples which indicates that both R_q and Wenzel roughness factor are generally following a similar trend. Moreover, these small fluctuations can be justified by the Cassie and Baxter model, and various amounts of *f* (the ratio of the solid–liquid contact area to the area of projection of the droplet) for different samples.

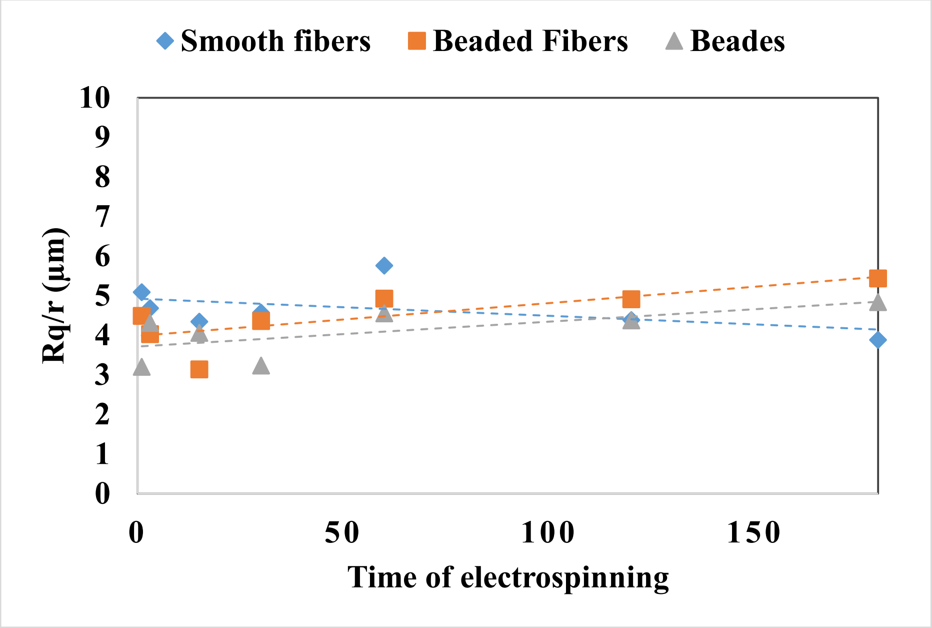

Figure 6. 14: changes of the ratio of Rq/r by the time of electrospinning

6.3.3. Observation of the rose petal behaviour in PS electrospun samples

The PS electrospun samples showed a high level of water adhesion despite of exhibiting a high contact angle. This phenomenon is known as rose petal effect. The rose petal behaviour is shown in the Figure 6. 15. Pisuchpen et al. and Guangming et al. also reported the same behavior for PVA and Polyimid electrospun samples, respectively (Pisuchpen et al. 2011; Guangming et al. 2014; Gong et al. 2012). Some researches assumed that the water adhesion is due to the collapse of the surface fibrous structures and the removal of air voids (Pisuchpen et al. 2011). This characteristic, proposed as the "Petal effect" by Feng et al. is also postulated to be originated from the "Cassie impregnating wetting state" in which water soaks large hollows on the surface whereas leaving the small voids dry (see Figure 6.4) (Feng et al. 2008). Nonwetting over these tiny voids, comparable to that shown in the Cassie-Baxter model, enables a high advancing contact angle, making the surface appear hydrophobic on the macroscopic level. However, the migration of water to the larger and wettable hollows can result in a low receding contact angle and high hysteresis. Although the hysteresis of contact angle can characterize the water adhesion on a surface, the water permeation can discriminate the “Lotus effect” from the “Petal effect” (Feng et al. 2008). The hierarchical structural surfaces of the PS electrospun samples, assembled of micro- and nanoscale roughness, result in various sized grooves (Bhushan and Nosonovsky 2010). Water can permeate to the larger voides, but not to the very small ones which can cause this phenomenon on the surfaces of the electrospun samples.

Figure 6. 15: Observation of the rose petal effec on the PS electrospun samples

6.3.4. Effect of CNC incorporation on the hydrophobicity of the electrospun samples

Samples containing variously modified CNCs were prepared and discussed in Chapters 4 and 5. The surface properties of these samples are discussed in this section. As Figure 6.16 shows, the addition of CNC-1, CNC-2 resulted in a drop in contact angle which can be attributed to the hydrophobicity of the CNC, and change in the roughness of the fibers (see Figure 6.17). As discussed in Chapter 4, the dimensions of the fibers changed by the CNC inclusion resulting in the fluctuation of the roughness. However, CNC-g incorporation gave a rise to the contact angle which can be explained by the beaded structure of this sample as well as the hydrophobic chemical structure of this type of modified CNC. Moreover, unlike CNC-1 and CNC-2 which caused a drop in the fiber roughness, incorporation of CNC-g did not influence the surface roughness.

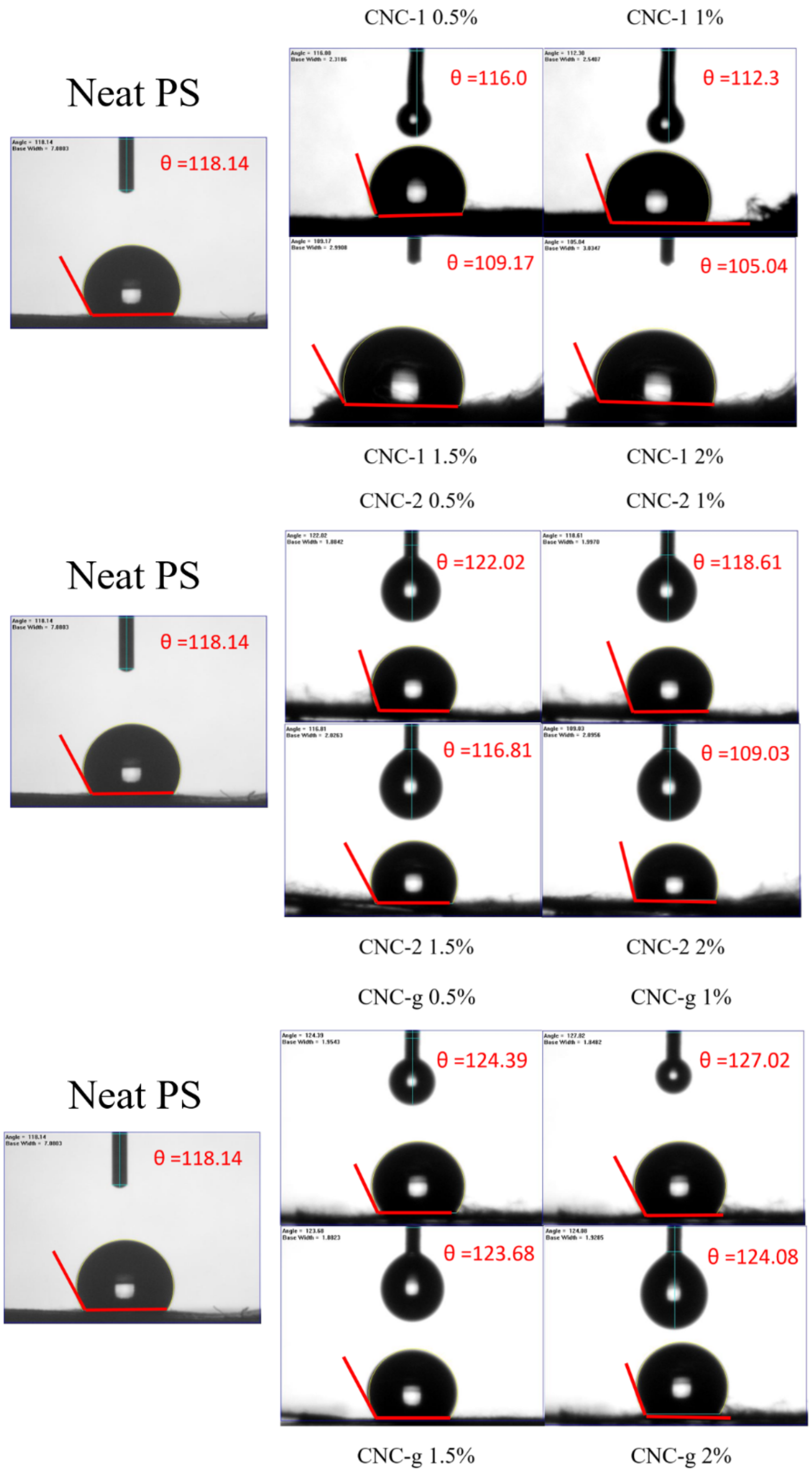

Figure 6. 16: The water contact angle changes by the CNC incorporation

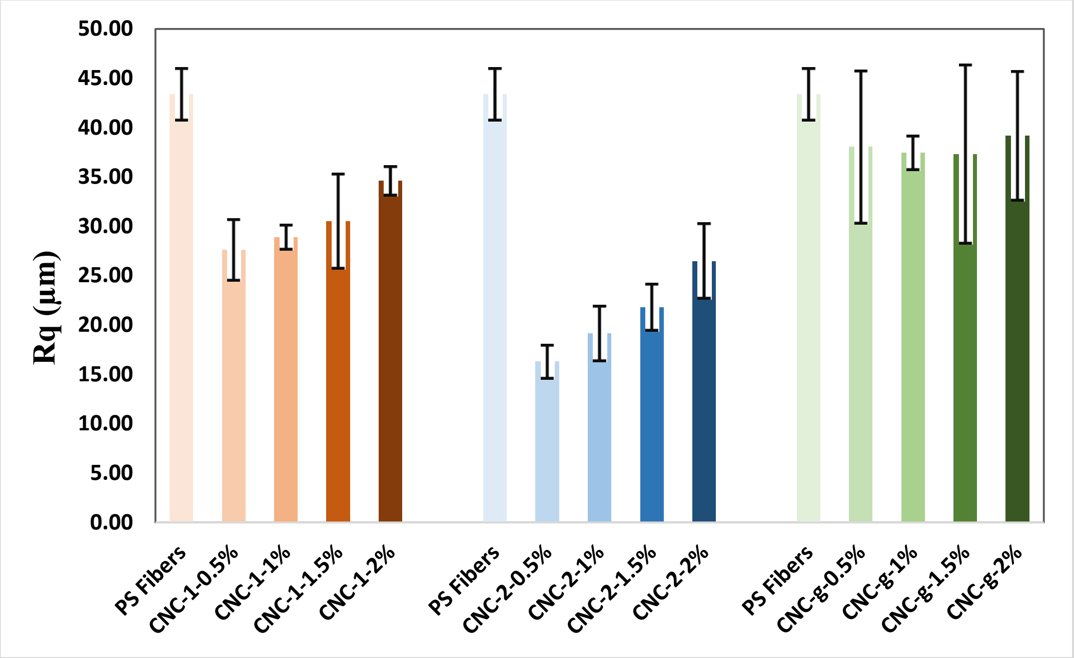

Figure 6. 17: The root mean squared of the linear roughness of different CNC/PS electrospun samples

The effects of fiber alignment on the CNC/PS electrospun products were also investigated. As Figure 6.18 illustrates, alignment of the fibers resulted in the smaller water contact angel which can be justified by their lower roughness, and more ordered structures. On the ordered structures of the aligned electrospun samples, tiny grooves were replaced with tiny voids. This can give rise to the drainage of the water droplet and consequently smaller contact angle.

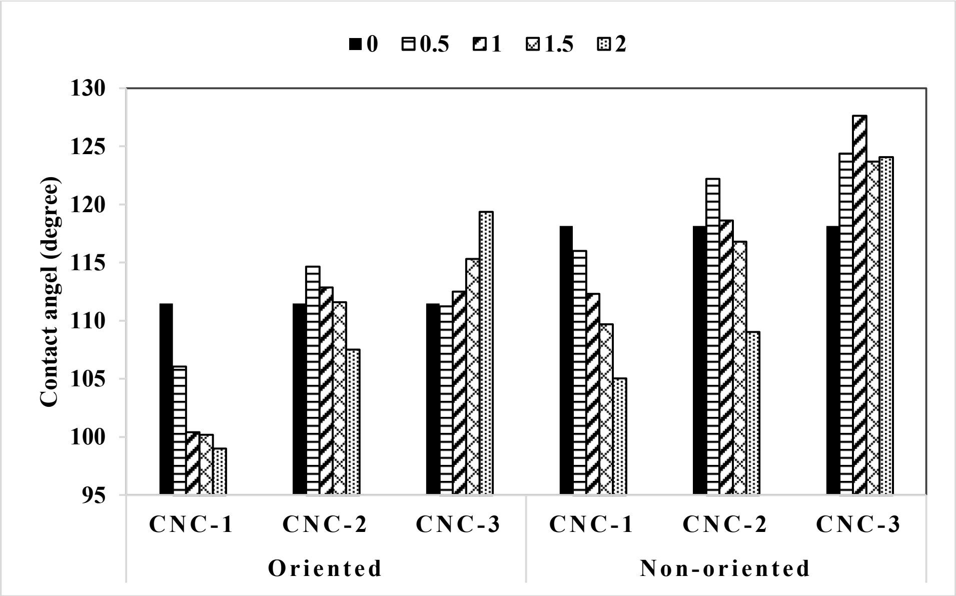

Figure 6. 18: The water contact angle measurements of the oriented and non-oriented CNC/PS electrospun samples

6.4. Conclusion

In this Chapter, the surface properties and wettability of the electrospun samples were studied by means of contact angle and roughness measurements. Three different structures of the neat PS including smooth electrospun fibers, beaded fiber, and electrosprayed spheres were prepared by means of different solvent collections. The beaded fiber structure showed the highest contact angles; however, there is a potential for electrosprayed samples to give a rise to superhydrophobic surface by longer times of electrospraying. Moreover, rose petal effect was observed in electrospun samples which can be attributed to their hairiness and hierarchical surface structures. Finally, addition of CNC can affect the fiber surface properties by changing the roughness and the surface energy; however, the type of these effects can vary based on the types of the CNC modification. Besides, alignment of the fibers caused a drop in contact angle and roughness which can explained by more ordered structure of the oriented CNC/PS samples.

Chapter 7

7. Conclusion and recommendation for future work

7.1. Conclusion

This thesis mainly concentrated on the production of Cellulose nanocrystals (CNC) reinforced PS fibers by means of the electrospinning technique. In this technique, PS solution in a proper solvent is subjected to a high voltage electrical field to stretch and form continuous fibers and fiber mats. Cellulose nanocrystals (CNCs) were chosen as natural reinforcing nanoparticles because of their biocompatibility, high mechanical stiffness, and high strength. Evaluation of the morphological, mechanical, and surface behaviours of these electrospun products are the main objectives of this PhD thesis.

To prepare the best structured fibrous material, firstly, the preparation process of neat PS fibers were optimized. Several PS solvents including dimethyl formaldehyde (DMF), toluene, dichloromethane, tetrahydrofuran, and chloroform were considered as electrospinning solvent for PS. Then, the obtained morphologies of the electrospun samples were analyzed and compared based on the characteristics of the solvents and PS solutions. Among these solvents, dimethyl formaldehyde (DMF) was found the best electrospinning solvent of PS owing to its high conductivity and dielectric constant. Moreover, the viscoelastic behaviour of the PS solution in DMF during electrospinning helped produce the smoothest and narrowest fibers.

After production of an optimized PS electrospun sample, CNC were considered as a reinforcement means to improve its mechanical properties. However, hydrophilic characteristic of CNC makes it less favorable to disperse it uniformly in the hydrophobic PS matrix. Therefore, to improve the interfacial interaction of CNC with PS matrix, CNC nanoparticles were first modified by different functional chemical groups. In this work, three types of modified CNC were used. The modifications included replacement of hydroxyl groups through substitutive reactions with the para nitro benzene (CNC-1), three fluorocarbon benzene (CNC-2), and grafted PS chains (CNC-g). Then, these modified CNCs were used to reinforce PS fibers that were produced using electrospinning technique. Firstly, dispersion behaviour of these modified CNC in DMF were evaluated by means of turbidity metre technique. CNC-2 was the most compatible sample in DMF followed by CNC-g, CNC-1 and unmodified CNC (CNC-R) respectively. These dispersions behaviours reflects the electron pair donation of the DMF, and the strong electron pair acceptor functional groups of –NO2 and –CF3 on CNC-1 and CNC-2 respectively.

All CNC/PS electrospun fibers were collected into both randomly oriented, and aligned structures. To that end, a flat stationary plate, and a rotating drum was considered as collectors in order to induce randomly oriented, and aligned structures in electrospun products, respectively. The effects of modifications on the fiber morphologies were studied through SEM images. In the case of the randomly collected fibers, the inclusion of CNC-1 and CNC-2 resulted in smoother fibers structure and an increase in fibers diameter. On the other hand, beaded fibers, with smaller diameters, were obtained by adding CNC-g and CNC-R. These obtained morphologies can be explained by the excel dispersions of CNC-1 and CNC-2 in DMF in comparison with the CNC-g and CNC-R ones. Moreover, possible entanglements of short grafted PS chains on CNC-g resulted in the agglomeration of CNCs leading to bead formations in fiber structures. In case of oriented electrospun products, the optimum orientation were obtained for the neat PS, and CNC/PS fibrous samples. Five constant speeds of 500 RPM, 1000 RPM, 1500 RPM, 2000 RPM and 3000 RPM were considered to evaluate the effects of the rotating drum speed on both alignments and morphology of the electrospun fibers by means of SEM microscopy. The rotating drum speed of 2000 RPM resulted in the best alignment of fibrous structures because of the possible harmonisation of the frequencies in the rotating drum and the impinging electrospun jet during electrospinning. It was also found that higher PS concentrations resulted in the smoother and thicker electrospun fibers collected on rotating drum. However, higher rotating drum speeds resulted in thinner fibers for all concentrations of PS. Higher speeds of drum could also help remove the beaded structures. Similarly, inclusion of the CNC-1 and CNC-2 to the fiber resulted in a smooth and bead free fiber structures, but beaded fibers, were obtained by addition of CNC-R and CNC-g at low or zero rotor speeds. In the case of CNC-g, the beaded structures disappeared at higher speeds of drum. However, the best rotor speeds to obtain optimum fiber alignments were slightly different for the CNC reinforced fiber and the neat PS fibers.

Mechanical properties of the produced electrospun mats of these fibers were evaluated by means of tensile tests as well as dynamic mechanical analysis (DMA). The effects of CNC inclusion and fiber alignments on the elastic modulus, strength and maximum strain of the fiber mats were investigated by conducting tensile tests. Besides, using DMA results, storage moduli, loss moduli, and damping factors of the electrospun samples were measured and compared. Inclusion of all modified CNCs were resulted in higher mechanical performance of the electrospun products. In the case of CNC-1, or CNC-2, higher concentrations of CNCs brought about higher elastic moduli as well as storage moduli. Among the samples, the oriented PS mats with 0.5 wt. % CNC-g showed the best mechanical gain. The elastic modulus (E) and storage modulus (E') of this samples increased 910% and 250%, respectively. This outstanding improvement can be attributed to the better interfacial interaction of CNC and PS matrix. However, higher concentrations of CNC-g led to a decrease in mechanical performance of the electrospun products. This issue can be explained by the beaded structures of these sample at higher CNC concentrations, observed in SEM images. Finally, alignments of the electrospun fibers led to averages of 450% improvement in stiffness, and 250% increment in storage modulus with inclusion of 2 wt. % of various CNCs.

The surface properties and wettability of the electrospun samples were also studied by means of contact angle and roughness measurements. Three different structures of the neat PS including smooth electrospun fibers, beaded fiber, and electrosprayed spheres, were prepared by using different solvent collections. The beaded fiber structure resulted in the highest contact angle; however, there is a potential for electrosprayed samples to give a rise to superhydrophobic surface after longer times of electrospraying. Moreover, electrospun samples showed the rose petal effect which can be attributed to their hairiness and hierarchical surface structures. Finally, addition of CNC can change the surface properties due to the changes in roughness, and the surface energy based on the types of the CNC modification. Besides, alignment of the fibers caused a drop in contact angle and roughness which can be explained by an increase in the structure order for the oriented CNC/PS samples.

The main objective of this study which was the reinforcements of electrospun PS fibers was well achieved, and all of the modifications of the CNC were helpful to gain striking mechanical improvements with low percentages of CNC inclusions. Consequently, this project can successfully contribute to the composite manufacturing industries.

7.2 Recommendations for future projects

Although a noticeable improvement in mechanical properties of the CNC reinforced electrospun PS products (non-oriented mats and oriented webs) was achieved in this study, there is still a lot to be done for their mechanical improvements. The studies conducted in the present thesis are based on small percentages of the CNC incorporations, and further improvements can be expected when higher concentrations of CNC-1 (CNC-NO2) and CNC-2 (CNC-CF3) are incorporated into the fibers. Additionally, based on the results of the mechanical properties obtained for the samples containing CNC-g (PS grafted CNC), this type of CNC modification shown the best compatibility with PS matrix. However, just low concentrations of them can be applied in electrospun fibers due to the possible chain entanglements, and beads formation. The chemical structure of this type of modified CNC were not investigated thoroughly. By acquiring the knowledge about the length of grafted PS chains and the techniques of controlling their length, their applications in electrospun samples as reinforcement can be improved. As a general trend, lower length of the grafted chains on CNC is preferred because of the lower possibility of the chain entanglements, and beads formation.

Moreover, there are many possible applications for the CNC/PS electrospun products including adhesive layers in composites with sandwich structures. Therefore, evaluation of the improved mechanical performance of the electrospun samples in the final application can be an interesting study. For instance, how a CNC reinforced adhesive layer can prevent or delay the delamination of the the sandwich structured composites.

Finally, as discussed in Chapter 6, PS electrospun product can be a good candidate for superhydrophobicity due to their low surface energy, and their rough structures. In addition, because of the surface hairiness, the petal effect were observed on the surfaces of these samples.

However, the highest contact angle obtained in this study were around 140° which is lower than the required contact angle for superhydrophobicity. Therefore, it is suggested to modify the surface of these products to get a higher surface hydrophobicity for possible application in microdroplet transportations.

Reference

Affdl, J. C.Halpin, and J. L. Kardos. 1976. “The Halpin?Tsai Equations: A Review.” *Polymer Engineering & Science* 16 (5): 344–52. doi:10.1002/pen.760160512.

Ago, Mariko, Joseph E. Jakes, and Orlando J. Rojas. 2013. “Thermomechanical Properties of Lignin-Based Electrospun Nanofibers and Films Reinforced with Cellulose Nanocrystals: A Dynamic Mechanical and Nanoindentation Study.” *ACS Applied Materials and Interfaces* 5 (22): 11768–76. doi:10.1021/am403451w.

Ago, Mariko, Kunihiko Okajima, Joseph E. Jakes, Sunkyu Park, and Orlando J. Rojas. 2012. “Lignin-Based Electrospun Nanofibers Reinforced with Cellulose Nanocrystals.” *Biomacromolecules* 13 (3): 918–26. doi:10.1021/bm201828g.

Ahmed, S, and F R Jones. 1990. “A Review of Particulate Reinforcing Theories for Polymer Composites.” *Journal of Materials Science,* 25 (12): 4933–42.

Akabori, Kei-ichi, Keiji Tanaka, Toshihiko Nagamura, Atsushi Takahara, and Tisato Kajiyama. 2005. “Molecular Motion in Ultrathin Polystyrene Films: Dynamic Mechanical Analysis of Surface and Interfacial Effects.” *Macromolecules* 38 (23): 9735–41. doi:10.1021/ma051143e.

An, H., C. Shin, and G. G. Chase. 2006. “Ion Exchanger Using Electrospun Polystyrene Nanofibers.” *Journal of Membrane Science* 283 (1–2): 84–87. doi:10.1016/j.memsci.2006.06.014.

Arinstein, Arkadii, Michael Burman, Oleg Gendelman, and Eyal Zussman. 2007. “Effect of Supramolecular Structure on Polymer Nanofibre Elasticity.” *Nature Nanotechnology* 2 (1): 59–62. doi:10.1038/nnano.2006.172.

Aslanzadeh, Samira, Zhengxiang Zhu, Qi Luo, Behzad Ahvazi, Yaman Boluk, and Cagri Ayranci. 2016. "Electrospinning of Colloidal Lignin in Poly(ethylene Oxide) *N* , *N* - Dimethylformamide Solutions." *Macromolecular Materials and Engineering* 301 (4): 401–13. doi:10.1002/mame.201500317.

Aussawasathien, D., S. Sahasithiwat, and L. Menbangpung. 2008. "Electrospun Camphorsulfonic Acid Doped Poly(o-Toluidine)-Polystyrene Composite Fibers: Chemical Vapor Sensing." *Synthetic Metals* 158 (7): 259–63. doi:10.1016/j.synthmet.2008.01.007.

Baji, Avinash, Yiu Wing Mai, Shing Chung Wong, Mojtaba Abtahi, and Pei Chen. 2010. "Electrospinning of Polymer Nanofibers: Effects on Oriented Morphology, Structures and Tensile Properties." *Composites Science and Technology* 70 (5). Elsevier Ltd: 703–18. doi:10.1016/j.compscitech.2010.01.010.

Baji, Avinash, Yiu Wing Mai, Shing Chung Wong, Mojtaba Abtahi, and Xusheng Du. 2010. "Mechanical Behavior of Self-Assembled Carbon Nanotube Reinforced Nylon 6,6 Fibers." *Composites Science and Technology* 70 (9). Elsevier Ltd: 1401–9. doi:10.1016/j.compscitech.2010.04.020.

Baker, Simon C., Neil Atkin, Paul A. Gunning, Nick Granville, Karen Wilson, Darren Wilson, and Jennifer Southgate. 2006. "Characterisation of Electrospun Polystyrene Scaffolds for Three-Dimensional in Vitro Biological Studies." *Biomaterials* 27 (16): 3136–46. doi:10.1016/j.biomaterials.2006.01.026.

Bashouti, M., W. Salalha, M. Brumer, E. Zussman, and E. Lifshitz. 2006. "Alignment of Colloidal CdS Nanowires Embedded in Polymer Nanofibers by Electrospinning." *ChemPhysChem* 7 (1): 102–6. doi:10.1002/cphc.200500428.

Bellani, Caroline F., Eric Pollet, Anne Hebraud, Fabiano V. Pereira, Guy Schlatter, Luc Avérous, Rosario E.S. Bretas, and Marcia C. Branciforti. 2016. “Morphological, Thermal, and Mechanical Properties of Poly(ε-Caprolactone)/poly(ε-Caprolactone)-Grafted-Cellulose Nanocrystals Mats Produced by Electrospinning.” *Journal of Applied Polymer Science* 133 (21): 4–11. doi:10.1002/app.43445.

Bercea, Maria, and Patrick Navard. 2000. “Shear Dynamics of Aqueous Suspensions of Cellulose Whiskers.” *Macromolecules* 33 (16): 6011–16. doi:10.1021/ma000417p.

Berriot, J., F. Lequeux, L. Monnerie, H. Montes, D. Long, and P. Sotta. 2002. “Filler-Elastomer Interaction in Model Filled Rubbers, a 1H NMR Study.” *Journal of Non-Crystalline Solids* 307–310: 719–24. doi:10.1016/S0022-3093(02)01552-1.

Berriot, Julien, Hélène Montes, Francois Lequeux, Didier Long, and Paul Sotta. 2002. “Evidence for the Shift of the Glass Transition near the Particles in Silica-Filled Elastomers.” *Macromolecules* 35 (26): 9756–62. doi:10.1021/ma0212700.

Bhattarai, Narayan, Dennis Edmondson, Omid Veiseh, Frederick A. Matsen, and Miqin Zhang. 2005. “Electrospun Chitosan-Based Nanofibers and Their Cellular Compatibility.” *Biomaterials* 26 (31): 6176–84. doi:10.1016/j.biomaterials.2005.03.027.

Bhushan, B., and M. Nosonovsky. 2010. “The Rose Petal Effect and the Modes of Superhydrophobicity.” *Philosophical Transactions of the Royal Society A: Mathematical, Physical and Engineering Sciences* 368 (1929): 4713–28. doi:10.1098/rsta.2010.0203.

Blaker, J. J., V. Maquet, R. Jérôme, A. R. Boccaccini, and S. N. Nazhat. 2005. “Mechanical Properties of Highly Porous PDLLA/Bioglass® Composite Foams as Scaffolds for Bone Tissue Engineering.” *Acta Biomaterialia* 1 (6): 643–52. doi:10.1016/j.actbio.2005.07.003.

Boger, David V., and Hang Nguyen. 1978. “A Model Viscoelastic Fluid.” *Polymer Engineering and Science* 18 (13). Wiley-Blackwell: 1037–43. doi:10.1002/pen.760181311.

Boluk, Yaman, and Christophe Danumah. 2014. “Analysis of Cellulose Nanocrystal Rod Lengths by Dynamic Light Scattering and Electron Microscopy.” *Journal of Nanoparticle Research* 16 (1). doi:10.1007/s11051-013-2174-4.

Boluk, Yaman, Roya Lahiji, Liyan Zhao, and Mark T. McDermott. 2011. “Suspension Viscosities and Shape Parameter of Cellulose Nanocrystals (CNC).” *Colloids and Surfaces A: Physicochemical and Engineering Aspects* 377 (1–3). Elsevier B.V.: 297–303. doi:10.1016/j.colsurfa.2011.01.003.

Boluk, Yaman, and B Schreiber H. 1986. “Interfacial Interactions and the Properties of Filled Polymers: I. Dynamic-Mechanical Responses.” *Polymer Composites* 7 (5).

Botaro, Vagner Roberto, and Alessandro Gandini Ã. 1998. “Chemical Modi ® Cation of the Surface of Cellulosic ® Bres . 2 . Introduction of Alkenyl Moieties via Condensation Reactions Involving Isocyanate Functions.” *Cellulose* 5 (2): 65–78. doi:10.1023/A:1009216729686.

Brown, William Fuller. 1953. “Dielectric Constant Theory for Polar Liquids.” *The Journal of Chemical Physics* 21 (8). American Institute of Physics: 1327–32. doi:10.1063/1.1699214.

Buchko, C J, L C Chen, Y Shen, and D C Martina. 1999. “Processing and Microstructural Characterization of Porous Biocompatible\rprotein Polymer Thin Films.” *Polymer* 40: 7397–7407. doi:10.1016/S0032-3861(98)00866-0.

Bush, John W.M. 2004. “MIT Lecture Notes on Surface Tension, Lecture 1.” *Massachusetts*

Institute of Technology, 1–4. doi:10.13040/IJPSR.0975-8232.7(2).531-42.

Cacciotti, Ilaria, Elena Fortunati, Debora Puglia, Josè Maria Kenny, and Francesca Nanni. 2014. "Effect of Silver Nanoparticles and Cellulose Nanocrystals on Electrospun Poly(lactic) Acid Mats: Morphology, Thermal Properties and Mechanical Behavior." *Carbohydrate Polymers* 103 (1). Elsevier Ltd.: 22–31. doi:10.1016/j.carbpol.2013.11.052.

Can-Herrera, L. A., A. Ávila-Ortega, S. de la Rosa-García, A. I. Oliva, J. V. Cauich-Rodríguez, and J. M. Cervantes-Uc. 2016. "Surface Modification of Electrospun Polycaprolactone Microfibers by Air Plasma Treatment: Effect of Plasma Power and Treatment Time." *European Polymer Journal* 84. Elsevier Ltd: 502–13. doi:10.1016/j.eurpolymj.2016.09.060.

Casper, C L, and J S Stephens. 2004. "Controlling Surface Morphology of Electrospun Polysterene Fibers: Effect of Humidity and Molecular Weight in Electrospinning Process." *Macromolecules* 37: 573–78.

Changsarn, Sutheerat, James D. Mendez, Kadhiravan Shanmuganathan, E. Johan Foster, Christoph Weder, and Pitt Supaphol. 2011. "Biologically Inspired Hierarchical Design of Nanocomposites Based on Poly(ethylene Oxide) and Cellulose Nanofibers." *Macromolecular Rapid Communications* 32 (17): 1367–72. doi:10.1002/marc.201100183.

Chen, Dan, Tianxi Liu, Xiaoping Zhou, Wuiwui Chauhari Tjiu, and Haoqing Hou. 2009. "Electrospinning Fabrication of High Strength and Toughness Polyimide Nanofiber Membranes Containing Multiwalled Carbon Nanotubes." *The Journal of Physical Chemistry. B* 113 (29): 9741–48. doi:10.1021/jp9025128.

Chen, Zonggang, Xiumei Mo, and Fengling Qing. 2007. "Electrospinning of Collagen-Chitosan Complex." *Materials Letters* 61 (16): 3490–94. doi:10.1016/j.matlet.2006.11.104.

Chevigny, Chloé, Florent Dalmas, Emanuela Di Cola, Didier Gigmes, Denis Bertin, François Boué, and Jacques Jestin. 2011. "Polymer-Grafted-Nanoparticles Nanocomposites: Dispersion, Grafted Chain Conformation, and Rheological Behavior." *Macromolecules* 44 (1): 122–33. doi:10.1021/ma101332s.

Colby, Ralph, Michael Rubinstein, Mohamed Daoud, Ralph Colby, Michael Rubinstein, and Mohamed Daoud. 1994. "Hydrodynamics of Polymer Solutions via Two-Parameter Scaling To Cite This Version : HAL Id : Jpa-00248044 Hydrodynamics Polymer."

Cooper, Ashleigh, Rachael Oldinski, Hongyan Ma, James D. Bryers, and Miqin Zhang. 2013. "Chitosan-Based Nanofibrous Membranes for Antibacterial Filter Applications." *Carbohydrate Polymers* 92 (1). Elsevier Ltd.: 254–59. doi:10.1016/j.carbpol.2012.08.114.

Coran, A. Y., K. Boustany, and P. Hamed. 1971. "Unidirectional Fiber–polymer Composites: Swelling and Modulus Anisotropy." *Journal of Applied Polymer Science* 15 (10): 2471–85. doi:10.1002/app.1971.070151014.

Corcione, Carola Esposito, and Mariaenrica Frigione. 2012. "Characterization of Nanocomposites by Thermal Analysis." *Materials* 5 (12): 2960–80. doi:10.3390/ma5122960.

Costa, P., J. Silva, V. Sencadas, R. Simoes, J. C. Viana, and S. Lanceros-M??ndez. 2013. "Mechanical, Electrical and Electro-Mechanical Properties of Thermoplastic Elastomer Styrene-Butadiene-Styrene/multiwall Carbon Nanotubes Composites." *Journal of Materials Science* 48 (3): 1172–79. doi:10.1007/s10853-012-6855-7.

Counto, Upendra J. 1964. "The Effect of the Elastic Modulus of the Aggregate on the Elastic Modulus, Creep and Creep Recovery of Concrete." *Magazine of Concrete Research* 16 (48): 129–38. doi:10.1680/macr.1964.16.48.129.

Daga, Vikram K., Matthew E. Helgeson, and Norman J. Wa. 2006. "Electrospinning of Neat and Laponite-Filled Aqueous Poly(ethylene Oxide) Solutions." *Electrospinning Is Reported for Viscoelastic Aqueous Solutions of Poly(ethylene Oxide) (PEO) and with Added Nanoclay (Laponite). A Weak Correlation between Fiber Diameter and the Spinning Solution's Zero-Shear Viscosity Is Observed and Compared with Previ* 44: 1608–17. doi:10.1002/polb.

Dalmas, Florent, Jean Yves Cavaillé, Catherine Gauthier, Laurent Chazeau, and Rémy Dendievel. 2007. "Viscoelastic Behavior and Electrical Properties of Flexible Nanofiber Filled Polymer Nanocomposites. Influence of Processing Conditions." *Composites Science and Technology* 67 (5): 829–39. doi:10.1016/j.compscitech.2006.01.030.

Dankovich, Theresa a., and Derek G. Gray. 2011. "Contact Angle Measurements on Smooth Nanocrystalline Cellulose (I) Thin Films." *Journal of Adhesion Science and Technology* 25 (6–7): 699–708. doi:10.1163/016942410X525885.

Deitzel, J.M, J Kleinmeyer, D Harris, and N.C Beck Tan. 2001. "The Effect of Processing Variables on the Morphology of Electrospun Nanofibers and Textiles." *Polymer* 42 (1): 261–72. doi:10.1016/S0032-3861(00)00250-0.

Demir, M. M., I. Yilgor, E. Yilgor, and B. Erman. 2002. "Electrospinning of Polyurethane Fibers." *Polymer* 43 (11): 3303–9. doi:10.1016/S0032-3861(02)00136-2.

Dersch, R., Taiqi Liu, A. K. Schaper, A. Greiner, and J. H. Wendorff. 2003. "Electrospun Nanofibers: Internal Structure and Intrinsic Orientation." *Journal of Polymer Science, Part A: Polymer Chemistry* 41 (4): 545–53. doi:10.1002/pola.10609.

Dong, Hong. 2015. "Handbook of Polymer Nanocomposites. Processing, Performance and Application – Volume C: Polymer Nanocomposites of Cellulose Nanoparticles" C: 323–41.

doi:10.1007/978-3-642-38649-7.

Dong, Hong, Kenneth E. Strawhecker, James F. Snyder, Joshua a. Orlicki, Richard S. Reiner, and Alan W. Rudie. 2012. "Cellulose Nanocrystals as a Reinforcing Material for Electrospun Poly(methyl Methacrylate) Fibers: Formation, Properties and Nanomechanical Characterization." *Carbohydrate Polymers* 87 (4). Elsevier Ltd.: 2488–95. doi:http://dx.doi.org/10.1166/jbmb.2009.1016.

Dong, S., and R. Gauvin. 1993. "Application of Dynamic Mechanical Analysis for the Study of the Interfacial Region in Carbon Fiber/epoxy Composite Materials." *Polymer Composites* 14 (5): 414–20. doi:10.1002/pc.750140508.

Dontula, P., C. W. Macosko, and L. E. Scriven. 1998. "Model Elastic Liquids with Water-Soluble Polymers." *AIChE Journal* 44 (6). American Institute of Chemical Engineers: 1247–55. doi:10.1002/aic.690440603.

Drew, Christopher, Xianyan Wang, Lynne Samuelson, and Jayant Kumar. 2003. "The Effect of Viscosity and Filler on Electrospun Fiber Morphology." *Journal of Macromolecular Science, Part A* 40 (12): 1415–22. doi:10.1081/MA-120025320.

Eda, Goki, and Satya Shivkumar. 2007. "Bead-to-Fiber Transition in Electrospun Polystyrene." *Journal of Applied Polymer Science* 106: 475–87.

Eichhorn, S. J., a. Dufresne, M. Aranguren, N. E. Marcovich, J. R. Capadona, S. J. Rowan, C. Weder, et al. 2010. "Review: Current International Research into Cellulose Nanofibres and Nanocomposites." *Journal of Materials Science* 45 (1): 1–33. doi:10.1007/s10853-009-3874-0.

Elkhaldi, Raed M., Serkan Guclu, and Ismail Koyuncu. 2016. “Enhancement of Mechanical and Physical Properties of Electrospun PAN Nanofiber Membranes Using PVDF Particles.” *Desalination and Water Treatment*. doi:10.1080/19443994.2016.1159253.

Esfandarani, M. Salehi, M. S. Johari, R. Amrollahi, and M. Karimi. 2011. “Laser Induced Surface Modification of Clay-PAN Composite Nanofibers.” *Fibers and Polymers* 12 (6): 715–20. doi:10.1007/s12221-011-0715-y.

Fallahi, Dellaram, Mehdi Rafizadeh, Naser Mohamaddi, and Behrooz Vahidi. 2008. “Effect of Applied Voltage on Jet Electriccurrent and Flow Rate in Electrospinningof Polyacrylonitrile Solutions.” *Polymer International* 57 (April): 171–80. doi:10.1002/pi.

Favier, V., G. R. Canova, S. C. Shrivastava, and J. Y. Cavaillé. 1997. “Mechanical Percolation in Cellulose Whisker Nanocomposites.” *Polymer Engineering and Science* 37 (10): 1732–39. doi:10.1002/pen.11821.

Feigin, Robert I., and Donald H. Napper. 1980. “Depletion Stabilization and Depletion Flocculation.” *Journal of Colloid And Interface Science* 75 (2): 525–41. doi:10.1016/0021-9797(80)90475-0.

Feng, Lin, Shuhong Li, Huanjun Li, Jin Zhai, Yanlin Song, Lei Jiang, and Daoben Zhu. 2002. “Super-Hydrophobic Surface of Aligned Polyacrylonitrile Nanofibers.” *Angewandte Chemie - International Edition* 41 (7): 1221–23. doi:10.1002/1521-3773(20020402)41:7<1221::AID-ANIE1221>3.0.CO;2-G.

Feng, Lin, Yanan Zhang, Jinming Xi, Ying Zhu, Nü Wang, Fan Xia, and Lei Jiang. 2008. “Petal Effect: A Superhydrophobic State with High Adhesive Force.” *Langmuir* 24 (8): 4114–19. doi:10.1021/la703821h.

Ferry, J D. 1948. "Viscoelastic Properties of Polymer Solutions." *Journal of Research of the National Bureau of Standards* 41 (1): 53–62. doi:10.1007/BF01534283.

Fong, H, H Fong, I Chun, I Chun, D Reneker, and D Reneker. 1999. "Beaded Nano Bers Formed during Electrospinning." *Polymer* 40: 4585–92.

Forrest, James A., and Kari Dalnoki-Veress. 2001. "The Glass Transition in Thin Polymer Films." *Advances in Colloid and Interface Science* 94 (1–3): 167–96. doi:10.1016/S0001-8686(01)00060-4.

FRANCL, J., and W. D. KINGERY. 1954. "Thermal Conductivity: IX, Experimental Investigation of Effect of Porosity on Thermal Conductivity." *Journal of the American Ceramic Society* 37 (2): 99–107. doi:10.1111/j.1551-2916.1954.tb20108.x.

Gao, Dawei, Hui Qiao, Qingqing Wang, Yibing Cai, and Qufu Wei. n.d. "Structure , Morphology and Thermal Stability of Porous Carbon Nanofibers Loaded with Cobalt Nanoparticles" 851: 2–5.

Gennes, P G De. 2017. "Coil-Stretch Transition of Dilute Flexible Polymers under Ultrahigh Velocity Gradients Coil-Stretch Transition of Dilute Flexible Polymers under Ultrahigh Velocity Gradients" 5030 (1974). doi:10.1063/1.1681018.

Gonçalves, R.P., W.H. Ferreira, R.F. Gouvêa, and C.T. Andrade. 2017. "Effect of Chitosan on the Properties of Electrospun Fibers from Mixed poly(Vinyl Alcohol)/Chitosan Solutions." *Materials Research* 20 (4): 984–93. doi:10.1590/1980-5373-MR-2016-0618.

Gong, Guangming, Juntao Wu, Jingang Liu, Na Sun, Yong Zhao, and Lei Jiang. 2012. "Bio-Inspired Adhesive Superhydrophobic Polyimide Mat with High Thermal Stability." *Journal* *of Materials Chemistry* 22 (17): 8257. doi:10.1039/c2jm16503a.

Goodsell, Johnathan E, Robert J Moon, Alionso Huizar, and R Byron Pipes. 2014. "A Strategy for Prediction of the Elastic Properties of Epoxy-Cellulose Nanocrystal-Reinforced Fiber Networks." *Nordic Pulp & Paper Research Journal* 29 (1, SI): 85–94.

Gopal, Renuga, Satinderpal Kaur, Chao Yang Feng, Casey Chan, Seeram Ramakrishna, Shahram Tabe, and Takeshi Matsuura. 2007. "Electrospun Nanofibrous Polysulfone Membranes as Pre-Filters: Particulate Removal." *Journal of Membrane Science* 289 (1–2): 210–19. doi:10.1016/j.memsci.2006.11.056.

Guangming, Gong, Wu Juntao, Zhao Yong, Liu Jingang, Jin Xu, and Jiang Lei. 2014. "A Novel Fluorinated Polyimide Surface with Petal Effect Produced by Electrospinning." *Soft Matter* 10 (4): 549–52. doi:10.1039/c3sm52540f.

Gupta, Pankaj, Casey Elkins, Timothy E. Long, and Garth L. Wilkes. 2005. "Electrospinning of Linear Homopolymers of Poly(methyl Methacrylate): Exploring Relationships between Fiber Formation, Viscosity, Molecular Weight and Concentration in a Good Solvent." *Polymer* 46 (13): 4799–4810. doi:10.1016/j.polymer.2005.04.021.

H., Reneker Darrell, Alexander Yarin, Eyal Zussman, Sureeporn Koombhongse, and Woraphon Kataphinan. 2006. "Nanofiber Manufacturing : Toward Better Process Control." *ACS Symposium Series* 918: 7–20.

Habibi, Youssef, Lucian A. Lucia, and Orlando J. Rojas. 2010. "Cellulose Nanocrystals: Chemistry, Self-Assembly, and Applications." *Chemical Reviews* 110 (6): 3479–3500. doi:10.1021/cr900339w.

Haghi, a. K., and M. Akbari. 2007. “Trends in Electrospinning of Natural Nanofibers.” *Physica Status Solidi (A) Applications and Materials Science* 204 (6): 1830–34. doi:10.1002/pssa.200675301.

Hansen, Charles M. 2000. “Solubility Parameters — An Introduction.” *Hansen Solubility Parameters: A User’s Handbook*, 281. doi:doi:10.1201/9781420049312.ch1.

Hansen, Charles M. 2013. *Hansen Solubility Parameters A User’s Handbook*. *Journal of Chemical Information and Modeling*. Vol. 53. doi:10.1017/CBO9781107415324.004.

Hasan, O.a, and M.C Boyce. 1993. “Energy Storage during Inelastic Deformation of Glassy Polymers.” *Polymer* 34 (24): 5085–92. doi:10.1016/0032-3861(93)90252-6.

Herrera, N V, a P Mathew, L Y Wang, and K Oksman. 2011. “Randomly Oriented and Aligned Cellulose Fibres Reinforced with Cellulose Nanowhiskers, Prepared by Electrospinning.” *Plastics, Rubber and Composites* 40 (2): 57–64. doi:10.1179/174328911X12988622800891.

Heux, L., G. Chauve, and C. Bonini. 2000. “Nonflocculating and Chiral-Nematic Self-Ordering of Cellulose Microcrystals Suspensions in Nonpolar Solvents.” *Langmuir* 16 (21): 8210–12. doi:10.1021/la9913957.

Hiemenz. 1984. *Polymer Chemistry: The Basic Concepts*. New York.

Hohman, Moses M., Michael Shin, Gregory Rutledge, and Michael P. Brenner. 2001a. “Electrospinning and Electrically Forced Jets. I. Stability Theory.” *Physics of Fluids* 13 (8): 2221–36. doi:10.1063/1.1384013.

Hohman, M. M., Shin, M., Rutledge, G., & Brenner, M. P. (2001). Electrospinning and electrically forced jets. II. Applications " Journal of Applied Physics, 13(3018), 2221–2201.

http://doi.org/10.1063/1.1384013.

Hong, Xia, Xuefeng Gao, and Lei Jiang. 2007. "Application of Superhydrophobic Surface with High Adhesive Force in No Lost Transport of Superparamagnetic Microdroplet." *Journal of the American Chemical Society* 129 (6): 1478–79. doi:10.1021/ja065537c.

Hoy, K.L. 1970. "New Values of the Solubility Parameters from Vapor Pressure Data." *Journal of Paint Technology* 42 (541): 76–118.

Huan, Siqi, Long Bai, Guoxiang Liu, Wanli Cheng, and Guangping Han. 2015. "Electrospun Nanofibrous Composites of Polystyrene and Cellulose Nanocrystals: Manufacture and Characterization." *RSC Adv.* 5 (63). Royal Society of Chemistry: 50756–66. doi:10.1039/C5RA06117B.

Huan, Siqi, Guoxiang Liu, Guangping Han, Wanli Cheng, Zongying Fu, Qinglin Wu, and Qingwen Wang. 2015. "Effect of Experimental Parameters on Morphological, Mechanical and Hydrophobic Properties of Electrospun Polystyrene Fibers." *Materials* 8 (5): 2718–34. doi:10.3390/ma8052718.

Huang, Chaobo, Shuiliang Chen, Darrell H. Reneker, Chuilin Lai, and Haoqing Hou. 2006. "High-Strength Mats from Electrospun Poly(p-Phenylene Biphenyltetracarboximide) Nanofibers." *Advanced Materials* 18 (5): 668–71. doi:10.1002/adma.200501806.

Huang, F. L., Q. Q. Wang, Q. F. Wei, W. D. Gao, H. Y. Shou, and S. D. Jiang. 2010. "Dynamic Wettability and Contact Angles of Poly(vinylidene Fluoride) Nanofiber Membranes Grafted with Acrylic Acid." *Express Polymer Letters* 4 (9): 551–58. doi:10.3144/expresspolymlett.2010.69.

Huang, Jian, Lin Liu, and Juming Yao. 2011. “Electrospinning of Bombyx Mori Silk Fibroin Nanofiber Mats Reinforced by Cellulose Nanowhiskers.” *Fibers and Polymers* 12 (8): 1002–6. doi:10.1007/s12221-011-1002-7.

Huang, Zheng Ming, Chuang Long He, Aizhao Yang, Yanzhong Zhang, Xiao Jian Han, Junlin Yin, and Qingsheng Wu. 2006. “Encapsulating Drugs in Biodegradable Ultrafine Fibers through Co-Axial Electrospinning.” *Journal of Biomedical Materials Research - Part A* 77 (1): 169–79. doi:10.1002/jbm.a.30564.

Huang, Zheng Ming, Y. Z. Zhang, M. Kotaki, and S. Ramakrishna. 2003. “A Review on Polymer Nanofibers by Electrospinning and Their Applications in Nanocomposites.” *Composites Science and Technology* 63 (15): 2223–53. doi:10.1016/S0266-3538(03)00178-7.

Hubbe, Martin a., Orlando J. Rojas, Lucian a. Lucia, and Mohini Sain. 2008. “Cellulosic Nanocomposites: A Review.” *BioResources* 3 (3): 929–80. doi:10.15376/biores.3.3.929-980.

Iwamoto, Shinichiro, Weihua Kai, Akira Isogai, and Tadahisa Iwata. 2009. “Elastic Modulus of Single Cellulose Microfibrils from Tunicate Measured by Atomic Force Microscopy.” *Biomacromolecules* 10 (9): 2571–76. doi:10.1021/bm900520n.

Jarusuwannapoom, Teeradech, Walaiporn Hongrojjanawiwat, Sujinda Jitjaicham, Ladawan Wannatong, Manit Nithitanakul, Cattaleeya Pattamaprom, Piyawit Koombhongse, Ratthapol Rangkupan, and Pitt Supaphol. 2005. “Effect of Solvents on Electro-Spinnability of Polystyrene Solutions and Morphological Appearance of Resulting Electrospun Polystyrene Fibers.” *European Polymer Journal* 41 (3): 409–21. doi:10.1016/j.eurpolymj.2004.10.010.

Jia, Hongfei, Guangyu Zhu, Bradley Vugrinovich, Woraphon Kataphinan, Darrell H. Reneker, and Ping Wang. 2002. “Enzyme-Carrying Polymeric Nanofibers Prepared via Electrospinning for

Use as Unique Biocatalysts." *Biotechnology Progress* 18 (5): 1027–32. doi:10.1021/bp020042m.

Jin, Meihua, Xinjian Feng, Lin Feng, Taolei Sun, Jin Zhai, Tiejin Li, and Lei Jiang. 2005. "Superhydrophobic Aligned Polystyrene Nanotube Films with High Adhesive Force." *Advanced Materials* 17 (16): 1977–81. doi:10.1002/adma.200401726.

Jose, Moncy V., Vinoy Thomas, Kalonda T. Johnson, Derrick R. Dean, and Elijah Nyairo. 2009. "Aligned PLGA/HA Nanofibrous Nanocomposite Scaffolds for Bone Tissue Engineering." *Acta Biomaterialia* 5 (1). Acta Materialia Inc.: 305–15. doi:10.1016/j.actbio.2008.07.019.

Karatrantos, Argyrios, Nigel Clarke, and Martin Kr????ger. 2016. "Modeling of Polymer Structure and Conformations in Polymer Nanocomposites from Atomistic to Mesoscale: A Review." *Polymer Reviews* 56 (3). Taylor & Francis: 385–428. doi:10.1080/15583724.2015.1090450.

Kargarzadeh, Hanieh, Rasha M. Sheltami, Ishak Ahmad, Ibrahim Abdullah, and Alain Dufresne. 2015. "Cellulose Nanocrystal: A Promising Toughening Agent for Unsaturated Polyester Nanocomposite." *Polymer (United Kingdom)* 56. Elsevier Ltd: 346–57. doi:10.1016/j.polymer.2014.11.054.

Katta, P., M. Alessandro, R. D. Ramsier, and G. G. Chase. 2004. "Continuous Electrospinning of Aligned Polymer Nanofibers onto a Wire Drum Collector." *Nano Letters* 4 (11): 2215–18. doi:10.1021/nl0486158.

Kaur, Narinder, Vipin Kumar, and Sanjay R. Dhakate. 2016. "Synthesis and Characterization of Multiwalled CNT–PAN Based Composite Carbon Nanofibers via Electrospinning." *SpringerPlus* 5 (1). Springer International Publishing: 483. doi:10.1186/s40064-016-2051-6.

Ki, Chang Seok, Doo Hyun Baek, Kyung Don Gang, Ki Hoon Lee, In Chul Um, and Young Hwan Park. 2005. "Characterization of Gelatin Nanofiber Prepared from Gelatin-Formic Acid Solution." *Polymer* 46 (14): 5094–5102. doi:10.1016/j.polymer.2005.04.040.

Kim, Gil-Tae, Yu-Jin Hwang, Young-Chull Ahn, Hee-Soo Shin, Jae-Keun Lee, and Chang-Mo Sung. 2005. "The Morphology of Electrospun Polystyrene Fibers." *Korean Journal of Chemical Engineering* 22 (1): 147–53. doi:10.1007/BF02701477.

Kim, Hyun Suk, Kwangsok Kim, Hyoung Joon Jin, and In Joo Chin. 2005. "Morphological Characterization of Electrospun Nano-Fibrous Membranes of Biodegradable Poly(l-Lactide) and Poly(lactide-Co-Glycolide)." *Macromolecular Symposia* 224: 145–54. doi:10.1002/masy.200550613.

Kim, Jong-Sang, and Darrell H. Reneker. 1999. "Polybenzimidazole Nanofiber Produced by Electrospinning." *Polymer Engineering & Science* 39 (5): 849–54.

Kim, Kwan, Keun Lee, Myung Khil, Yo Ho, and Hak Kim. 2004. "The Effect of Molecular Weight and the Linear Velocity of Drum Surface on the Properties of Electrospun Poly(ethylene Terephthalate) Nonwovens." *Fibers and Polymers* 5 (2): 122–27. doi:10.1007/bf02902925.

Klemm, Dieter, Friederike Kramer, Sebastian Moritz, Tom Lindstr??m, Mikael Ankerfors, Derek Gray, and Annie Dorris. 2011. "Nanocelluloses: A New Family of Nature-Based Materials." *Angewandte Chemie - International Edition* 50 (24): 5438–66. doi:10.1002/anie.201001273.

Ko, Frank K., and Yuqin Wan. 2014. "Introduction to Nanofiber Materials," 282. doi:10.1017/CBO9781139021333.

Kongkhlang, Thontree, Kohji Tashiro, Masaya Kotaki, and Suwabun Chirachanchai. 2008.

“Electrospinning as a New Technique To Control the Crystal Morphology and Molecular Orientation of Polyoxymethylene Nanofibers Electrospinning as a New Technique To Control the Crystal Morphology and Molecular Orientation of Polyoxymethylene,” no. 12: 15460–66. doi:10.1021/ja804185s.

Kontou, E, and G Anthoulis. 2007. “The Effect of Silica Nanoparticles on the Thermomechanical Properties of Polystyrene.” *Polymer* 4: 3–6. doi:10.1002/app.

Koosha, Mojtaba, Hamid Mirzadeh, Mohammad Ali Shokrgozar, and Mehdi Farokhi. 2015. “Nanoclay-Reinforced Electrospun chitosan/PVA Nanocomposite Nanofibers for Biomedical Applications.” *RSC Adv.* 5 (14). Royal Society of Chemistry: 10479–87. doi:10.1039/C4RA13972K.

Koski, a., K. Yim, and S. Shivkumar. 2004. “Effect of Molecular Weight on Fibrous PVA Produced by Electrospinning.” *Materials Letters* 58 (3–4): 493–97. doi:10.1016/S0167-577X(03)00532-9.

Krause, W. E., E. G. Bellomo, and R. H. Colby. 2001. “Rheology of Sodium Hyaluronate under Physiological Conditions.” *Biomacromolecules* 2 (1): 65–69. doi:10.1021/bm0055798.

Larrondo, L, and R St John Manley. 1981. “Electrostatic Fiber Spinning from Polymer Melts. II. Examination of the Flow Field in an Electrically Driven Jet.” *... of Polymer Science: Polymer ...* 19: 921–32. doi:10.1002/pol.1981.180190602.

Lee, Jihoon, and Yulin Deng. 2012. “Increased Mechanical Properties of Aligned and Isotropic Electrospun PVA Nanofiber Webs by Cellulose Nanowhisker Reinforcement.” *Macromolecular Research* 20 (1): 76–83. doi:10.1007/s13233-012-0008-3.

Lee, Keun Hyung, Hak Yong Kim, Young Min La, Douk Rae Lee, and Nak Hyun Sung. 2002. "Influence of a Mixing Solvent with Tetrahydrofuran and N,N-Dimethylformamide on Electrospun Poly(vinyl Chloride) Nonwoven Mats." *Journal of Polymer Science, Part B: Polymer Physics* 40 (19): 2259–68. doi:10.1002/polb.10293.

Lemarchand, Caroline, Patrick Couvreur, Christine Vauthier, Dominique Costantini, and Ruxandra Gref. 2003. "Study of Emulsion Stabilization by Graft Copolymers Using the Optical Analyzer Turbiscan." *International Journal of Pharmaceutics* 254 (1): 77–82. doi:10.1016/S0378-5173(02)00687-7.

Li, Dan, Amit Babel, Samson a. Jenekhe, and Younan Xia. 2004. "Nanofibers of Conjugated Polymers Prepared by Electrospinning with a Two-Capillary Spinneret." *Advanced Materials* 16 (22): 2062–66. doi:10.1002/adma.200400606.

Li, Dan, Yuliang Wang, and Younan Xia. 2003. "Electrospinning of Polymeric and Ceramic Nanofibers as Uniaxially Aligned Arrays." *Nano Letters* 3 (8): 1167–71. doi:10.1021/nl0344256.

Li, Dan, and Younan Xia. 2004. "Direct Fabrication of Composite and Ceramic Hollow Nanofibers by Electrospinning." *Nano Letters* 4 (5): 933–38. doi:10.1021/nl049590f.

Li, Yue, Weiping Cai, Guotao Duan, Bingqiang Cao, Fengqiang Sun, and Fang Lu. 2005. "Superhydrophobicity of 2D ZnO Ordered Pore Arrays Formed by Solution-Dipping Template Method." *Journal of Colloid and Interface Science* 287 (2): 634–39. doi:10.1016/j.jcis.2005.02.010.

Li, Yue, Eun Je Lee, and Sung Oh Cho. 2007. "Superhydrophobic Coatings on Curved Surfaces Featuring Remarkable Supporting Force." *Journal of Physical Chemistry C* 111 (40): 14813–

17. doi:10.1021/jp073672l.

Lim, Jong-min, Gi-ra Yi, Jun Hyuk Moon, Chul-joon Heo, and Seung-man Yang. 2007. "Superhydrophobic Films of Electrospun Fibers with Multiple-Scale Surface Morphology," no. 20: 7981–89. doi:10.1021/la700392w.

Lin, Ning, and Alain Dufresne. 2013. "Supramolecular Hydrogels from in Situ Host-Guest Inclusion between Chemically Modified Cellulose Nanocrystals and Cyclodextrin." *Biomacromolecules* 14 (3): 871–80. doi:10.1021/bm301955k.

Ning Lin, and Alain Dufresne. 2014. "Nanocellulose in Biomedicine: Current Status and Future Prospect." *European Polymer Journal* 59. Elsevier Ltd: 302–25. doi:10.1016/j.eurpolymj.2014.07.025.

Lin Song, Qing Cai, Jianying Ji, Gang Sui, Yunhua Yu, Xiaoping Yang, Qi Ma, Yan Wei, and Xuliang Deng. 2008. "Electrospun Nanofiber Reinforced and Toughened Composites through in Situ Nano-Interface Formation." *Composites Science and Technology* 68 (15–16). Elsevier Ltd: 3322–29. doi:10.1016/j.compscitech.2008.08.033.

Lin, Tong, Hongxia Wang, Huimin Wang, and Xungai Wang. 2004. "The Charge Effect of Cationic Surfactants on the Elimination of Fibre Beads in the Electrospinning of Polystyrene." *Nanotechnology* 15 (9): 1375–81. doi:10.1088/0957-4484/15/9/044.

Liu, Dongyan, Xiaowen Yuan, and Debes Bhattacharyya. 2012. "The Effects of Cellulose Nanowhiskers on Electrospun Poly (Lactic Acid) Nanofibres." *Journal of Materials Science* 47 (7): 3159–65. doi:10.1007/s10853-011-6150-z.

Lu, Ping, and You-Lo Hsieh. 2009. "Cellulose Nanocrystal-Filled Poly(acrylic Acid)

Nanocomposite Fibrous Membranes." *Nanotechnology* 20 (41): 415604. doi:10.1088/0957-4484/20/41/415604.

Lu, Xiaofeng, Ce Wang, and Yen Wei. 2009. "One-Dimensional Composite Nanomaterials: Synthesis by Electrospinning and Their Applications." *Small* 5 (21): 2349–70. doi:10.1002/smll.200900445.

Luo, C. J., M. Nangrejo, and M. Edirisinghe. 2010. "A Novel Method of Selecting Solvents for Polymer Electrospinning." *Polymer* 51 (7). Elsevier Ltd: 1654–62. doi:10.1016/j.polymer.2010.01.031.

Luo, C. J., E. Stride, and M. Edirisinghe. 2012. "Mapping the Influence of Solubility and Dielectric Constant on Electrospinning Polycaprolactone Solutions." *Macromolecules* 45 (11): 4669–80. doi:10.1021/ma300656u.

Lynwood, Cole. 2018. *Polystyrene : Synthesis, Characteristics, and Applications*. Accessed May 27. https://books.google.ca/books/about/Polystyrene.html?id=AxuDoAEACAAJ&redir_esc=y.

Ma, Minglin, Malancha Gupta, Zhi Li, Lei Zhai, Karen K. Gleason, Robert E. Cohen, Michael F. Rubner, and Gregory C. Rutledge. 2007. "Decorated Electrospun Fibers Exhibiting Superhydrophobicity." *Advanced Materials* 19 (2): 255–59. doi:10.1002/adma.200601449.

Ma, Minglin, Randal M. Hill, Joseph L. Lowery, Sergey V. Fridrikh, and Gregory C. Rutledge. 2005. "Electrospun Poly(styrene-Block-Dimethylsiloxane) Block Copolymer Fibers Exhibiting Superhydrophobicity." *Langmuir* 21 (12): 5549–54. doi:10.1021/la047064y.

Ma, Minglin, Yu Mao, Malancha Gupta, Karen K. Gleason, and Gregory C. Rutledge. 2005.

“Superhydrophobic Fabrics Produced by Electrospinning and Chemical Vapor Deposition.” *Macromolecules* 38 (23): 9742–48. doi:10.1021/ma0511189.

Marega, Carla, Jenny Maculan, Gian Andrea Rizzi, Roberta Saini, Emanuele Cavaliere, Luca Gavioli, Mattia Cattelan, Giuseppe Giallongo, Antonio Marigo, and Gaetano Granozzi. 2015. “Polyvinyl Alcohol Electrospun Nanofibers Containing Ag Nanoparticles Used as Sensors for the Detection of Biogenic Amines.” *Nanotechnology* 26 (7). IOP Publishing: 75501. doi:10.1088/0957-4484/26/7/075501.

Mathew, G., J. P. Hong, J. M. Rhee, D. J. Leo, and C. Nah. 2006. “Preparation and Anisotropic Mechanical Behavior of Highly-Oriented Electrospun Poly(butylene Terephthalate) Fibers.” *Journal of Applied Polymer Science* 101 (3): 2017–21. doi:10.1002/app.23762.

McKee, Matthew G., Casey L. Elkins, and Timothy E. Long. 2004. “Influence of Self-Complementary Hydrogen Bonding on Solution Rheology/electrospinning Relationships.” *Polymer* 45 (26): 8705–15. doi:10.1016/j.polymer.2004.10.049.

McKinley, G. H. 2005. “Dimensionless Groups for Understanding Free Surface Flows of Complex Fluids.” *Soc. Rheology Bulletin* July (5): 8.

Medeiros, Eliton S., Luiz H C Mattoso, Edson N. Ito, Kay S. Gregorski, George H. Robertson, Richard D. Offeman, Delilah F. Wood, William J. Orts, and Syed H. Imam. 2008. “Electrospun Nanofibers of Poly(vinyl Alcohol) Reinforced with Cellulose Nanofibrils.” *Journal of Biobased Materials and Bioenergy* 2 (3): 231–42. doi:10.1166/jbmb.2008.411.

Menard, Kevin P. 1999. *DYNAMIC MECHANICAL ANALYSIS A Practical Introduction*. doi:doi:10.1201/9781420049183.ch2.

Michielsen, Stephen, and Hoon J. Lee. 2007. “Design of a Superhydrophobic Surface Using Woven Structures.” *Langmuir* 23 (11): 6004–10. doi:10.1021/la063157z.

Mohammadi, N., M. J. Mahjoob, B. Kaffashi, and S. Malakooti. 2010. “An Experimental Evaluation of Pre-Yield and Post-Yield Rheological Models of Magnetic Field Dependent Smart Materials.” *Journal of Mechanical Science and Technology* 24 (9): 1829–37. doi:10.1007/s12206-010-0607-x.

Mohammadian, M., and A. K. Haghi. 2014. “Systematic Parameter Study for Nano-Fiber Fabrication via Electrospinning Process.” *Bulgarian Chemical Communications* 46 (3): 545–55. doi:10.1016/j.polymer.2005.05.068.

Montes, H., F. Lequeux, and J. Berriot. 2003. “Influence of the Glass Transition Temperature Gradient on the Nonlinear Viscoelastic Behavior in Reinforced Elastomers.” *Macromolecules* 36 (21): 8107–18. doi:10.1021/ma0344590.

Moon, R J, a Martini, J Nairn, J Simonsen, and J Youngblood. 2011. *Cellulose Nanomaterials Review: Structure, Properties and Nanocomposites*. *Chem Soc Rev*. Vol. 40. doi:10.1039/c0cs00108b.

Morandi, Gaelle, Lindy Heath, and Wim Thielemans. 2009. “Cellulose Nanocrystals Grafted with Polystyrene Chains through Surface-Initiated Atom Transfer Radical Polymerization (SI-ATRP).” *Langmuir* 25 (14): 8280–86. doi:10.1021/la900452a.

Mortezaei, Mehrzad, Mohammad Hossein Navid Famili, and Mehrdad Kokabi. 2011. “The Role of Interfacial Interactions on the Glass-Transition and Viscoelastic Properties of Silica/polystyrene Nanocomposite.” *Composites Science and Technology* 71 (8). Elsevier Ltd: 1039–45. doi:10.1016/j.compscitech.2011.02.012.

Mthethwa, T. P., M. J. Moloto, A. De Vries, and K. P. Matabola. 2011. “Properties of Electrospun CdS and CdSe Filled Poly(methyl Methacrylate) (PMMA) Nanofibres.” *Materials Research Bulletin* 46 (4). Elsevier Ltd: 569–75. doi:10.1016/j.materresbull.2010.12.022.

Nakajima, A., K. Hashimoto, and T. Watanabe. 2001. “Recent Studies on Super-Hydrophobic Films.” *Monatshefte Fur Chemie* 132 (1): 31–41. doi:10.1007/s007060170142.

Ndoro, Tinashe V M, Michael C. Böhm, and Florian Müller-Plathe. 2012. “Interface and Interphase Dynamics of Polystyrene Chains near Grafted and Ungrafted Silica Nanoparticles.” *Macromolecules* 45 (1): 171–79. doi:10.1021/ma2020613.

Nelson, Andrew, and Terence Cosgrove. 2004. “Dynamic Light Scattering Studies of Poly(ethylene Oxide) Adsorbed on Laponite: Layer Conformation and Its Effect on Particle Stability.” *Langmuir* 20 (24): 10382–88. doi:10.1021/la049323p.

Nielsen, Lawrence E. 1967. “Mechanical Properties of Particulate-Filled Systems.” *Journal of Composite Materials* 1 (1): 100–119. doi:10.1177/002199836700100110.

Nuraje, Nurxat, Waseem S. Khan, Yu Lei, Muhammet Ceylan, and Ramazan Asmatulu. 2013. “Superhydrophobic Electrospun Nanofibers.” *J. Mater. Chem. A* 1 (6): 1929–46. doi:10.1039/C2TA00189F.

Oguzlu, Hale, and Yaman Boluk. 2017. “Interactions between Cellulose Nanocrystals and Anionic and Neutral Polymers in Aqueous Solutions.” *Cellulose* 24 (1). Springer Netherlands: 131–46. doi:10.1007/s10570-016-1096-6.

Öner, Didem, and Thomas J. McCarthy. 2000. “Ultrahydrophobic Surfaces. Effects of Topography Length Scales on Wettability.” *Langmuir* 16 (20): 7777–82. doi:10.1021/la000598o.

Park, Joung-Man, Ga-Young Gu, Zuo-Jia Wang, Dong-Jun Kwon, Pyeong-Su Shin, Jin-Yeong Choi, Lawrence DeVries K, Jin-Yeong Choi, and K Lawrence Devries. 2015. “Mechanical and Electrical Properties of Electrospun CNT/PVDF Nanofiber for Micro- Actuator Applications.” *Advanced Composite Materials*. doi:10.1080/09243046.2015.1082714.

Pavel Kiselev, and Rosell-Llompart Joan. 2012. “Highly Aligned Electrospun Nanofibers by Elimination of the Whipping Motion.” *Journal of Applied Polymer Science* 5 (3): 2423–41.

Pawley, James B. 2006. *Handbook of Biological Confocal Microscopy*. 3rded. Madison: Springer International Publishing.

Peresin, M., Y. Habibi, J. Zoppe, J. Pawlak, and O. Rojas. 2010. “Nanofiber Composites of Polyvinyl Alcohol and Cellulose Nanocrystals: Manufacture and Characterisation.” *Biomacromolecules* 11: 674–81.

Peresin, Maria Soledad, Arja Helena Vesterinen, Youssef Habibi, Leena Sisko Johansson, Joel J. Pawlak, Alexander A. Nevzorov, and Orlando J. Rojas. 2014. “Crosslinked PVA Nanofibers Reinforced with Cellulose Nanocrystals: Water Interactions and Thermomechanical Properties.” *Journal of Applied Polymer Science* 131 (11): 1–12. doi:10.1002/app.40334.

Pham, Quynh P, Upma Sharma, and Antonios G Mikos. 2006. “Electrospinning of Polymeric Nanofibers for Tissue Engineering Applications: A Review.” *Tissue Engineering* 12 (5): 1197–1211. doi:10.1089/ten.2006.12.1197.

Pisuchpen, Thanarath, Navarun Chaim-Ngoen, Narupol Intasanta, Pitt Supaphol, and Voravee P. Hoven. 2011. “Tuning Hydrophobicity and Water Adhesion by Electrospinning and Silanization.” *Langmuir* 27 (7): 3654–61. doi:10.1021/la104978e.

Politechnika Warszawska. Instytut Techniki Cieplnej., Karol, and Tomasz S. Wiśniewski. 2011. “A Review of Models for Effective Thermal Conductivity of Composite Materials.” *Journal of Power Technologies* 95 (1). Warsaw University of Technology, Institut of Heat Engineering: 14–24. http://papers.itc.pw.edu.pl/index.php/JPT/article/view/463.

Reichardt, C. (Christian), and T. (Thomas) Welton. 2010. *Solvents and Solvent Effects in Organic Chemistry.* Wiley-VCH.

Reneker, D. H., W. Kataphinan, A. Theron, E. Zussman, and A. L. Yarin. 2002. “Nanofiber Garlands of Polycaprolactone by Electrospinning.” *Polymer* 43 (25): 6785–94. doi:10.1016/S0032-3861(02)00595-5.

Reneker, Darrell H., Alexander L. Yarin, Hao Fong, and Sureeporn Koombhongse. 2000. “Bending Instability of Electrically Charged Liquid Jets of Polymer Solutions in Electrospinning.” *Journal of Applied Physics* 87 (9): 4531–47. doi:10.1063/1.373532.

Roghani-Mamaqani, Hossein, Vahid Haddadi-Asl Mohammad Najafi, and Mehdi Salami-Kalajahi. 2010. “Preparation of Nanoclay-Dispersed Polystyrene Nanofibers via Atom Transfer Radical Polymerization and Electrospinning.” *Polymers and Polymer Composites* 120: 1431–38. doi:10.1002/app.33119.

Rojas, Orlando J., and Gerardo A. Montero Youssef Habibi. 2009. “Electrospun Nanocomposites from Polystyrene Loaded with Cellulose Nanowhiskers.” *Journal of Applied Polymer Science* 113: 927–35. doi:10.1002/app.

Rošic, R., J. Pelipenko, P. Kocbek, S. Baumgartner, M. Bešter-Rogač, and J. Kristl. 2012. “The Role of Rheology of Polymer Solutions in Predicting Nanofiber Formation by Electrospinning.” *European Polymer Journal* 48 (8): 1374–84.

doi:10.1016/j.eurpolymj.2012.05.001.

Samir A, Alloin F, Dufresne A. 2005. "Review of Recent Research into Cellulosic Whisker, Their Properties and Their Application in Nanocomposites Field." *Biomacromolecules* 6: 612–26. doi:10.1021/bm0493685.

Sas, Iurii, Russell E. Gorga, Jeff A. Joines, and Kristin A. Thoney. 2012. "Literature Review on Superhydrophobic Self-Cleaning Surfaces Produced by Electrospinning." *Journal of Polymer Science, Part B: Polymer Physics* 50 (12): 824–45. doi:10.1002/polb.23070.

Sato, Yoshiyasu, and Junji Furukawa. 1963. "A Molecular Theory of Filler Reinforcement Based upon the Conception of Internal Deformation (A Rough Approximation of the Internal Deformation)." *Rubber Chemistry and Technology*. doi:10.5254/1.3539632.

Seeram Ramakrishna, Kazutoshi Fujihara, Wee-Eong Teo, Teik-Cheng Lim, Zuwei Ma. 2005. *An Introduction to Electrospinning Process*. *Man-Made Textiles in India*. doi:10.1142/9789812567611.

Sepe, Michael P. 1998. "Dynamic Mechanical Analysis for Plastics Engineering" 20 (12): 204. doi:10.1002/9780470423837.ch5.

Shang, H. M., Y. Wang, K. Takahashi, G. Z. Cao, D. Li, and Y. N. Xia. 2005. "Nanostructured Superhydrophobic Surfaces." *Journal of Materials Science* 40 (13): 3587–91. doi:10.1007/s10853-005-2892-9.

Sharp, J. S., and J. A. Forrest. 2003. "Free Surfaces Cause Reductions in the Glass Transition Temperature of Thin Polystyrene Films." *Physical Review Letters* 91 (23). American Physical Society: 235701. doi:10.1103/PhysRevLett.91.235701.

Sheikh, Faheem a, Hyung Woo Ju, Bo Mi Moon, Hyun Jung Park, Jung Ho Kim, Ok Joo Lee, and Chan Hum Park. 2013. “A Novel Approach to Fabricate Silk Nanofibers Containing Hydroxyapatite Nanoparticles Using a Three-Way Stopcock Connector.” *Nanoscale Research Letters* 8 (1): 303. doi:10.1186/1556-276X-8-303.

Shenoy, Suresh L., W. Douglas Bates, Harry L. Frisch, and Gary E. Wnek. 2005a. “Role of Chain Entanglements on Fiber Formation during Electrospinning of Polymer Solutions: Good Solvent, Non-Specific Polymer-Polymer Interaction Limit.” *Polymer* 46 (10): 3372–84. doi:10.1016/j.polymer.2005.03.011.

Shin, C. 2006. “Filtration Application from Recycled Expanded Polystyrene.” *Journal of Colloid and Interface Science* 302 (1): 267–71. doi:10.1016/j.jcis.2006.05.058.

Shirole, Anuja, Janak Sapkota, E. Johan Foster, and Christoph Weder. 2016. “Shape Memory Composites Based on Electrospun Poly(vinyl Alcohol) Fibers and a Thermoplastic Polyether Block Amide Elastomer.” *ACS Applied Materials and Interfaces* 8 (10): 6701–8. doi:10.1021/acsami.6b00834.

Sihn, Sangwook, Ran Y. Kim, Wansoo Huh, Kwang Hoon Lee, and Ajit K. Roy. 2008. “Improvement of Damage Resistance in Laminated Composites with Electrospun Nano-Interlayers.” *Composites Science and Technology* 68 (3–4): 673–83. doi:10.1016/j.compscitech.2007.09.015.

Small, P. a. 1953. “Some Factors Affecting the Solubility of Polymers.” *Journal of Applied Chemistry* 3 (2): 71–80. doi:10.1002/jctb.5010030205.

Smallwood, Ian M. 1997. *Handbook of Organic Solvent Properties*. *International Journal of Adhesion and Adhesives*. Vol. 17. London: Arnold. New York. doi:10.1016/S0143-

7496(97)88687-3.

Solak, Ali Osman, Laura R. Eichorst, William J. Clark, and Richard L. McCreery. 2003. “Modified Carbon Surfaces As ‘organic Electrodes’ that Exhibit Conductance Switching.” *Analytical Chemistry* 75 (2): 296–305. doi:10.1021/ac026107h.

Spychal, T., D. Lath, and D. Berek. 1979. “Thermodynamic and Hydrodynamic Properties of the the Systems Polymer-Tetrahydrofuran-Water: 1. Solution Properties of Polystyrene.” *Polymer* 20 (4): 437–42. doi:10.1016/0032-3861(79)90067-3.

Stefanis, Emmanuel, and Costas Panayiotou. 2008. “Prediction of Hansen Solubility Parameters with a New Group-Contribution Method.” *International Journal of Thermophysics* 29 (2): 568–85. doi:10.1007/s10765-008-0415-z.

Sukigara, Sachiko, Milind Gandhi, Jonathan Ayutsede, Michael Micklus, and Frank Ko. 2003. “Regeneration of Bombyx Mori Silk by Electrospinning - Part 1: Processing Parameters and Geometric Properties.” *Polymer* 44 (19): 5721–27. doi:10.1016/S0032-3861(03)00532-9.

Sullivan, Erin M., Robert J. Moon, and Kyriaki Kalaitzidou. 2015. “Processing and Characterization of Cellulose Nanocrystals/polylactic Acid Nanocomposite Films.” *Materials* 8 (12): 8106–16. doi:10.3390/ma8125447.

Sun, Chenggui, Yaman Boluk, and Cagri Ayranci. 2015. “Investigation of Nanofiber Nonwoven Meshes Produced by Electrospinning of Cellulose Nanocrystal Suspensions in Cellulose Acetate Solutions.” *Cellulose* 22 (4). Springer Netherlands: 2457–70. doi:10.1007/s10570-015-0665-4.

Sun, Zaicheng, Joseph M. Deitzel, Jeff Knopf, Xing Chen, and John W. Gillespie. 2012. “The

Effect of Solvent Dielectric Properties on the Collection of Oriented Electrospun Fibers." *Journal of Applied Polymer Science* 125 (4). Wiley-Blackwell: 2585–94. doi:10.1002/app.35454.

Sundaray, Bibekananda, V. Subramanian, T. S. Natarajan, Rong Zheng Xiang, Chia Cheng Chang, and Wun Shain Fann. 2004. "Electrospinning of Continuous Aligned Polymer Fibers." *Applied Physics Letters* 84 (7): 1222–24. doi:10.1063/1.1647685.

Supaphol, Pitt, Chidchanok Mit-Uppatham, and Manit Nithitanakul. 2005. "Ultrafine Electrospun Polyamide-6 Fibers: Effect of Emitting Electrode Polarity on Morphology and Average Fiber Diameter." *Journal of Polymer Science, Part B: Polymer Physics* 43 (24): 3699–3712. doi:10.1002/polb.20671.

Tadros, Th.F. 1996. "Correlation of Viscoelastic Properties of Stable and Flocculated Suspensions with Their Interparticle Interactions." *Advances in Colloid and Interface Science* 68: 97–200. doi:10.1016/S0001-8686(96)90047-0.

Takayanagi, Motowo, Shinsaku Uemura, and Shunsuke Minami. 1964. "Application of Equivalent Model Method to Dynamic Rheo-Optical Properties of Crystalline Polymer." *Journal of Polymer Science Part C: Polymer Symposia* 5 (1): 113–22. doi:10.1002/polc.5070050111.

Tan, E. P S, S. Y. Ng, and C. T. Lim. 2005. "Tensile Testing of a Single Ultrafine Polymeric Fiber." *Biomaterials* 26 (13): 1453–56. doi:10.1016/j.biomaterials.2004.05.021.

Teo, W E, and S Ramakrishna. 2006. "A Review on Electrospinning Design and Nanofibre Assemblies." *Nanotechnology* 17 (14): R89–106. doi:10.1088/0957-4484/17/14/R01.

Theron, A, E Zussman, and A L Yarin. 2001. "Electrostatic Field-Assisted Alignment of

Electrospun Nanofibres." *Nanotechnology* 12 (3): 384–90. doi:10.1088/0957-4484/12/3/329.

Thomas, Vinoy, Moncy V. Jose, S. Chowdhury, Jonathan F. Sullivan, Derrick R. Dean, and Yogesh K. Vohra. 2006. "Mechano-Morphological Studies of Aligned Nanofibrous Scaffolds of Polycaprolactone Fabricated by Electrospinning." *Journal of Biomaterials Science, Polymer Edition* 17 (9): 969–84. doi:10.1163/156856206778366022.

Uyar, Tamer, and Flemming Besenbacher. 2008. "Electrospinning of Uniform Polystyrene Fibers: The Effect of Solvent Conductivity." *Polymer* 49 (24). Elsevier Ltd: 5336–43. doi:10.1016/j.polymer.2008.09.025.

Van Es, M, F Xiqiao, J Van Turnhout, E Van der Giessen, S Al-Malaika, and A W Golovoy. 2001. "Specialty Polymer Additives: Principles and Applications." *Malden, MA, USA: Blackwell Science*. Malden: Blackwell Science.

Victor M. Starov, Manuel G. Velarde, Clayton J. Radke. 2007. *Wetting and Spreading*. *CRC Press*. CRC Press.

Viet, David, Stephanie Beck-Candanedo, and Derek G. Gray. 2007. "Dispersion of Cellulose Nanocrystals in Polar Organic Solvents." *Cellulose* 14 (2). Kluwer Academic Publishers: 109–13. doi:10.1007/s10570-006-9093-9.

Wagner, Herman L. 1985. "The Mark–Houwink–Sakurada Equation for the Viscosity of Atactic Polystyrene." *Journal of Physical and Chemical Reference Data*. doi:10.1063/1.555740.

Wanasekara, N. D., R. P. O. Santos, C. Douch, E. Frollini, and S. J. Eichhorn. 2016. "Orientation of Cellulose Nanocrystals in Electrospun Polymer Fibres." *Journal of Materials Science* 51 (1). Springer US: 218–27. doi:10.1007/s10853-015-9409-y.

Wang, Biao, Ying Sun, and Huaping Wang. 2010. “Preparation and Properties of Electrospun PAN/Fe3O4 Magnetic Nanofibers.” *Journal ofAppliedPolymer Science* 115: 1781–86.

Wang, Chi, Chia Hung Hsu, and Jian Hua Lin. 2006. “Scaling Laws in Electrospinning of Polystyrene Solutions.” *Macromolecules* 39 (22): 7662–72. doi:10.1021/ma060866a.

Wang, Mao, Hyoung-Joon Jin, David L. Kaplan, and Gregory C. Rutledge. 2004. “Mechanical Properties of Electrospun Silk Fibers.” *Macromolecules* 37 (18): 6856–64. doi:10.1021/ma048988v.

Wang, Xuefen, In Chul Um, Dufei Fang, Akio Okamoto, Benjamin S. Hsiao, and Benjamin Chu. 2005. “Formation of Water-Resistant Hyaluronic Acid Nanofibers by Blowing-Assisted Electro-Spinning and Non-Toxic Post Treatments.” *Polymer* 46 (13): 4853–67. doi:10.1016/j.polymer.2005.03.058.

Wang, Yazhou, Bochu Wang, Weili Qiao, and Tieying Yin. 2010. “A Novel Controlled Release Drug Delivery System for Multiple Drugs Based on Electrospun Nanofibers Containing Nanoparticles.” *Journal of Pharmaceutical Sciences* 99 (12). Elsevier Masson SAS: 4805–11. doi:10.1002/jps.22189.

Wannatong, Ladawan, Anuvat Sirivat, and Pitt Supaphol. 2004. “Effects of Solvents on Electrospun Polymeric Fibers: Preliminary Study on Polystyrene.” *Polymer International* 53 (11): 1851–59. doi:10.1002/pi.1599.

Wong, Shing Chung, Avinash Baji, and Siwei Leng. 2008. “Effect of Fiber Diameter on Tensile Properties of Electrospun Poly(ε-Caprolactone).” *Polymer* 49 (21): 4713–22. doi:10.1016/j.polymer.2008.08.022.

Worzakowska, Marta. 2015. “Thermal and Mechanical Properties of Polystyrene Modified with Esters Derivatives of 3-Phenylprop-2-En-1-Ol.” *Journal of Thermal Analysis and Calorimetry* 121 (1). Springer Netherlands: 235–43. doi:10.1007/s10973-015-4547-7.

Wu, Qiang, Yujie Meng, Siqun Wang, Yanjun Li, Shenyun Fu, Lingfei Ma, and David Harper. 2014. “Rheological Behavior of Cellulose Nanocrystal Suspension: Influence of Concentration and Aspect Ratio.” *Journal of Applied Polymer Science* 131 (15): 1–8. doi:10.1002/app.40525.

Wu, Xiang Fa, and Alexander L. Yarin. 2013. “Recent Progress in Interfacial Toughening and Damage Self-Healing of Polymer Composites Based on Electrospun and Solution-Blown Nanofibers: An Overview.” *Journal of Applied Polymer Science* 130 (4): 2225–37. doi:10.1002/app.39282.

Wu, Xiawa, Robert J. Moon, and Ashlie Martini. 2013. “Crystalline Cellulose Elastic Modulus Predicted by Atomistic Models of Uniform Deformation and Nanoscale Indentation.” *Cellulose* 20 (1): 43–55. doi:10.1007/s10570-012-9823-0.

Xu, C. Y., R. Inai, M. Kotaki, and S. Ramakrishna. 2004. “Aligned Biodegradable Nanofibrous Structure: A Potential Scaffold for Blood Vessel Engineering.” *Biomaterials* 25 (5): 877–86. doi:10.1016/S0142-9612(03)00593-3.

Xu, Chengyu, Ryuji Inai, Masaya Kotaki, and Seeram Ramakrishna. 2004. “Electrospun Nanofiber Fabrication as Synthetic Extracellular Matrix and Its Potential for Vascular Tissue Engineering.” *Tissue Engineering* 10 (7–8): 1160–68. doi:10.1089/ten.2004.10.1160.

Xu, Desheng, Veronica Sanchez-Romaguera, Silvia Barbosa, Will Travis, Jos de Wit, Paul Swan, and Stephen George Yeates. 2007. “Inkjet Printing of Polymer Solutions and the Role of

Chain Entanglement." *Journal of Materials Chemistry* 17 (46): 4902. doi:10.1039/b710879f.

Xu, Xuezhu, Fei Liu, Long Jiang, J. Y. Zhu, Darrin Haagenson, and Dennis P. Wiesenborn. 2013. "Cellulose Nanocrystals vs. Cellulose Nanofibrils: A Comparative Study on Their Microstructures and Effects as Polymer Reinforcing Agents." *ACS Applied Materials and Interfaces* 5 (8): 2999–3009. doi:10.1021/am302624t.

Yang, Qingbiao, L. I. Zhenyu, Youliang Hong, Yiyang Zhao, Shilun Qiu, C. E. Wang, and Yen Wei. 2004. "Influence of Solvents on the Formation of Ultrathin Uniform Poly(vinyl Pyrrolidone) Nanofibers with Electrospinning." *Journal of Polymer Science, Part B: Polymer Physics* 42 (20): 3721–26. doi:10.1002/polb.20222.

Yarin, A L, S Koombhongse, and D H Reneker. 2002. "Bending Instability in Electrospinning of Nanofibers Bending Instability in Electrospinning of Nanofibers" 3018 (2001). doi:10.1063/1.1333035.

Yasuda, T., T. Okuno, and H. Yasuda. 1994. "Contact Angle of Water on Polymer Surfaces." *Langmuir* 10 (7): 2435–39. doi:10.1021/la00019a068.

Yordem, O. S., M. Papila, and Y. Z. Menceloglu. 2008. "Effects of Electrospinning Parameters on Polyacrylonitrile Nanofiber Diameter: An Investigation by Response Surface Methodology." *Materials and Design* 29 (1): 34–44. doi:10.1016/j.matdes.2006.12.013.

Yu, Jian H., Sergey V. Fridrikh, and Gregory C. Rutledge. 2006. "The Role of Elasticity in the Formation of Electrospun Fibers." *Polymer* 47 (13): 4789–97. doi:10.1016/j.polymer.2006.04.050.

Yuan, XiaoYan Y., YuanYuan Y. Zhang, Cunhai Dong, and Jing Sheng. 2004. "Morphology of

Ultrafine Polysulfone Fibers Prepared by Electrospinning." *Polymer International* 53 (11): 1704–10. doi:10.1002/pi.1538.

Zeng, Jing, Xiaoyi Xu, Xuesi Chen, Qizhi Liang, Xinchao Bian, Lixin Yang, and Xiabin Jing. 2003. "Biodegradable Electrospun Fibers for Drug Delivery." *Journal of Controlled Release* 92 (3): 227–31. doi:10.1016/S0168-3659(03)00372-9.

Zhai, Lei, Fevzi C. Cebeci, Robert E. Cohen, and Michael F. Rubner. 2004. "Stable Superhydrophobic Coatings from Polyelectrolyte Multilayers." *Nano Letters* 4 (7): 1349–53. doi:10.1021/nl049463j.

Zhang, Yanzhong, Hongwei Ouyang, Teck Lim Chwee, Seeram Ramakrishna, and Zheng Ming Huang. 2005. "Electrospinning of Gelatin Fibers and gelatin/PCL Composite Fibrous Scaffolds." *Journal of Biomedical Materials Research - Part B Applied Biomaterials* 72 (1): 156–65. doi:10.1002/jbm.b.30128.

Zhou, Chengjun, Raymond Chu, Rhonna Wu, and Qinglin Wu. 2011. "Electrospun Polyethylene Oxide/cellulose Nanocrystal Composite Nanofibrous Mats with Homogeneous and Heterogeneous Microstructures." *Biomacromolecules* 12 (7): 2617–25. doi:10.1021/bm200401p.

Zhou, Chengjun, Qingfeng Shi, Weihong Guo, Lekeith Terrell, Ammar T. Qureshi, Daniel J. Hayes, and Qinglin Wu. 2013. "Electrospun Bio-Nanocomposite Scaffolds for Bone Tissue Engineering by Cellulose Nanocrystals Reinforcing Maleic Anhydride Grafted PLA." *ACS Applied Materials and Interfaces* 5 (9): 3847–54. doi:10.1021/am4005072.

Zhou, Chengjun, Qingwen Wang, and Qinglin Wu. 2012. "UV-Initiated Crosslinking of Electrospun Poly(ethylene Oxide) Nanofibers with Pentaerythritol Triacrylate: Effect of

Irradiation Time and Incorporated Cellulose Nanocrystals." *Carbohydrate Polymers* 87 (2). Elsevier Ltd.: 1779–86. doi:10.1016/j.carbpol.2011.09.095.

Zhou, Chengjun, and Qinglin Wu. 2012. "Recent Development in Applications of Cellulose Nanocrystals for Advanced Polymer-Based Nanocomposites by Novel Fabrication Strategies." *Nanocrystals – Synthesis, Characterization and Applications Properties.*, 103–20. doi:10.5772/46512.

Zhou, Zhengping, Xiang Fa Wu, Yichun Ding, Meng Yu, Youhao Zhao, Long Jiang, Chengluan Xuan, and Chengwen Sun. 2014. "Needleless Emulsion Electrospinning for Scalable Fabrication of Core-Shell Nanofibers." *Journal of Applied Polymer Science* 131 (20): 1–9. doi:10.1002/app.40896.

Zhou, Zhengping, Xiang Fa Wu, Xueqin Gao, Long Jiang, Yong Zhao, and Hao Fong. 2011. "Parameter Dependence of Conic Angle of Nanofibres during Electrospinning." *Journal of Physics D: Applied Physics* 44 (43). doi:10.1088/0022-3727/44/43/435401.

Zong, Xinhua, Kwangsok Kim, Dufei Fang, Shaofeng Ran, Benjamin S. Hsiao, and Benjamin Chu. 2002. "Structure and Process Relationship of Electrospun Bioabsorbable Nanofiber Membranes." *Polymer* 43 (16): 4403–12. doi:10.1016/S0032-3861(02)00275-6.

Zoppe, Justin O., Maria S. Peresin, Youssef Habibi, Richard a. Venditti, and Orlando J. Rojas. 2009. "Reinforcing Poly(ε-Caprolactone) Nanofibers with Cellulose Nanocrystals." *ACS Applied Materials and Interfaces* 1 (9): 1996–2004. doi:10.1021/am9003705.

Zussman, E., D. Rittel, and A. L. Yarin. 2003. "Failure Modes of Electrospun Nanofibers." *Applied Physics Letters* 82 (22): 3958–60. doi:10.1063/1.1579125.